Stable isotopes of volatile elements as a window into the crust and mantle beneath Icelandic volcanoes

Eemu Ranta

Faculty of Earth Sciences
University of Iceland
2022

Stable isotopes of volatile elements as a window into the crust and mantle beneath Icelandic volcanoes

Eemu Ranta

Dissertation submitted in partial fulfillment of a
Philosophiae Doctor degree in Geology

PhD Committee

Dr. Sæmundur A. Halldórsson
Dr. Andri Stefánsson
Institute of Earth Sciences, University of Iceland

Dr. Peter H. Barry
Woods Hole Oceanographic Institution, USA

Opponents

Dr. Jacqueline E. Dixon
College of Marine Science, University of South Florida, USA

Dr. James Farquhar
Department of Geology, University of Maryland, USA

Faculty of Earth Sciences
School of Engineering and Natural Sciences
University of Iceland
Reykjavik, February 2022

Stable isotopes of volatile elements as a window into the crust and mantle beneath Icelandic volcanoes
Dissertation submitted in partial fulfillment of a *Philosophiae Doctor* degree in Geology

Copyright © 2022 Eemu Ranta
All rights reserved

Faculty of Earth Sciences
School of Engineering and Natural Sciences
University of Iceland
Sturlugata 7
102 Reykjavik
Iceland

Telephone: 525 4000

Bibliographic information:
Eemu Ranta, 2022, *Stable isotopes of volatile elements as a window into the crust and mantle beneath Icelandic volcanoes*, PhD dissertation, Faculty of Earth Sciences, University of Iceland, 217 pp.

Author ORCID: 0000-0003-3685-334X
ISBN: 978-9935-9555-5-5

Printing: Háskólaprent
Reykjavik, Iceland, February 2022

Abstract

Volatile species (e.g., H_2O, He, B, CO_2, S, Cl) and their isotopes in volcanic materials provide a unique, but underexplored archive of information about magmatic processes and planetary evolution. This study aims to improve our understanding regarding the origins of volatiles in ocean island basalts and the roles played by volatiles in evolving magmas in the crust. To this end, data are presented on the abundances and isotopic compositions of volatiles in lavas and hydrothermal fluids from active volcanoes in Iceland. Special focus is given to the Kverkfjöll volcanic system, for which a comprehensive geochemical dataset is provided. The main results are: (1) Chlorine isotope ratios of silicic volcanic rocks are introduced as a novel tracer of fluid-melt interaction in silicic magma domains, showing that magmatic brine assimilation may be a fundamental, but previously unrecognized process during rhyolite genesis. (2) Sulfur isotopic compositions of Icelandic basalts are shown to reflect both crustal magma evolution and mantle heterogeneity. Distinct $\Delta^{33}S$-$\delta^{34}S$ signatures are assigned for recycled and primordial mantle components. (3) Deep intrusive degassing is identified as the source of CO_2 and S in Icelandic volcanic-hydrothermal systems, which are proposed to be the main conduits of mantle-to-atmosphere degassing for these volatiles. (4) The geochemistry of the Kverkfjöll magma suite highlights the lithospheric lid control on mantle melting, and an asymmetric distribution of enriched components in the Iceland mantle (5) A subduction fluid-enriched mantle component beneath Iceland is suggested to explain the chlorine-enrichment and back-arc basin-like isotopic signatures of hydrogen, helium, boron, sulfur and chlorine of the Kverkfjöll basalts.

Útdráttur

Reikul efni og sér í lagi samsætur þeirra (t.d. H_2O, He, B, CO_2, S, Cl), veita margvíslegar upplýsingar um kvikuferli sem og uppsprettur þeirra í möttli og skorpu. Í þessari ritgerð eru lagðar fram fimm greinar þar sem reikul efni, uppleyst í kviku og í jarðhitavökva, eru könnuð með það að markmiði að auka skilning okkar á skorpuferlum, djúpstæðri og grunnstæðri kvikuafgösum. Sérstök áhersla var lögð á að rannsaka basalt og jarðhitavökva úr Kverkfjalla-eldstöðvakerfniu m.t.t. þessara markmiða. Niðurstöður eru eftirfarandi: (1) Nota má samsætur klórs í súru íslensku bergi til að varpa ljósi á samspil vökva og bráðar. Sýnt er fram á að áður óþekkt ferli, meltun kvikupækla, er að öllum líkindum grundvallarþáttur við myndun súrs bergs hér á landi sem og annars staðar. (2) Samsætur brennisteins í íslensku basalti bera vott um flókin skorpuferli ásamt margbreytilegum uppsprettum brennisteins í íslenska jarðmöttlinum. (3) Djúpstæð kvikuafgösum gegnum jarðhitakerfi Kverkfjalla og Öskju er helsta uppspretta CO_2 og S og er útstreymi þeirra frá möttli til andrúmslofts rakið. (4) Jarðefnafræði bergs úr Kverkfjallakerfinu er best skýrð með hliðsjón að þykku steinhveli sem líklegt er að stjórni lengd bræðlusúlu undir svæðinu sem og ósamhverfu í möttulþáttum eins og þeir birtast okkur í basalti Miðhálendisins. (5) Uppleyst reikulefni í basalti Kverkfjalla–kerfisins bera keim af möttli sem endurtekið hefur verið auðgaður með vökvum er losa frá sökkvandi úthafsfleka á niðurstreymisflekamótum.

Dedicated to Pauliina and Neeme
who remind me every day that life is more than rocks

Preface

This thesis is based on research carried out at the University of Iceland between August 2017 and December 2021. The PhD project was funded for three consecutive years by the Nordic Volcanological Center and for a fourth year by the University of Iceland Doctoral Research Fund. The outcome is presented in five manuscripts, of which, at the time of writing, one is published, one has been submitted and three are in preparation. The manuscripts are listed below in their order of appearance in the thesis:

I. **Ranta, E**., Halldórsson, S.A., Barnes, J.D., Jónasson, K., Stefánsson, A. (2021) Chlorine isotope ratios record magmatic brine assimilation during rhyolite genesis. *Geochemical Perspectives Letters*, 15, 35-39

II. **Ranta, E.**, Gunnarsson-Robin, J., Halldórsson, S.A., Ono, S., Izon, G., Jackson, M.G., Reekie, C.D.J., Jenner, F.E., Gudfinnsson, G.H., Jónsson, O.P., Stefánsson, A. (in review) Ancient and recycled sulfur sampled by the Iceland mantle plume. Submitted to *Earth and Planetary Science Letters*

III. **Ranta, E.**, Stefánsson, A., Gunnarsson-Robin, J., Barry, P., Ono, S., Kleine, B., Ricci, A., Fiebig, J., Kjartansdóttir, R., Halldórsson, S.A. (in prep.) Deep and shallow magma degassing and volatile fluxes through volcanic hydrothermal systems – insights from the Askja and Kverkfjöll volcanoes, Iceland. In preparation for *Geochmica et Cosmochimica Acta*, or similar

IV. **Ranta, E.**, Halldórsson, S.A., Nykänen, V., Kaikkonen, R., Gudfinnsson, G.H., Barry, P.H., O'Brien, H., Rasmussen, M.B., Gunnarsson-Robin, J., Marshall, E.W., Stefánsson, A., Bali, E., Jackson, M.G., Grönvold, K. (in prep.) Geochemistry of basalts of the Kverkfjöll volcanic system, Iceland: Bridging the gap between rift and off-rift magmatism. In preparation for *Journal of Petrology*, or similar

V. **Ranta, E.**, Halldórsson, S.A., Barnes, J.D., Matthews, S., Kleine, B.I., Marshall, E.W., Jackson, M.G., Bali, E., Barry, P.H., Stefánsson, A., Gudfinnsson, G.H., Grönvold, K. (in prep.) A whiff of subduction fluids in the Iceland mantle. In preparation for *Earth and Planetary Science Letters*, or similar

Additionally, contributions were made to the following articles that are not included in the thesis:

Marshall, E.W., **Ranta, E.**, Halldórsson, S.A., Caracciolo, A., Bali, E., Jeon, H., Whitehouse, M.J., Barnes, J.D., Stefánsson, A. (2022) Boron isotope evidence for the presence of devolatilized and rehydrated subducted materials in the Icelandic mantle source. *Earth and Planetary Science Letters* 577:117229

Taracsák, Z., Neave, D.A., Beaudry, P., Gunnarsson-Robin, J., Burgess, R., Edmonds, M., Halldórsson, S.A., Longpré, M-A., Ono, S., **Ranta, E.**, Stefánsson, A., Turchyn, A.V., EIMF, Hartley, M.E. (2021) Instrumental mass fractionation during sulfur isotope analysis by secondary ion mass spectrometry in natural and synthetic glasses. *Chemical Geology* 578:120318

Byrne, D.J., Broadley, M.W., Halldórsson, S.A., **Ranta, E.**, Ricci, A., Tyne, R.L., Stefánsson, A., Ballentine, C.J., Barry, P.H. (2021) The use of noble gas isotopes to trace subsurface boiling temperatures in Icelandic geothermal systems. *Earth and Planetary Science Letters* 560:116805

Halldórsson, S.A., Hilton, D.R., Marshall, E.W., **Ranta, E.**, Ingvason, A., Chakraborty, S., Gunnarsson-Robin, J., Rasmussen, M.B., Gibson, S.A., Ono, S., Scarsi, P., Abebe, T., Hopp, J., Barry, P.H., Castillo, P.R. (2022) Evidence from gas-rich ultramafic xenoliths for superplume-derived recycled volatiles in the East African sub-continental mantle. *Chemical Geology* 589:120682

Halldórsson, S.A. and 29 other authors (in review) Rapid source shifting of a deep magmatic system revealed by the Fagradalsfjall eruption, Iceland. Submitted to *Nature*

Table of Contents

List of Figures

List of Tables

All supplementary data tables are provided in digital format and can be accessed via the skemman.is portal along with an electronic version of this thesis.

Abbreviations

BABB – back-arc basin basalt

δ (‘delta’) – denotes the isotope ratio of a specified element in a sample relative to a standard, usually given in ‰ (‘per mil’).

Δ (‘capital delta’) – denotes either isotopic fractionation between two phases or mass independent isotope fractionation, usually given in ‰ (‘per mil’)

DMM – depleted MORB Mantle

EM – enriched mantle

EMW – enriched mantle wedge

Ga – billion years ago

ka – thousand years ago

KVK – Kverkfjöll volcanic system

LLSVP – large low-shear velocity province

Ma – million years ago

MAR – Mid-Atlantic Ridge

MI – melt inclusion

MORB – mid-ocean ridge basalt

NRZ – Northern Rift Zone

OIB – ocean island basalt

RP – Reykanes Peninsula

SIVZ – South Iceland Volcanic Zone

SNVZ – Snæfellsnes Volcanic Zone

ULVZ – Ultra low-velocity zone

WRZ – Western Rift Zone

ÖVB – Öræfajökull Volcanic Belt

Acknowledgements

Left foot forward and right foot back, goes the science waltz. I am lucky to be able to say that my first steps as a scientist—sideways, backward, forward—have been more of joy than of despair thanks to the enduring support from family, friends, supervisors, peers and scientists that I have been surrounded by during my four years and counting in Iceland.

I wish to thank my wonderful supervisor Sæmi. You handed me a study area that was so easy to fall in love with. During the years you taught me how to be a scientist, pushing, but gently, and giving enough, but not too much space. I am thankful to Andri, my second supervisor, for all the support during the years, and for being a formidable field, lab and science teacher in all things hydrothermal and beyond. I wish to also thank Pete Barry of my PhD committee for following the project from the first field trip to last minute revisions, for making the best noble gas analyses, and for being awesome.

For giving me the confidence to pursue the academic path I thank my BSc and MSc supervisors Gabrielle Stockmann and Thomas Wagner for their early and continuing support. I am very thankful to my many coauthors with whom I can feel that geology is best done together. I wish to especially thank Shuhei Ono for hosting me for several weeks at his breathtaking stable isotope lab at MIT. There are so many colleagues I would like to thank for sharing the years with me. Alberto Caracciolo, Andrea Ricci, Barbara Kleine, Daniel Ben-Yehoshua, Deirdre Clarke, Ed Marshall, Jóhann Gunnarsson Robin, Maarit Kalliokoski, Martin Voigt, Matylda Heřmanská, Nína Aradóttir, Ríkey Kjartansdóttir, Simon Matthews, Stefan Peters, Quinten van der Meer, Talfan Barnie and Wesley Farnsworth, for starters! Work is a pleasure when you are among friends.

Among many good companions in the field I would like to especially thank Arola Moreras Marti, Dave Byrne, Mike Broadley, who tagged along to Kverkfjöll in 2017; Kate Gallagher and Kalli Stefánsson, with whom I got to spend three unforgettable days up in Hveradalur, and nights waking up to the ice calving into the Gengissig lagoon; Ed, Margaret Hartley, Guðmundur Guðfinsson and Dan Colman who joined me in the search for the source of the Hveragil hot river (which remains hidden from us humans); Matt Jackson for following me to the Cliffs of Certain Death at Askja and still being my friend; Maja Bar Rasmussen, for doing most of these things, and also for driving Bjössi's jeeps to the far Highlands three times, and for being the best office mate one could have hoped for for four years.

Without funders, little science would get done. I thank NordVulk for entrusting me and this project funding for three years and the NordVulk captain Rikke Pedersen who somehow always makes your life easier. I also gratefully acknowledge funding from the University of Iceland Doctoral Fund for an additional year that made it possible to connect all (okay, some of) the loose threads.

My close family keeps lifting me up. I wish to thank: My parents Pihla and Aarne; you are my academic and actual life role models and have always been supportive of my endeavors (even when I dropped out of school to play in a metal band). My 7-year-old Neeme; you are the best volcanologist I know and my best friend. My other half, Pauliina; you always encourage me to do things you think are important to me, but the most important thing to me by far is to get to share a life with you. Lastly, thank you to the many people not mentioned—friends, relatives, colleagues. Your support and general kindness have been overwhelming.

1 Introduction

The *raison d'être* of igneous geochemistry—study of the chemistry of volcanic materials—is that the chemical makeup of lavas and volcanic gases provide first-hand information about the inner workings of volcanoes as well as the Earth's interior that is otherwise unattainable. A critical way to study the mantle—the rocky layer between the crust and the core that makes up about 84% of the Earth's volume—is to study the composition of basalts that are formed through partial melting of the mantle (Fig. 1.1, Green and Ringwood 1967, Hofmann 1997). However, to reach the surface, basaltic melts must travel through the crust, which in Iceland is between 15 and 40 km thick. During the crustal passage, basaltic melts may dwell for long periods in crustal magma storage zones, where they experience a range of magmatic processes that include assimilation of crustal materials, fractional crystallization, melt mixing and degassing (Fig. 1.1). All of these processes change the primary, mantle-derived chemical makeup of basaltic melts. On one hand, these secondary chemical fingerprints can be used to glean information about magmatic processes that take place in the crust. On the other hand, the crustal magmatic processing obfuscates the basaltic window into the mantle and needs to be unraveled to deduce the mantle signal.

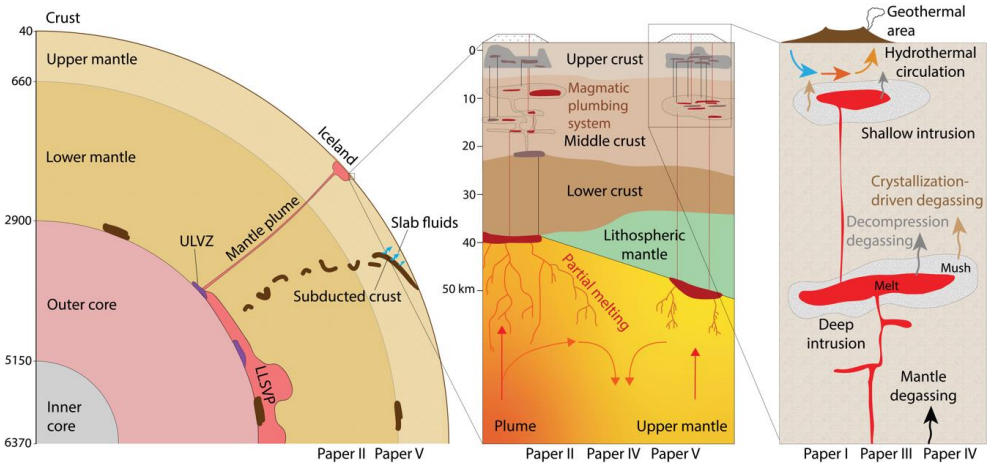

Figure 1.1 Cartoons of Earth's layers (left), drawn approximately to scale, the lithosphere (center) and middle-upper crust underlaying Iceland (right). The research questions that can be addressed by the study of igneous volatiles encompass planetary, lithospheric and upper crustal (and smaller) scales. The five thesis papers are marked below the panels that most closely correspond to their research questions

Lithophile (rock-loving) elements experience, and therefore keep track of many important events experienced by magmas. Although volatile elements—elements such as H, He, B, C, N, S and Cl, that preferably form gaseous or aqueous molecules at the Earth's surface—are only present in minor or trace amounts in most igneous rocks, they play an outsize role

as the drivers of eruptions, and as the elements that form the atmosphere and sustain life (Rollinson 2009). Volatiles in basalts keep a record of shallow and deep Earth processes that is complementary to the lithophiles. Despite their potential to address a wide spectrum of key Earth Science problems, the use of volatile elements and their stable isotopes in igneous geochemistry has been limited due to analytical challenges (White 2015). Recently, improvements in analytical capabilities have made the volatile element archive in volcanic materials more accessible, forming the impetus for this thesis.

1.1 Aims

In this thesis, magmatic processes and mantle geochemistry are explored through the lense of volatile elements and their isotopic compositions (δD, $^{3}He/^{4}He$, $\delta^{11}B$, $\delta^{13}C$, $\Delta^{33}S$-$\delta^{34}S$, $\delta^{37}Cl$). The sample material comprises igneous rocks (focusing on basalts and rhyolites) and thermal fluids (fumarole gases and hot spring waters) collected from active volcanoes in Iceland.

The three principal aims of the PhD project are to:

- Build up a better understanding of crustal magmatic process from the point-of-view of magmatic volatiles in volcanic materials.
- Investigate deep Earth volatile cycles and the mantle beneath Iceland, by using volatile isotope systematics of lavas and hydrothermal fluids.
- Conduct the first petrological and geochemical survey of the Kverkfjöll volcanic system in Iceland, including both its magma suite and its geothermal area.

1.2 Mantle geochemistry

Because the mantle is inaccessible for direct observation, its composition and structure must be studied by indirect means. The most comprehensive source of information about the composition of the mantle come from studies of mid-ocean ridge and ocean island basalts (MORBs and OIBs, respectively). A striking feature of MORBs is their relatively uniform chemical composition across the global mid-ocean ridge system (Gale et al. 2013) – by far the largest volcanic manifestation on Earth, transecting 60,000 km of the planet's surface. This suggests that the upper mantle (extending to a depth of ~670 km) that melts to form MORBs must have a rather *homogeneous* composition (Engel et al. 1965, Langmuir et al. 1992). Nevertheless, notable geochemical *heterogeneity* in MORB exists at both global (Dupre and Allegre 1983) and local scales (Goldstein et al. 2008, Shimizu et al. 2016). These heterogeneities can only partially be explained by melting processes, instead suggesting that the upper mantle is spotted with so called recycled components—derivatives of continental and oceanic crustal materials that have been introduced to the mantle by subduction or delamination (Plank and Langmuir 1998, Dixon et al. 2017, Richter et al. 2020, Yang et al. 2021).

Nevertheless, the relatively subtle heterogeneity present in MORBs pales in comparison to the wide variety of chemical signatures present in anomalous volcanism on the ocean floor, that is found in basaltic seamounts, oceanic plateaus and ocean islands (Kurz et al. 1982, White and Hofmann 1982, Hofmann 1997, 2003). Some ocean islands or archipelagos, such as Iceland, Hawaii, Galapagos and Samoa, likely owe their existence to

deep-rooted mantle plumes (Jackson et al. 2017), which can be traced via seismic tomography all the way to the core-mantle boundary at a depth of ~2900 km (Fig. 1.1a; Montelli et al. 2006, French and Romanowicz 2015). By extension, the large chemical variability displayed by OIBs suggests that considerable chemical *heterogeneity* prevails in the lower mantle. The chemical difference between MORBs and OIBs must reflect planetary scale, long-term evolution of the mantle. Therefore, the geochemistry of OIBs can shed light on the ancient history of Earth and its deep structure (Koppers et al. 2021).

Among the principal goals of mantle geochemistry is to answer questions such as: *What different domains exist in the mantle? What is their origin? How are they related to the evolution of the Earth?* Extensive geochemical studies of OIBs through the last half century have led to the discovery of about half a dozen "animals" in the "mantle zoo", that is, distinct mantle components with characteristic compositions and *radiogenic* isotope signatures (Zindler and Hart 1986, Hofmann 1997, Stracke et al. 2005). The depleted MORB mantle (DMM) has been depleted in incompatible elements because partial melts of the upper mantle have, through time, formed the Earth's crust (Workman and Hart 2005). Enriched mantle components (EM1 and EM2)—so called because they have elevated concentrations of incompatible trace elements as well as radiogenic isotope signatures indicative of long-term incompatible trace element enrichment—demonstrate the return of crustal components that were subducted into the mantle (Zindler and Hart 1986, Hart 1988, Jackson et al. 2007, Cabral et al. 2013). The "high-^{3}He/^{4}He" mantle is marked by high relative abundance of the primordial ^{3}He isotope originating from the Earth's accretion from a proto-solar disc, which shows that relatively undegassed and primordial domains remain in the planet's interior (Moreira 2013).

All hotspots with EM-type characteristics appear to be situated above large, continent-sized regions at the core-mantle boundary that attenuate seismic waves, known as large low shear velocity provinces (LLSVPs; Fig. 1.1; Jackson et al. 2018). The correlation between EM hotspots and LLSVPs suggests that these may be global storage regions for recycled materials (Jackson et al. 2018, 2021). The link between LLSVPs and the high-^{3}He/^{4}He mantle is less certain (Jackson et al. 2021), although at least Hawaiian, Samoan and Icelandic plumes appear to be rooted at Ultra Low Velocity Zones (ULVZ) associated with LLSVPs (Fig. 1.1; Yuan and Romanowicz 2017, Williams et al. 2019).

High-^{3}He/^{4}He basalts in Iceland show excesses of ^{129}Xe and deficits of ^{182}W—decay products of the now-extinct short-lived radiogenic isotopes ^{129}I and ^{182}Hf, respectively—relative to the DMM. These anomalies indicate that the Iceland plume samples an ancient mantle reservoir that formed >4.45 billion years ago (Mukhopadhyay 2012, Mundl-Petermeier et al. 2019, Williams et al. 2019), which is older than any preserved terrestrial rock on the surface, even predating the moon-forming impact. Icelandic basalts additionally show DMM- and EM-like chemical signatures (Hanan et al. 2000, Peate et al. 2010), with the distribution of mantle components varying spatially across Iceland (Kokfelt et al. 2006, Peate et al. 2010, Hardardóttir et al. 2018, Rasmussen et al. 2020). Thus, Iceland offers a unique setting for investigating both the deep and shallow mantle as well as the early planetary evolution. These themes are explored in Papers II, IV and V.

1.3 Icelandic volcanism

The Iceland Plateau sits on the mid-Atlantic ridge—on the plate boundary between the North American and Eurasian plates—but marks a region of unusually voluminous magmatism that has generated a large ocean island. The reason for its abundant volcanism

is the coexistence of two fundamental planetary scale forces: plate spreading and a mantle upwelling, or mantle plume, that brings hot material from the lower mantle toward the surface (Morgan 1971). Acting together, this plume-ridge interaction results in excessive melting of the mantle and one of Earth's most volcanically active regions. The Iceland plume is considered to be the modern-day manifestation of a long-lived mantle plume that first impinged the Earth's crust approximately 62 Ma, giving rise to the flood basalts of the North Atlantic Igneous Province that are today found on both sides of the North Atlantic, from West Greenland to the Scottish Isles (Saunders et al. 1997).

Today, about 30 active volcanic systems are distributed across three rift segments that mark the subaerial plate boundary, as well as three off-rift volcanic zones (Fig. 1.2). These span almost all forms of terrestrial volcanism, as well as lava compositions ranging from basalts to rhyolites, offering a smorgasbord of research opportunities for geoscientists.

Accordingly, studies of Icelandic volcanoes have long played a central role in the fields of volcanology (Walker 1963, 1983, Thorarinsson et al. 1964, Thordarson and Self 1993), petrology (Carmichael 1964, Sigurdsson and Sparks 1981, Óskarsson et al. 1982, Maclennan 2008), mantle geochemistry (Schilling 1973, Condomines et al. 1983, Jackson et al. 2020) and hydrothermal geochemistry (Arnórsson 1970, Sano et al. 1985, Poreda et al. 1992, Barry et al. 2014, Stefánsson et al. 2017, Bali et al. 2020). As the field advances and new analytical methods emerge, Iceland remains an important global testing ground for new ideas.

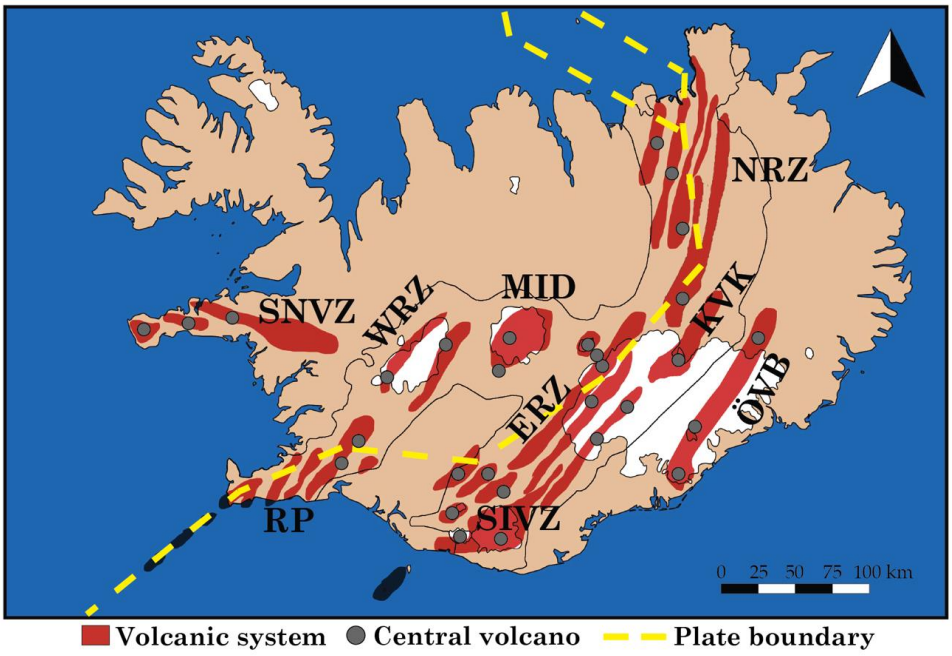

Figure 1.2 Volcanic zones of Iceland. ERZ: Eastern Rift Zone. KVK: Kverkfjöll volcanic system. MID: Mid-Iceland volcanic belt. NRZ: Northern Rift Zone. RP: Reykjanes Peninsula. SNVZ: Snæfellsnes Volcanic Zone. SIVZ: South Iceland Volcanic Zone. WRZ: Western Rift Zone. ÖVB: Öræfajökull Volcanic Belt.

1.4 The Kverkfjöll volcanic system

Special attention in this thesis is given to the Kverkfjöll volcanic system in the central highlands of Iceland (Figs. 1.3 and 1.4). Kverkfjöll's central volcano and the connected fissure swarm make up one of Iceland's ~30 active volcanic systems. Kverkfjöll is situated at an unusual structural position in between the main rift axis of the Northern Rift Zone and the off-rift Öræfajökull Volcanic Belt (ÖVB). The subaerial part of the fissure swarm is defined by Pleistocene eruptive fissures that have formed subglacially erupted pillow basalt and hyaloclastite ridges and post-glacial scoria cones and lava flows, of which the latest, Lindahraun, was erupted approximately 700 CE. The central stratovolcano—Iceland's third tallest mountain (1934 m.a.s.l.)—is situated at the margin of the Vatnajökull ice cap and hosts two, ice filled calderas (Fig. 1.3). The Hveradalur geothermal area is located at an altitude of 1500-1700 m.a.s.l. on the eastern rim of the NE caldera (Fig. 1.4a)—higher than any other Icelandic geothermal area—and is one of Iceland's most active high temperature geothermal areas (Oddsson 2016).

Although limited geochemical data from Kverkfjöll are available (e.g, Sigvaldason et al. 1974, Sigvaldason and Óskarsson 1976), a comprehensive petrological and geochemical characterization of the system is missing from the published literature. The existing data suggests that the Kverkfjöll basalts are some of the most chlorine- (Sigvaldason and Óskarsson 1976, 1986) and water-rich (Nichols et al. 2002, Höskuldsson et al. 2006) in Iceland, but the origin of this apparent volatile-enrichment remains unclear. Similarly, the geochemistry of the hydrothermal fluids at Kverkfjöll had only been explored in a reconnaissance study (Ólafsson et al. 2000), leaving open questions about the hydrogeology and volatile origin of the system. Because of these knowledge gaps, Kverkfjöll was chosen as the main study area for this PhD project. The geochemistry of the Kverkfjöll hydrothermal fluids and its magma suite is explored in Papers IV and V

1.5 Volcanic hydrothermal systems

Heating up surrounding groundwater is a way for a shallow magmatic intrusion to cool itself (Fig. 1.1). The result is a volcanic geothermal system, an underground convection cell that works as an interface between a magmatic intrusion and the atmosphere. The heated steam and water manifest at the surface as fumaroles and hot springs, that can be sampled to gain information about the subsurface system and the magmatic source itself.

Iceland has ~33 high-temperature geothermal systems, defined by temperatures above 200°C below a depth of 1 km (Arnórsson et al. 2008). Some of these have been harnessed to provide heat and to produce electricity, but many remote systems, such as those at the Askja and Kverkfjöll volcanic systems, remain in their natural state.

In this thesis, focus is given to the role of volcanic hydrothermal systems as conduits of magmatic volatiles degassing from magmatic intrusions. The channeling of mantle-derived volatiles via volcanic hydrothermal systems plays a potentially important, but poorly constrained role in global volatile cycles (Taran 2009, Stefánsson et al. 2016). Hydrothermal fluids from the Askja and Kverkfjöll volcanoes were studied in this thesis to better quantify the magmatic volatile input into Icelandic hydrothermal fluids.

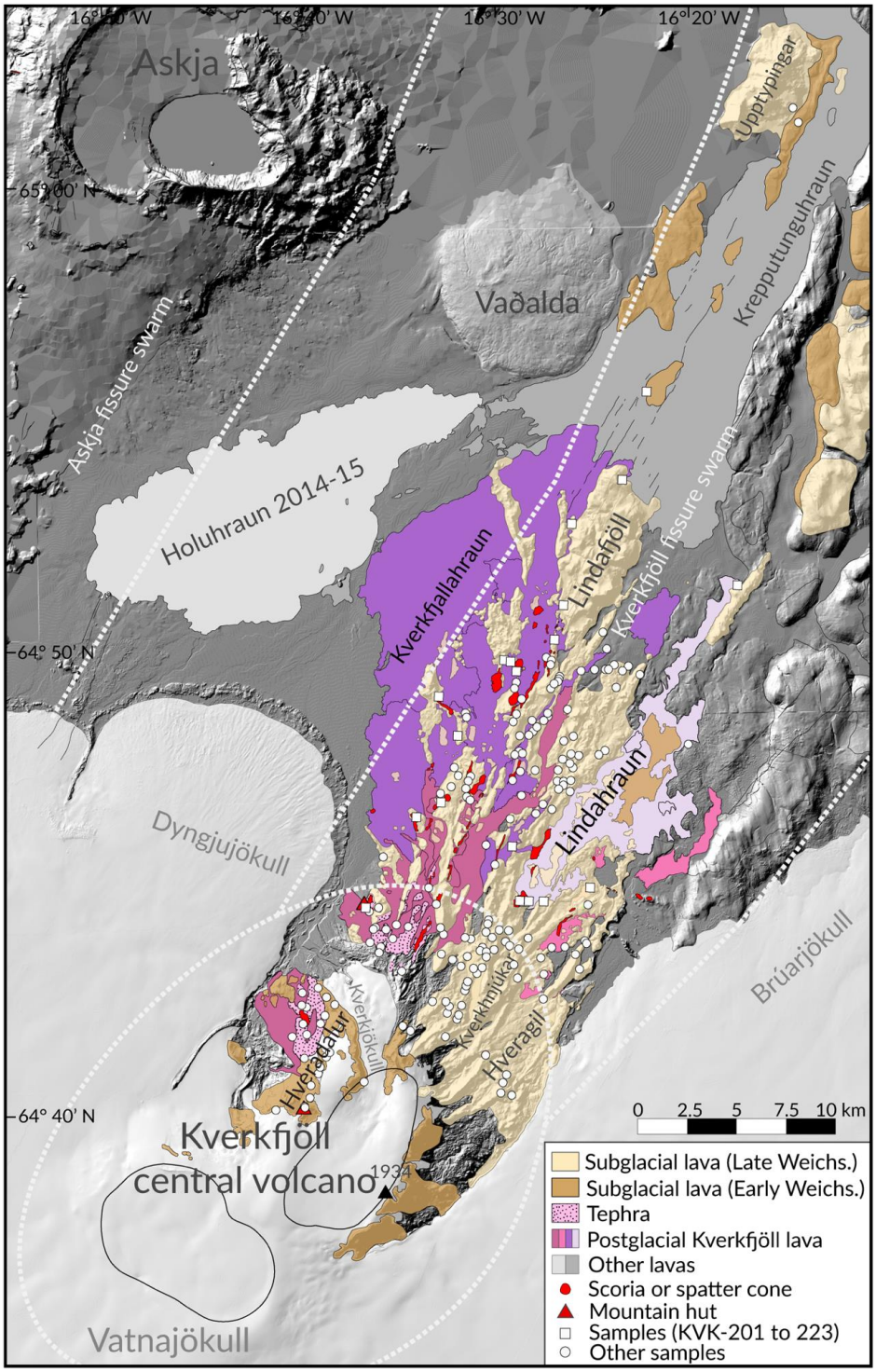
16° 40' W
16° 30' W
16° 20' W
65° 00' N
64° 50' N
64° 40' N
Askja
Vaðalda
Upptypningar
Krepputunguhraun
Askja fissure swarm
Holuhraun 2014-15
Kverkfjallahraun
Lindafjöll
Kverkfjöll fissure swarm
Lindahraun
Dyngjujökull
Brúarjökull
Kverkhnjúkar
Hveragil
Kverkjökull
Hveradalur
Kverkfjöll
central volcano
1934
Vatnajökull
0 2.5 5 7.5 10 km
Subglacial lava (Late Weichs.)
Subglacial lava (Early Weichs.)
Tephra
Postglacial Kverkfjöll lava
Other lavas
Scoria or spatter cone
Mountain hut
Samples (KVK-201 to 223)
Other samples

Figure 1.3 (previous page) Geological map of Kverkfjöll. Locations of rock samples used in this study are shown. Dashed white lines indicate the approximate limits of the Askja and Kverkfjöll fissure swarms and the Kverkfjöll central volcano (after Hjartardóttir and Einarsson 2012). Outlines and distinctions of the geological units are based on the map of Sigurgeirsson et al. (2015). Background digital elevation model is from the National Land Survey of Iceland.

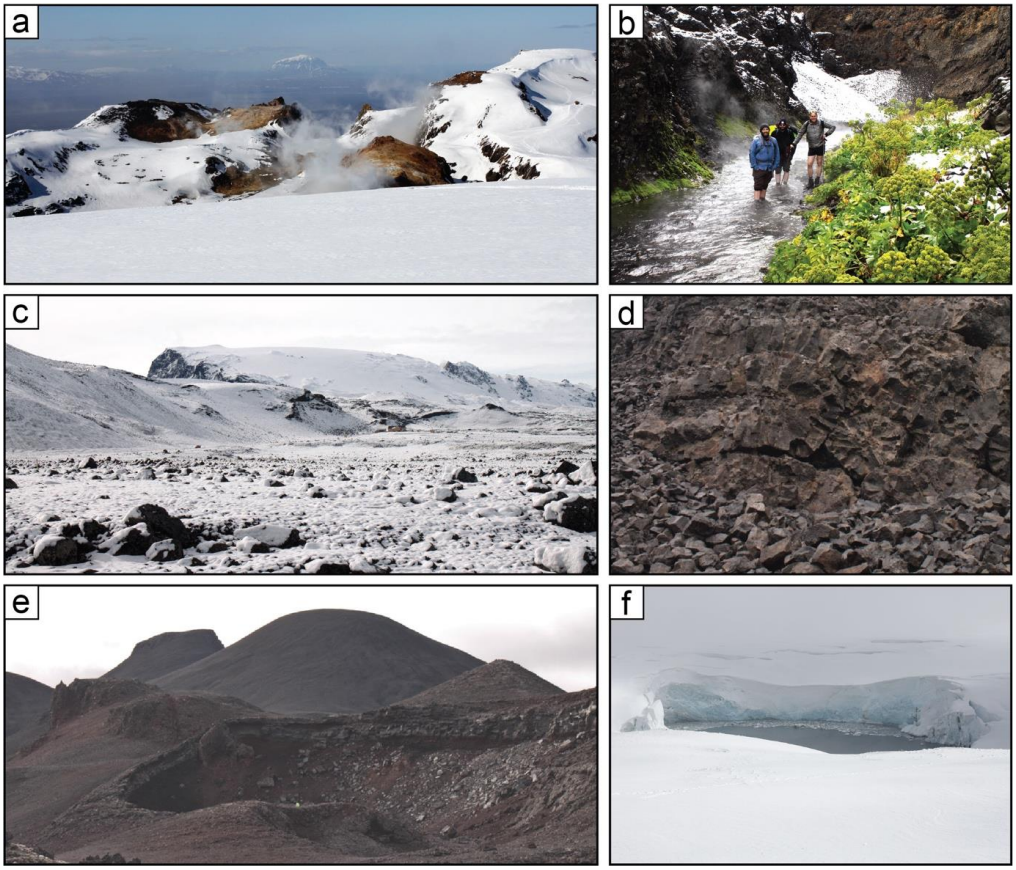

Figure 1.4 Field pictures. (a) View from Vatnajökull, looking N over the Hveradalur geothermal area of Kverkfjöll. Askja and Mt. Herðubreið visible in upper left and center, respectively. (b) Lower Hveragil river on the eastern flank of Kverkfjöll. The hot (30-60 °C) and mildly alkaline (pH up to 9) thermal river supports a population of angelica in the middle of the barren highlands. (c) Western side of Kverkfjöll mountain seen from north. The Sigurðarskáli mountain hut in right center. Steam from Hveradalur geothermal area is visible. (d) Characteristically large subglacial pillow basalts (up to 2 m diameter) from a pillow ridge in the Kverkfjöll fissure swarm. (e) One of the Lindahraun craters from ~700 CE, the latest known Kverkfjöll eruption. A barely visible, yellow-vested geoscientist for scale. (f) The geothermally heated, 0.5 km wide glacial lagoon Gengissig in Kverkfjöll (1600 m.a.s.l).

1.6 Volatiles as an archive of information on volcanic processes and planetary evolution

Because of their chemical nature, volatiles are subject to a range of geological processes not experienced by non-volatile elements. For example, exsolution of volatiles from magmas and associated bubble formation and expansion drives eruptions. Over geological timescales, magmatic degassing regulates the composition of the atmosphere. In crustal magmatic storage zones, magmatic volatile phases co-exist and interact with melts in ways that are not fully understood, but that could be important for influencing eruptibility of magmas (Edmonds and Woods 2018) and in redistribution and concentration of metals, such as copper, to form certain types of ore deposits (Blundy et al. 2015; this theme is expanded on in Paper I). Determining the distribution of water and carbon in the mantle is important in a further sense, because it influences mantle dynamics by lowering the melting temperature of mantle rocks (e.g., Peslier 2017). Indeed, the anomalously high magma production beneath Iceland may be partly attributed to an elevated H_2O content of the underlying mantle plume (Nichols et al. 2002). The study of volatiles in volcanic materials also takes a center stage in addressing fundamental geological problems related to the early differentiation and accretion history of the Earth and the origin of its water and other volatiles (Marty 2020), and the subsequent evolution of the mantle (Bekaert et al. 2021).

A key way to study volatiles in geological media is to study isotopes—elements with same number of protons but different number of neutrons in their nuclei. Ratios of stable isotopes (e.g., $^{2}H/^{1}H$, $^{13}C/^{12}C$, $^{33}S/^{32}S$, $^{34}S/^{32}S$ or $^{37}Cl/^{35}Cl$) remain unchanged if "left standing" but change during chemical reactions (like oxidation or reduction), phase changes (such as evaporation or melting) and physical processes (like diffusion of an element across a chemical or thermal gradient) mainly because of the different masses of the isotopes. Therefore, an isotope ratio of an element holds the memory of both the original ratio of an element and the processes that it has experienced.

For example, upon ascent of a basaltic melt, decompression leads to the exsolution of CO_2(gas) formed from CO_3^{2-}, the main dissolved carbon species in a basaltic melt. The carbon in the gas becomes enriched in the heavier isotope ($^{13}C/^{12}C$ increases). Conversely, C remaining in the melt will become "depleted" in the heavier isotope ($^{13}C/^{12}C$ decreases). By determining the $^{13}C/^{12}C$ of the CO_2 in fumarole gases or fluid inclusions of igneous minerals, it is possible to evaluate whether it has a magmatic origin and how deep the source melt is situated (Boudoire et al. 2018; Paper IV). Isotopic fractionations are largest at low temperatures at the Earth's surface (< 100 °C), but typically insignificantly small at the high temperatures prevailing in the Earth's mantle or in basaltic magmas (> 1000 °C). Thus, subducted crustal materials, that have been subjected to low-T surface processes, introduce characteristic isotopic signals into the mantle which can be recognized if these are incorporated into MORBs or OIBs.

Constraining the volatile element abundances and isotopic signatures in OIBs and their mantle sources is crucial to gain a better understanding of global volatile cycles, and thereby the evolution of the atmosphere, crust and mantle over geological time. Recent studies on volatile stable isotopes in OIBs show large heterogeneity for boron (Walowski et al. 2021, Marshall et al. 2022), nitrogen (Halldórsson et al. 2016b), sulfur (Cabral et al. 2014, Delavault et al. 2016, Dottin et al. 2020a, b) and chlorine (John et al. 2010, Halldórsson et al. 2016a). However, key pieces of data from important global endmembers like Iceland are missing.

Figure 1.3 Methods (a) Sampling fumarole gas into duplicate copper tubes for noble gas analysis. Víti, Askja. (b) Sulfur extraction setup at IES. (c) Electron probe microanalyzer at the Institute of Earth Sciences. (d) A fumarole sample in a two-port "Giggenbach" bottle hooked into the inlet system of a gas chromatograph at IES. (e) View of an olivine crystal from Kverkfjöll with four visible melt inclusions. The exposed melt inclusion has a vapor or shrinkage bubble. (f) Glass shards from subglacial pillow basalt rims, crushed, cleaned and sieved preparation for δD analysis. (g) Fourier-transform infrared spectrometer used for analysis of H_2O-CO_2 contents in glass and melt inclusions, IES. (h) Fumarole gas H_2S precipitated has ZnS in preparation for S extractions. (i) The custom-built fluorination and purification inlet system for multiple sulfur isotope analysis at MIT, USA (j) A thin section image of a subglacial pillow basalt with crystalline interior (dark), glassy rim (bottle brown), and travertine layers (white-beige) precipitated from the Hveragil thermal river, Kverkfjöll.

A common limiting factor in mantle volatile studies is the poor availability of undegassed samples that retain their primary volatile content. Lavas erupted to the surface are typically highly degassed, as most H_2O, CO_2 and S present in deep melts is lost through decompression degassing when melts ascend toward the surface (e.g., Dixon et al. 1995). A key advantage utilized in this study is the wide availability of subglacially erupted basalts in Iceland (Fig. 1.4d).

These were erupted under high enough pressure—below up to 2 km thick ice sheets during Pleistocene glacial periods—to retain much of their pre-eruptive volatile content. Specifically, the rapidly quenched glassy rims of subglacial pillow basalts (Fig. 1.5f), abundant in Iceland, provide a highly suitable material for both petrological (Paper IV) and volatile isotope studies in this thesis (Papers II, V).

Furthermore, access to active volcanic hydrothermal systems in Iceland makes it possible to, in theory, capture the volatiles that degas from magmatic intrusions *ex situ*. This complementary record of magmatic volcatiles can be used to reconstruct a more complete record of the fluxes of deep volatiles to the crust and the atmosphere (Paper III).

1.7 Samples and analytical methods

1.7.1 Samples

For Paper I, rock samples from the collections of the Icelandic Institute of Natural History were made available by Kristján Jónasson. Rock and glass samples analyzed for Paper II originate largely from a regional collection of subglacial glasses at the Institute of Earth Sciences, University of Iceland.

Lava, scoria and subglacial pillow basalt samples (n = 23) from the Kverkfjöll area were collected in 2017 (Fig. 1.4) and form the basis for Papers IV and V. Paper IV additionally benefits from a set of ~200 rock samples collected during multiple previous sampling campaigns conducted between the 1970's and 1990's under the auspices of the Nordic Volcanological Center (formerly, Nordic Volcanological Institute).

Thermal fluids (fumarole gases and hot spring waters) and non-thermal waters from Askja and Kverkfjöll (n = 37) were sampled during four field trips in the summers of 2017-2019 (Fig. 3). Fumarole discharges were collected into evacuated two-port glass bulbs (Giggenbach flasks) through a basic (KOH) solution used to trap CO_2 and H_2S (Fig. 1.5d). Additionally, fumarole vapors were sampled to copper tubes for noble gas analysis (Fig. 1.5a), and to flow-through flasks for $\delta^{13}C$ analysis. Water samples were pumped through a filter to sample-washed polypropylene bottles.

1.7.2 Analytical methods

The work in this thesis relies on a broad palette of analytical techniques used to determine elemental abundances and isotope ratios in rock, gas and water samples. A more thorough description of each individual method is provided in the relevant thesis chapters. The following techniques were used:

- Electron probe microanalysis (EPMA; Fig. 1.5c), used for determining concentrations of ~10 major and minor elements in minerals and glasses, as well as S and Cl concentrations in glasses and melt inclusions (down to ~50 ppm level).
- Inductively coupled plasma optical emission spectroscopy (ICP-OES), used for major and minor element concentrations in water samples.
- Gas chromatography (GC; Fig. 1.5d), used for analysis of gas species in fumarole gases.
- Laser ablation inductively coupled plasma mass spectrometry (LA-ICP-MS), for *in situ* analysis of ~40 trace elements in glasses (down to ~10 ppb level).
- Solution ICP-MS, used for analysis of trace elements in water samples.

- Fourier-transform infrared spectroscopy (FTIR; Fig. 1.5g) was used for determining H_2O and CO_2 concentrations in glasses and melt inclusions.
- Multi-collector ICP-MS, used for measuring isotope ratios of lead.
- Isotope ratio mass spectrometry (IRMS; Fig. 1.5i), for determining isotope ratios of H, C, O, S and Cl in water, gas and rock samples.
- Titrations, for determining CO_2 and S concentrations in waters and gases
- Dissolution and ion chromatography, to isolate Pb from rocks for isotope analysis
- Extraction and purification of S from solid, gas and water samples for isotope analysis (Figs. 1.5b,h).

1.8 Summary of papers

1.8.1 Paper I

Ranta, E., Halldórsson, S.A., Barnes, J.D., Jónasson, K., Stefánsson, A. (2021) Chlorine isotope ratios record magmatic brine assimilation during rhyolite genesis. *Geochemical Perspectives Letters*, 15, 35-39

Chlorine-rich magmatic fluids are closely linked to the late-stage evolution of silicic intrusions and play a major part during the formation of critical ore deposits. However, how these saline fluids, or brines, interact with melts and affect active volcanic processes in crustal silicic magma mushes is poorly known. In particular, very limited prior data on the chlorine isotopic compositions of silicic rocks (i.e., rhyolites or dacites) exist in the published literature (Barnes et al. 2014). The aim of this study was to bridge this knowledge gap by acquiring chlorine isotope data for silicic and intermediate volcanic rocks from a total of 8 volcanic systems in Iceland. Importantly, the $\delta^{37}Cl$ systematics of basaltic rocks from the same volcanic systems had been well established by a previous study (Halldórsson et al. 2016a), providing an anchor point for interpreting the new data.

A new and unexpected result of the study is that silicic rocks (rhyolites and dacites) are systematically shifted to more negative $\delta^{37}Cl$ values compared to corresponding basalts and intermediate rocks. The magnitude of these shifts (up to –2.9‰) is too large to be explained by conventional magmatic or volcanic processes like fractional crystallization or degassing. Instead, it is suggested that the cause for the large negative $\delta^{37}Cl$ shifts is assimilation of magmatic brines, that have been formed by previous generations of intrusions in long-lived magmatic mush systems. Based on recent theoretical, experimental and empirical findings, it is shown that magmatic brines may acquire highly negative $\delta^{37}Cl$ values. This mechanism by which silicic melts interact with brines is a new concept that needs to be added to the emerging view of the silicic magma mush. We propose that assimilation of magmatic brines is likely to be a common process accompanying rhyolite genesis.

1.8.2 Paper II

Ranta, E., Gunnarsson-Robin, J., Halldórsson, S.A., Ono, S., Izon, G., Jackson, M.G., Reekie, C.D.J., Jenner, F.E., Guðfinnsson, G.H., Jónsson, O.P., Stefánsson, A. (in review) Ancient and recycled sulfur sampled by the Iceland mantle plume. Submitted to *Earth and Planetary Science Letters*

This study presents quadruple sulfur isotopic compositions as well as S concentration, major and trace element data of 59 subglacial glasses from active volcanic zones in Iceland. The aim of the study was to investigate the behavior of sulfur during crustal magma evolution and the S isotopic signatures of Icelandic mantle components. The data record both mantle source signatures as well as the fractionation of immiscible sulfide liquids from Icelandic melts below ~6 wt.% MgO, which is shown to have a subtle, but measurable effect on $\delta^{34}S$. Many Icelandic basalts record small shifts toward negative $\Delta^{33}S$ signatures (down to -0.050 ‰) and lower $\delta^{34}S$ (down to -2.5 ‰) relative to MORBs. These signatures are interpreted to signal involvement of a subduction fluid-enriched component in the Iceland mantle. However, samples with high $^{3}He/^{4}He$ and negative $\mu^{182}W$—sampling primordial plume-derived material—describe a trend toward chondritic $\Delta^{33}S$ and $\delta^{34}S$ values of ~0 ‰, and are distinct from the depleted upper mantle that has a sub-chondritic $\delta^{34}S$ signature of -1.3 ‰. These results illuminate the diverse origins of volatiles in the Iceland mantle, and provide new constraints on the formation of the primordial high-$^{3}He/^{4}He$ reservoir.

1.8.3 Paper III

Ranta, E., Stefánsson, A., Gunnarsson-Robin, J., Barry, P., Ono, S., Kleine, B., Ricci, A., Fiebig, J., Kjartansdóttir, R., Halldórsson, S.A. (in prep.) Deep and shallow magma degassing and volatile fluxes through volcanic hydrothermal systems – insights from the Askja and Kverkfjöll volcanoes, Iceland. In preparation for *Geochmica et Cosmochimica Acta*, or similar

Determining the origin of each volatile species present in hydrothermal fluids is a central objective of geothermal research. It is well established that volatiles in geothermal fluids can be sourced from meteoric water, seawater, crustal brines, degassing of shallow- or deep-seated magmas reservoirs. However, the contribution of magmatic volatiles into hydrothermal fluids is not well constrained. This is because on their path from a reservoir to the surface, primary volatile signatures of hydrothermal fluids are perturbed by secondary processes such as boiling, mixing, redox reactions and fluid-rock interaction. In this project, we aim to unravel this complexity using modelling and a concentrated dataset on volatile concentrations (H_2O, H_2S, SO_2, H_2, N_2, Ar, He, Cl, B, CO_2), stable isotopes (δD, $\delta^{13}C$, $\delta^{18}O$, $\delta^{33,34,36}S$) and ratios of $^{3}He/^{4}He$ in gas and water samples from the geothermal systems of the Askja and Kverkfjöll volcanoes. Importantly, a complementary volatile dataset on the host rocks is available from the Kverkjöll rocks (Paper 5), constraining a crucial model end-member. Together, the combined information enables us to identify and quantify the magmatic component in the hydrothermal fluids, which makes it possible to constrain deep and shallow volatile fluxes from magmatic intrusions that are channeled via volcanic hydrothermal systems to the atmosphere. The approach developed here can be adapted in similar studies of other geothermal systems in the future.

1.8.4 Paper IV

Ranta, E., Halldórsson, S.A., Nykänen, V., Kaikkonen, R., Guðfinnsson, G.H., Barry, P.H., O'Brien, H., Rasmussen, M.B., Gunnarsson-Robin, J., Marshall, E.W., Stefánsson, A., Bali, E., Jackson, M.G., Grönvold, K. (in prep.) Geochemistry of basalts of the Kverkfjöll volcanic system, Iceland: Bridging the gap between rift and off-rift magmatism. In preparation for *Journal of Petrology*, or similar

This chapter presents the first comprehensive geochemical dataset from the magma suite of the Kverkfjöll volcanic system in central Iceland. The dataset comprises major element data from subglacial glasses, scoria, whole rocks and melt inclusions and minerals, as well as trace element and He-Ne-Ar-O-Pb isotope data from select subglacial glasses. The results highlight some unusual characteristics of the Kverkfjöll magmas, such as their narrow compositional range (80% of the samples have 4-5 wt.% MgO) and a tendency for eruptions to occur close to a nominal melt density maximum. Further, a geochemical comparison between Kverkfjöll and its nearest neighboring volcanic zones highlights the primary role of the lithospheric lid in controlling the degree of mantle melting in Iceland. It is further shown that Kverkfjöll basalts sample a ^{208}Pb-enriched (high Δ^{208}Pb) mantle component with MORB-like ^{3}He/^{4}He of ~8.5 R_A. This EM2-flavored component appears to be only sampled by volcanoes located to the east of the Northern Rift Zone, revealing an asymmetric distribution of enriched components in the Iceland mantle.

1.8.5 Paper V

Ranta, E., Halldórsson, S.A., Barnes, J.D., Matthews, S., Kleine, B.I., Marshall, E.W., Jackson, M.G., Bali, E., Barry, P.H., Stefánsson, A., Guðfinnsson, G.H., Grönvold, K. (in prep.) A whiff of subduction fluids in the Iceland mantle. In preparation for *Earth and Planetary Science Letters*, or similar

To further investigate the origin of the Kverkfjöll mantle source, this paper focuses on the volatile elemental abundances (H_2O, CO_2, Cl, S) in subglacial glasses and melt inclusions, as well as the hydrogen and chlorine isotope composition (δD and δ^{37}Cl) of subglacial pillow glasses. The volatile signature of the Kverkfjöll basalts—elevated Cl/K coupled to high δD (up to -50 ‰), a seawater-like δ^{37}Cl signature, and previously reported high δ^{11}B, low δ^{34}S and a MORB-like ^{3}He/^{4}He—is clearly distinct from both the depleted North Atlantic mantle and the Icelandic high ^{3}He/^{4}He plume component, instead resembling back-arc basins basalts. We ascribe this similarity to the presence a subduction fluid enriched mantle wedge (EMW) type component in the Iceland mantle. These findings align with previously observed CO_2, H_2O and D enrichments in North Atlantic and Arctic mid-ocean ridge basalts, suggesting that the EMW component is not necessarily carried from the lower mantle by the Iceland plume, but rather, may be a North Atlantic mantle anomaly inherited from Phanerozoic subduction events.

References

Arnórsson, S. (1970). Underground temperatures in hydrothermal areas in Iceland as deduced from the silica content of the thermal water. *Geothermics*, *2*, 536-541.

Arnórsson, S., Axelsson, G., & Sæmundsson, K. (2008). Geothermal systems in Iceland. *Jökull*, *58*, 269-302.

Bali, E., Aradi, L. E., Zierenberg, R., Diamond, L. W., Pettke, T., Szabó, Á., Gudfinnsson, G.H., Fridleifsson, G.Ó., & Szabó, C. (2020). Geothermal energy and ore-forming potential of 600° C mid-ocean-ridge hydrothermal fluids. *Geology*, *48*(12), 1221-1225.

Barnes, J. D., Prather, T. J., Cisneros, M., Befus, K., Gardner, J. E., & Larson, T. E. (2014). Stable chlorine isotope behavior during volcanic degassing of H_2O and CO_2 at Mono Craters, CA. *Bulletin of Volcanology*, *76*(3), 1-13.

Barry, P. H., Hilton, D. R., Füri, E., Halldórsson, S. A., & Grönvold, K. (2014). Carbon isotope and abundance systematics of Icelandic geothermal gases, fluids and subglacial basalts with implications for mantle plume-related CO2 fluxes. *Geochimica et Cosmochimica Acta*, *134*, 74-99.

Bekaert, D. V., Turner, S. J., Broadley, M. W., Barnes, J. D., Halldórsson, S. A., Labidi, J., Wade, J., Walowski, K.J., & Barry, P. H. (2021). Subduction-driven volatile recycling: a global mass balance. *Annual Review of Earth and Planetary Sciences*, *49*, 37-70.

Blundy, J., Mavrogenes, J., Tattitch, B., Sparks, S., & Gilmer, A. (2015). Generation of porphyry copper deposits by gas–brine reaction in volcanic arcs. *Nature Geoscience*, *8*(3), 235-240.

Boudoire, G., Rizzo, A. L., Di Muro, A., Grassa, F., & Liuzzo, M. (2018). Extensive CO_2 degassing in the upper mantle beneath oceanic basaltic volcanoes: First insights from Piton de la Fournaise volcano (La Réunion Island). *Geochimica et Cosmochimica Acta*, *235*, 376-401.

Cabral, R. A., Jackson, M. G., Rose-Koga, E. F., Koga, K. T., Whitehouse, M. J., Antonelli, M. A., Farquhar, J., Day, J.M.D.m & Hauri, E. H. (2013). Anomalous sulphur isotopes in plume lavas reveal deep mantle storage of Archaean crust. *Nature*, *496*(7446), 490-493.

Carmichael, I. S. E. (1964). The petrology of Thingmuli, a Tertiary volcano in eastern Iceland. *Journal of Petrology*, *5*(3), 435-460.

Condomines, M., Grönvold, K., Hooker, P. J., Muehlenbachs, K., O'Nions, R. K., Oskarsson, N., & Oxburgh, E. R. (1983). Helium, oxygen, strontium and neodymium isotopic relationships in Icelandic volcanics. *Earth and Planetary Science Letters*, *66*, 125-136.

Delavault, H., Chauvel, C., Thomassot, E., Devey, C. W., & Dazas, B. (2016). Sulfur and lead isotopic evidence of relic Archean sediments in the Pitcairn mantle plume. *Proceedings of the National Academy of Sciences*, *113*(46), 12952-12956.

Dixon, J. E., Stolper, E. M., & Holloway, J. R. (1995). An experimental study of water and carbon dioxide solubilities in mid-ocean ridge basaltic liquids. Part I: calibration and solubility models. *Journal of Petrology*, *36*(6), 1607-1631.

Dixon, J. E., Bindeman, I. N., Kingsley, R. H., Simons, K. K., Le Roux, P. J., Hajewski, T. R., Swart, P., Langmuir, C.H., Ryan, J.G., Walowski, K.J., & Wallace, P. J. (2017). Light stable isotopic compositions of enriched mantle sources: Resolving the dehydration paradox. *Geochemistry, Geophysics, Geosystems*, *18*(11), 3801-3839.

Dottin III, J. W., Labidi, J., Jackson, M. G., Woodhead, J., & Farquhar, J. (2020a). Isotopic evidence for multiple recycled sulfur reservoirs in the Mangaia mantle plume. *Geochemistry, Geophysics, Geosystems*, *21*(10), e2020GC009081.

Dottin III, J. W., Labidi, J., Lekic, V., Jackson, M. G., & Farquhar, J. (2020b). Sulfur isotope characterization of primordial and recycled sources feeding the Samoan mantle plume. *Earth and Planetary Science Letters*, *534*, 116073.

Dupré, B., & Allègre, C. J. (1983). Pb–Sr isotope variation in Indian Ocean basalts and mixing phenomena. *Nature*, *303*(5913), 142-146.

Edmonds, M., & Woods, A. W. (2018). Exsolved volatiles in magma reservoirs. *Journal of Volcanology and Geothermal Research*, *368*, 13-30.

Engel, A. J., Engel, C. G., & Havens, R. G. (1965). Chemical characteristics of oceanic basalts and the upper mantle. *Geological Society of America Bulletin*, *76*(7), 719-734.

French, S. W., & Romanowicz, B. (2015). Broad plumes rooted at the base of the Earth's mantle beneath major hotspots. *Nature*, *525*(7567), 95-99.

Goldstein, S. L., Soffer, G., Langmuir, C. H., Lehnert, K. A., Graham, D. W., & Michael, P. J. (2008). Origin of a 'Southern Hemisphere'geochemical signature in the Arctic upper mantle. *Nature*, *453*(7191), 89-93.

Gale, A., Dalton, C. A., Langmuir, C. H., Su, Y., & Schilling, J. G. (2013). The mean composition of ocean ridge basalts. *Geochemistry, Geophysics, Geosystems*, *14*(3), 489-518.

Green, D. H., & Ringwood, A. E. (1967). The genesis of basaltic magmas. *Contributions to Mineralogy and Petrology*, *15*(2), 103-190.
Halldórsson, S. A., Barnes, J. D., Stefánsson, A., Hilton, D. R., Hauri, E. H., & Marshall, E. W. (2016a). Subducted lithosphere controls halogen enrichments in the Iceland mantle plume source. *Geology*, *44*(8), 679-682.
Halldórsson, S. A., Hilton, D. R., Barry, P. H., Füri, E., & Grönvold, K. (2016b). Recycling of crustal material by the Iceland mantle plume: new evidence from nitrogen elemental and isotope systematics of subglacial basalts. *Geochimica et Cosmochimica Acta*, *176*, 206-226.
Hanan, B. B., Blichert-Toft, J., Kingsley, R., & Schilling, J. G. (2000). Depleted Iceland mantle plume geochemical signature: Artifact of multicomponent mixing?. *Geochemistry, Geophysics, Geosystems*, *1*(4).
Harðardóttir, S., Halldórsson, S. A., & Hilton, D. R. (2018). Spatial distribution of helium isotopes in Icelandic geothermal fluids and volcanic materials with implications for location, upwelling and evolution of the Icelandic mantle plume. *Chemical Geology*, *480*, 12-27.
Hart, S. R. (1988). Heterogeneous mantle domains: signatures, genesis and mixing chronologies. *Earth and Planetary Science Letters*, *90*(3), 273-296.
Hjartardóttir, Á. R., & Einarsson, P. (2012). The Kverkfjöll fissure swarm and the eastern boundary of the Northern Volcanic Rift Zone, Iceland. *Bulletin of volcanology*, *74*(1), 143-162.
Hofmann, A. W. (1997). Mantle geochemistry: the message from oceanic volcanism. *Nature*, *385*(6613), 219-229.
Hofmann, A. W. (2003). Sampling mantle heterogeneity through oceanic basalts: isotopes and trace elements. *Treatise on geochemistry*, *2*, 568.
Höskuldsson, A., Sparks, R. S., & Carroll, M. R. (2006). Constraints on the dynamics of subglacial basalt eruptions from geological and geochemical observations at Kverkfjöll, NE-Iceland. *Bulletin of volcanology*, *68*(7), 689-701.
Jackson, M. G., Hart, S. R., Koppers, A. A., Staudigel, H., Konter, J., Blusztajn, J., Kurz, M., & Russell, J. A. (2007). The return of subducted continental crust in Samoan lavas. *Nature*, *448*(7154), 684-687.
Jackson, M. G., Konter, J. G., & Becker, T. W. (2017). Primordial helium entrained by the hottest mantle plumes. *Nature*, *542*(7641), 340-343.
Jackson, M. G., Becker, T. W., & Konter, J. G. (2018). Geochemistry and distribution of recycled domains in the mantle inferred from Nd and Pb isotopes in oceanic hot spots: Implications for storage in the large low shear wave velocity provinces. *Geochemistry, Geophysics, Geosystems*, *19*(9), 3496-3519.
Jackson, M. G., Blichert-Toft, J., Halldórsson, S. A., Mundl-Petermeier, A., Bizimis, M., Kurz, M. D., Price, A.A., Hardadóttir, S., Willhite, L.N., Breddam, K., Becker, T.W., & Fischer, R. A. (2020). Ancient helium and tungsten isotopic signatures preserved in mantle domains least modified by crustal recycling. *Proceedings of the National Academy of Sciences*, *117*(49), 30993-31001.
Jackson, M. G., Becker, T. W., & Steinberger, B. (2021). Spatial characteristics of recycled and primordial reservoirs in the deep mantle. *Geochemistry, Geophysics, Geosystems*, *22*(3), e2020GC009525.
John, T., Layne, G. D., Haase, K. M., & Barnes, J. D. (2010). Chlorine isotope evidence for crustal recycling into the Earth's mantle. *Earth and Planetary Science Letters*, *298*(1-2), 175-182.
Koppers, A. A., Becker, T. W., Jackson, M. G., Konrad, K., Müller, R. D., Romanowicz, B., Steinberger, B., & Whittaker, J. M. (2021). Mantle plumes and their role in Earth processes. *Nature Reviews Earth & Environment*, *2*(6), 382-401.
Kokfelt, T. F., Hoernle, K. A. J., Hauff, F., Fiebig, J., Werner, R., & Garbe-Schoenberg, D. (2006). Combined trace element and Pb-Nd–Sr-O isotope evidence for recycled oceanic crust (upper and lower) in the Iceland mantle plume. *Journal of Petrology*, *47*(9), 1705-1749.
Kurz, M. D., Jenkins, W. J., & Hart, S. R. (1982). Helium isotopic systematics of oceanic islands and mantle heterogeneity. *Nature*, *297*(5861), 43-47.
Langmuir, C. H., Klein, E. M., & Plank, T. (1992). Petrological systematics of mid-ocean ridge basalts: Constraints on melt generation beneath ocean ridges. *Mantle flow and melt generation at mid-ocean ridges*, *71*, 183-280.
Maclennan, J. (2008). Concurrent mixing and cooling of melts under Iceland. *Journal of Petrology*, *49*(11), 1931-1953.
Marshall, E. W., Ranta, E., Halldórsson, S. A., Caracciolo, A., Bali, E., Jeon, H., Whitehouse, M.J., Barnes, J.D., & Stefánsson, A. (2022). Boron isotope evidence for devolatilized and rehydrated recycled materials in the Icelandic mantle source. *Earth and Planetary Science Letters*, *577*, 117229.
Marty, B. (2020). Origins and early evolution of the atmosphere and the oceans. *Geochemical Perspectives*, *9*(2), 135-136.

Moreira, M. (2013). Noble gas constraints on the origin and evolution of Earth's volatiles. *Geochemical Perspectives*, *2*(2), 229-230.
Morgan, W. J. (1971). Convection plumes in the lower mantle. *Nature*, *230*(5288), 42-43.
Montelli, R., Nolet, G., Dahlen, F. A., & Masters, G. (2006). A catalogue of deep mantle plumes: New results from finite-frequency tomography. *Geochemistry, Geophysics, Geosystems*, *7*(11).
Mukhopadhyay, S. (2012). Early differentiation and volatile accretion recorded in deep-mantle neon and xenon. *Nature*, *486*(7401), 101-104.
Mundl-Petermeier, A., Walker, R. J., Jackson, M. G., Blichert-Toft, J., Kurz, M. D., & Halldórsson, S. A. (2019). Temporal evolution of primordial tungsten-182 and 3He/4He signatures in the Iceland mantle plume. *Chemical Geology*, *525*, 245-259.
Oddsson, B. (2016). Heat transfer in volcanic settings: Application to lava-ice interaction and geothermal areas. PhD dissertation, Faculty of Earth Science, University of Iceland, 106 pp.
Ólafsson, M., Torfason, H., & Grönvold, K. (2000). Surface exploration and monitoring of geothermal activity in the Kverkfjöll geothermal area, central Iceland. *World Geothermal Congress 2000*, 1539-1545.
Óskarsson, N., Sigvaldason, G. E., & Steinthorsson, S. (1982). A dynamic model of rift zone petrogenesis and the regional petrology of Iceland. *Journal of Petrology*, *23*(1), 28-74.
Peate, D. W., Breddam, K., Baker, J. A., Kurz, M. D., Barker, A. K., Prestvik, T., Grassineau, N., & Skovgaard, A. C. (2010). Compositional characteristics and spatial distribution of enriched Icelandic mantle components. *Journal of Petrology*, *51*(7), 1447-1475.
Peslier, A. H., Schönbächler, M., Busemann, H., & Karato, S. I. (2017). Water in the Earth's interior: Distribution and origin. *Space Science Reviews*, *212*(1), 743-810.
Plank, T., & Langmuir, C. H. (1998). The chemical composition of subducting sediment and its consequences for the crust and mantle. *Chemical geology*, *145*(3-4), 325-394.
Poreda, R. J., Craig, H., Arnorsson, S., & Welhan, J. A. (1992). Helium isotopes in Icelandic geothermal systems: I. ^{3}He, gas chemistry, and ^{13}C relations. *Geochimica et Cosmochimica Acta*, *56*(12), 4221-4228.
Ranta, E., Halldórsson, S. A., Barnes, J. D., Jónasson, K., & Stefánsson, A. (2021). Chlorine isotope ratios record magmatic brine assimilation during rhyolite genesis. *Geochemical Perspectives Letters*, *16*, 35-39.
Rasmussen, M. B., Halldórsson, S. A., Gibson, S. A., & Guðfinnsson, G. H. (2020). Olivine chemistry reveals compositional source heterogeneities within a tilted mantle plume beneath Iceland. *Earth and Planetary Science Letters*, *531*, 116008.
Richter, M., Nebel, O., Maas, R., Mather, B., Nebel-Jacobsen, Y., Capitanio, F. A., Dick, H.J.B., & Cawood, P. A. (2020). An Early Cretaceous subduction-modified mantle underneath the ultraslow spreading Gakkel Ridge, Arctic Ocean. *Science advances*, *6*(44), eabb4340.
Rollinson, H. R. (2009). *Early Earth systems: a geochemical approach*. John Wiley & Sons, 296 pp.
Sano, Y., Urabe, A., Wakita, H., Chiba, H., & Sakai, H. (1985). Chemical and isotopic compositions of gases in geothermal fluids in Iceland. *Geochemical journal*, *19*(3), 135-148.
Saunders, A. D., Fitton, J. G., Kerr, A. C., Norry, M. J., Kent, R. W., Mahoney, J. J., & Coffin, M. F. (1997). The north Atlantic igneous province. *Geophysical Monograph-American Geophysical Union*, *100*, 45-94.
Schilling, J. G. (1973). Iceland mantle plume: geochemical study of Reykjanes Ridge. *Nature*, *242*(5400), 565-571.
Shimizu, K., Saal, A. E., Myers, C. E., Nagle, A. N., Hauri, E. H., Forsyth, D. W., Kamenetsky, V.S., & Niu, Y. (2016). Two-component mantle melting-mixing model for the generation of mid-ocean ridge basalts: implications for the volatile content of the Pacific upper mantle. *Geochimica et Cosmochimica Acta*, *176*, 44-80.
Sigvaldason, G. E., Steinthorsson, S., Oskarsson, N., & Imsland, P. (1974). Compositional variation in recent Icelandic tholeiites and the Kverkfjöll hot spot. *Nature*, *251*(5476), 579-582.
Sigvaldason, G. E., & Óskarsson, N. (1976). Chlorine in basalts from Iceland. *Geochimica et Cosmochimica Acta*, *40*(7), 777-789.
Sigvaldason, G. E., & Óskarsson, N. (1986). Fluorine in basalts from Iceland. *Contributions to Mineralogy and Petrology*, *94*(3), 263-271.
Sigurdsson, H., & Sparks, R. S. J. (1981). Petrology of rhyolitic and mixed magma ejecta from the 1875 eruption of Askja, Iceland. *Journal of Petrology*, *22*(1), 41-84.
Sigurgeirsson, M.Á., Hjartarson, Á., Kaldal, I., Sæmundsson, K., Kristinsson, S.G., & Víkingsson, S. (2015). Geological Map of the Northern Volcanic Zone, Iceland. Southern Part. 1:100 000. Reykjavík: Iceland GeoSurvey.

Stefánsson, A., Sveinbjörnsdóttir, Á. E., Heinemeier, J., Arnórsson, S., Kjartansdóttir, R., & Kristmannsdóttir, H. (2016). Mantle CO_2 degassing through the Icelandic crust: evidence from carbon isotopes in groundwater. *Geochimica et Cosmochimica Acta*, *191*, 300-319.

Stefánsson, A., Hilton, D. R., Sveinbjörnsdóttir, Á. E., Torssander, P., Heinemeier, J., Barnes, J. D., Ono, S., Halldórsson, S.A., Fiebig, J., & Arnórsson, S. (2017). Isotope systematics of Icelandic thermal fluids. *Journal of Volcanology and Geothermal Research*, *337*, 146-164.

Stracke, A., Hofmann, A. W., & Hart, S. R. (2005). FOZO, HIMU, and the rest of the mantle zoo. *Geochemistry, geophysics, geosystems*, *6*(5).

Taran, Y. A. (2009). Geochemistry of volcanic and hydrothermal fluids and volatile budget of the Kamchatka–Kuril subduction zone. *Geochimica et Cosmochimica acta*, *73*(4), 1067-1094.

Thorarinsson, S., Einarsson, T., Sigvaldason, G., & Elisson, G. (1964). The submarine eruption off the Vestmann Islands 1963–64. *Bulletin Volcanologique*, *27*(1), 435-445.

Thordarson, T., & Self, S. (1993). The Laki (Skaftár Fires) and Grímsvötn eruptions in 1783–1785. *Bulletin of Volcanology*, *55*(4), 233-263.

Walker, G.P.L. (1963). The Breiddalur central volcano, eastern Iceland. *Quarterly Journal of the Geological Society*, *119*(1-4), 29-63.

Walker, G. P. (1983). Ignimbrite types and ignimbrite problems. *Journal of volcanology and geothermal research*, *17*(1-4), 65-88.

Walowski, K. J., Kirstein, L. A., De Hoog, J. C. M., Elliott, T., Savov, I. P., & Jones, R. E. (2021). Boron recycling in the mantle: Evidence from a global comparison of ocean island basalts. *Geochimica et Cosmochimica Acta*, *302*, 83-100.

Williams, C. D., Mukhopadhyay, S., Rudolph, M. L., & Romanowicz, B. (2019). Primitive helium is sourced from seismically slow regions in the lowermost mantle. *Geochemistry, Geophysics, Geosystems*, *20*(8), 4130-4145.

White, W. M., & Hofmann, A. W. (1982). Sr and Nd isotope geochemistry of oceanic basalts and mantle evolution. *Nature*, *296*(5860), 821-825.

White, W. M. (2015). Isotope geochemistry. John Wiley & Sons, 496 pp.

Workman, R. K., & Hart, S. R. (2005). Major and trace element composition of the depleted MORB mantle (DMM). *Earth and Planetary Science Letters*, *231*(1-2), 53-72.

Yang, A. Y., Langmuir, C. H., Cai, Y., Michael, P., Goldstein, S. L., & Chen, Z. (2021). A subduction influence on ocean ridge basalts outside the Pacific subduction shield. *Nature communications*, *12*(1), 1-10.

Yuan, K., & Romanowicz, B. (2017). Seismic evidence for partial melting at the root of major hot spot plumes. *Science*, *357*(6349), 393-397.

Zindler, A., & Hart, S. (1986). Chemical geodynamics. *Annual review of earth and planetary sciences*, *14*(1), 493-571

2 Paper I

Chlorine isotope ratios record magmatic brine assimilation during rhyolite genesis

Eemu Ranta[1], Sæmundur A. Halldórsson[1], Jaime D. Barnes[2], Kristján Jónasson[3], Andri Stefánsson[1]

[1]*Nordic Volcanological Center, Institute of Earth Sciences, University of Iceland, Iceland*
[2]*Department of Geological Sciences, University of Texas at Austin, USA*
[3]*Icelandic Institute of Natural History, Iceland*

Published in 2021 in *Geochemical Perspectives Letters* (vol. 15, pp. 35-39).
Reprinted under Creative Commons License CC BY-NC-ND 4.0.

Geochemical Perspectives Letters

© 2021 The Authors
Published by the European Association of Geochemistry

Chlorine isotope ratios record magmatic brine assimilation during rhyolite genesis

E. Ranta[1*], S.A. Halldórsson[1], J.D. Barnes[2], K. Jónasson[3], A. Stefánsson[1]

OPEN ACCESS
doi: 10.7185/geochemlet.2101

Abstract

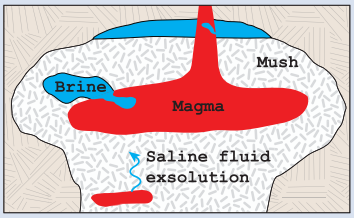

Magmatic volatile phases within crustal silicic magma domains influence key volcanic processes such as the build up to eruptions and formation of magmatic-hydrothermal ore deposits. However, the extent and nature of fluid-melt interaction in such environments is poorly understood, as geochemical signals in volcanic rocks originating from pre-eruptive volatile processes are commonly overprinted by syn-eruptive degassing. Here, we use $\delta^{37}Cl$ as a conservative tracer of brine-melt interaction on a broad suite of silicic volcanic rocks from Iceland. We find that the $\delta^{37}Cl$ values of silicic rocks are systematically shifted to more negative values compared to associated basalts and intermediate rocks by up to 2.9 ‰. These large shifts cannot be explained by well known processes inherent to silicic magma genesis, including crustal assimilation, mineral-melt fractionation and syn-eruptive degassing. Instead, we show that low $\delta^{37}Cl$ values in silicic rocks can be attributed to assimilation of magmatic brines that are formed and stored in long lived crustal magma mushes. Our results indicate that magmatic brine assimilation is a fundamental, but previously unrecognised part of rhyolite genesis.

Received 23 July 2020 | Accepted 24 November 2020 | Published 13 January 2021

Introduction

Magmatic volatiles play a fundamental part during silicic magma genesis and the formation of associated ore deposits. Chlorine is among the most abundant volatile elements in igneous rocks and may become concentrated enough in late stage silicic melts to exsolve and form hydrosaline liquids, *i.e.* high density Cl-enriched aqueous fluids or hydrosaline brines (Webster, 2004). As chlorine is a hydrophile element, its isotopic fingerprint has been used to trace volatile sources in igneous rocks and hydrothermal fluids (Barnes *et al.*, 2008; Li *et al.*, 2015). Lavas associated with subduction zones and oceanic islands have a range of $\delta^{37}Cl$ values from −3 to +3 ‰, likely due to incorporation of subduction fluids, recycled marine sediments and altered oceanic crust into the mantle (John *et al.*, 2010; Barnes and Sharp, 2017). In contrast, the depleted upper mantle (DMM) has a restricted $\delta^{37}Cl$ variability of −0.2 ± 0.3 ‰ (Sharp *et al.*, 2013), reflecting the limited $\delta^{37}Cl$ fractionation from high temperature magmatic processes (Schauble *et al.*, 2003). The majority of chlorine isotope studies on igneous rocks have been conducted on basaltic rocks, whereas published $\delta^{37}Cl$ data for silicic rocks is limited, with 40 out of 44 published analyses coming from a single volcanic system, the Mono Craters, USA (Barnes *et al.*, 2014). This study was designed to explore if and how $\delta^{37}Cl$ systematics can provide new insights into silicic magmatic processes such as assimilation and brine-melt interaction, using Iceland as a test site.

Chlorine Isotope Systematics in Silicic Rocks

We present new $\delta^{37}Cl$ and $\delta^{18}O$ data for a sample set (n = 16) focusing on neovolcanic extrusive silicic (SiO_2 > 65 wt. %) and intermediate (SiO_2 = 52-65 wt. %) rocks from Iceland (Tables S-1, S-2). Together with previously published $\delta^{37}Cl$ and $\delta^{18}O$ data on Icelandic basalts (Halldórsson *et al.*, 2016), the samples represent the full chemical range between subalkaline-tholeiitic rift zone, and transitional to alkaline propagating rift and off-rift magma suites in Iceland (Fig. S-1), spanning a SiO_2 range of 44.4-77.7 wt. % and Cl concentrations between 17 and 3988 ppm (Figs. 1, S-2). The samples cover the main types of silicic rocks in Iceland, *i.e.* dacites and alkaline and subalkaline rhyolites (Jónasson, 2007), and include both obsidians and tephras (*i.e.* products of effusive *vs.* explosive eruptions). All studied volcanoes are situated on land and are free of seawater influence (Halldórsson *et al.*, 2016).

Significant Cl variation is present at any given SiO_2 content in the basaltic (17–1269 ppm), intermediate (130–942 ppm) and silicic (282–3988 ppm) samples (Fig. S-2). These ranges are similar to published Cl concentrations in melt inclusions (MIs) from corresponding locations (Fig. S-3). The $\delta^{37}Cl$ value of all analysed samples (n = 14) vary from −1.9 to +1.3 ‰ (1σ = ±0.2 ‰) (Fig. 1a,b). The basaltic (n = 3) and intermediate (n = 4) samples have $\delta^{37}Cl$ values between −0.4 and +1.3 ‰, overlapping with the known range of Icelandic basalts of −0.6 to +1.4 ‰ (Halldórsson *et al.*, 2016). In contrast, the $\delta^{37}Cl$ values of

1. Nordic Volcanological Center, Institute of Earth Sciences, University of Iceland, 102 Reykjavík, Iceland
2. Department of Geological Sciences, University of Texas, Austin, Texas 78712, USA
3. Icelandic Institute of Natural History, 210 Garðabær, Iceland
* Corresponding author (email: eemu@hi.is)

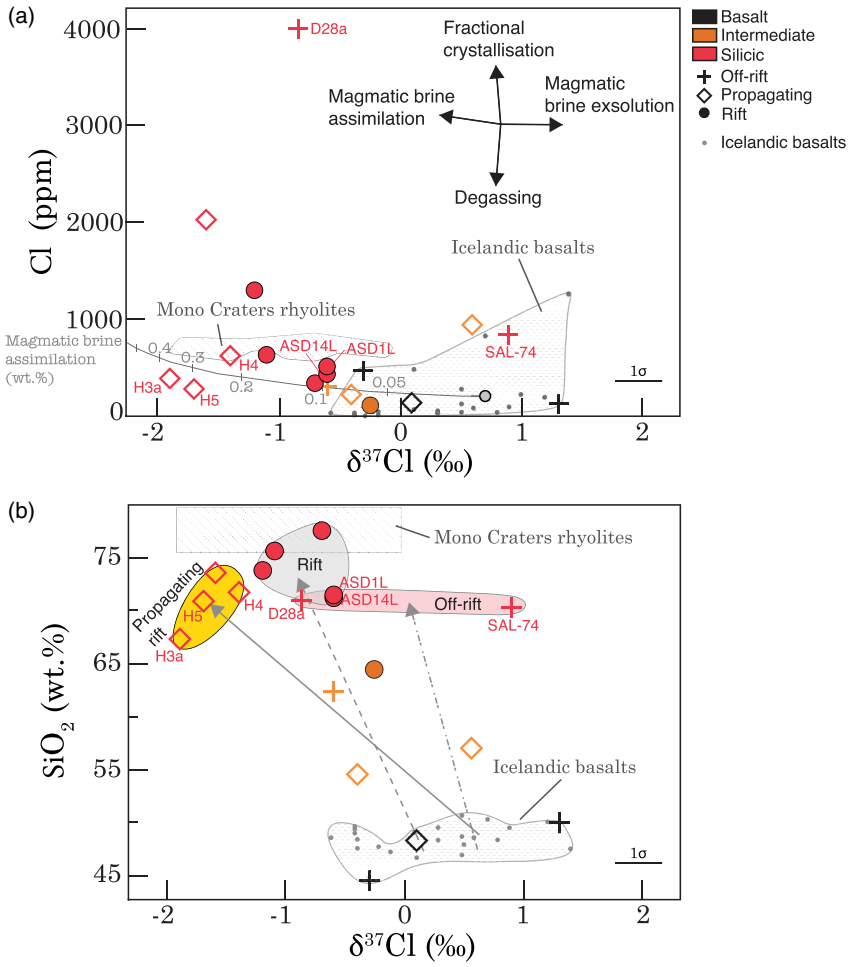

Figure 1 Chlorine isotope variations *vs*. **(a)** Cl concentrations and **(b)** SiO_2. Silicic rocks in Iceland have lower $\delta^{37}Cl$ values than basalts (data from Halldórsson *et al.*, 2016), overlapping with rhyolites from the Mono Craters, USA (Barnes *et al.*, 2014). Arrows in **(a)** indicate the effects of the small equilibrium isotope fractionations caused by fractional crystallisation and degassing, and the large kinetic isotope fractionation during magmatic brine exsolution (Fortin *et al.*, 2017) and assimilation on the $\delta^{37}Cl$ and Cl composition of silicic melts. The gray curve in **(a)** shows the effect of magmatic brine assimilation (in wt. %) on the Cl-$\delta^{37}Cl$ values of a hypothetical rhyolite melt with an average propagating rift basalt $\delta^{37}Cl$ value of +0.7 ‰. The negative $\delta^{37}Cl$ shifts between silicic rocks and basalts are illustrated in **(b)** by arrows anchored at the average SiO_2 concentrations and $\delta^{37}Cl$ values of the rift, propagating rift and off-rift basalts. The 1σ uncertainty is ±0.2 ‰ for $\delta^{37}Cl$.

the silicic samples from this study (n = 8) and those previously published (n = 3; Halldórsson *et al.*, 2016) deviate from the basaltic-intermediate range towards more negative values of −1.9 to −0.6 ‰ (Fig. 1b), except for a single outlier (SAL-74) with $\delta^{37}Cl = +0.9$ ‰.

Local $\delta^{37}Cl$ variability in Icelandic rhyolites appears to be small (≤0.5 ‰ for Hekla: H3, H4, H5; and Askja: ASD1L, ASD14L) compared to the large range of −1.9 to 0.0 ‰ reported for the Mono Crater rhyolites (Barnes *et al.*, 2014) (Fig. 1). Rift, propagating rift and off-rift samples define distinct fields in the SiO_2-$\delta^{37}Cl$ and $\delta^{18}O$-$\delta^{37}Cl$ diagrams (Figs. 1b, 2), suggesting a possible correlation between volcano-tectonic setting and $\delta^{37}Cl$ (see Supplementary Information S-2).

Origin of Large $\delta^{37}Cl$ Variability: Sources Versus Processes

Our dataset demonstrates that silicic rocks in Iceland have more negative $\delta^{37}Cl$ values relative to associated basalts and intermediate rocks. Whereas basalts inherit the $\delta^{37}Cl$ signatures of their mantle sources (Halldórsson *et al.*, 2016), the shift to more negative $\delta^{37}Cl$ values in silicic rocks must reflect a process or a combination of processes taking place during rhyolite genesis, such as mineral-melt fractionation, degassing and/or assimilation.

Rayleigh $\delta^{37}Cl$ fractionations between HCl(g), minerals and silicic melt are expected to be small, based on theoretical equilibrium fractionation factors of Schauble *et al.* (2003)

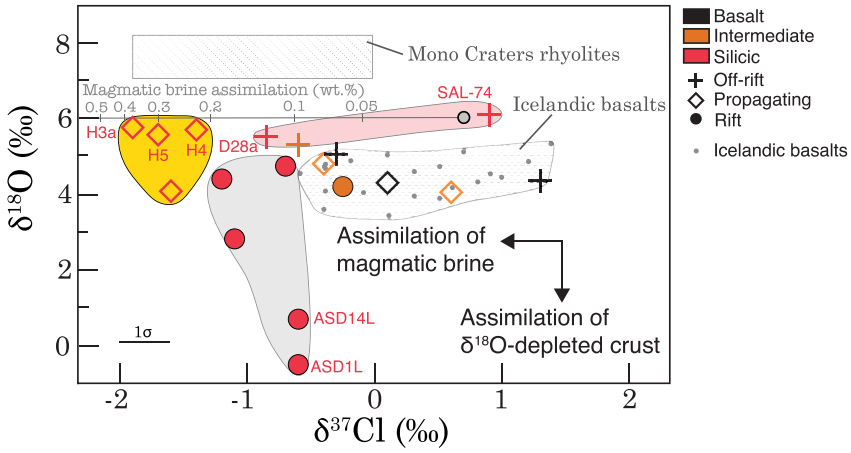

Figure 2 The $\delta^{18}O$-$\delta^{37}Cl$ systematics of silicic rocks. Low $\delta^{18}O$ values of rift-related silicic rocks result from assimilation of hydrothermally altered, $\delta^{18}O$-depleted crust. Lack of correlation between $\delta^{18}O$ and $\delta^{37}Cl$ indicates that negative $\delta^{37}Cl$ values of rhyolites are not caused by crustal assimilation. The gray line shows the effect of magmatic brine assimilation in wt. % (Supplementary Information S-4). Mono Craters field is drawn after data reported in Newman *et al.* (1988) and Barnes *et al.* (2014). The 1σ uncertainty is ±0.2 ‰ for $\delta^{37}Cl$, and smaller than the size of the symbols for $\delta^{18}O$.

extrapolated to magmatic temperatures ($\Delta^{37}Cl_{mineral\text{-}melt} \approx \Delta^{37}Cl_{vapour\text{-}melt} \approx 0.2$ ‰ at 600 °C). Thus, even extreme cases of 90 % Cl removal by fractional apatite crystallisation or open system degassing of HCl(g) only fractionate the $\delta^{37}Cl_{melt}$ values by about −0.5 ‰. However, modal apatite abundances in our samples are low (<2 %) and similar Cl concentrations in MIs and matrix glasses imply an insignificant degree of syn-eruptive chlorine degassing (Fig. S-3). Therefore, the combined effect of fractional crystallisation and degassing on $\delta^{37}Cl_{melt}$ values of our samples is negligible (<0.2 ‰). Moreover, similar $\delta^{37}Cl$ values of both obsidians and tephras indicate that $\delta^{37}Cl$ fractionation is independent of eruption type and occurs within the crustal magma domain prior to eruptions.

To test if assimilation of altered basaltic crust causes negative $\delta^{37}Cl$ shifts between rhyolites and basalts, we analysed the $\delta^{18}O$ compositions of our samples (Fig. 2). In Iceland, low $\delta^{18}O_{rock}$ values relative to pristine basaltic values (+4.8 to +5.8 ‰; Thirlwall *et al.*, 2006) are used to recognise assimilation (or partial melting) of altered crust, which has been shifted to low $\delta^{18}O$ signatures (≤+2 ‰) by hydrothermal alteration with low $\delta^{18}O$ meteoric water (Gautason and Muehlenbachs, 1998). We note that basalts and intermediate rocks from all three volcanic settings display $\delta^{18}O$ values between +3.4 and +5.2 ‰ (Fig. 2), typical for Icelandic basalts (Thirlwall *et al.*, 2006). Silicic rocks from the propagating rift and off-rift zones have basalt-like $\delta^{18}O$ values of +4.0 to +6.1 ‰, whereas the lower and more variable $\delta^{18}O$ values from −0.5 to +4.7 ‰ in the rift zone rhyolites (Fig. 2) indicate variable degrees of crustal assimilation.

However, there is no correlation between $\delta^{37}Cl$ and $\delta^{18}O$ (Fig. 2). For example, silicic samples with the most negative (H3a) and positive $\delta^{37}Cl$ values (SAL-74) have normal $\delta^{18}O$ values, while the two samples with the lowest $\delta^{18}O$ values (ASD1L, ASD14L) show relatively small $\delta^{37}Cl$ shifts. This indicates that the negative $\delta^{37}Cl$ shifts in Icelandic rhyolites are not caused by assimilation of $\delta^{18}O$-depleted altered crust, but by an additional process. Conversely, this suggests that hydrothermally altered crust in Iceland has a basalt-like $\delta^{37}Cl$ range, consistent with the basalt-like $\delta^{37}Cl$ values in Icelandic hydrothermal fluids (Stefánsson and Barnes, 2016) and the lack of $\delta^{37}Cl$ fractionation resulting from hydrothermal alteration (Cullen *et al.*, 2019). In contrast, boron another fluid-mobile element, displays anomalous positive $\delta^{11}B$ values in Icelandic silicic rocks that correlate with decreasing $\delta^{18}O$, and that have thus been explained by crustal assimilation (Rose-Koga and Sigmarsson, 2008).

Extensive previous work on the Hekla volcano demonstrates that for non-volatile element stable isotope systems studied thus far, fractionations between rhyolites and basalts are either negligible or can be explained by fractional crystallisation (Supplementary Information S-4). Our silicic Hekla samples (H3a, H4, H5) display the largest $\delta^{37}Cl$ shifts (up to −2.9 ‰) compared to corresponding basalts (Fig. 1). This comparison highlights that $\delta^{37}Cl$ selectively records a process relating to the pre-eruptive volatile history of silicic magmas that is not recorded by other, non-volatile stable isotope systems. Indeed, a complicated pre-eruptive volatile history is also reflected by high Cl variability in Icelandic propagating rift and rift rhyolites (50 to 2600 ppm) (Fig. S-2), likely reflecting a combination of fractional crystallisation, partial melting, accumulation of fractional melts from volatile heterogeneous sources as well as episodic exsolution and resorption of magmatic volatile phases, including magmatic brines (Webster *et al.*, 2019; Supplementary Information S-3; Fig. 3a).

Chlorine isotope systematics provide a strict constraint on the nature of a potential assimilant, which must have a negative $\delta^{37}Cl$ and elevated concentrations of Cl compared to the rhyolites. These criteria best match a fluid assimilant with high Cl concentrations ($Cl_{assimilant}/Cl_{rhyolite} >> 1$) and low $\delta^{37}Cl$ (<−3 ‰) (Fig S-4). Magmatic hydrosaline fluids have by definition high Cl concentrations and may acquire highly negative $\delta^{37}Cl$ values during exsolution from dacitic (and more silicic) melts due to kinetic diffusion effects, that cause considerable fractionation of up to $\Delta^{37}Cl_{fluid\text{-}melt} = -5$ ‰ even at high temperatures (Fortin *et al.*, 2017) (Fig. 3b). Therefore, in terms of predicted Cl-$\delta^{37}Cl$ values, magmatic brine is an assimilant that near-perfectly matches the observed $\delta^{37}Cl$ shifts in Icelandic rhyolites (Fig. S-4). Anomalously negative $\delta^{37}Cl$ values of down to −5.6 ‰ have been reported for saline fluid inclusions in porphyry copper and iron oxide-copper-gold deposits, showing that low $\delta^{37}Cl$ brines do exist in magmatic-hydrothermal environments (Gleeson and Smith, 2009; Nahnybida *et al.*, 2009).

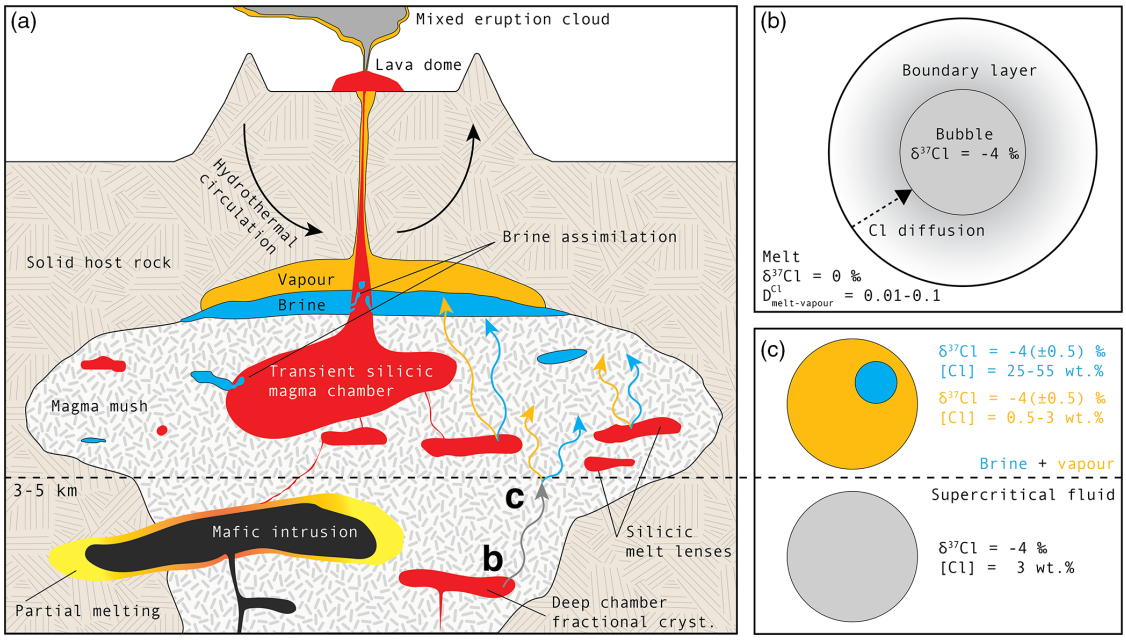

Figure 3 **(a)** A model of magmatic brine formation and assimilation in a long lived upper crustal magma mush. **(b)** Magmatic fluids exsolve from silicic melts during late stage crystallisation and acquire negative $\delta^{37}Cl$ values through kinetic fractionation (Fortin *et al.*, 2017). **(c)** Decompression-driven phase separation of a supercritical fluid produces a NaCl-rich brine and a NaCl-poor vapour with a maximum fractionation of $\Delta^{37}Cl_{liquid\text{-}vapour} = \pm 0.5$ ‰ (Liebscher *et al.*, 2006).

Assimilation of Magmatic Brines

The presence of magmatic brine is a widely reported phenomenon associated with silicic and intermediate magmas in the upper crust. For example, brines are found in magmatic fluid inclusions and are implicated in the formation of magmatic-hydrothermal ore deposits globally (Audétat *et al.*, 2008), including in Iceland (Kremer and Bird, 2018). Crystallisation of silicic melts that stall in the crust lead to late stage exsolution of magmatic brines or hydrosaline fluids. Magmatic brines may form by direct exsolution from melts with moderate Cl/H_2O ratios (>0.05 for granitic melts; Webster, 2004) at pressures below about 1.5 kbar, by phase separation of a magmatic fluid into low NaCl vapour and a high NaCl brine (up to NaCl > 85 wt. %) during decompression (Fig. 3c), or by condensation of magmatic vapour (Webster and Mandeville, 2007). Magmatic brines are less dense and stable to lower temperatures compared to melts, and once formed, may accumulate in pore space or pool in roof zones of magma mushes forming lenses (Fig. 3a) that can stay stable for over 1 Myr (Blundy *et al.*, 2015; Afanasyev *et al.*, 2018; Edmonds and Woods, 2018). Individual accumulations of silicic melts form over short time scales (0.01 to 1 kyr time scales) compared to the long lifetimes of the silicic magma mushes that they are part of (100 kyr – 1 Myr time scales) (Padilla *et al.*, 2016; Cooper, 2019). Thus, cycles of silicic melt production and crystallisation lead to repeated production and accumulation of magmatic brines in long lived magma mushes.

Our samples are chlorine undersaturated, similar to the majority of felsic melt inclusions globally (Webster *et al.*, 2019). We envision that such chlorine undersaturated melts may, prior to or during eruptions, assimilate ambient low $\delta^{37}Cl$ magmatic brines that have been formed by previous generations of silicic intrusions within the same, long lived silicic magma mush (Fig. 3a). Our bulk assimilation model shows that modest amounts (*ca.* 0.5 wt. %) of addition of magmatic brines with $NaCl_{equivalent} = 16.5$ wt. % and $\delta^{37}C_{fluid} = -4$ ‰ is sufficient to explain the maximum observed $\delta^{37}Cl$ shift of −2.9 ‰ between silicic rocks and basalts in our samples (Figs. 1b, S-4, S-5). Assimilation of brines has been previously demonstrated to take place in submarine basalts, that may directly assimilate seawater-derived brines (Kendrick *et al.*, 2013), and in silicic melts, where surplus Cl contents have been interpreted as assimilation of hydrosaline fluids of unknown origin (Webster *et al.*, 2019).

The common association of silicic magmas with brines and the dominantly negative $\delta^{37}Cl$ signatures observed in silicic volcanic rocks that are difficult to reconcile with other known magmatic processes suggest that magmatic brine assimilation may be a fundamental process in silicic, long lived magma mushes. Our results highlight that little is still known about the storage and evolution of hydrosaline liquids in magma mushes. The details of physical and chemical interactions between brines and melts should be a fruitful target of future research aiming to improve our understanding of silicic magmatism. Finally, we note that low $\delta^{37}Cl$ magmatic vapours and/or liquids residing in the roof zones of magma mushes may become incorporated in eruption clouds or shallow hydrothermal systems (Fig. 3a). This process could, instead of direct degassing of magmatic Cl, offer an alternative explanation to the association of volcanic activity with negative $\delta^{37}Cl$ signatures in thermal springs and fumaroles in Guadeloupe, Martinique (Li *et al.*, 2015) and the Izu-Bonin-Mariana arc (Barnes *et al.*, 2008) as well as volcanic gases in Stromboli, Italy (Liotta *et al.*, 2017).

Acknowledgements

ER acknowledges support from NordVulk and the University of Iceland Research Fund. SAH acknowledges support from the Icelandic Research Fund (Grant #196139-051). We would like to thank Guðmundur H. Guðfinnsson for assistance with EPMA analysis and Enikő Bali for help with FTIR. We thank Maja Bar Rasmussen, Edward W. Marshall and Olgeir Sigmarsson for fruitful discussions. Níels Óskarsson is thanked for sharing previously unpublished data for Askja and Hekla samples. Cin-Ty Lee is acknowledged for smooth editorial handling of the manuscript. We are grateful to Shanaka de Silva and an anonymous reviewer for constructive comments that helped improve the manuscript. Isabelle Chambefort and two anonymous reviewers are thanked for helpful comments on a previous version of the manuscript.

Editor: Cin-Ty Lee

Additional Information

Supplementary Information accompanies this letter at https://www.geochemicalperspectivesletters.org/article2101.

© 2021 The Authors. This work is distributed under the Creative Commons Attribution Non-Commercial No-Derivatives 4.0 License, which permits unrestricted distribution provided the original author and source are credited. The material may not be adapted (remixed, transformed or built upon) or used for commercial purposes without written permission from the author. Additional information is available at https://www.geochemicalperspectivesletters.org/copyright-and-permissions.

Cite this letter as: Ranta, E., Halldórsson, S.A., Barnes, J.D., Jónasson, K., Stefánsson, A. (2021) Chlorine isotope ratios record magmatic brine assimilation during rhyolite genesis. *Geochem. Persp. Let.* 16, 35–39.

References

Afanasyev, A., Blundy, J., Melnik, O., Sparks, S. (2018) Formation of magmatic brine lenses via focussed fluid-flow beneath volcanoes. *Earth and Planetary Science Letters* 486, 119–128.

Audétat, A., Pettke, T., Heinrich, C.A., Bodnar, R.J. (2008) The composition of magmatic-hydrothermal fluids in barren and mineralized intrusions. *Economic Geology* 103, 877–908.

Barnes, J.D., Sharp, Z.D. (2017) Chlorine isotope geochemistry. *Reviews in Mineralogy and Geochemistry* 82, 345–378.

Barnes, J.D., Sharp, Z.D., Fischer, T.P. (2008) Chlorine isotope variations across the Izu-Bonin-Mariana arc. *Geology* 36, 883–886.

Barnes, J.D., Prather, T.J., Cisneros, M., Befus, K., Gardner, J.E., Larson, T.E. (2014) Stable chlorine isotope behavior during volcanic degassing of H_2O and CO_2 at Mono Craters, CA. *Bulletin of Volcanology* 76, 805.

Blundy, J., Mavrogenes, J., Tattitch, B., Sparks, S., Gilmer, A. (2015) Generation of porphyry copper deposits by gas–brine reaction in volcanic arcs. *Nature Geoscience* 8, 235.

Cooper, K.M. (2019) Time scales and temperatures of crystal storage in magma reservoirs: Implications for magma reservoir dynamics. *Philosophical Transactions of the Royal Society A* 377, 20180009.

Cullen, J.T., Hurwirz, S., Barnes, J.D., Lassiter, J.C., Penniston-Dorland, S., Kasemann, S.A., Thordsen, J.J. (2019) Temperature-Dependent variations in mineralogy, major element chemistry and the stable isotopes of boron, lithium and chlorine resulting from hydration of rhyolite: Constraints from hydrothermal experiments at 150 to 350° C and 25 MPa. *Geochimica et Cosmochimica Acta* 261, 269–287.

Fortin, M.A., Watson, E.B., Stern, R. (2017) The isotope mass effect on chlorine diffusion in dacite melt, with implications for fractionation during bubble growth. *Earth and Planetary Science Letters* 480, 15–24.

Edmonds, M., Woods, A.W. (2018) Exsolved volatiles in magma reservoirs. *Journal of Volcanology and Geothermal Research* 368, 13–30.

Gautason, B., Muehlenbachs, K. (1998) Oxygen isotopic fluxes associated with high-temperature processes in the rift zones of Iceland. *Chemical Geology* 145, 275–286.

Gleeson, S.A., Smith, M.P. (2009) The sources and evolution of mineralising fluids in iron oxide–copper–gold systems, Norrbotten, Sweden: Constraints from Br/Cl ratios and stable Cl isotopes of fluid inclusion leachates. *Geochimica et Cosmochimica Acta* 73, 5658–5672.

Halldórsson, S.A., Barnes, J.D., Stefánsson, A., Hilton, D.R., Hauri, E.H., Marshall, E.W. (2016) Subducted lithosphere controls halogen enrichments in the Iceland mantle plume source. *Geology* 44, 679–682.

John, T., Layne, G.D., Haase, K.M., Barnes, J.D. (2010) Chlorine isotope evidence for crustal recycling into the Earth's mantle. *Earth and Planetary Science Letters* 298, 175–182.

Jónasson, K. (2007) Silicic volcanism in Iceland: Composition and distribution within the active volcanic zones. *Journal of Geodynamics* 43, 101–117.

Kendrick, M.A., Arculus, R., Burnard, P., Honda, M. (2013) Quantifying brine assimilation by submarine magmas: Examples from the Galápagos Spreading Centre and Lau Basin. *Geochimica et Cosmochimica Acta* 123, 150–165.

Kremer, C.H., Bird, D.K. (2018) Fluid origin and evolution of Cu-Pb-Zn mineralization in rhyolite breccias in the Lón area, southeastern Iceland. *Journal of Volcanology and Geothermal Research* 349, 177–191.

Li, L., Bonifacie, M., Aubaud, C., Crispi, O., Dessert, C., Agrinier, P. (2015) Chlorine isotopes of thermal springs in arc volcanoes for tracing shallow magmatic activity. *Earth and Planetary Science Letters* 413, 101–110.

Liebscher, A., Barnes, J., Sharp, Z. (2006) Chlorine isotope vapor–liquid fractionation during experimental fluid-phase separation at 400 C/23 MPa to 450 C/42 MPa. *Chemical Geology* 234, 340–345.

Liotta, M., Rizzo, A.L., Barnes, J.D., D'Auria, L., Martelli, M., Bobrowski, N., Wittmer, J. (2017) Chlorine isotope composition of volcanic rocks and gases at Stromboli volcano (Aeolian Islands, Italy): Inferences on magmatic degassing prior to 2014 eruption. *Journal of Volcanology and Geothermal Research* 336, 168–178.

Nahnybida, T., Gleeson, S.A., Rusk, B.G., Wassenaar, L.I. (2009) Cl/Br ratios and stable chlorine isotope analysis of magmatic–hydrothermal fluid inclusions from Butte, Montana and Bingham Canyon, Utah. *Mineralium Deposita* 44, 837.

Newman, S., Epstein, S., Stolper, E. (1988) Water, carbon dioxide, and hydrogen isotopes in glasses from the ca. 1340 AD eruption of the Mono Craters, California: constraints on degassing phenomena and initial volatile content. *Journal of Volcanology and Geothermal Research* 35, 75–96.

Padilla, A.J., Miller, C.F., Carley, T.L., Economos, R.C., Schmitt, A.K., Coble, M.A., Wooden, J.L., Fisher, C.-M., Vervoort, J.D., Hanchar, J.M. (2016) Elucidating the magmatic history of the Austurhorn silicic intrusive complex (southeast Iceland) using zircon elemental and isotopic geochemistry and geochronology. *Contributions to Mineralogy and Petrology* 171, 69.

Rose-Koga, E.F., Sigmarsson, O. (2008) B–O–Th isotope systematics in Icelandic tephra. *Chemical Geology* 255, 454–462.

Schauble, E.A., Rossman, G.R., Taylor Jr., H.P. (2003) Theoretical estimates of equilibrium chlorine-isotope fractionations. *Geochimica et Cosmochimica Acta* 67, 3267–3281.

Sharp, Z.D., Mercer, J.A., Jones, R.H., Brearley, A.J., Selverstone, J., Bekker, A., Stachel, T. (2013) The chlorine isotope composition of chondrites and Earth. *Geochimica et Cosmochimica Acta* 107, 189–204.

Stefánsson, A., Barnes, J.D. (2016) Chlorine isotope geochemistry of Icelandic thermal fluids: Implications for geothermal system behavior at divergent plate boundaries. *Earth and Planetary Science Letters* 449, 69–78.

Thirlwall, M.F., Gee, M.A.M., Lowry, D., Mattey, D.P., Murton, B.J., Taylor, R.N. (2006) Low $\delta^{18}O$ in the Icelandic mantle and its origins: Evidence from Reykjanes Ridge and Icelandic lavas. *Geochimica et Cosmochimica Acta* 70, 993–1019.

Webster, J.D. (2004) The exsolution of magmatic hydrosaline chloride liquids. *Chemical Geology 210,* 33–48.

Webster, J.D., Mandeville, C.W. (2007) Fluid immiscibility in volcanic environments. *Reviews in Mineralogy and Geochemistry* 65, 313–362.

Webster, J.D., Iveson, A.A., Rowe, M.C., Webster, P.M. (2019) Chlorine and felsic magma evolution: Modeling the behavior of an under-appreciated volatile component. *Geochimica et Cosmochimica Acta* 271, 248–288.

3 Paper II

Ancient and recycled sulfur sampled by the Iceland mantle plume

Eemu Ranta[1], Jóhann Gunnarsson-Robin[1], Sæmundur A. Halldórsson[1], Shuhei Ono[2], Gareth Izon[2], Matthew G. Jackson[3], Callum D.J. Reekie[4], Frances E. Jenner[5], Guðmundur H. Guðfinnsson[1], Ólafur P. Jónsson[1], Andri Stefánsson[1]

[1]*Nordic Volcanological Center, Institute of Earth Sciences, University of Iceland, Iceland*
[2]*Department of Earth, Atmospheric and Planetary Sciences, Massachusetts Institute of Technology, USA*
[3]*Department of Earth Science, University of California, Santa Barbara, USA*
[4]*Department of Earth Sciences, University of Cambridge, UK*
[5]*School of Environment, Earth and Ecosystem Sciences, The Open University, UK*

Manuscript has been submitted to *Earth and Planetary Science Letters*

3.1 Abstract

Stable sulfur isotope ratios of mid-ocean ridge and ocean island basalts (MORBs and OIBs) preserve unique information about early Earth processes and the long-term volatile cycles between Earth's mantle and the surface. Icelandic basalts present ideal material to examine the oldest known terrestrial mantle reservoir, accessed through a deep-rooted mantle plume, but their multiple sulfur isotope systematics have not been explored previously. Here, we present new sulfur concentration (30-1570 ppm) and isotope data ($\delta^{34}S$ = –2.5 to +3.8 ‰ and $\Delta^{33}S$ = –0.045 to +0.016 ‰; vs. Canyon Diablo Troilite) from a sample suite (N = 62) focused on subglacially erupted basaltic glasses obtained from Iceland's neovolcanic zones. Using these data along with trace element systematics to account for the effects of magmatic processes (degassing and immiscible sulfide melt formation) on $\delta^{34}S$, we show that primitive (MgO > 6 wt.%), undegassed glasses accurately record the $\delta^{34}S$ signatures of their mantle sources. Compared to the depleted MORB source mantle (DMM; $\delta^{34}S$ = –1.3±0.3 ‰), the Iceland mantle is shown to have a greater range of $\delta^{34}S$ values between –2.5 and –0.1%. Similarly, Icelandic basalts are characterized by more variable and negatively shifted $\Delta^{33}S$ values (–0.035 to +0.013 ‰) relative to DMM (0.004±006 ‰). Negative $\delta^{34}S$-$\Delta^{33}S$ signatures are most prominent in basalts from the Snæfellsnes Volcanic Zone and the Kverkfjöll volcanic system, which also have the lowest, most MORB-like $^{3}He/^{4}He$ (8–9 R/R_A, where R_A is the $^{3}He/^{4}He$ of air) and the highest Ba/La (up to 12) in Iceland. We propose that subduction fluid-enriched, mantle wedge type material, possibly present in the North Atlantic upper mantle, constitutes a low-$\delta^{34}S$-$\Delta^{33}S$ component in the Icelandic mantle. This suggests that volatile heterogeneity in Iceland, and potentially at other OIBs, may originate not only from diverse plume-associated mantle components, but also from a heterogeneous ambient upper mantle. By contrast, a set of samples with high $^{3}He/^{4}He$ (up to 25.9 R/R_A) and negative $\mu^{182}W$ anomalies define an ancient lower mantle reservoir with a near-chondritic $\Delta^{33}S$ and $\delta^{34}S$ signature of ~0 ‰. The difference between DMM and the high high-$^{3}He/^{4}He$ mantle may reflect separate conditions during core-mantle differentiation, or a previously unidentified flux of sulfur from the core to the high-$^{3}He/^{4}He$ reservoir.

3.2 Introduction

Mass-independent S isotope fractionation signatures (S-MIF; $\Delta^{33}S \neq 0$) measured in sulfides from the South Pacific Pitcairn and Mangaia hotspots provide remarkable evidence for the recycling of Archean sedimentary material through ocean island basalts (OIBs) (Cabral et al. 2013; Delavault et al. 2016). By contrast, the depleted upper mantle (DMM) as sampled by mid-ocean ridge basalts (MORBs) features chondritic $\Delta^{33}S$ values (~0‰) coupled with a sub-chondritic $\delta^{34}S$ signature (–1.28±0.33‰; Labidi et al. 2013), which requires that ~97% of Earth's sulfur partitioned to the core during core-mantle differentiation (Labidi et al. 2013, 2016; Labidi and Cartigny 2016). Determining the multiple sulfur isotopic composition of high-$^{3}He/^{4}He$ OIBs, which are thought to tap primordial lower mantle reservoirs (Yuan and Romanowicz 2017; Mundl-Petermeier et al. 2020), could provide additional constraints on the timing and nature of Early Earth processes. However, to date, published data are limited to two highly degassed high-$^{3}He/^{4}He$ samples from Samoa (Dottin et al. 2020a).

The mantle plume beneath Iceland samples what is thought to be the oldest and most primordial material available on Earth (i.e., a part of the deep mantle that has remained

unstirred by mantle processes since at least 4.45 Ga). Such an ancient origin is supported by the highest modern terrestrial mantle $^{3}He/^{4}He$ values (Harðardóttir et al. 2018), negative $\mu^{182}W$ anomalies (Mundl-Petermeier et al. 2019) and ^{129}Xe-excesses that could have been generated only in the earliest Hadean (Mukhopadhyay 2012). Additionally, the geochemical variability of Icelandic basalts suggests the presence of one or more recycled components and the ambient DMM in the mantle beneath Iceland (Hanan et al. 2000; Macpherson et al. 2005; Halldórsson et al. 2016a,b; Harðardóttir et al. 2018; Rasmussen et al. 2020). Due to the unique dual role of sulfur as a volatile element in near-surface processes and its strong partitioning to the core during core-mantle differentiation, the $\delta^{34}S$ and $\Delta^{33}S$ composition of Icelandic basalts could provide unique constraints on both the early planetary history of Earth and the deep recycling of sulfur through the mantle.

Previously published $\delta^{34}S$ values for Icelandic basalts range from –2.0 to 0.4‰ (Torssander 1989), but are difficult to interpret in terms of source values due to their highly degassed nature. In this study, we combine a newly developed HF extraction protocol (Labidi et al. 2012) with improved mass spectroscopy (Ono et al. 2006) to generate a high precision quadruple sulfur isotope dataset (^{32}S, ^{33}S, ^{34}S and ^{36}S) measured from dissolved sulfide (S^{2-}) in a large set of subglacial basaltic glasses. Importantly, our subglacial glass samples are largely devoid of secondary $\delta^{34}S$ shifts imposed by degassing and assimilation of seawater-derived sulfate. Instead, the data illuminate the effects of immiscible sulfide melt formation during crustal magmatic evolution on $\delta^{34}S$, and enables us to constrain the $\delta^{34}S$ and $\Delta^{33}S$ signatures of ancient and recycled mantle components beneath Iceland.

3.3 Samples & Methods

3.3.1 Samples

Our sample set (n = 62) focuses on Pleistocene subglacial glasses (n = 59; Fig. 3.1), i.e., the quenched rims of pillow lavas that were erupted beneath glaciers or ice sheets. The samples were collected from the three currently active on-land rift zones of Iceland, i.e., the Northern, Western (including the Reykjanes Peninsula) and Eastern Rift Zones (NRZ, WRZ and ERZ, respectively), that mark the boundary between the North American and Eurasian plates (Fig. 3.1). Samples were also collected from two active volcanic zones that are located away from the rifts: The South Iceland Volcanic Zone (SIVZ), which is the southward propagating tip of the ERZ, and the off-rift Snæfellsnes Volcanic Zone (SNVZ) (Fig. 3.1). Together, the samples represent most of the geochemical variability of the Icelandic magma series (0.1–10.1 wt.% MgO; Fig. 3.2). The rift zone lavas are tholeiitic, while the SIVZ and SNVZ lavas are transitional to alkaline. To assess the sulfur isotope systematics of a single magmatic lineage, 15 samples were included from the Kverkfjöll volcanic system, located in the south-eastern flank of the NRZ.

Most subglacial glasses (n = 45) were quenched under sufficiently high pressure to prevent significant S degassing (Supplementary Information). Moreover, the potential effect of crustal assimilation on S isotopic compositions of Icelandic basalts is likely to be small because of the higher S content of deep, undegassed melts (400-1600 ppm) relative to hydrothermally altered crust which is expected to be S-depleted due to degassing and leaching of sulfur by hydrothermal fluids (Alt et al. 1995; Gunnarsson-Robin et al. 2017). An additional advantage of the subglacial glasses is that they are unaffected by assimilation of seawater sulfate-derived S, a process which is known to increase both measured S concentrations and $\delta^{34}S$ values in submarine pillow glasses (Labidi et al.

2014). Absence of seawater-influence in Icelandic subglacial basalts is demonstrated by lack of elevated Cl/K ratios above ~0.10 (Halldórsson et al. 2016a). Thus, subglacial glasses closely capture the pre-eruptive melt compositions with respect to S concentrations and $\delta^{34}S$, presenting an advantage over the subaerial samples targeted in the only previous sulfur isotope appraisal in Iceland (Fig. 3.3a; Torssander, 1989) and many previous sulfur isotope studies on OIBs (e.g., Dottin et al. 2020a), where $\delta^{34}S$ (but not $\Delta^{33}S$) has been modified by shallow-level degassing. Three subaerial lavas (A-THO, B-ALK, I-ICE) are included to examine the effect of near-surface degassing on S concentrations and $\delta^{34}S$.

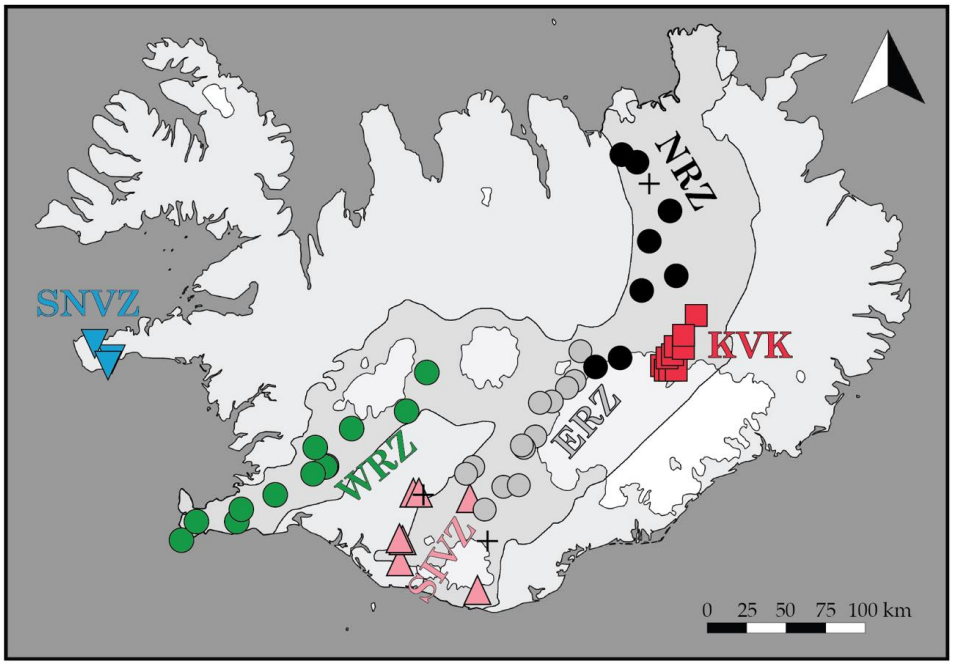

Figure 3.1 Map of Iceland showing sample locations of 59 subglacial pillow rim glass (circles, squares, triangles) and 3 subaerial lava samples (black crosses) analyzed in this study. The grey shaded area depicts presently active rift zones and the SIVZ propagating rift. Symbol types and colors used here to discriminate samples from different volcanic regions are maintained in all figures. Abbreviations: ERZ = Eastern Rift Zone, KVK = Kverkfjöll volcanic system, NRZ = Northern Rift Zone, SIVZ = South Iceland Volcanic Zone, SNVZ = Snæfellsnes Volcanic Zone, WRZ = Western Rift Zone and Reykjanes Peninsula.

3.3.2 Major and trace elements

Major element and S concentrations in glasses were determined by electron probe microanalysis (EPMA) using the JEOL JXA-8230 SuperProbe at the Institute of Earth Sciences, University of Iceland, following the protocol outlined in Bali et al. (2018). Sulfur concentrations were determined using a wavelength-dispersive spectrometer equipped with a PET crystal detector. A 10-15µm diameter diffuse beam was used, operating at a current of 20nA and a voltage of 15keV, with peak and background counting times of 100s. Pyrite was used as a primary standard, used for calibrating the S Kα peak. Reported concentrations represent averages of 6-11 spot analyses on polished glass grains, with typical standard deviations of ±5%. Sulfur concentrations were also determined for the USNM reference glasses VG-2 (1371±35ppm S, 1σ), 113716 (1004±15ppm S, 1σ) and A99 (119±37ppm S, 1σ), which agree with previously reported values (Table S7). Sulfur

concentrations determined for the Icelandic glasses A35, A36 and STAP-1 agree within uncertainty with previously reported S concentrations measured via secondary ion mass spectrometry (Taracsák et al. 2021)

Trace element analysis was performed using inductively coupled plasma mass spectrometry (ICP-MS) at the Scripps Institution of Oceanography, as well as laser ablation ICP-MS (LA-ICP-MS) at the Research School of Earth Sciences, Australian National University and at the Geological Survey of Finland. Additional details on analytical protocols are provided in the Supplementary Information.

3.3.3 Sulfur extraction protocol

Sulfur was extracted from powdered hand-picked glasses or rock fragments and converted to Ag_2S(s) via the coupled HF dissolution/Cr reduction method using an all-teflon extraction line (Labidi et al. 2012). Sulfide (S^{2-}) was released as H_2S(g) and flushed within a nitrogen stream via a water trap before being precipitated as Ag_2S(s) in a $AgNO_3$ trapping solution. The resultant Ag_2S(s) was heated at 80 °C for 3-6 hours, cleaned in triplicate using deionized water (18.2MΩ·cm) prior to being dried and weighed. Gravimetric extraction yields were calculated relative to the EPMA-derived S concentrations, and were found to vary between 60 and 110%. Rather than incomplete extractions, this relatively large spread in yields probably reflects a combination of variable crystal contents and $S^{6+}/\Sigma S$ of the extracted material as well as weighing errors (Supplementary Information). Importantly, no relationship between yields and measured S isotope values was identified (Figs. S1d and S2). Repeated extractions of the relatively aphyric glass STAP-1 returned an average yield of 91±11% (1σ, n = 10).

3.3.4 Sulfur isotope analysis

Sulfur isotope ratios were determined via dual-inlet isotope ratio mass spectrometry (IRMS) at the Stable Isotope Geobiology Laboratory at the Massachusetts Institute of Technology (MIT) following the methodology described by Ono et al. (2006, 2012). Here, approximately 2 mg of Ag_2S was converted into SF_6(g) via overnight reaction with F_2(g) at 300°C. The resultant SF_6(g) was initially purified cryogenically before being isolated by preparative tandem-column (molecular sieve 5 Å and HayesepQ) gas chromatography. The purified analyte was introduced to a Thermo Scientific MAT 253 IRMS instrument where the mass/charge ratios 127, 128, 129, 131, corresponding to $^{32,33,34,36}SF_5^+$ ions, were measured. The $^{34}S/^{32}S$ data are reported in δ-notation relative to the Vienna Cañon Diablo Troilite (VCDT), following:

$$\delta^{34}S_{sample} = \frac{(^{34}S/^{32}S)_{sample} - (^{34}S/^{32}S)_{VCDT}}{(^{34}S/^{32}S)_{VCDT}} \quad (1)$$

The VCDT scale is defined by the IAEA-S-1 standard with a $\delta^{34}S_{VCDT}$ value of -0.3‰ (Coplen and Krouse, 1998). Deviation from a mass-dependent fractionation line is reported in Δ notation as

$$\Delta^x S = \ln(\delta^x S + 1) - \theta^x \ln(\delta^{34} S + 1) \quad (2)$$

where x = 33 or 36, θ^{33} = 0.515 and θ^{36} = 1.90. Replicate analyses of an in-house Ag_2S standard (Ono-Ag_2S), the IAEA-S-1 reference material and three subglacial glasses are reported in Tables S1 and S2. Based on 18 analyses of Ono-Ag_2S during our sessions, long-term $\delta^{34}S$, $\Delta^{33}S$ and $\Delta^{36}S$ reproducibilities are estimated at 0.12, 0.004, and 0.086‰ (all 1σ), respectively (Fig. S1a-c). Repeat measurements of IAEA-S-1 yield respective $\delta^{34}S$, $\Delta^{33}S$ and $\Delta^{36}S$ values of -1.19±0.17‰, +0.100±0.004‰ and -0.669±0.068‰, relative to the MIT reference gas SG1 (Table S1). Given the lack of reference materials with certified $\Delta^{33}S_{CDT}$ and $\Delta^{36}S_{CDT}$ values, different laboratories have defined the CDT-scale via measurements of IAEA-S-1 and CDT (Table S3, Fig. S3). Because no CDT measurements have been conducted at the MIT lab, we anchor the CDT scale by defining the respective $\Delta^{33}S_{CDT}$ and $\Delta^{36}S_{CDT}$ values of IAEA-S-1 as +0.109 and –0.730‰, which represents the average of previously established IAEA-S-1 values (Supplementary Information). This makes it possible to compare our dataset with previously published multiple sulfur isotope datasets for MORBs and OIBs.

The relatively large uncertainty associated with $\Delta^{36}S$ measurements results from the low natural abundance of ^{36}S (0.015%) and potential isobaric interferences on mass 131 (Ono et al. 2006). While $\Delta^{36}S$ data is reported for completeness, its large uncertainty relative to the subdued variability within our samples limits its utility beyond that of $\Delta^{33}S$.

3.4 Results

Sulfur concentration and isotope data as well as major and trace element abundances are reported in Tables S4 and S5.

Sulfur concentrations. The samples (including both subaerial lavas and subglacial glasses) display variable S concentrations from 30 to 1570 ppm. Overall, S concentrations increase from 300-800ppm in the most primitive subglacial glasses (9-10 wt.% MgO) to a peak of 1200-1570ppm at 6 wt.% MgO, before decreasing to about 1100 ppm at 4 wt.% MgO (Fig. 3.2a). A subset of the subglacial glasses deviates from these trends toward lower S concentrations (Fig. 3.2a). The lowest sulfur contents are seen in the subaerial lavas (30 to 70 ppm). The main trend closely follows the pre-eruptive sulfur concentrations as recorded by melt inclusion datasets available for Icelandic basalts (Fig. 3.2a). Of the other examined trace elements, only Cu shows a similar trend (Fig. 3.2b). Hereafter, the two distinct melt evolution trends defined by S and Cu are referred to as Phase 1 (MgO > 6 wt.%) and Phase 2 (MgO < 6 wt.%).

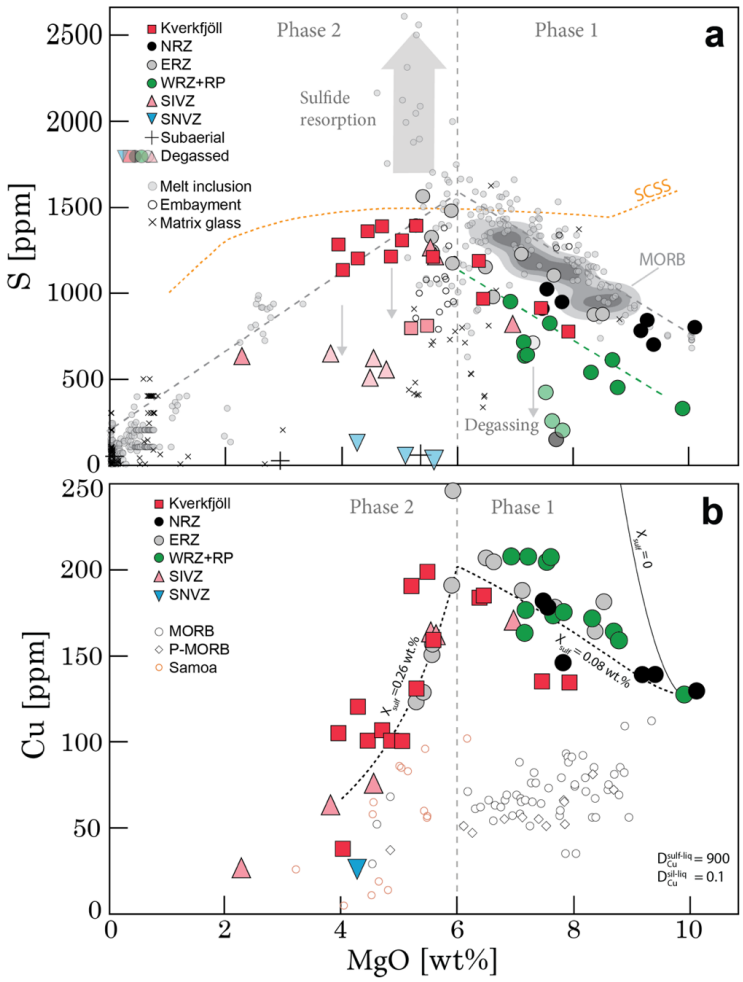

Figure 3.2 Sulfur and copper systematics. (a) S versus MgO. Data from this study are superimposed on published melt inclusion data from Iceland (compilation from Ranta et al. 2021). The melt inclusion data define an undegassed S evolution trend (dashed grey lines) with an inflection point at MgO ≈ 6 wt.%, separating two distinct phases of melt evolution. In Phase 1, the WRZ basalts define a parallel, lower-S trend, indicated by the green dashed line. Over-enrichments in S are recorded by a subset of basaltic melt inclusions, which at other localities has been explained by resorption of sulfides (Reekie et al. 2019; Wieser et al. 2020). Samples deemed to have lost a significant amount of S by degassing are shown as transparent symbols (Supplementary Information). The $SCSS^{2-}$ curve in (a) (orange) in was calculated for the 2.5 kbar model after Fortin et al. (2015). (b) Cu versus MgO. A clear inflection point at MgO ≈ 6 wt.% signals the onset, or acceleration, of sulfide fractionation. The observed trends indicate fractionation of about 0.08 wt.% sulfide melt between MgO = 6–10 wt.% (Phase 1) and 0.26 wt.% between MgO = 4-6 wt.% (Phase 2) (dashed grey line; see Supplementary material for model details). The modelled fractional crystallization trajectory for X_{sulf} = 0 (black line) greatly overestimates Cu concentrations. MORB (white circles) data are sourced from Labidi et al. (2012, 2013, 2014) and Labidi and Cartigny (2016). Plume-influenced MORB data (P-MORB) covering the LOMU, Discovery and Shona anomalies in the South Mid-Atlantic Ridge are from Labidi et al. (2013). Samoan (orange circles) data are from Labidi et al. (2015).

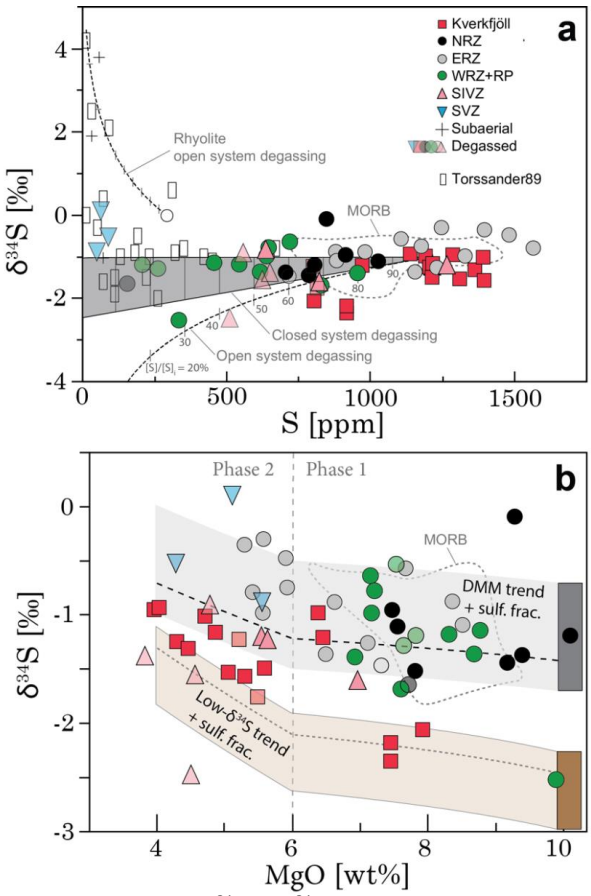

Figure 3.3 Effects of magmatic processes on $\delta^{34}S$. (a) $\delta^{34}S$ versus S concentrations. The effect of degassing on δ34S in Icelandic samples is clearly illustrated by generally increasing $\delta^{34}S$ at low S concentrations. Large scatter in previously published data on Iceland (white rectangles; T89; Torssander 1989) demonstrates the advantage of using relatively undegassed subglacial glasses for studying pre-eruptive S isotope compositions. All undegassed Icelandic basalts have negative $\delta^{34}S$ values. Shaded grey field represents closed system degassing of a basaltic melt with δ34S = -1 % and S = 1200 ppm, assuming a fractionation factor of $\Delta^{34}S_{gas-melt}$ = 0 to +1.4 ‰. Lower dashed line shows open system degassing path for the same melt for of $\Delta^{34}S_{gas-melt}$ = +1.4. Upper dashed model line shows the effect open system degassing of a hypothetical undegassed rhyolitic melt with S = 300ppm and $\delta^{34}S$ = 0‰ (white circle). Model details are explained in the Supplementary Information. (b) $\delta^{34}S$ versus MgO. Redox buffering of S following sulfide fractionation may lead to increasingly positive $\delta^{34}S_{sulfide}$ values during melt evolution (shaded fields). However, a DMM-like mantle component cannot by itself explain the most negative $\delta^{34}S_{sulfide}$ values in the primitive (MgO > 6 wt.%) samples. Instead, an additional mantle component with more negative $\delta^{34}S$ signature is implicated. Modelled $\delta^{34}S$sulfide trajectories for hypothetical DMM (MgO = 10 wt%, $\delta^{34}S$ = –1.44 ‰, S = 750 ppm, $S^{6+}/\Sigma S$ = 0.18; similar to NAL-611) and "low-$\delta^{34}S$ component" (MgO = 10 wt%, $\delta^{34}S$ = –2.5 ‰, S = 400ppm, $S^{6+}/\Sigma S$ = 0.24; similar to MID-1) primary mantle melts are shown by dashed lines. The NRZ sample HS92-15 is an outlier with a clearly less negative $\delta^{34}S$ value of -0.1‰ compared to other NRZ samples. Degassed samples are shown for reference (transparent symbols). MORB field drawn from the references given in Fig. 3.2.

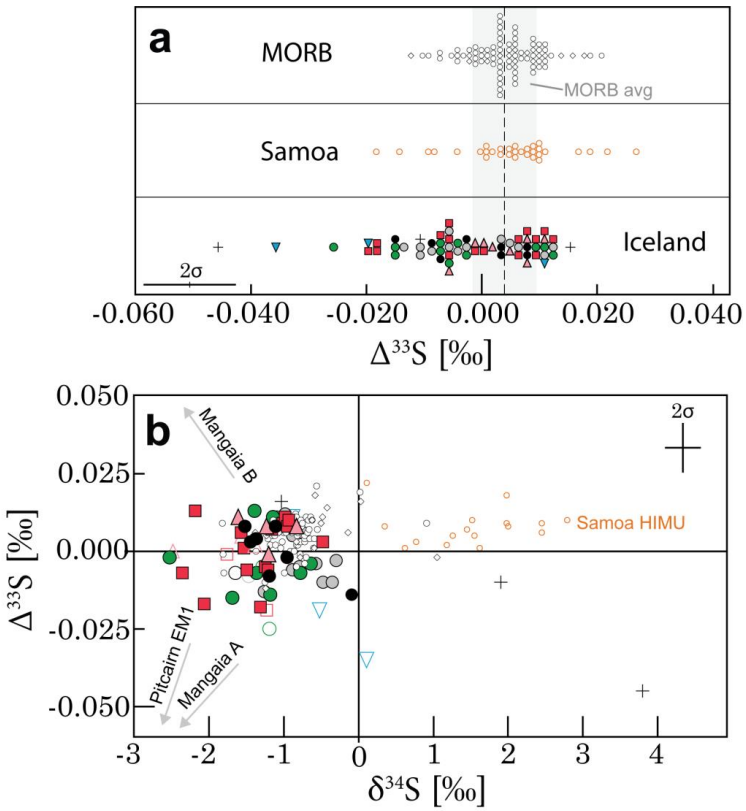

Figure 3.4 (a) A compilation of basaltic glass-derived $\Delta^{33}S$ data. Iceland samples overlap with MORBs and Samoan OIBs but are shifted toward more negative $\Delta^{33}S$. Negative $\Delta^{33}S$ values in MORBs are uncommon. Grey field and dashed line show the MORB average (0.004±0.006, 1σ). (b) $\Delta^{33}S$ vs. $\delta^{34}S$ systematics. Available hotspot S isotope data from Iceland, Samoa (orange circles; Labidi et al. 2015; Dottin et al. 2020a, Dottin et al. 2021), Mangaia and Pitcairn seem to describe a positive correlation between $\Delta^{33}S$ and $\delta^{34}S$ which is also present in the Archaean sediment record (Johnston et al. 2011). However, a break from this trend is represented by the Mangaian HIMU endmember B ($\delta^{34}S$ = –7.5‰, $\Delta^{33}S$ = +0.200‰; Dottin et al. 2020b). Notably, very few data plot in the 2nd quadrant. Grey arrows point toward the Mangaia HIMU endmember A ($\delta^{34}S$ = –22‰, $\Delta^{33}S$ = –0.600‰; Cabral et al. 2014) and B and the Pitcairn EM1 component ($\delta^{34}S$ = –6 ‰, $\Delta^{33}S$ = –0.800 ‰; Delavault et al. 2016). Degassed Samoan samples from Dottin et al. (2020), and MORBs that have assimilated seawater sulfate have been filtered out following Labidi et al. (2014). Symbols and MORB data as in Fig. 3.2.

Sulfur isotopes. The overall variation in $\delta^{34}S$ captured within our Icelandic samples (subaerial and subglacial) is –2.5 to +3.8‰ (Fig. 3.3a). This range is similar to previously reported $\delta^{34}S$ data for Icelandic lavas (Torssander 1989; Fig. 3.3a) and exceeds the $\delta^{34}S$ range displayed by MORBs (–1.8 to +1.0‰, n = 68; Labidi and Cartigny 2016 and sources therein). Nevertheless, positive values are clearly linked to degassed samples (Fig. 3.3a; Section 4.1; Torssander 1989), while undegassed basaltic glasses display a more limited range of $\delta^{34}S$ values from –2.5 to –0.1‰. Thus, Icelandic basalts lack the positive $\delta^{34}S$ values characteristic of OIBs from Samoa (Labidi et al. 2015) and the Canary Islands (Beaudry et al. 2018). The most negative $\delta^{34}S$ values are observed in the most primitive Kverkfjöll basalts NAL-356 (–2.3 ‰) and NAL-585 and (–2.0‰) and in the highly primitive (MgO = 9.9 wt.%) and geochemically depleted WRZ sample MID-1 (–2.5 ‰). The $\delta^{34}S$ values generally increase with decreasing MgO, a trend that is most clear in the ERZ and Kverkfjöll sample suites (Fig 3.3b).

The $\Delta^{33}S$ values of the entire dataset vary between –0.045 and +0.016‰, or between –0.035 to +0.010‰ (±0.013, 1σ) if subaerial samples are excluded (Fig. 3.4). The Icelandic glasses have an average $\Delta^{33}S$ value of -0.002±0.010 ‰ (1σ, n = 59) and extend to more negative values compared to Samoan OIBs (0.005±0.009‰; 1σ, n = 32; Labidi et al. 2015, Dottin et al. 2020a, Dottin et al. 2021) and MORBs (0.004±0.006‰ (1σ, n = 68; Labidi et al. 2012, 2013, 2014, Labidi and Cartigny 2016; Fig. 3.4). Although their average $\Delta^{33}S$ values overlap within 1σ, a statistical student's t test indicates that, as a whole, Icelandic basalts reflect a different population from both Samoan OIBs and MORBs (p value < 0.0015).

3.5 Discussion

3.5.1 Magmatic degassing and S oxidation state

Sulfur degassing from low-H_2O basaltic magmas typically commences at pressures of ~150MPa (Wallace and Edmonds 2011). Thus, degassing should not significantly affect the pre-eruptive S inventory of Icelandic basalts, which are typically stored at considerably higher pressures of ~200-600MPa (Neave and Putirka 2017). Therefore, any S degassing observed in subglacial glasses is related to syn-eruptive degassing (Fig. 3.2a; Supplementary Information). Degassing can lead to either positive or negative $\delta^{34}S$ fractionation, expressed as $\varepsilon^{34}S_{gas-melt}$ (see Eq. 13 for definition; note that ε is used here for the fractionation factor to avoid confusion with Δ, which is used for denoting S-MIF). The sign of $\varepsilon^{34}S_{gas-melt}$ is determined by the S speciation of the gas, $SO_2/(SO_2+H_2S)$, and the melt, $S^{6+}/\Sigma S$, respectively (Fig. S4; Supplementary Information). For example, the sign of $\varepsilon^{34}S_{gas-melt}$ is positive during degassing of oxidized gases from reduced melts (high $SO_2/(SO_2+H_2S)$ and low $S^{6+}/\Sigma S$) and negative during the converse (low $SO_2/(SO_2+H_2S)$ and high $S^{6+}/\Sigma S$; Fig. S4).

The $S^{6+}/\Sigma S$ has been previously measured in three Icelandic samples included in this study (A35, A36 and STAP-1) at 0.03 to 0.09±0.20 (Taracsák et al. 2021). These values are consistent with a $S^{6+}/\Sigma S$ range between c. 0.05 and 0.40 estimated with Eq. 21 for Icelandic basaltic melts (Supplementary Information), and with a range of c. 0.05 to 0.30 measured in similarly oxidized, undegassed OIBs at Samoa and Hawaii (Jugo et al. 2010, Labidi et al. 2015, Brounce et al. 2017). Using this range of $S^{6+}/\Sigma S$ and $SO_2/(SO_2+H_2S) > 10$, calculated with the D-Compress program (Burgisser et al. 2015; Fig. S5), we estimate a modest, and positive $\varepsilon^{34}S_{gas-melt}$ between +0.3 to +1.4‰ (Fig. S4a). Thus, only minor $\delta^{34}S$ fractionation of less than –0.3 ‰ is expected for the melt phase during up to 20 % degassing (Fig. 3.3a). Therefore, identifying and filtering out samples that have only experienced minor amounts of degassing is not necessary, as they closely record the $\delta^{34}S$ values of the undegassed melts.

In contrast, degassing-induced changes in $\delta^{34}S$ toward more positive values are seen clearly in more evolved subaerial lavas from this study (A-THO, I-ICE) and from Torssander (1989) (Fig. 3.3a). This indicates a negative $\varepsilon^{34}S_{gas-melt}$ fractionation factor, which may suggest that these melts are more oxidized (Fig. S4b). As the $\delta^{34}S$ values are affected by degassing, the degassed samples (subaerial lavas, A1, A3, A6, A32, THOR-1, STORID-1, SELJA-1, SAL-601, BOTN-1, HNAUS-1, OLAF-1, NAL-460, KVK-202, KVK-205) are excluded from Figs. 5a, 6a and 7a and are not considered in subsequent discussion on $\delta^{34}S$ signatures.

3.5.2 Sulfide immiscibility

Quantifying sulfide melt formation

Immiscible sulfide melts effectively sequester S and chalcophile elements, such as Cu, from magmas that are sulfide saturated (Bézos et al. 2005; Jenner et al., 2010, Reekie et al. 2019). The observed trend of decreasing Cu concentrations with decreasing MgO below c. 6 wt.% (Fig. 3.2b) clearly implicates sequestration of Cu by an immiscible sulfide melt, as has been previously noted in Icelandic whole-rock data (Momme et al. 2003). An analogous trend is observed for S and S/Dy, but is less distinct due to degassing-induced scatter (Figs. 3.2a and S9b).

The kinks observed at MgO = 6 wt% for Cu, S and Cu/Y define the boundary between Phase 1 (between MgO = 6-10 wt.%) and Phase 2 (MgO = 4-6 wt.%; Figs. 3.2 and S9). Similar phases have been identified for Samoan basalts (Labidi et al., 2015). The weight fraction of fractionated sulfide (X_{sulf}) during both phases can be quantified using

$$X_{sulf} = \frac{D_{Cu}^{min-liq} - D_{Cu}^{sil-liq}}{D_{Cu}^{sulf-liq} - D_{Cu}^{sil-liq}} \quad (3)$$

where $D_{Cu}^{min-liq}$, the empirical bulk partition coefficient of Cu between crystallizing minerals and silicate melt, is estimated using the observed Cu trends (see Labidi et al. 2014; Supplementary Information). The partition coefficients of Cu between silicate minerals and silicate melt, $D_{Cu}^{min-liq}$, and between sulfide and silicate melts, $D_{Cu}^{sulf-liq}$ are taken as 0.1 and 900, respectively (Lee et al. 2012; Labidi et al. 2014). This yields X_{sulf} = 800ppm for Phase 1 and 2580ppm for Phase 2 for Icelandic melts. Physical evidence of sulfide saturation during Phase 2 is preserved as Cu-rich sulfide globule inclusions observed in melt inclusions (Fig. S8). However, the apparent early fractionation of sulfides during Phase 1 may be an artefact of the sulfide fractionation model, as the relatively low S contents in Phase 1 melts fall below [$SCSS^{2-}$] (S concentrations at sulfide saturation; Fig. 3.2a; Fortin et al. 2015). Alternatively, the lower-than-expected increase of Cu and the negatively sloping Cu/Y trend during Phase 1 could be a result of melt-mixing processes (c.f. Shorttle and Maclennan 2011).

We interpret these results to show that Icelandic melts become sulfide saturated below MgO = 6 wt.% (cf. Halldórsson et al. 2018). In this respect, Icelandic melts contrast with MORBs, as MORBs fractionate sulfides throughout their crustal evolution path (Bézos et al. 2005; Fig. 3.2b). Instead, this behavior is more similar to arc-related magmas, where the onset of magnetite crystallization leads a reduction in melt f_{O2}, triggering sulfide saturation at about 2-3 wt.% MgO (Jenner et al. 2010), a process also suggested to explain the Cu versus MgO trend observed at Samoa (Labidi et al. 2015). However, in the Icelandic magma series, the onset of Phase 2 clearly predates the onset of magnetite formation, which is observed only in glasses with MgO < 5 wt.%. A more complex pattern of multiple starts and stops in sulfide saturation during magmatic evolution that are reported for basalts from the Kilauea volcano in Hawaii (Wieser et al., 2020) are not strictly required to explain the Iceland data, although we cannot rule out the possibility that some melts were sulfide saturated at higher pressures and became undersaturated upon ascent to higher level crustal magma chambers (Reekie et al. 2019; Wieser et al. 2020).

Effect of sulfide fractionation on $\delta^{34}S$ evolution of Icelandic basalts

In a non-redox buffered system, sulfide fractionation leads to an increase in the melt $S^{6+}/\Sigma S$ and thereby an increase in $\delta^{34}S_{\Sigma S}$ values (where $\Sigma S = S^{6+} + S^{2-}$) because S^{6+} is isotopically heavier than S^{2-} ($\varepsilon^{34}S_{sulfate\text{-}sulfide} \approx +3‰$ at T = 1250°C; Supplementary Information). In this case, no change in melt $\delta^{34}S_{sulfide}$ values should be observed (Fig. S7; Labidi et al. 2015). However, if $S^{6+}/\Sigma S$ is buffered during sulfide fractionation by another multivalent element, conversion of S^{6+} to S^{2-} leads to a gradual increase in both melt $\delta^{34}S_{\Sigma S}$ and $\delta^{34}S_{sulfide}$ (Fig. 3.3b; Supplementary Information). This buffering effect means that the $\delta^{34}S$ values of moderately oxidized basalts that have fractionated sulfides, like those in Iceland, may be more positive than their mantle sources (c.f. Labidi et al. 2015). Iron may act as a redox buffer through the following electron-exchange reaction (Fig. S6; Jugo et al. 2010, Nash et al. 2019):

$$S^{6+} + 8Fe^{2+} \rightleftharpoons S^{2-} + 8Fe^{3+} \quad (4)$$

In the Kverkfjöll samples, a subtle trend of increasing $\delta^{34}S_{sulfide}$ from –2.2‰ to –0.9‰ is observed during melt evolution between 7.5 to 4.0 wt.% MgO (Fig. 3.3b). A parallel $\delta^{34}S_{sulfide}$ versus MgO trend defined by the WRZ-ERZ-NRZ samples is offset to more positive $\delta^{34}S_{sulfide}$ values by ~0.5‰. The observed trends could be explained by redox buffering-induced $\delta^{34}S$ fractionation during sulfide melt formation. However, the large $\delta^{34}S$ variability in more primitive samples (MgO > 6 wt.%) cannot be explained by melt derivation from a homogenous mantle, even if sulfide formation during Phase 1 is allowed (Fig. 3.3b). Instead, the data are most easily explained by primitive melt variability of $\delta^{34}S_{sulfide}$ between approximately –2.5 and –0.1‰, as the low $\delta^{34}S_{sulfide}$ values of the Kverkfjöll samples NAL-356 and NAL-585, and the WRZ sample MID-1 require a parental melt with a distinctly lower $\delta^{34}S_{sulfide}$ compared to the remaining WRZ-ERZ-NRZ samples.

3.5.3 Sulfur heterogeneity in the Iceland mantle

Given that S isotope fractionation during partial melting is negligible, the $\delta^{34}S$, $\Delta^{33}S$ and $\Delta^{36}S$ values of mantle protoliths are passed on to primary mantle melts (Labidi and Cartigny 2016). While subsequent melt mixing in lower crustal or sub-Moho magma reservoirs is known to blunt the most extreme mantle source signatures, bulk measurements of relatively primitive glasses are able to capture a major part of the chemical heterogeneity in the Iceland mantle (Shorttle and Maclennan 2011). Other types of crustal magmatic processing, such as sulfide immiscibility and crustal assimilation, are only expected to have a minor effect on the $\delta^{34}S$ signatures of primitive (MgO > 6 wt.%), undegassed samples (Sections 4.1 and 4.2). We consider the $\delta^{34}S$ values of such samples to be representative of primary melt compositions within instrumental error. Degassed samples, and samples with MgO lower than 6 wt.% are filtered out in Figs. 6a, 7a and 8a. The $\Delta^{33}S$ values are not affected by either degassing or sulfide melt fractionation (Labidi et al. 2014), so all $\Delta^{33}S$ glass analyses are thought to reflect source values and are plotted in Figs. 5-8.

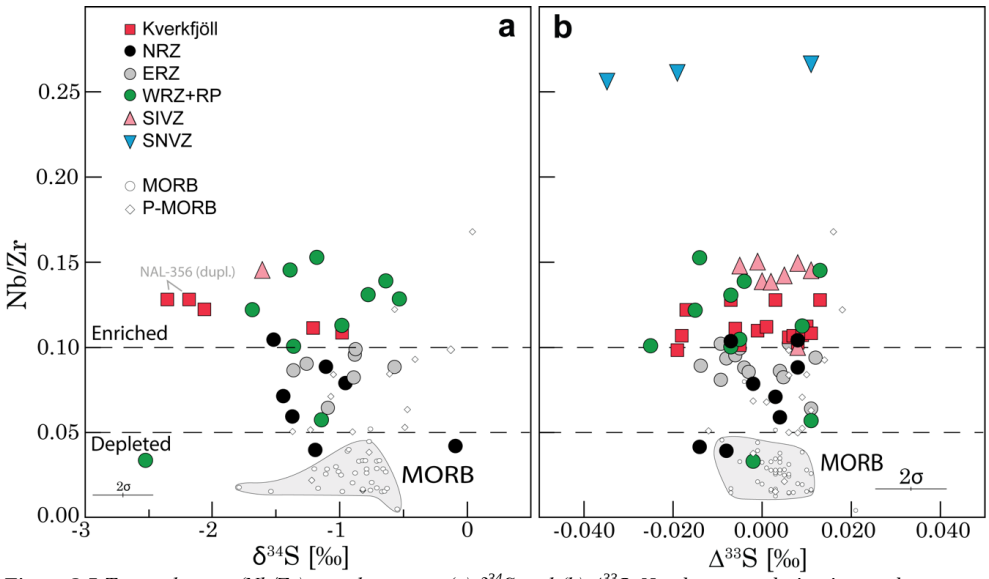

Figure 3.5 Trace element (Nb/Zr) enrichment vs. (a) $\delta^{34}S$ and (b) $\Delta^{33}S$. No clear correlation is seen between trace element enrichment, as measured by Nb/Zr, and $\delta^{34}S$ or $\Delta^{33}S$. The greatest variation in $\delta^{34}S$ values is observed in both the depleted (Nb/Zr < 0.05) and the enriched glasses (Nb/Zr > 0.10), while moderately enriched samples fall within the MORB field (light grey). Both depleted and enriched samples trend toward negative $\Delta^{33}S$ compared to MORBs. Samples that have experienced degassing or considerable sulfide fractionation (MgO < 6 wt.%) may have altered $\delta^{34}S$ values and have been filtered out from (a) (see sections 4.1 and 4.2). MORB samples that have assimilated seawater sulfate have been filtered out from (a) following Labidi et al. (2014). The entire dataset is shown in (b), as $\Delta^{33}S$ is not affected by magmatic processes. MORB and P-MORB data as in Fig. 3.2.

Mantle sulfur isotopic signatures and relationship to other mantle source indicators

The large $\delta^{34}S$ variability identified in the Iceland mantle ($\delta^{34}S$ = –2.5 to –0.1‰) exceeds that of unaltered MORBs and points to mantle heterogeneity with respect to sulfur (Figs. 3.3, 3.5-3.7). If sulfur shares a common history with known Icelandic mantle components, a correlation is expected between $\delta^{34}S$-$\Delta^{33}S$ and traditional tracers of mantle heterogeneity, such as Nb/Zr, $^{3}He/^{4}He$ and $^{206}Pb/^{204}Pb$.

The three most depleted samples (Nb/Zr < 0.05) show the greatest variation in $\delta^{34}S$ values, representing the full of range of Icelandic mantle values of –2.5 to –0.1‰ (Fig. 3.5a). Similar, but slightly smaller $\delta^{34}S$ variation of -2.3 to -0.6‰ is found in the most enriched samples (Nb/Zr > 0.10). Whereas enriched trace element signatures in Iceland are tied to enriched radiogenic isotope signatures (Shorttle and Maclennan 2011), the apparent lack of correlation of Nb/Zr with $\delta^{34}S$ or $\Delta^{33}S$ (Fig. 3.5) indicates that sulfur is partly decoupled from the lithophile, non-volatile elements and their isotopes. However, $\delta^{34}S$-$\Delta^{33}S$ signatures can be tied to Icelandic mantle components using available $^{206}Pb/^{204}Pb$ and $^{3}He/^{4}He$ data (Figs. 3.6, 3.7 and S11), which have been used to demarcate primordial, recycled, and local DMM components in the Iceland plume (e.g., Hanan et al. 2000, Füri et al. 2010). Four mantle components are required to explain the combined $^{3}He/^{4}He$-$\delta^{34}S$-$\Delta^{33}S$-$^{206}Pb/^{204}Pb$ systematics:

(1) Local DMM contributes a low-$^{3}He/^{4}He$ (8±1 R_A) Icelandic end-member with typical MORB-like $\delta^{34}S$ = -1.3‰ and $\Delta^{33}S$ = 0‰. The samples closest to the DMM component come from the NRZ (cf. Hanan et al. 2000).

(2) Plume 1 component has a moderate $^{206}Pb/^{204}Pb$ of 18.2-18.5 and is tied to one of the highest $^{3}He/^{4}He$ of 33.6 R_A measured in present-day hotspots (Jackson et al. 2020), representing an ancient lower mantle component. This component has DMM-like $\Delta^{33}S$ of 0‰. The $\delta^{34}S$ signature of the Plume 1 component is less negative than DMM (-1.3‰), approaching a chondritic value of ~0‰ (see section 4.4). Plume 1 is expressed most clearly by the high-$^{3}He/^{4}He$ ERZ-NRZ basalts in central Iceland, close to the suggested center of the plume (Rasmussen et al. 2020).

(3) Plume 2 is a second Icelandic high-$^{3}He/^{4}He$ component (up to 25.7 R_A) marked by more radiogenic $^{206}Pb/^{204}Pb$ (19.1-19.3) compared to the Plume 1 component (Mundl-Petermeier et al. 2019, Jackson et al. 2020). It is exclusively sampled by the propagating rift volcanoes in the SIVZ, which have an average $\Delta^{33}S$ value of 0.004±0.005‰. The $\delta^{34}S$ signature of Plume 2 is assumed to be –1.6‰ based on the most primitive SIVZ sample THRI-2. Plume 2 component is thought to represent intermingling of primordial mantle with recycled oceanic crust (Rasmussen et al. 2020). This proposed origin of Plume 2 component is consistent with its apparent DMM-like $\delta^{34}S$-$\Delta^{33}S$ signature, as the $\delta^{34}S$ of oceanic lithosphere is approximately preserved during subduction to the deep mantle (Alt 1995; Li et al. 2020).

(4) To explain the low-$\delta^{34}S$ trend defined by Kverkfjöll lavas (Section 4.2; Fig. 3.3b) and the tendency of Iceland lavas toward negative $\Delta^{33}S$ signatures compared to DMM (Fig. 3.4), we propose a previously unrecognized Icelandic mantle component – Enriched Mantle Wedge (EMW). Based on the $^{3}He/^{4}He$-$\delta^{34}S$-$\Delta^{33}S$ systematics (Fig. 7), EMW is assigned negative $\delta^{34}S_{\Sigma S}$ and $\Delta^{33}S$ values of –2.5‰ and –0.040%, respectively, and a DMM-like $^{3}He/^{4}He$ of 8 R_A. EMW is sampled most clearly by Kverkfjöll lavas, but its influence is seen across lavas from all rift zones as negatively trending $\delta^{34}S$ and $\Delta^{33}S$ values with decreasing $^{3}He/^{4}He$ (Fig. 3.7). The three lowest-$\delta^{34}S$ samples (MID-1, NAL-356, NAL-585) all have similar $^{206}Pb/^{204}Pb$ of 18.4-18.5, which is taken as the signature of EMW. The SNVZ basalts also have MORB-like $^{3}He/^{4}He$ and the lowest $\Delta^{33}S$ (down to –0.035‰) in Iceland, suggesting contributions from the EMW component (Fig. 3.7b). However, as the SNVZ samples are evolved and highly degassed, their source $\delta^{34}S$ signature cannot be inferred.

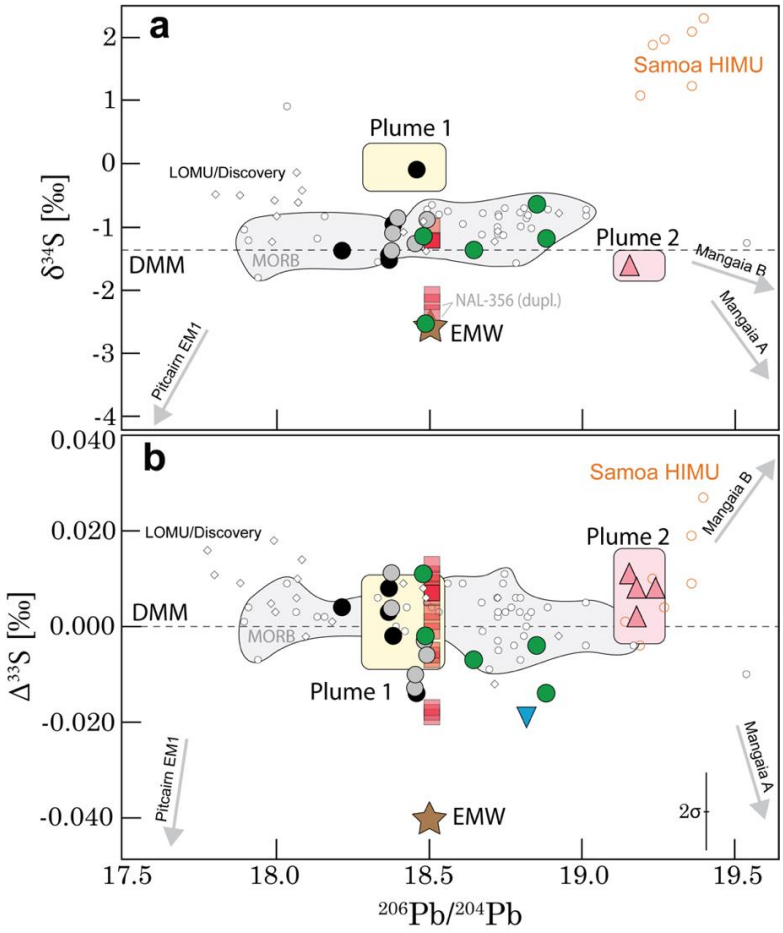

Figure 3.6 Lead and sulfur isotope relationships. (a) $\delta^{34}S$ versus $^{206}Pb/^{204}Pb$. The $\delta^{34}S$ values of Icelandic glasses partly overlap with those of MORBs (grey field). Notably, the anomalously negative $\delta^{34}S$ values at Kverkfjöll and the WRZ sample MID-1 are both associated with a $^{206}Pb/^{204}Pb$ value of ~18.5. (b) Icelandic glasses show a greater variability in $\Delta^{33}S$ values compared to MORBs and have overall negative $\Delta^{33}S$ values that seem to converge at the EMW component. Notably, the SIVZ samples, that have the highest $^{206}Pb/^{204}Pb$ in Iceland (> 19.0) lack anomalous $\Delta^{33}S$ values. Pb isotope data for the Icelandic samples are sourced from Halldórsson et al. (2016a) and Jackson et al. (2020). The value $^{206}Pb/^{204}Pb$ = 18.508 reported for KVK-77 by Halldórsson et al. (2016a) is assumed for all KVK samples (transparent symbols). EMW = subduction fluid-enriched mantle wedge. Symbols and MORB data as in Fig. 3.2.

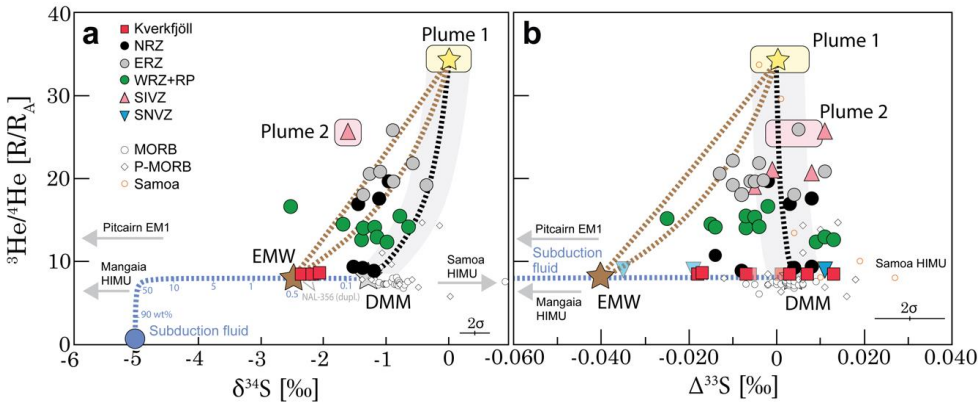

Figure 3.7 Sulfur and helium isotope relationships. (a) The $^3He/4He$ vs. $\delta^{34}S$ systematics of Icelandic lavas can be explained by three-component mixing of DMM ($^3He/^4He = 8R_A$, $\delta^{34}S = –1.3‰$; grey star), Plume 1 mantle ($^3He/^4He = 33.6R_A$, $\delta^{34}S = 0‰$; yellow star) and EMW (subduction fluid-enriched mantle wedge; $^3He/^4He = 8R_A$, $\delta^{34}S = -2.5‰$; brown star). The Plume 2 component (cf. Fig. 3.6) sampled by SIVZ lavas (pink field) has high $^3He/^4He$ (~$25R_A$) and $\Delta^{33}S \approx 0‰$, but its $\delta^{34}S$ signature is only constrained by a single sample. The EMW component that gives rise to the low-$\delta^{34}S$ and low $^3He/^4He$ Kverkfjöll lavas is created by adding ~0.5 wt.% subduction derived fluid (blue circle) with a composition of $\delta^{34}S = –5‰$, S = 9620 ppm, similar to subduction fluids released from metasediments during devolatilization at ~100 km depth (Li et al. 2020). (b) $^3He/^4He$ versus $\Delta^{33}S$. There is a clear tendency toward negative $\Delta^{33}S$ values in Icelandic lavas compared to DMM. This can be explained if the EMW component has a $\Delta^{33}S$ value of –0.040‰, which requires a subduction fluid component with $\Delta^{33}S = –0.130‰$. The $\Delta^{33}S$ variability decreases with increasing $^3He/^4He$ to values ~0 ‰, which is taken as the $\Delta^{33}S$ signature of the Plume 1 component. Two SNVZ (BOTN-1 and OLAF-1) and Kverkfjöll samples (KVK-147 and KVK-168) with degassed $^3He/^4He$ are projected to the $^3He/^4He = 9.0$ and $8.5R_A$, which are representative of Snæfellsnes and Kverkfjöll lavas and geothermal fluids, respectively (Harðardóttir et al. 2018). Binary mixing curves are shown by dashed lines. Two binary mixing lines between EMW and Plume are shown scenario with [He]Plume1/[He]EMW of 1 (straight line) and 0.5 (curved line). End-member compositions are given in Table S6. The composition of the EMW component is chosen arbitrarily as the least extreme composition that is required to explain the most negative $\Delta^{33}S$ and $\delta^{34}S$ values. Sample filtering, references and the Mangaia HIMU, Samoa and Pitcairn EM1 compositions as in Figs. 3-4. Helium isotope data for the Iceland samples from Macpherson et al. (2005), Füri et al. (2010) and Halldórsson et al. (2016b). MORB and P-MORB data as in Fig. 3.2.

Origin of recycled sulfur in the Iceland mantle

Previous observations of non-zero $\Delta^{33}S$ values in OIBs from Mangaia (Cabral et al. 2014; Dottin et al. 2020b) and Pitcairn (Delavault et al. 2016) provide evidence for the resurgence of deep recycled Archaean sediments – the only known major terrestrial reservoir with S-MIF signatures ($\Delta^{33}S$ between –2.5 and 11.5‰; Johnston 2011). The large negative $\Delta^{33}S$ anomalies at Pitcairn and Mangaia (down to –0.8 ‰) are coupled to highly negative $\delta^{34}S$ (Cabral et al. 2014, Delavault et al. 2016). Subducted sediments are also thought to form a positive $\delta^{34}S$ end-member in the MORB source mantle (Labidi et al. 2013, 2014), the Samoan EM2 component (Labidi et al. 2015, Dottin et al. 2021), as well as the Canary Islands HIMU component (Beaudry et al. 2018), which all lack resolvable $\Delta^{33}S$ anomalies.

Negative $\Delta^{33}S$ and $\delta^{34}S$ values in Icelandic basalts are tied to a mantle component with MORB-like $^3He/^4He$ and $^{206}Pb/^{204}Pb$ (Figs. 6-7 and S11), but also elevated Ba/La (Fig. S10). These characteristics are compatible with subduction fluid-enriched mantle wedge (EMW) type component, i.e., a DMM-like component that has been enriched with sediment-derived fluids from a subducting plate (cf. Richter et al. 2020).

Influx of subduction-related volatiles to the upper mantle from subducting slabs is thought to contribute to the volatile heterogeneity of MORB sources (Dixon et al. 2017), including the North Atlantic mantle, as well as Iceland (Halldórsson et al. 2016b; Hauri et al. 2018, Richter et al. 2020). As ambient DMM constitutes a geochemical endmember in Icelandic basalts (Hanan et al. 2000), it is worthwhile to entertain the possibility that the EMW component represents a local upper mantle anomaly resulting from shallow subduction-fluid metasomatism, rather than a deep-sourced plume component.

Plausible past subduction events in the region that could have produced the EMW component include Palaeozoic subduction episodes that lead to the closure of the proto-Atlantic Iapetus ocean (Halldórsson et al. 2016b; Hauri et al. 2018) and the Early Cretaceous South Anuyi subduction event (145-120 Ma; Richter et al. 2020).

Subduction fluids are potent agents of mantle metasomatism, and may transport 6-20% of the S budget of the slab to the the mantle wedge region at 30-230km depth (Jégo and Dasgupta 2013; Li et al. 2020). Fluids equilibrated with subducting metasediments at ~100km depth have highly negative $\delta^{34}S$ values (as low as -8 ‰) and high sulfur concentrations of ~1 wt.% (Li et al. 2020). Sediment-derived fluids could also acquire measurable negative $\Delta^{33}S$ signatures through even minor incorporation of Archaean sediments derived from continental margins adjacent to the subduction zone. Thus, subduction fluid metasomatism could potentially lead to lowered $\delta^{34}S$ and $\Delta^{33}S$ of the mantle wedge. Indeed, a similar process was suggested by Giuliani et al. (2016) to explain low-$\delta^{34}S$ sulfides in peridotite xenoliths from the sub-continental lithospheric mantle of the Kaapvaal craton, South Africa. The EMW component can be created by an admixture of DMM, and ~0.5 wt.% of metasediment-derived subduction fluid with moderately negative $\delta^{34}S$ and $\Delta^{33}S$ signatures of –5 ‰ and –0.130‰, respectively (Fig. 3.7).

Subduction fluids are also enriched in fluid-mobile elements like Ba, leading to elevated Ba/La in arc and back-arc basin basalts and mantle wedges (Leeman et al. 1994). A negative correlation is observed between Ba/La and $^{3}He/^{4}He$ in Icelandic basalts (Fig. S10), supporting the presence of an Icelandic mantle component that resembles subduction fluid-enriched DMM. For example, the Kverkfjöll and SNVZ samples that have the lowest $^{3}He/^{4}He$, $\delta^{34}S$ and $\Delta^{33}S$ values in Iceland, also have highest Ba/La (10.4-12.4). A fluid-enriched source for the SNVZ basalts is also suggested by their elevated W concentrations (Mundl-Petermeier et al. 2019).

As opposed to a deep-sourced plume component, the EMW may represent a shallow low-$\delta^{34}S$-$\Delta^{33}S$ mantle anomaly in the North Atlantic upper mantle, created during past subduction events in the region, that has become captured *en passant* by the upwelling Iceland mantle plume. However, the data presented here does not rule out the alternative possibility that EMW could be a subduction-fluid enriched component that is an inherent part of the lower mantle Iceland plume source.

3.5.4 Implications For The Origin Of Sulfur In The Primordial Mantle

Assuming that the association of high-$^{3}He/^{4}He$ Iceland samples with ^{129}Xe anomalies and negative $\mu^{182}W$ (where $\mu^{182}W$ represents deviations of the modern upper mantle $^{182}W/^{184}W$ in ppm) is indicative of an early-Hadean origin (>4.45Ga; Mukhopadhyay 2012; Mundl-Petermeier et al. 2019), the formation of the high-$^{3}He/^{4}He$ mantle domain predates the oldest surviving terrestrial crust (Jack Hill zircons, up to 4.40Ga; Wilde et al. 2001) and the peak of late accretion at 4.2-4.0Ga (Bottke and Norman 2017). This ancient mantle domain may be associated spatially with ultra-low seismic wave velocity zones (ULVZs) identified

at the base of the mantle at the roots of the high-$^3He/^4He$ plumes Hawaii, Iceland and Samoa (Yuan and Romanowicz 2017, Mundl-Petermeier et al. 2020). The hot, potentially partly molten state of ULVZs could promote transport of elements, including S, across the core-mantle boundary (Rizo et al. 2019, Mundl-Petermeier et al. 2020). Further, depletions of highly siderophile elements (HSEs) in high-$^3He/^4He$ lavas relative to chondrites indicate that the high-$^3He/^4He$ mantle domain experienced core extraction (Mundl et al. 2017, Mundl-Petermeier et al. 2020), similarly to the DMM. Core-mantle segregation is thought to have produced the negative $\delta^{34}S$ signature of the DMM, because the metallic iron alloy that forms the core is enriched in ^{34}S during metal-silicate equilibration (i.e., $\varepsilon^{34}S_{metal\text{-}silicate} > 0$; Labidi et al. 2013, 2016, Labidi and Cartigny 2016). According to this model, the high-$^3He/^4He$ mantle would also be expected to have a sub-chondritic, negative $\delta^{34}S$ signature, but this has not been previously constrained by empirical data. The sulfur isotopic fingerprints of high-$^3He/^4He$ samples from Iceland have the potential to constrain key questions remaining about Early Earth processes, such as the nature and extent of core-mantle interaction experienced by the ancient high-$^3He/^4He$ mantle (e.g., Mundl-Petermeier et al. 2020).

Icelandic high-$^3He/^4He$ lavas (> $15R/R_A$) from the NRZ and ERZ, that sample the highest proportion of the Plume 1 component, have distinctly less negative $\delta^{34}S$ values (–1.4 to –0.4‰) compared to the samples with MORB-like $^3He/^4He$ of 8 to $9.5R_A$ from Kverkfjöll and NRZ, that have $\delta^{34}S$ between –2.2 and –1.2‰. Although the $\delta^{34}S$ range of the high-$^3He/^4He$ NRZ-ERZ lavas (–1.4 to –0.4‰) is negative and intermediate between DMM (–1.3±0.3‰) and chondrites (0.0±0.3‰, Labidi et al. 2013), we note that if the overall trend of increasing $\delta^{34}S$ with increasing $^3He/^4He$ is extrapolated to $34R_A$ (Plume 1), it is consistent with a near-chondritic $\delta^{34}S$ value of up to 0 ‰ for the Plume 1 component (Fig. 3.7a). It is worth to note that this conclusion holds even if the bulk $\delta^{34}S$ value is corrected for minor presence of sulfate in ERZ samples: If the $S^{6+}/\Sigma S$ of the ERZ is taken as 0.03-0.07, as reported by Taracsák et al. (2021) for the high-$^3He/^3He$ ERZ samples A35 and A36 (also included in this study), the ERZ bulk $\delta^{34}S$ values would be shifted by c. +0.1 to +0.2‰ (calculated with Eq.12; Supplementary Information) relative to the measured $\delta^{34}S_{sulfide}$ values, shifting the projected Plume 1 component by a similar amount to a bulk $\delta^{34}S$ value of up to c. +0.2‰. This minor correction would still leave the Plume 1 component within the chondritic $\delta^{34}S$ range (0.0±0.3‰).

The contrasting $\delta^{34}S$ signatures of DMM (sub-chondritic) and high-$^3He/^4He$ mantle (approximately chondritic) present an apparent paradox. Below, we discuss mechanisms that could affect the S isotopic composition of the two mantle reservoirs differently.

First, it is conceivable that sulfur was extracted from the high-$^3He/^4He$ mantle during core formation at conditions where $^{34}S/^{32}S$ fractionation is negligible. If the high-$^3He/^4He$ mantle equilibrated with a metallic iron alloy at higher temperature compared to the DMM, the accompanying $\varepsilon^{34}S_{metal\text{-}silicate}$ fractionation factor could be considerably smaller. However, extrapolation of $\varepsilon^{34}S_{metal\text{-}silicate}$ from experimental conditions (up to 1.5 GPa and 1650°C; Labidi et al. 2016) to lower mantle conditions (up to 136GPa and ~4000K at the core-mantle boundary at present) is difficult because of the opposing effects of increasing T (decreases $^{34}S/^{32}S$ fractionation) and P (increases $^{34}S/^{32}S$ fractionation; Labidi and Cartigny 2016). Alternatively, rather than resulting from metal/silicate equilibrium, it is possible that the S isotopic signature of the high-$^3He/^4He$ mantle is controlled by equilibrium with a sulfide liquid phase ("Hadean matte"; O'Neill 1991) which is associated with negligible $^{34}S/^{32}S$ fractionation (Labidi and Cartigny 2016). Although the fraction of S in the bulk mantle affected by sulfide-silicate equilibrium is estimated to be less than ~10% (Labidi and Cartigny 2016), the high-$^3He/^4He$ mantle could be disproportionally affected

compared to the DMM due to its location at the base of the mantle, where a 2-35km layer of sulfide liquid is thought to have ponded at the late stage of core-mantle differentiation (Savage et al. 2015). Either of these scenarios could potentially explain the contrasting $\delta^{34}S$ signatures of the high-$^{3}He/^{4}He$ mantle and the DMM by only invoking core extraction from the silicate mntle.

An additional phenomenon that could influence the S isotopic composition of the high-$^{3}He/^{4}He$ mantle is material exchange between the core and the mantle, which has been recently suggested to explain negative $\mu^{182}W$ anomalies present in high-$^{3}He/^{4}He$ lavas (Mundl et al. 2017, Rizo et al. 2019, Mundl-Petermeier et al. 2020, Jackson et al. 2020). The core is Earth's main reservoir of both W (500ppb), with very low $\mu^{182}W$ (–220ppm; Mundl-Petermeier et al., 2019, 2020; Rizo et al. 2019), and S, with a 100-fold higher S content relative to the mantle (approximately 2 wt.% and 200ppm, respectively) and an assumed chondritic $\Delta^{33}S$-$\delta^{34}S$ signature (Labidi et al. 2013). Thus, incorporation of small amounts of core-derived W and S in the high $^{3}He/^{4}He$ mantle could simultaneously explain both the negative $\mu^{182}W$ signature and a shift toward chondritic $\delta^{34}S$ values.

Further, combined $^{3}He/^{4}He$-$\Delta^{33}S$-$\mu^{182}W$ data from Iceland and Samoa – the only high-$^{3}He/^{4}He$ locations where coupled data are available – show that Samoan and Icelandic basalts converge toward near-0 $\Delta^{33}S$ values with increasing $^{3}He/^{4}He$ (Fig. 3.7b) and decreasing $\mu^{182}W$ (Fig. 3.8). The chondritic $\Delta^{33}S$ signature of high-$^{3}He/^{4}He$ lavas corroborates the suggestion that they sample a primordial mantle *least* modified by subducted crustal materials (Jackson et al. 2020). Due to the observed coupling between $^{3}He/^{4}He$-$\Delta^{33}S$-$\delta^{34}S$-$\mu^{182}W$ systematics (Figs. 3.7 and 3.8), it is important to explore whether a single process could explain the $\delta^{34}S$-$\Delta^{33}S$-$\mu^{182}W$ signature of the high-$^{3}He/^{4}He$ mantle.

Two main scenarios have been proposed to explain the negative correlation between $\mu^{182}W$ and $^{3}He/^{4}He$ in OIBs. Mundl-Petermeier et al. (2020) hypothesized that equilibration of the metallic outer core and a basal layer of a primordial magma ocean could produce a remnant lower mantle reservoir with core-like $\mu^{182}W$ signature without elevated HSE abundances. However, if the the $\varepsilon^{34}S_{metal\text{-}silicate}$ fractionation factor remains positive at lower mantle P-T-conditions (Labidi et al. 2016), applied to S, the core-mantle equilibration model of Mund-Petermeier et al. (2020) would generate (or maintain) a negative $\delta^{34}S$ signature for the high-$^{3}He/^{4}He$ mantle.

As an alternative process of adding negative $\mu^{182}W$ core material to the lower mantle, Rizo et al. (2019) showed that Si-Mg-Fe oxides that exsolve from the outer core preferentially incorporate W over HSEs. These oxides are buoyant and would accumulate at the core-mantle boundary, potentially contributing to the selective transport of core-derived W to the lower mantle. It is conceivable that sulfur with a near-chondritic isotopic composition could be transported to the lower mantle through this or a similar process.

At present, more studies are required to assess the respective effects of the two core-mantle exchange models on the $\delta^{34}S$ isotopic composition of the high-$^{3}He/^{4}He$ mantle, as key parameters, such as partitioning of S to Si-Mg-Fe oxides and the $\varepsilon^{34}S_{metal\text{-}silicate}$ fractionation factor at high P and T remain poorly constrained.

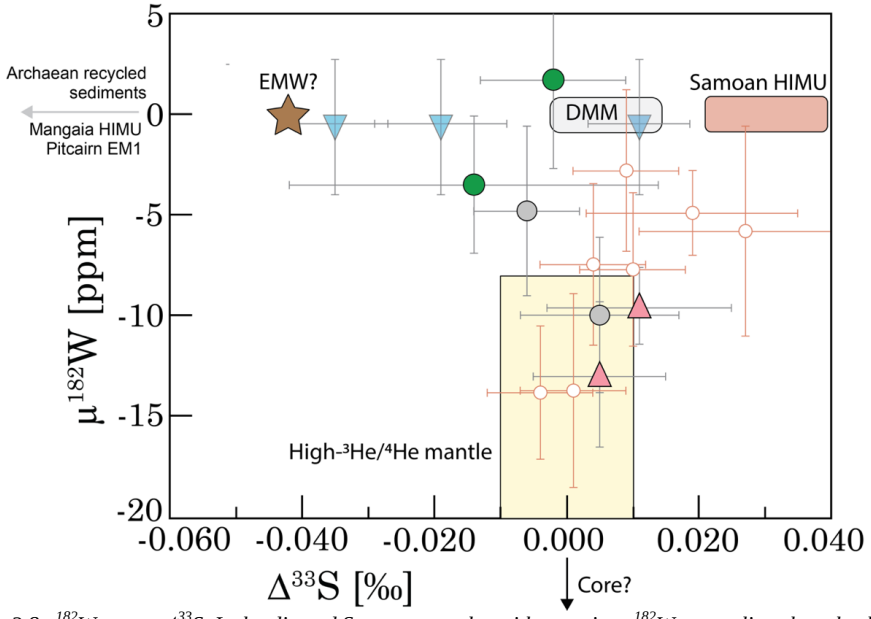

Figure 3.8 $\mu^{182}W$ versus $\Delta^{33}S$. Icelandic and Samoan samples with negative $\mu^{182}W$ anomalies, that also have high $^{3}He/^{4}He$, converge toward a chondritic $\Delta^{33}S \approx 0‰$, which is taken as a signature of an early-differentiated, ancient mantle reservoir. Samples with $\mu^{182}W$ approaching 0 exhibit larger variation in $\Delta^{33}S$, with Icelandic samples pulling toward negative and Samoan toward positive $\Delta^{33}S$ values. The $\mu^{182}W$ signature of the SNVZ samples is taken as the average of two other SNVZ samples SNS-206 (–0.6ppm) and SNS-214 (–0.7ppm) reported by Mundl-Petermeier et al. (2019). The $\mu^{182}W$ data for all Iceland samples are sourced from Mundl-Petermeier et al. (2019), except for sample A24 which is from Jackson et al. (2020). $\Delta^{33}S$ and $\mu^{182}W$ data for Samoa are sourced from Dottin et al. (2020a). Error bars represent 2SE for both $\mu^{182}W$ and $\Delta^{33}S$. Arrows point toward $\Delta^{33}S$-$\mu^{182}W$ compositions of Mangaia, Pitcairn and Earth's core based on Cabral et al. (2013), Labidi et al. (2013), Delavault et al. (2016) and Mundl et al. (2017). Symbols as in Fig. 3.2.

3.6 Conclusions

This study presents major and trace element, S concentration and multiple S isotope data acquired from 62 samples covering the main neovolcanic zones of Iceland. Focusing on undegassed, subglacial basaltic glasses, the data provide a unique window to the sulfur isotopic evolution of OIB magmas and constrains the $\delta^{34}S$-$\Delta^{33}S$ signatures of various Icelandic mantle components. Undegassed Icelandic basaltic glasses contain between 300 and 1570 ppm of S and reach sulfide saturation at MgO ≈ 6 wt.%, which leads to S and Cu depletions concurrent with increasing $\delta^{34}S$ during subsequent melt evolution. The observed $\delta^{34}S$ (–2.5 to -0.1‰) and $\Delta^{33}S$ (–0.035 to +0.011‰) variability expressed by primitive Icelandic basalts exceeds that measured in MORBs. We infer an Icelandic mantle component with negative $\delta^{34}S$ = –2.5 wt.% and negative $\Delta^{33}S$ = –0.40‰ that is associated with MORB-like $^{3}He/^{4}He$ ($8R_A$) and elevated Ba/La (>12). We suggest that this mantle component (EMW) represents subduction fluid-enriched mantle wedge-type material present in the local upper mantle, that became entrained in the Iceland plume *en route* to the surface, although a deeper recycled component cannot be ruled out. High-$^{3}He/^{4}He$ and low-$\mu^{182}W$ samples trend toward chondritic $\Delta^{33}S$ and $\delta^{34}S$ values of ~0 ‰. A near-chondritic $\delta^{34}S$ signature inferred for the ancient high-$^{3}He/^{4}He$ reservoir is difficult to reconcile with the sub-chondritic $\delta^{34}S$ signature of DMM, and may suggest either that the two mantle domains experienced core extractions at different conditions during planetary

differentiation, or alternatively, points toward a previously unidentified flux of S from the core to the high-$^{3}He/^{4}He$ reservoir. Although many open questions remain, the $\delta^{34}S$-$\Delta^{33}S$ signatures of Icelandic basalts provide important constraint for future models on the nature and extent of chemical interactions between the core and the mantle during early planetary differentiation, as well as the recycling of S through the deep and shallow mantle.

3.7 Acknowledgements

This study has been supported by NordVulk fellowships awarded to ER and JGR, as well as a University of Iceland Research Fund Doctoral grant awarded to ER. SAH acknowledges support from the Icelandic Research Fund (Grant #196139-051) and the University of Iceland Research Fund. GI acknowledges the financial support of the Simons Foundation under the auspices of the SCOL incentive awarded to Roger Summons at MIT. William Olszewski's reliable help with the SF_6 GC-IRMS line at MIT is thankfully acknowledged. Hugh O'Brien at GTK was of great help during trace element analysis of the KVK samples. Simon Matthews and Maja Bar Rasmussen are thanked for commenting on early versions of the manuscript. We are thankful to Maryjo Brounce and an anonymous reviewer for helpful comments on a previous version of the manuscript.

3.8 References

Alt, J. C. (1995) Sulfur isotopic profile through the oceanic crust: sulfur mobility and seawater-crustal sulfur exchange during hydrothermal alteration. *Geology*, *23*, 585–588.

Beaudry, P., Longpré, M. A., Economos, R., Wing, B. A., Bui, T. H., & Stix, J. (2018). Degassing-induced fractionation of multiple sulphur isotopes unveils post-Archaean recycled oceanic crust signal in hotspot lava. *Nature communications*, *9*(1), 1-12.

Bézos, A., Lorand, J. P., Humler, E., & Gros, M. (2005). Platinum-group element systematics in Mid-Oceanic Ridge basaltic glasses from the Pacific, Atlantic, and Indian Oceans. *Geochimica et Cosmochimica Acta*, *69*(10), 2613-2627.

Bottke, W. F., & Norman, M. D. (2017). The late heavy bombardment. *Annual Review of Earth and Planetary Sciences*, *45*.

Brounce, M., Stolper, E., & Eiler, J. (2017). Redox variations in Mauna Kea lavas, the oxygen fugacity of the Hawaiian plume, and the role of volcanic gases in Earth's oxygenation. *Proceedings of the National Academy of Sciences*, *114*(34), 8997-9002.

Burgisser, A., Alletti, M., & Scaillet, B. (2015). Simulating the behavior of volatiles belonging to the C–O–H–S system in silicate melts under magmatic conditions with the software D-Compress. *Computers & Geosciences*, *79*, 1-14.

Cabral, R. A., Jackson, M. G., Rose-Koga, E. F., Koga, K. T., Whitehouse, M. J., Antonelli, M. A., Farquhar, J., Day, J.M.D., & Hauri, E. H. (2013). Anomalous sulphur isotopes in plume lavas reveal deep mantle storage of Archaean crust. *Nature*, *496*(7446), 490-493.

Coplen, T. B., & Krouse, H. R. (1998). Sulphur isotope data consistency improved. *Nature*, *392*(6671), 32-32.

Delavault, H., Chauvel, C., Thomassot, E., Devey, C. W., & Dazas, B. (2016). Sulfur and lead isotopic evidence of relic Archean sediments in the Pitcairn mantle plume. *Proceedings of the National Academy of Sciences*, *113*(46), 12952-12956.

Dixon, J. E., Bindeman, I. N., Kingsley, R. H., Simons, K. K., Le Roux, P. J., Hajewski, T. R., Swart, P., Langmuir, C.H., Ryan, J.G., Walowski, K.J., Wada, I., & Wallace, P. J. (2017). Light stable isotopic compositions of enriched mantle sources: Resolving the dehydration paradox. *Geochemistry, Geophysics, Geosystems*, *18*(11), 3801-3839.

Dottin III, J. W., Labidi, J., Lekic, V., Jackson, M. G., & Farquhar, J. (2020a). Sulfur isotope characterization of primordial and recycled sources feeding the Samoan mantle plume. *Earth and Planetary Science Letters*, *534*, 116073.

Dottin III, J. W., Labidi, J., Jackson, M. G., Woodhead, J., & Farquhar, J. (2020b) Isotopic evidence for multiple recycled sulfur reservoirs in the Mangaia mantle plume. *Geochemistry, Geophysics, Geosystems*, e2020GC009081.

Dottin III, J. W., Labidi, J., Jackson, M. G., & Farquhar, J. (2021). Sulfur isotope evidence for a geochemical zonation of the Samoan mantle plume. *Geochemistry, Geophysics, Geosystems*, e2021GC009816.

Giuliani, A., Fiorentini, M. L., Martin, L. A., Farquhar, J., Phillips, D., Griffin, W. L., & LaFlamme, C. (2016). Sulfur isotope composition of metasomatised mantle xenoliths from the Bultfontein kimberlite (Kimberley, South Africa): contribution from subducted sediments and the effect of sulfide alteration on S isotope systematics. *Earth and Planetary Science Letters*, *445*, 114-124.

Gunnarsson-Robin, J., Stefánsson, A., Ono, S., & Torssander, P. (2017). Sulfur isotopes in Icelandic thermal fluids. *Journal of Volcanology and Geothermal Research*, *346*, 161-179.

Halldórsson, S. A., Barnes, J. D., Stefánsson, A., Hilton, D. R., Hauri, E. H., & Marshall, E. W. (2016a). Subducted lithosphere controls halogen enrichments in the Iceland mantle plume source. *Geology*, *44*(8), 679-682.

Halldórsson, S. A., Hilton, D. R., Barry, P. H., Füri, E., & Grönvold, K. (2016b). Recycling of crustal material by the Iceland mantle plume: New evidence from nitrogen elemental and isotope systematics of subglacial basalts. *Geochimica et Cosmochimica Acta*, *176*, 206-226.

Halldórsson, S. A., Bali, E., Hartley, M. E., Neave, D. A., Peate, D. W., Guðfinnsson, G. H., Bindeman, I., Whitehouse, M.J., Riishuus, M.S., Pedersen, G.B.M., Jakobsson, S., Askew, R., Gallagher, C.R., Guðmundsdóttir, E.R., Gudnason, J., Moreland, W.M., Óskarsson, B.V., Nikkola, P., Reynolds, H.I., Schmith, H., & Thordarson, T. (2018). Petrology and geochemistry of the 2014–2015 Holuhraun eruption, central Iceland: compositional and mineralogical characteristics, temporal variability and magma storage. *Contributions to Mineralogy and Petrology*, *173*(8), 64.

Hanan, B. B., Blichert-Toft, J., Kingsley, R., & Schilling, J. G. (2000). Depleted Iceland mantle plume geochemical signature: Artifact of multicomponent mixing?. *Geochemistry, Geophysics, Geosystems*, *1*(4).

Harðardóttir, S., Halldórsson, S. A., & Hilton, D. R. (2018). Spatial distribution of helium isotopes in Icelandic geothermal fluids and volcanic materials with implications for location, upwelling and evolution of the Icelandic mantle plume. *Chemical Geology*, *480*, 12-27.

Hauri, E. H., Maclennan, J., McKenzie, D., Gronvold, K., Oskarsson, N., & Shimizu, N. (2018). CO2 content beneath northern Iceland and the variability of mantle carbon. *Geology*, *46*(1), 55-58.

Jackson, M. G., Blichert-Toft, J., Halldórsson, S.A., Mundl-Petermeier, A., Bizimis, M., Kurz, M.D., Price, A.A., Harðardóttir, S. , Willhite, L.N.,. Breddam, K., Becker, T.W., Fischer, R.A. (2020) Ancient helium and tungsten isotopic signatures preserved in mantle domains least modified by crustal recycling. *Proceedings of the National Academy of Sciences*, *117*(49), 30993-31001.

Jégo, S. & Dasgupta, R (2013). Fluid-present melting of sulfide-bearing ocean-crust: experimental constraints on the transport of sulfur from subducting slab to mantle wedge. *Geochimica et Cosmochimica Acta, 110,* 106–134.

Jenner, F. E., O'Neill, H. S. C., Arculus, R. J., & Mavrogenes, J. A. (2010). The magnetite crisis in the evolution of arc-related magmas and the initial concentration of Au, Ag and Cu. *Journal of Petrology*, *51*(12), 2445-2464.

Johnston, D. T. (2011). Multiple sulfur isotopes and the evolution of Earth's surface sulfur cycle. *Earth-Science Reviews*, *106*(1-2), 161-183.

Jugo, P.J., Wilke, M., & Botcharnikov, R.E. (2010). Sulfur K-edge XANES analysis of natu- ral and synthetic basaltic glasses: implications for S speciation and S content as function of oxygen fugacity. *Geochimica et Cosmochimica Acta*, *74*(20), 5926–5938.

Labidi, J., Cartigny, P., Birck, J. L., Assayag, N., & Bourrand, J. J. (2012). Determination of multiple sulfur isotopes in glasses: A reappraisal of the MORB δ34S. *Chemical Geology*, *334*, 189-198.

Labidi, J., Cartigny, P., & Moreira, M. (2013). Non-chondritic sulphur isotope composition of the terrestrial mantle. *Nature*, *501*(7466), 208-211.

Labidi, J., Cartigny, P., Hamelin, C., Moreira, M., & Dosso, L. (2014). Sulfur isotope budget (32S, 33S, 34S and 36S) in Pacific–Antarctic ridge basalts: A record of mantle source heterogeneity and hydrothermal sulfide assimilation. *Geochimica et Cosmochimica Acta*, *133*, 47-67.

Labidi, J., Cartigny, P., & Jackson, M. G. (2015). Multiple sulfur isotope composition of oxidized Samoan melts and the implications of a sulfur isotope 'mantle array' in chemical geodynamics. *Earth and Planetary Science Letters*, *417*, 28-39.

Labidi, J., & Cartigny, P. (2016). Negligible sulfur isotope fractionation during partial melting: Evidence from Garrett transform fault basalts, implications for the late-veneer and the hadean matte. *Earth and Planetary Science Letters*, *451*, 196-207.

Labidi, J., Shahar, A., Le Losq, C., Hillgren, V. J., Mysen, B. O., & Farquhar, J. (2016). Experimentally determined sulfur isotope fractionation between metal and silicate and implications for planetary differentiation. *Geochimica et Cosmochimica Acta*, *175*, 181-194.

Lee, C. T. A., Luffi, P., Chin, E. J., Bouchet, R., Dasgupta, R., Morton, D. M., Le Roux, V., Yin, Q., & Jin, D. (2012). Copper systematics in arc magmas and implications for crust-mantle differentiation. *Science*, *336*(6077), 64-68

Leeman, W. P., Carr, M. J., & Morris, J. D. (1994). Boron geochemistry of the Central American volcanic arc: constraints on the genesis of subduction-related magmas. *Geochimica et Cosmochimica Acta*, *58*(1), 149-168.

Li, J. L., Schwarzenbach, E. M., John, T., Ague, J. J., Huang, F., Gao, J., Klemd, R., Whitehouse, M., & Wang, X. S. (2020). Uncovering and quantifying the subduction zone sulfur cycle from the slab perspective. *Nature Communications*, *11*(1), 1-12.

Macpherson, C. G., Hilton, D. R., Day, J. M., Lowry, D., & Grönvold, K. (2005). High-$^{3}He/^{4}He$, depleted mantle and low-$\delta^{18}O$, recycled oceanic lithosphere in the source of central Iceland magmatism. *Earth and Planetary Science Letters*, *233*(3-4), 411-427.

Mukhopadhyay, S. (2012). Early differentiation and volatile accretion recorded in deep-mantle neon and xenon. *Nature*, *486*(7401), 101-104.

Mundl, A., Touboul, M., Jackson, M. G., Day, J. M., Kurz, M. D., Lekic, V., Helz, R.T., & Walker, R. J. (2017). Tungsten-182 heterogeneity in modern ocean island basalts. *Science*, *356*(6333), 66-69.

Mundl-Petermeier, A., Walker, R. J., Jackson, M. G., Blichert-Toft, J., Kurz, M. D., & Halldórsson, S. A. (2019). Temporal evolution of primordial tungsten-182 and $^{3}He/^{4}He$ signatures in the Iceland mantle plume. *Chemical Geology*, *525*, 245-259.

Mundl-Petermeier, A., Walker, R. J., Fischer, R. A., Lekic, V., Jackson, M. G., & Kurz, M. D. (2020). Anomalous ^{182}W in high $^{3}He/^{4}He$ ocean island basalts: Fingerprints of Earth's core? *Geochimica et Cosmochimica Acta*, *271*, 194-211.

Neave, D. A., & Putirka, K. D. (2017). A new clinopyroxene-liquid barometer, and implications for magma storage pressures under Icelandic rift zones. *American Mineralogist*, *102*(4), 777-794.

Ono, S., Wing, B., Rumble, D., & Farquhar, J. (2006). High precision analysis of all four stable isotopes of sulfur (^{32}S, ^{33}S, ^{34}S and ^{36}S) at nanomole levels using a laser fluorination isotope-ratio-monitoring gas chromatography–mass spectrometry. *Chemical Geology*, *225*(1-2), 30-39.

Ono, S., Keller, N. S., Rouxel, O., & Alt, J. C. (2012). Sulfur-33 constraints on the origin of secondary pyrite in altered oceanic basement. *Geochimica et Cosmochimica Acta*, *87*, 323-340.

Ranta, E., Barnes, J.D., Halldórsson, S.A., Jónasson, K., Stefánsson A. (2021). Chlorine isotope ratios record magmatic brine assimilation during rhyolite genesis. *Geochemical Perspectives Letters*, *16*, 35-39.

Rasmussen, M. B., Halldórsson, S. A., Gibson, S. A., & Guðfinnsson, G. H. (2020). Olivine chemistry reveals compositional source heterogeneities within a tilted mantle plume beneath Iceland. *Earth and Planetary Science Letters*, *531*, 116008.

Reekie, C. D. J., Jenner, F. E., Smythe, D. J., Hauri, E. H., Bullock, E. S., & Williams, H. M. (2019). Sulfide resorption during crustal ascent and degassing of oceanic plateau basalts. *Nature communications*, *10*(1), 1-11.

Richter, M., Nebel, O., Maas, R., Mather, B., Nebel-Jacobsen, Y., Capitanio, F. A., Dick, H.J.B., & Cawood, P. A. (2020). An Early Cretaceous subduction-modified mantle underneath the ultraslow spreading Gakkel Ridge, Arctic Ocean. *Science advances*, *6*(44), eabb4340.

Rizo, H., Andrault, D., Bennett, N. R., Humayun, M., Brandon, A., Vlastélic, I., Moine, B., Poirier, A., Bouhifd, M.A. & Murphy, D. T. (2019). ^{182}W evidence for core-mantle interaction in the source of mantle plumes. *Geochemical Perspectives Letters*, *11*, 6-11.

Shorttle, O., & Maclennan, J. (2011). Compositional trends of Icelandic basalts: Implications for short–length scale lithological heterogeneity in mantle plumes. *Geochemistry, Geophysics, Geosystems*, *12*(11).

Taracsák, Z., Neave, D.A., Beaudry, P., Gunnarsson-Robin, J., Burgess, R., Edmonds, M., Halldórsson, S.A., Longpré, M-A., Ono, S., Ranta, E., Stefánsson, A., Turchyn, A.V., EIMF, Hartley, M.E. (2021) Instrumental mass fractionation during sulfur isotope analysis by secondary ion mass spectrometry in natural and synthetic glasses. *Chemical Geology* 578

Torssander, P. (1989). Sulfur isotope ratios of Icelandic rocks. *Contributions to Mineralogy and Petrology*, *102*(1), 18-23.

Wallace, P. J., & Edmonds, M. (2011). The sulfur budget in magmas: evidence from melt inclusions, submarine glasses, and volcanic gas emissions. *Reviews in Mineralogy and Geochemistry*, *73*(1), 215-246.

Wieser, P. E., Jenner, F., Edmonds, M., Maclennan, J., & Kunz, B. E. (2020). Chalcophile elements track the fate of sulfur at Kīlauea Volcano, Hawai'i. *Geochimica et Cosmochimica Acta*, *282*, 245-275.

Wilde, S. A., Valley, J. W., Peck, W. H., & Graham, C. M. (2001). Evidence from detrital zircons for the existence of continental crust and oceans on the Earth 4.4 Gyr ago. *Nature*, *409*(6817), 175-178.

Yuan K. & Romanowicz B. (2017) Seismic evidence for partial melting at the root of major hot spot plumes. *Science* 357, 393.

4 Paper III

Deep and shallow magma degassing and volatile fluxes through volcanic hydrothermal systems – insights from the Askja and Kverkfjöll volcanoes, Iceland

Eemu Ranta[1], Andri Stefánsson[1], Jóhann Gunnarsson-Robin[1], Peter H. Barry[2], Shuhei Ono[3], Barbara I. Kleine[1], Andrea Ricci[1], Jens Fiebig[4], Ríkey Kjartansdóttir[1], Sæmundur A. Halldórsson[1]

[1]*Nordic Volcanological Center, Institute of Earth Sciences, University of Iceland, Iceland*
[2]*Marine Chemistry and Geochemistry Department, Woods Hole Oceanographic Institution, USA*
[3]*Department of Earth, Atmospheric and Planetary Sciences, Massachusetts Institute of Technology, USA*
[4] *Institut für Geowissenschaften, Goethe Universität, Germany*

Manuscript to be submitted to *Geochimica et Cosmochimica Acta* (or similar)

4.1 Abstract

Mantle volatiles are transported to Earth's crust and atmosphere by basaltic volcanism. During eruptions, vast amounts of CO_2, S and Cl are released to the atmosphere during a short time-interval, with impacts ranging in size from the local environment to the global climate. However, the long-term potential for volatile release at surface from intrusive magmatism—which outsizes eruptive volumes by a factor of 2-30—is far greater, yet poorly constrained. Volcanic hydrothermal systems (VHSs) act as conduits for volatiles released from degassing intrusions and can thus be used to gauge the contribution of intrusive magmatism to global volatile cycles. Here, we present new compositional and isotopic (δD and $\delta^{18}O$-H_2O, $^3He/^4He$, $\delta^{13}C$-CO_2, $\Delta^{33}S$-$\delta^{34}S$-H_2S and SO_4) data for non-thermal and thermal waters and fumarole gases from the active Askja and Kverkfjöll volcanoes in central Iceland. The aim of this study is to constrain the contribution of intrusive magmatism to the volatile budget of geothermal fluids in Iceland.

The $CO_2/\Sigma S$ (10-30), $^3He/^4He$ (8.3-10.5 R_A), $\delta^{13}C$ (-4.1 to -0.2 ‰) and $\Delta^{33}S$-$\delta^{34}S$ (-0.031 to 0.003 ‰ and -1.5 to +3.6‰) values in Askja and Kverkfjöll high-gas flux fumaroles are consistent with a magmatic origin for CO_2 and S. Using modelled magmatic gas compositions and mass-balance calculations, we demonstrate that deep (0.5–5 kbar) decompression degassing of basaltic intrusions (330–5060 CO_2 kt/yr, 6–210 kt/yr S) is sufficient to account for the flux of CO_2 observed at Icelandic VHSs (~3300 kt/yr), but probably only supplies a part of their S flux (~220 kt/yr). Crystallization-driven degassing from maturing intrusions and leaching of crustal rocks are suggested as the most feasible additional sources of S. Only a minor proportion of the mantle flux of Cl is channeled via VHSs, whereas the H_2O flux remains poorly constrained, as magmatic signals in Icelandic VHSs are masked by a dominant meteoric water component.

4.2 Introduction

Volatile fluxes from the mantle—the main terrestrial reservoir of volatiles—to the atmosphere are mediated through the crust by volcanism. Long-term volcanic volatile fluxes are commonly extrapolated from direct measurements of volcanic gas plumes of erupting and persistently degassing volcanoes (e.g., Gerlach 1991, Andres and Kasgnoc 1998, Fischer 2008, Aiuppa et al. 2019). However, intrusive basaltic magmatism delivers ~2-30 times more mantle-derived material to the crust than subaerial eruptions (White et al. 2006) and thus has the potential to supply an order of magnitude higher flux of key volatiles like CO_2 and S to the atmosphere (Gerlach 1989). A major conduit of volatile transport between intrusions and the atmosphere are volcanic hydrothermal systems (VHSs), which thus play a potentially large, but relatively poorly constrained role in the global volatile cycles (e.g., Seward and Kerrick 1996, McGee et al. 2001, Taran 2009, Shinohara 2013, Barry et al. 2014, Stefánsson et al. 2016, Taran and Kalacheva 2018, Fischer and Aiuppa 2020). Such systems may further act as sinks of volatiles through mineralization reactions of, e.g., sulfides and carbonates, or, conversely, facilitate leaching of volatiles from the shallow country rocks.

VHSs are powered by magmatic intrusions that heat up surrounding groundwater that percolates through porous or fractured rocks to the surface, giving rise to thermal surface manifestations such as hot springs, fumaroles, acid lakes and steaming grounds.

Considerable efforts through the last century have been made to constrain the sources of the main volatile species present in such hydrothermal fluids (H_2, H_2O, B, CO_2, CH_4, N_2, Cl, H_2S, SO_2, noble gases) (Craig 1963, Sakai and Matsubaya 1977, Marty and Giggenbach 1990, Giggenbach 1992, Sano and Marty 1995, Stefánsson et al. 2017, Gunnarsson-Robin et al. 2017, Fiebig et al. 2019, Labidi et al. 2020). Some of the least melt-soluble volatiles, such as CO_2 and He, are likely to be mainly sourced from magmas, whereas others, like the heavy noble gases (Ne-Ar-Kr-Xe; Füri et al. 2010, Byrne et al. 2021) and N (Labidi et al. 2020) are mainly of atmospheric origin. More melt-soluble elements like B and Cl are thought to be derived in large part from the host rocks through fluid-rock reactions ('leaching'), whereas volatiles with intermediate solubility, like S may be sourced from both leaching and magmatic degassing (Gunnarsson-Robin et al. 2017). VHSs in Iceland—a subaerial portion of the mid-Atlantic ridge—are typically associated with active central volcanoes and caldera structures, where shallow (~2-6 km) magmatic intrusions provide the heat sources that drive hydrothermal circulation along faults and through porous, volcanic bed rock. These shallow intrusions likely represent the top of a multi-tier 'ladder' of intrusions that extends through the crust to the mantle (Maclennan 2019), which potentially provide a deep supply of magmatic gases to the overlying VHSs. Thus, Icelandic VHSs provide an opportunity to study the mantle-to-atmosphere transport of volatiles at a divergent plate boundary.

Here, we present major and trace element, stable isotope (δD, $\delta^{18}O$, $\delta^{13}C$, $\Delta^{33}S$-$\delta^{34}S$) and helium isotope ($^3He/^4He$) data for thermal and non-thermal waters and fumarole gases from the active Askja and Kverkfjöll volcanic systems, located in the Northern Rift Zone (NRZ) of Iceland (Figs. 4.1 and 4.2). These locations are advantageous for studying magmatic volatile input into VHSs, as the pre-eruptive volatile elemental and isotopic characteristics of the basalts from the area are well constrained (Chapters 2 and 5), and because the local crust—a major source of volatiles in many geothermal areas worldwide—is dominantly basaltic and volatile-poor. Further, the aquifers at Askja and Kverkfjöll are devoid of seawater, which is a major source of H_2O, B, Cl and S, and thus complicates the detection of magmatic signals in coastal and submarine VHSs (Stefánsson et al. 2017). We use our geochemical dataset, along with estimated magmatic gas compositions for three main purposes: (1) To evaluate which geochemical signals in surface thermal fluids are derived from magmatic gases emanating from crustal intrusions, (2) to determine the relative contributions of magmatic, crustal and meteoric sources of volatiles to VHSs and (3) to constrain the shallow and deep fluxes of mantle-derived volatiles to the atmosphere channeled via VHSs in Iceland.

4.3 Geological Setting

The Northern Rift Zone (NRZ) of Iceland (Fig. 4.1a) is a subaerial portion of the divergent plate boundary that separates the Eurasian and North American tectonic plates. The NRZ hosts five active central volcanoes named, from north to south, Theistareykir, Krafla, Fremrinámar, Askja and Kverkfjöll, all with their own high-temperature geothermal areas (Ármannsson 2016).

Kverkfjöll is a mature volcanic system at the SE end of the NRZ. It comprises a central stratovolcano, partly covered by the Vatnajökull ice cap, and a connecting fissure swarm (Fig. 4.2b). Kverkfjöll is considered to be an active volcano with dozens of basaltic eruptions during the Holocene, although no historical (< 1100 yr) eruptions are known (Óladóttir et al. 2011). A vigorous geothermal system at Kverkfjöll is manifested on the

surface at several locations around the 3 x 8 km large and 100 m deep, ice-filled NE caldera (Fig. 4.1d, 4.2). A large vapor-dominated geothermal area is centered along a fault on the NW caldera rim at 1550-1700 m elevation. This area is divided into the three separate areas Efri and Neðri Hveradalur, and Hveratagl, that together host dozens of individual fumaroles, boiling pots, mud pools and several ice caves, as well as two ice-dammed geothermal lakes Galtarlón and Gengissig (Thórarinsson 1953, Ólafsson 2000, Oddsson 2016) (Fig. 4.1d; Fig. 4.2).

Hydrothermal explosions have occurred at Gengissig and its vicinity in 1959, 1968 and 2013 (Montanaro et al. 2016 and references therein). Two thermal rivers, Volga and Hveragil, flow down the southern and eastern caldera rims, respectively, (Fig. 4.1d) with temperatures of up to 26°C and 61.5°C, respectively (Ólafsson et al. 2000, this study). Hveragil is characterized by up to 0.5 m thick, layered travertine deposits along its banks (Fig. 4.2). Minor geothermal activity has been occasionally observed as hot vapor or heated grounds on the high slopes of the steep NE cliffs of the caldera and close to the highest top Jörfi (1933 m.a.s.l.) (Thórarinsson 1953, Ólafsson et al. 2000), but are considered to be subordinate compared to the other geothermal manifestations (Oddsson 2016). Oddsson (2016) concluded that the total geothermal heat output of Kverkfjöll amounts to 265±72 MW spread over a geothermal area of 2-2.5 km^2.

Askja is a bimodal and productive volcanic system comprising a fissure swarm and a central volcano. Askja last erupted in 1961 in a relatively small basaltic fissure eruption on the eastern caldera wall that formed the Vikrahraun lava field (Thorarinsson and Sigvaldason 1962). The latest-formed of its four nested calderas, formed following a rhyolitic VEI 5 eruption in 1875 (Hartley and Thorvaldson 2012), is occupied by the 10.7 km^2 large and up to 217 m deep Lake Öskjuvatn (~1052 m.a.s.l). The main geothermal activity at Askja is at present found in three areas around Lake Öskjuvatn: Víti and Bátshraun in the NE, at Suðurbotnar to the SE and at Mývetningahraun and below Þorvaldstindur in the SW (Fig. 4.3c; Jónasson and Einarsson 2009). The Suðurbotnar geothermal area was partly covered by a large landslide in July 2014 (Gylfadóttir et al. 2017). The geothermal activity extends to the Öskjuvatn lake, at least to a depth of 80 m (Ólafsson 1980), but its full extent and distribution on the lake floor are not well known. A hydrothermal explosion crater Víti, formed in connection to the 1875 eruption (Sparks et al. 1981), today hosts an acid thermal lake and several moderately active fumaroles. Both the 1875 and 1961 eruptions were preceded by increased fumarolic activity (Thorarinsson and Sigvaldason 1962).

4.4 Methods

4.4.1 Sampling and major element analysis

A total of 16 fumarole discharge samples, 13 thermal waters and 8 non-thermal water samples were collected from Askja and Kverkfjöll during three field seasons between 2017 and 2019. All fumarole vapors were near to local boiling point temperatures (~94.5-96.5°C at altitudes of 1050-1700m). Thermal and non-thermal waters were filtered on-site through 0.2 µm mesh cellulose acetate filters and collected in polypropylene (PP) tubes that were washed three times with the sample. Sample splits for ICP-OES analysis were acidified on site to 1% HNO_3 (Merck Suprapur®). Vapor samples for major gas analysis were collected in evacuated borosilicate glass gas bulbs (100 to 350 ml) including 10-35 ml of 50% KOH solution (Fig. 4.3e), following Arnórsson et al. (2006).

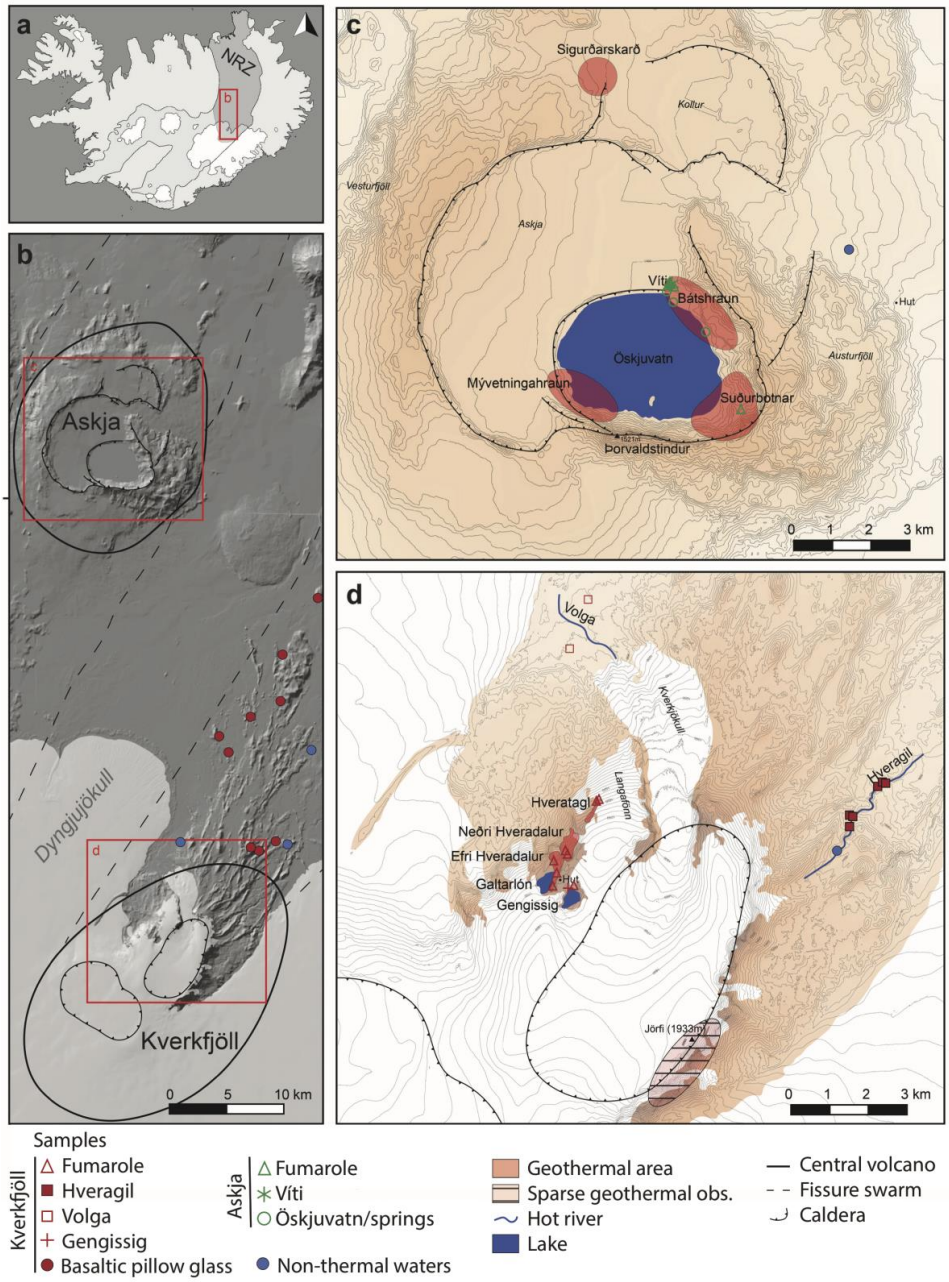

Figure 4.1 (a,b) Map of Iceland, the northern rift zone (NRZ) and the study areas (red boxes). (c) The Askja volcano and its four geothermally active areas. (d) Kverkfjöll volcano and geothermal manifestations: The Hveradalur geothermal area, two glacial lagoon, Galtarlón and Gengissig, and two thermal river Volga and Hveragil. Outlines of the geothermal areas and caldera faults based on Jónasson and Einarsson (2009), Sigurgeirsson et al. 2015 and Oddsson (2016). Locations of subglacial glasses samples in Ranta et al. (2021b) are shown as red circles.

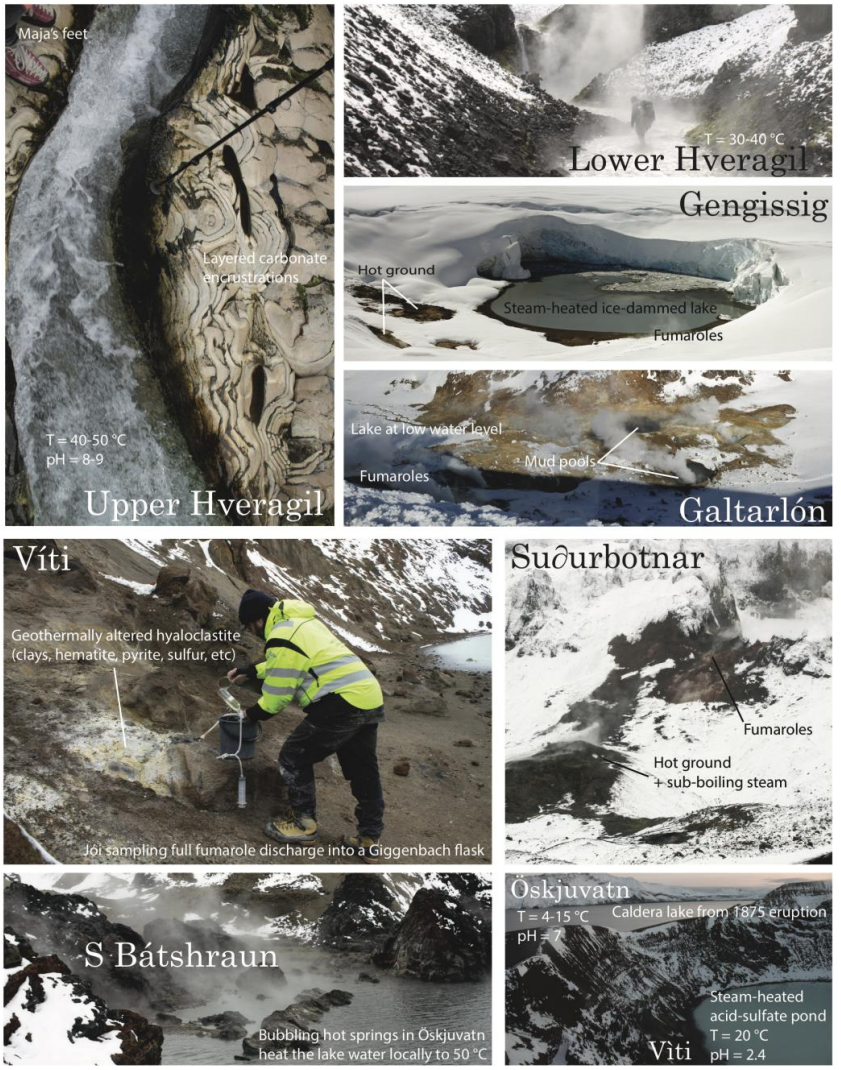

Figure 4.2 Geothermal manifestations at Kverkfjöll and Askja. (a)-(b) Upper and lower portions of the Hveragil thermal river at Kverkfjöll. Hveragil water is mildly alkaline (pH = 8-9) with temperatures decreasing from T = 60°C to T ≈ 30 °C from the upper to lower parts. (c)-(d) Gengissig and Galtarlón are steam-heated lakes located near the top of Hveradalur, at the edge of the Vatnajökull glacier. They occasionally drains in small jökulhlaups. Vigorous boiling-point fumaroles and mud-pools typical of the Hveradalur area are seen in (d). Much of the thermally active area is occasionally covered by the Galtarlón lagoon, which in the image is at low level, with an ice cover. (e) Fumarole sampling by the Víti pond at the Askja volcano. (f) Suðurbotnar thermal area in SE Askja. Hot grounds with sub-boiling steam, seen in the foreground, are typical in the easter margin of Lake Öskjuvatn. Several boiling-point fumaroles and high-T altered kaolonite-pyrite deposits are seen at higher altitude. (g) Bubbling hot springs are commonly found emanating from the floor of Lake Öskjuvatn, heating the lake water to > 50 °C. (h) The Öskjuvatn crater lake and the Víti acid pond seen from the north.

Separate vapor condensate samples were collected into PP tubes for $\delta D\text{-}H_2O$ and $\delta^{18}O\text{-}H_2O$ analysis. Samples for noble gas analyses were taken from 8 fumarole into copper tubes that were pre-flushed for ~15 min through a water lock and then sealed by cold-welding. Dry gas samples were collected for $\delta^{13}C\text{-}CO_2$ analysis from two Kverkfjöll fumaroles into a two-port borosilicate glass tubes that were pre-flushed with sample gas ~10 times.

Major element concentrations in waters were determined by ICP-OES at the Institute of Earth Sciences (IES), University of Iceland. The concentrations of non-condensable gases (H_2, N_2, O_2, Ar, CH_4) were determined by gas chromatography at IES, and water concentrations estimated gravimetrically. The H_2S concentration in the fumarole discharge was determined by Hg-acetate titration from the condensed steam fraction. The ΣCO_2 concentrations in both gas and water samples were determined by a modified alkali titration (Arnórsson et al. 2006). Major gas and noble gas isotope data for 4 fumarole samples from 2017 have been published previously by Byrne et al. (2021).

4.4.2 Hydrogen and oxygen isotope analysis

Hydrogen and oxygen isotope compositions of H_2O in water and gas condensate samples were determined by isotope ratio mass spectrometry (IRMS) at IES, using a Finnigan MAT 251 instrument. Data are reported in δ notation relative to VSMOW (Vienna Standard Mean Ocean Water) as δD and $\delta^{18}O$. Standard deviations of long-term repeat measurements are on average 0.7 ‰ and 0.05 ‰ for δD and $\delta^{18}O$, respectively (1σ).

4.4.3 Helium isotope analysis

Helium (^3He and ^4He) isotopes and ^{20}Ne were analyzed at the Woods Hole Oceanographic Institute, US, following methods outlined in Byrne et al. (2021). The helium isotope ratios ($^3He/^4He$) are reported relative to the atmospheric ratio ($R_a = 1.4 \times 10^{-6}$) and corrected for air contamination using $^4He/^{20}Ne$ (Hilton 1996). The corrections are minor (0.00 to 0.12 R_a) indicating that the samples are relatively unaffected by air-contamination. The estimated instrumental uncertainty (2σ) is between 0.22 and 0.44 R_a.

4.4.4 Carbon isotope analysis

The carbon isotopic composition of CO_2 on two dry-gas samples was measured at the Goethe University Frankfurt, Germany, with a Flash EA 1112 (Thermo) linked to the continuous flow system of a ThermoFischer MAT 253 IRMS, according to the protocol provided by Fiebig et al. (2004, 2007). Sample CO_2 was manually injected to the He-flow of the Flash EA, where it passes an oxidation reactor (Cr-oxide and silver-coated Co-oxide; 1020 °C), followed by a reduction reactor (Cu; 650 °C), a water trap and a GC (NC separation column; 40 °C) prior to transfer to the mass spectrometer. Two CO_2 standards were measured along with the samples ($\delta^{13}C$: -40.82‰ and -3.59‰; OzTech). A measurement sequence comprises four measurements of the reference gas followed by a standard/sample. At least two acquisitions per standard/sample were performed. Values represent the mean value of (corrected) single acquisitions. Reproducibility was better than ± 0.2‰ (1σ). Data are reported in δ notation relative to the (Vienna Pee Dee Belemnite (VPDB).

4.4.5 Sulfur isotope analysis

Sulfate (SO_4) in 6 water samples was precipitated as $BaSO_4$(s) by adding excess 1M $BaCl_2$ solution to a sample aliquot. The sample was then filtered through a 0.2 μm cellulose acetate filter and the $BaSO_4$ precipitate collected from the filter paper in deionized water, and dried. Analogously, sulfide (H_2S) in 14 fumarole gases was precipitated as ZnS(s) by adding excess 1M Zn-acetate solution to the gas condensates. The gas condensate containing ZnS(s) was then filtered, and ZnS(s) precipitate collected and dried. The resulting $BaSO_4$(s) and ZnS(s) precipitates were then dissolved, purified and extracted as Ag_2S(s) using "Thode" (Thode et al. 1961) and HCl extraction protocols (Alt and Shanks 1998), respectively, with modifications described in Gunnarsson-Robin et al. (2017).

All three stable sulfur isotope ratios ($^{33}S/^{32}S$, $^{34}S/^{32}S$, $^{36}S/^{32}S$) were determined by gas source dual-inlet IRMS using a Thermo Scientific MAT 253 at the Stable Isotope Geobiology Laboratory at the Massachusetts Institute of Technology using an analytical setup detailed by Ono et al. (2007, 2012) and Gunnarsson-Robin et al. (2017). In short, Ag_2S(s) is first fluorinated at ~300°C for > 6h, resulting in a full conversion of S to SF_6(g), which then passes a series of in-line cryogenic traps and a chromatographic purification step before introduction to the mass spectrometer. The samples were analyzed during the same sessions as data reported in Ranta et al. (2021b). The $^{34}S/^{32}S$ data are reported in standard δ notation relative to V-CDT (Vienna Canyon Diablo Troilite). The $^{33}S/^{32}S$ and $^{36}S/^{32}S$ data are reported as $\Delta^{33}S$ and $\Delta^{36}S$, defined as

$$\Delta^{x}S = \ln(\delta^{x}S + 1) - \theta^{x} \ln(\delta^{34}S + 1)\ ‰ \quad (1)$$

where Δ^x denotes the deviation of δ^xS from a mass-dependent fractionation line, where x = 33 or 36, and $\theta^{33} = 0.515$ and $\theta^{36} = 1.90$. Because the IAEA-S-1 lacks reference values for $\Delta^{33}S$ and $\Delta^{36}S$, they are anchored to the CDT scale using replicate measurements of the IAEA-S-1 reference material and average literature values of IAEA-S-1 vs. CDT. We use IAEA-S-1 $\Delta^{33}S_{CDT}$ and $\Delta^{36}S_{CDT}$ values of of +0.109 and –0.730‰, respectively (see Ranta et al. 2021b). Repeat measurements of IAEA-S-1 yield respective $\delta^{34}S$, $\Delta^{33}S$ and $\Delta^{36}S$ values of -1.19±0.17‰, +0.100±0.004‰ and -0.669±0.068‰, relative to the MIT reference gas SG1. The analytical uncertainties are 0.12, 0.004, and 0.086 ‰ (all 1σ) for $\delta^{34}S$, $\Delta^{33}S$ and $\Delta^{36}S$, respectively, based on the long-term reproducibility of an in-house Ag_2S (Sigma Aldrich) standard.

4.5 Results

4.5.1 Water compositions

The chemical compositions of non-thermal and thermal waters at Kverkfjöll and Askja are reported in Table 4.1 and Figs. S1-S3. The non-thermal waters collected at both localities are characterized by low total dissolved solid concentrations (TDS; 53-130 ppm) and low total dissolved carbon (ΣCO_2 = 23-53 ppm) and SO_4 (0.9-18 ppm) content (Fig. S2a).

At Kverkfjöll, the thermal Hveragil river water has low SO_4 contents (17-44 ppm) coupled to high ΣCO_2 content (up to 580 ppm) as well as neutral to alkaline pH values (7.2-8.9) and moderate temperatures (18.7-61.5 °C; Fig. S2a). The B, Cl, SiO_2 (Fig. S1) and ΣCO_2 concentrations of the Hveragil all show linear correlations with temperature.

At Askja, the Lake Öskjuvatn water has low temperature (T = 12.5°C), close to neutral pH (7.0), and elevated SO_4 content (460 ppm) and relatively high concentrations of ΣCO_2 (163 ppm), SiO_2 (94 ppm) and Cl (46 ppm). The Víti crater lake water is warmer (T = 20°C) and acidic (pH = 2.5), with low concentrations of ΣCO_2 (below detection limit) and Cl (1.6-4.7 ppm), but high concentrations of SO_4 (490 ppm) and SiO_2 (155 ppm). A circumneutral hot spring (pH = 6.4, T = 52°C) on the outer southern rim of the Víti crater has anomalous high concentrations of ΣCO_2 (630 ppm), SO_4^{2-} (820 ppm), Cl (141 ppm) and SiO_2 (142 ppm).

4.5.2 Fumarole compositions

The vapor compositions of fumarole discharges at Kverkfjöll and Askja are reported in Table 4.2 and shown in Figs. S2 and S3 together with previously published data (Poreda et al. 1992, Ólafsson et al. 2000, Stefánsson 2017). The fumarole discharges at Kverkfjöll are dominated by water (H_2O = 98.3-99.7 mol.%), which is typical for Icelandic fumaroles (Stefánsson 2017), followed by CO_2 (2450-15510 μmol/mol) and H_2S (94-631 μmol/mol; Fig. S2c). The CH_4 concentrations at Kverkfjöll (1.6-15.0 μmol/mol) are generally higher than at Askja at (0.9-3.6 μmol/mol; Fig. S2d).

The fumarole discharge at Askja has lower water content (H_2O = 96.90-98.00 mol.%) compared to most other Icelandic geothermal areas (Stefánsson 2017), followed by CO_2 (18650-28600 μmol/mol) and H_2S (790-1770 μmol/mol). A fumarole sample from Suðurbotnar has an anomalous composition, with H_2S concentrations below detection and high CH_4 (10 μmol/mol). No significant temporal changes are observed in the available vapor major gas data from Kverkfjöll and Askja from 1983 to present (Poreda et al. 1992, Ólafsson et al. 2000).

4.5.3 Hydrogen and oxygen isotopes

Non-thermal stream waters in the Kverkfjöll area (n = 4) have δD values between –100.1 and –95.2 ‰ and $\delta^{18}O$ values between –13.9 and –13.3 ‰, falling approximately on the Global Meteoric Water Line (GMWL; $\delta D = 8 \times \delta^{18}O + 10$; Table 4.1; Fig. 4.3a). These values agree well with the local precipitation in the central highlands (Árnason 1976). The Hveragil water records δD-$\delta^{18}O$ values extending from local non-thermal waters down to lower values of –107.8 % and –14.5 ‰, respectively. The Kverkfjöll fumaroles record some of the lowest δD and $\delta^{18}O$ values in Iceland, with fumarole vapors from Hveratagl showing values as low as –140.8 and –19.7 ‰ (Ólafsson et al. 2000; Fig. 4.3a). Higher δD and $\delta^{18}O$ values in the Kverkfjöll fumaroles of up to –108 ‰ and –10 ‰, respectively, coincide with increasingly positive d_O (difference in $\delta^{18}O$ between the sample and GMWL at a given δD value) of up to +5 ‰.

Local melt water stream at Askja has δD and $\delta^{18}O$ values of –92.5 and –12.9 ‰, respectively, reflecting the local precipitation (Árnason 1976). Near-shore samples taken from lake Öskjuvatn have somewhat higher δD and $\delta^{18}O$ values and display minor positive oxygen isotope shifts. The highest δD, $\delta^{18}O$ and d_O values at Askja are recorded from Víti at –76.2 ‰, –7.7 ‰ and +3 ‰, respectively. Compared to the thermal and non-thermal waters, the Askja fumaroles have more negative δD (between –124 and –104 ‰) and $\delta^{18}O$ (–17.3 to –14.0 ‰), and plot close to the GMWL.

Table 4.1 Chemical and isotope compostion of water samples

Sample ID	Location	Type [a]	Latitude (N)	Longitude (W)	T °C	pH	SiO_2 ppm	B ppm	Na ppm	K ppm	Ca ppm	Mg ppm
Kverkfjöll												
18-ER/KVK-01	Kreppa tributary	cs	64°42.576'	016°28.952'	5	7.54	8.15		1.82	0.25	2.55	1.15
18-ER/KVK-02	Hveragil	tr	64°41.589'	016°30.756'	35	8.90	113	0.176	182	15.9	15.2	26.5
18-ER/KVK-03	Hveragil	tr	64°41.642'	016°30.661'	22	8.10	50.3	0.080	97.6	6.57	12.9	22.6
18-ER/KVK-04	Hveragil	tr	64°41.619'	016°30.675'	19	8.01	43.9	0.067	84.7	5.71	12.7	20.5
18-ER/KVK-05	Lindaá	cs	64°48.319'	016°22.314'	3	8.49	16.2	0.022	19.8	0.97	5.10	5.04
18-ER/KVK-06	Sigurðarskáli	cs	64°44'48.7"	016°37'57.8"	6	7.18	9.46		4.12	0.38	8.11	2.23
18-ER/KVK-07	Volga	tr	64°44'08.1"	016°40'07.5"	20	7.76	96.1	0.661	93.6	9.46	22.8	11.2
18-ER/KVK-08	Hveragil	tr	64°41.158'	016°31.684'	35	8.54	96.4	0.184	199	15.2	10.9	27.6
18-ER/KVK-09	Hveragil	tr	64°41.149'	016°31.623'	44	8.57	130	0.201	204	18.4	17.9	28.2
18-ER/KVK-10	Arnardalsá	cs	65°07.473'	015°58.036'	3	8.94	16.9	0.015	12.2	0.41	4.81	1.49
19-EM-KVK-1	Hveragil	tr	64°41'04.8"	016°31'41.9"	48		132	0.190	202	19.7	18.1	27.9
19-ER/KVK-07	Gengissig	s	64°40'11.2"	016°41'10.6"	10	6.64	59.0	0.070	14.5	2.89	42.1	5.24
19-ER/KVK-08	Hveragil, upper	cs	64°40'42.3"	016°32'09.5"	2	7.83	6.90		5.66	0.30	8.12	1.73
19-ER/KVK-10	Volga	tr	64°43'19.1"	016°40'56.0"	26	7.79	110	0.744	106	11.5	23.0	10.6
Askja												
18-ER/ASK-05	Öskjuvatn	l	65°02'43.3"	016°43'30.9"	13	6.96	93.6	0.352	130	6.65	108	29.5
18-ER/ASK-06	Öskjuvatn	ts	65°02'44.3"	016°43'32.7"	52	6.41	142	0.576	205	10.4	336	81.9
18-ER/ASK-07	Víti	ts	65°02'47.4"	016°43'31.2"	20	2.43	156	0.090	12.0	3.55	46.0	19.8
18-ER/ASK-08	Víti	ts	65°02'49.0"	016°43'35.4"	20	2.45	155	0.084	8.43	1.75	43.0	18.9
18-ER/ASK-09	NE Askja caldera	cs	65°03.345'	016°37.575'	1	7.68	14.2	0.014	8.38	0.35	10.5	2.49
19-ER/ASK-01	Öskjuvatn	ts	65°02'10.4"	016°42'17.7"	50	7.86	153	0.077	113	6.43	44.3	11.7
19-ER/Jök-01	Jökulsaá-á-Fjöllum	cs	65°00'51.0"	016°15'03.3"	6	8.08	17	2.74	15.8	0.83	13.9	4.36

Table 4.1 (continued)

Sample ID	Fe ppm	Al ppm	F ppm	Cl ppm	ΣCO_2 ppm	SO_4 ppm	$\delta D\text{-}H_2O$ ‰	$\delta^{18}O\text{-}H_2O$ ‰	$\delta^{34}S_{V\text{-}CDT}\text{-}SO_4$ ‰		$\Delta^{33}S_{CDT}\text{-}SO_4$ ‰		$\Delta^{36}S_{CDT}\text{-}SO_4$ ‰	
Kverkfjöll														
18-ER/KVK-01	0.008	0.028	0.04	0.78	37.0	0.87	-99.3	-13.63						
18-ER/KVK-02	b.d.	0.023	0.77	35.3	570	32.9	-104.1	-14.19						
18-ER/KVK-03	b.d.	0.017	0.48	13.7	253	19.8	-102.2	-14.10						
18-ER/KVK-04	b.d.	0.018	0.42	11.5	229	17.4	-100.4	-14.01						
18-ER/KVK-05	b.d.	0.024	0.15	3.74	53.0	6.24	-100.1	-13.91						
18-ER/KVK-06	0.006	0.025	0.08	0.55	23.0	10.1	-99.5	-13.62						
18-ER/KVK-07	0.011	0.049	0.51	52.7	165	50.4	-103.8	-13.96	2.46	±0.12	-0.003	±0.014	0.049	±0.041
18-ER/KVK-08	0.030	0.068	0.76	33.8	399	43.7	-102.8	-14.03						
18-ER/KVK-09	b.d.	0.046	0.85	40.7	431	35.8	-105.4	-14.32	4.89	±0.12	-0.007	±0.007	0.062	±0.054
18-ER/KVK-10	0.024	0.084	0.13	1.78	34.0	2.0	-89.9	-12.34						
19-EM-KVK-1	0.008	0.009	n.d.	39.4	384	35.2	-103.6	-14.34	4.57	±0.12	0.004	±0.014	0.023	±0.025
19-ER/KVK-07	b.d.	b.d.	n.d.	b.d.	68.0	103	-99.5	-13.27						
19-ER/KVK-08	0.031	0.039	n.d.	b.d.	39.0	1.11	-95.2	-13.30						
19-ER/KVK-10	0.025	0.015	n.d.	60.5	180	49.7	-101.8	-13.56						
Askja														
18-ER/ASK-05	0.281	13.5	0.53	46.5	163	462	-90.2	-11.62	3.68	±0.12	-0.010	±0.025	0.042	±0.090
18-ER/ASK-06	2.46	13.6	0.06	141	628	822	-91.2	-11.77	5.69	±0.12	0.015	±0.010	0.011	±0.063
18-ER/ASK-07	29.5	13.5	0.02	4.70	b.d.	492	-76.2	-7.71						
18-ER/ASK-08	28.9	13.7	0.02	1.59	b.d.	496	-76.8	-7.69	-1.85	±0.12	0.020	±0.006	-0.116	±0.073
18-ER/ASK-09	0.294	0.160	0.10	1.33	34.0	17.9	-92.5	-12.94						
19-ER/ASK-01	0.018	0.025	n.d.	4.57	221	142	-12.1	-89.15						
19-ER/Jök-01	0.120	0.114	n.d.	b.d.	64.0	11.6	-14.7	-104.50						

[a] cs = cold stream or river; tr = thermal river; l = lake; ts = thermal spring

Table 4.2 Chemical and isotope compostion of fumarole vapor

Sample	Location	Latitude (N)	Longitude (W)	H_2O µmol/mol	CO_2 µmol/mol	H_2S µmol/mol	H_2 µmol/mol	O_2 µmol/mol	N_2 µmol/mol	Ar µmol/mol	CH_4 µmol/mol
Kverkfjöll											
19-ER/KVK-01	Efri Hveradalur	64°40'21.2"	016°41'35.6"	996605	2799	237	338	0.56	16	0.2	3.9
19-ER/KVK-02	Efri Hveradalur	64°40'16.1"	016°41'38.2"	993266	6294	224	156	1.40	49	1.2	8.4
19-ER/KVK-03	Efri Hveradalur	64°40'36.8"	016°41'17.3"	994031	5431	262	226	0.44	36	0.9	12.2
19-ER/KVK-04	Neðri Hveradalur	64°40'38.7"	016°41'19.5"	994778	4482	293	340	0.80	94	1.3	9.0
19-ER/KVK-05	Galtarlón	64°40'30.5"	016°41'32.9"	996823	2453	414	51	8.90	243	3.3	4.8
19-ER/KVK-06	Gengissig	64°40'15.4"	016°41'04.7"	993023	6649	140	148	0.58	30	0.5	10.2
17-KVE-01[a]	Hveratagl			987143	11331	345	687	1.02	478	7.2	7.69
17-KVE-02[a]	Hveratagl			983415	15506	631	374	0.97	59	1.2	11.98
17-KVE-03[a]	Hveratagl										
Askja											
17-ASK-01[a]	Víti			980054	18653	963	250	0.43	70	8.9	2.42
17-ASK-03[a]	Víti			979968	18673	794	522	1.63	39	0.9	0.97
18-ER/ASK-01	Víti	65°02'49.5"	016°43'26.8"	977123	20538	1654	635	0.84	47	1.0	0.9
18-ER/ASK-02	Víti	65°02'49.2"	016°43'26.6"	974911	23091	1195	514	5.15	277	4.7	1.46
18-ER/ASK-03	Víti	65°02'49.0"	016°43'25.6"	969275	28619	1769	160	3.43	166	4.2	3.59
18-ER/ASK-04	Víti	65°02'47.2"	016°43'28.8"	973050	25319	1541	8	0.35	78	2.1	1.14
19-ER/ASK-02	Suðurbotnar	65°00'57.7"	016°40'56"	96167	31982	0	282	20	530	8	10

Table 4.2 (continued)

Sample	$\delta D\text{-}H_2O$ ‰	$\delta^{18}O\text{-}H_2O$ ‰	^4He cm^3STP/cm^3 $(x10^{-7})$	$^3He/^4He$ R_M/R_A		$^4He/^{20}N$	X	$^3He/^4He$ R_C/R_A	$\delta^{13}C\text{-}CO_2$ ‰	$\delta^{34}S_{V\text{-}CDT}\text{-}H_2S$ ‰		$\Delta^{33}S_{CDT}\text{-}H_2S$ ‰		$\Delta^{36}S_{CDT}\text{-}H_2S$ ‰	
Kverkfjöll															
19-ER/KVK-01	-107.8	-10.85	11.6	8.47	±0.28	24.10	75.6	8.57	-1.5	4.82	±0.12	-0.031	±0.013	0.28	±0.111
19-ER/KVK-02	-107.6	-11.80	8.2	8.28	±0.22	15.30	48.0	8.43	-0.2	4.65	±0.12	-0.013	±0.013	0.206	±0.073
19-ER/KVK-03	-112.5	-12.36	20.6	8.37	±0.27	33.92	106	8.44		2.22	±0.12	-0.005	±0.005	0.157	±0.036
19-ER/KVK-04	-118.3	-13.79	21.8	8.52	±0.22	56.30	177	8.56		2.13	±0.12	-0.012	±0.010	0.205	±0.067
19-ER/KVK-05	-109.5	-11.79	8.6	8.58	±0.32	21.11	66.3	8.70		1.26	±0.12	0.003	±0.007	0.164	±0.054
19-ER/KVK-06	-111.8	-13.95	23.1	8.24	±0.27	47.51	149	8.28		3.01	±0.12	-0.012	±0.012	0.133	±0.059
17-KVE-01[a]			126.0	8.3	±0.34	37.7	157	8.35		3.63	±0.12	-0.015	±0.011	0.225	±0.034
17-KVE-02[a]			112.0	8.42	±0.33	142.5	587	8.44		1.41	±0.12	-0.008	±0.005	0.043	±0.067
17-KVE-03[a]										1.14	±0.12	-0.001	±0.017	0.058	±0.031
Askja															
17-ASK-0[a]			47.1	10.33	±0.40	318.2	1316	10.33		-1.47	±0.12	-0.002		0.049	
17-ASK-03[a]			43.3	10.15	±0.42	343.7	1415	10.15							
18-ER/ASK-01	-104.2	-14.22	15.49	10.23	±0.44	103.8	325	10.26		1.14	±0.12	-0.012	±0.014	0.032	±0.076
18-ER/ASK-02	-124.0	-17.26								1.28	±0.12	-0.017	±0.008	0.243	±0.064
18-ER/ASK-03	-117.8	-16.52								0.13	±0.12	-0.012	±0.009	0.075	±0.046
18-ER/ASK-04	-111.6	-13.96								-1.24	±0.12	0.002	±0.005	0.087	±0.097
19-ER/ASK-02															

[a] Major gas and noble gas isotope data from Byrne et al. (2021)

4.5.4 Helium isotopes

Fumarole vapor helium isotope ($^3He/^4He$) compositions from Kverkfjöll and Askja are reported in Table 4.2 and Fig. 4.3b and S5 together with previously reported data (Poreda et al. 1992, Füri et al. 2010, Byrne et al. 2021). The measured $^3He/^4He$ are 8.28-8.70 R_c/R_A for Kverkfjöll and 10.15-10.33 R_c/R_A for Askja (this study, Byrne et al. 2021). These recent values agree within error with $^3He/^4He$ values of 8.54-8.84 R_a (Kverkfjöll) and 10.45 R_a (Askja) measured about 30 years prior by Poreda et al. (1992), and 8.43–9.14 R_a (Kverkfjöll) and 9.08-9.70 R_a (Askja) measured about 10 years prior by Füri et al. (2010). Generally, the $^3He/^4He$ measured in fumaroles and hot springs at Kverkfjöll and Askja are similar to $^3He/^4He$ measured in olivine crystals and basaltic glasses least affected by degassing in Pleistocene lavas from the two volcanoes (Macpherson et al. 2005, Hardardóttir et al. 2018).

4.5.5 Carbon isotopes

The $\delta^{13}C\text{-}CO_2$ was determined in two fumarole dry gas samples from Kverkfjöll (–1.5 ‰ and –0.2 ‰; Table 4.2; Fig. 4.3c). These values are slightly less negative than published $\delta^{13}C\text{-}CO_2$ data from Kverkfjöll fumaroles of -4.1 ‰ (Poreda et al. 1992) and -2.43 and -1.98 ‰ (Barry et al. 2014).

4.5.6 Sulfur isotopes

The multiple sulfur isotope composition ($\delta^{34}S$ and $\Delta^{33}S$) of H_2S from 12 fumaroles and SO_4 for 5 thermal waters is reported in Tables 4.1 and 4.2 and Fig. 4.3d. The $\delta^{34}S\text{-}H_2S$ values in fumaroles from Kverkfjöll (+1.14 to +4.82 ‰) are distinctly more positive relative to Askja (–1.47 to +1.28 ‰; Fig. 4.3c). The $\Delta^{33}S\text{-}H_2S$ values of the Kverkfjöll and Askja fumaroles show a similar range of (–0.031 to +0.003 ‰). The thermal waters have a range of $\delta^{34}S\text{-}SO_4$ (–1.85 to +5.69 ‰) and $\Delta^{33}S\text{-}SO_4$ (–0.010 to +0.020 ‰).

The Askja $\delta^{34}S$ range is typical of meteoric water-fed VHSs in Iceland like Kerlingarfjöll, Geysir and Krafla (Stefánsson et al. 2015, Gunnarsson-Robin et al. 2017), whereas the $\delta^{34}S$ values of the Kverkfjöll fumaroles are the most positive of the meteoric water-fed VHSs in Iceland. The $\Delta^{33}S$ compositions of Kverkfjöll and Askja fumaroles and thermal waters are similar to those previously reported from geothermal wells, fumaroles and hot springs from meteoric water-fed VHSs in Iceland (Stefánsson et al. 2015; Gunnarsson-Robin et al. 2017, 2020), and indistinguishable from the $\Delta^{33}S$ range of Icelandic basalts (–0.045 to +0.016; Ranta et al. 2021b).

4.6 Discussion

4.6.1 Hydrothermal fluid chemical and isotope composition and secondary processes

The elemental and isotopic composition of thermal fluids sampled at the surface are affected by shallow secondary processes such as depressurization boiling, mixing, conductive cooling, oxidation and fluid-mineral reactions (e.g., Arnórsson et al. 2007). These need to be accounted for and quantified in order to estimate the composition of the hydrothermal source fluid, here referred to as the ‘reservoir fluid’.

Reservoir fluid temperature and composition

The temperature and composition of the reservoir liquid of Kverkfjöll was reconstructed from the measured compositions of fumaroles and the Hveragil hot spring water using the silica-enthalpy method (Fig. S1; Truesdell and Fournier 1977) and gas thermometers (Arnórsson and Gunnlaugsson 1985, Arnórsson et al. 1998, Byrne et al. 2021), as well as additional standard techniques outlined in the footnotes of Table 3 and the Supplementary Information. The silica-enthalpy mixing model yields a reservoir liquid temperature of ~280°C for Kverkfjöll, which agrees well with major (280±30 °C; Arnórsson et al. 1998) and noble gas thermometers (300±30 °C; Byrne et al. 2021). The reconstructed reservoir fluid composition of Kverkfjöll for selected elements is B = 0.8 ppm, Cl = 160 ppm, SiO_2 = 530 ppm, ΣCO_2 = 5400 ppm and ΣS = 200 ppm (full composition shown in Table 3). The full reservoir fluid composition of the Askja system could not be reconstructed, because there are no surface outflows of the reservoir liquid.

The δD-$\delta^{18}O$-$\delta^{13}C$-$\Delta^{33}S$-$\delta^{34}S$ signature of the reservoir fluid was estimated from the measured fumarole isotope values by modelling isotope fractionation between aqueous and gaseous species upon adiabatic boiling from 280°C to 100°C using methods described by Stefánsson et al. (2015, 2016, 2017) (Fig. 4.3). Isotope equilibrium fractionation factors used were taken from Horita and Wesolowski (1994) for δD and $\delta^{18}O$, from Stefánsson et al. (2016) for $\delta^{13}C$ and from Stefánsson et al. (2015) for $\Delta^{33}S$ and $\delta^{34}S$.

The δD and $\delta^{18}O$-H_2O composition of the reservoir fluid for Kverkfjöll is estimated at –95.2±4.7 ‰ and –9.2±1.1 ‰, respectively, suggesting that the Kverkfjöll reservoir is sourced from a local meteoric groundwater reservoir that experienced considerable water-rock interaction (Fig. 4.3a). The modelled $\delta^{13}C$-CO_2 value of the reservoir fluid is –1.8 ± 1.6 ‰ (Fig. 4.3c), whereas the $\Delta^{33}S$ and $\delta^{34}S$ ranges of the reservoir fluids are estimated at –0.006±0.010 ‰ (Fig. 4.3d) and +0.9±1.4 ‰, respectively.

Notably, depressurization boiling imposes large fractionations on δD-H_2O(v) (~ –15 ‰) and $\delta^{18}O$-H_2O(v) values (~ –3.2 ‰), explaining the lower δD and $\delta^{18}O$-H_2O values of most of the fumaroles relative to the reservoir liquid . By contrast, the effects of boiling on $\delta^{13}C$-CO_2(v) and $\delta^{34}S$-H_2S(v) are relatively minor (smaller than –0.5‰ and +1.3 ‰, respectively) (Fig. 4.3) and the effect on $\Delta^{33}S$ is insignificant (<0.001 ‰). Thus, the measured $\delta^{13}C$-CO_2 and $\delta^{34}S$-H_2S values of fumaroles closely reflect the reservoir fluid composition, although $\delta^{34}S$ values in low-gas flux fumaroles may be affected by additional shallow secondary processes (see section 4.6.4).

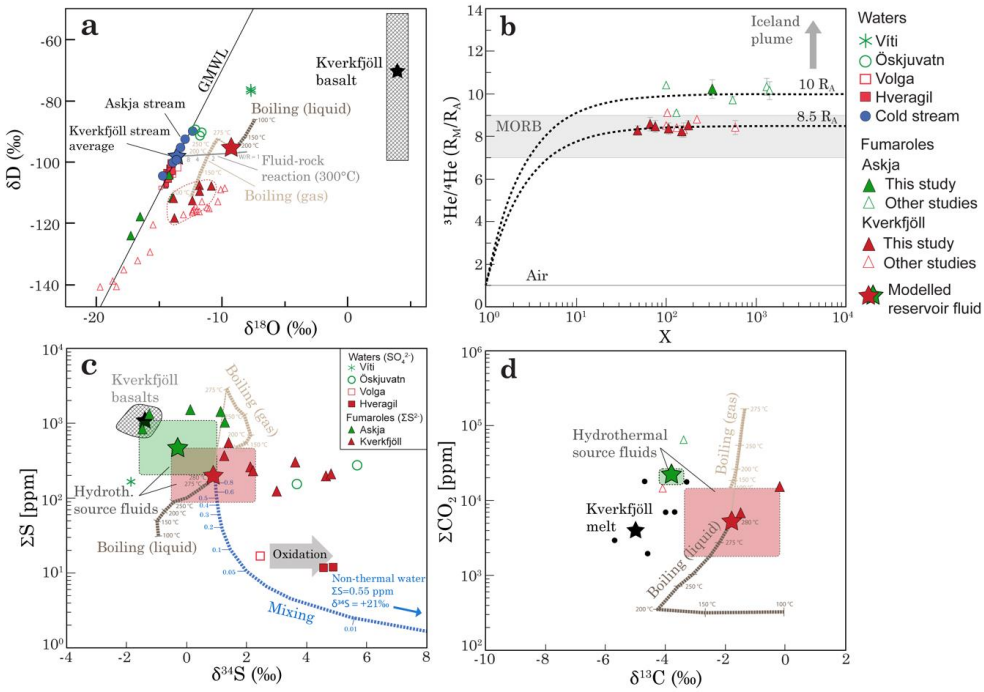

Figure 4.3 Helium, carbon and sulfur isotopes. (a) Water isotopes. Positive $\delta^{18}O$ shifts in the fumaroles indicate a local meteoric water reservoir that has experienced extensive fluid-rock interaction (white star). Fluid-rock interaction of meteoric water with basalt at 300 °C (grey curve) was simulated using PHREEQC, Parkhurst and Appelo (1999) and available mineral-water isotope fractionation factors (Kleine et al. 2020,Supplementary Information) (b) Measured $^3He/^4He$ versus the X-factor. Mixing lines are shown for mixing between air and components with $^3He/^4He$ of 10 R_A and 8.5 R_A, corresponding to the average $^3He/^4He$ signatures of Askja and Kverkfjöll signatures, respectively. The X factor is used to quantify air contamination in the sample, and is calculated as $X = \left[\frac{4He}{20Ne}\right]_{sample} / \left[\frac{4He}{20Ne}\right]_{air}$ *(e.g. Hilton 1996). All samples have high X values (>> 10), signaling minimal air contamination. Kverkfjöll samples plot within the mid-ocean ridge basalt (MORB) field (8±1 RA; Graham 2002), whereas higher $^3He/^4He$ at Askja suggest a component derived from the high-$^3He/^4He$ component of the Iceland plume (>30 R_A, Jackson et al. 2020). (c) ΣS versus $\delta^{34}S$ in H_2S(g) and SO_4(lq). The $\delta^{34}S$-H_2S values of the Askja fumaroles are consistent with a magmatic gas source for S, whereas the positive $\delta^{34}S$-H_2S of the Kverkfjöll fumaroles may suggest an additional S source from 2nd degassing of intrusions or leaching of host rocks with positive $\delta^{34}S$. The positive $\delta^{34}S$-SO_4 of hot springs is compatible with oxidation of ΣS^{2-} from a one-phase reservoir (Hveragil) liquid or fumarolic H_2S (Lake Öskjuvatn). Mixing line between the estimated Kverkfjöll reservoir liquid composition (yellow star) and meteoric water (Stefánsson et al. 2015) is shown with a blue dashed line. (d) ΣC versus $\delta^{13}C$. Model curves following depressurization boiling are shown for both liquid (tan) and vapor (dark brown) phases in (a), (c) and (d). Analytical uncertainties (1σ) are smaller than the sizes of the symbols except for $^3He/^4He$. Red and green stars and boxes indicate the average values and variation of modelled reservoir fluid compositions of Kverkfjöll and Askja, respectively.*

Table 4.3: Kverkfjöll reservoir fluid compostion

Entity	Unit	Value	Method
T	°C	280±30	a
pH		6.8	b
SiO_2	ppm	525	a
B	ppm	0.76	c
Na	ppm	270	d
K	ppm	24	d
Ca	ppm	0.16	d
Mg	ppm	0.002	d
Fe	ppm	0.26	d
Al	ppm	0.53	d
F	ppm	3.71	c
Cl	ppm	164	c
CO_2	ppm	5400	e
H_2S	ppm	200	e
H_2	ppm	12	e
$\delta D\text{-}H_2O$	‰	-95.2±4.7	f
$\delta^{18}O\text{-}H_2O$	‰	-9.2±1.1	f
$\delta^{13}C\text{-}CO_2$	‰	-1.8±1.6	g
$\delta^{34}S\text{-}H_2S$	‰	+0.9±1.4	g
$\Delta^{33}S\text{-}H_2S$	‰	-0.006±0.010	g

a Calculated based on the SiO_2-enthalpy geothermometry assuming quartz saturation in the reservoir (Gunnarsson and Arnórsson 2000) and adiabatic boiling to 100°C together with gas H_2/Ar and H_2S/Ar geothermometry (Arnórsson et al. 1998).

b Stefánsson and Arnórsson (2002)

c Calculated based on linear relationship between SiO_2 and Cl aqeuous concentrations

d Based on temperature dependence of ion to proton ratios proposed by Arnórsson et al. (1983) and Stefánsson and Arnórsson (2000)

e Based on fumarole vapor compostion and assuming adiabatic boiling to reservoir temperatures and liquid only reservoir fluids

f Calculated from fumarole fluid isotope compostion taken into account adiabatic boiling from reservor liquid to 100°C and using isotope equilibrium fractionation of Horita and Wesolowski (1994)

g Calculated from fumarole fluid isotope compostion and taking into account adiabatic boiling from reservoir liquid to 100°C, aqueous and gaseous speciation and assuming equilibrium isotope fractionation. Fractionation factors from Stefánsson et al. (2014, 2015).

4.6.2 Deep magmatic volatile input to volcanic hydrothermal fluids

Magmatic intrusions to ~2-6 km depth below an active volcano may result in the development of an overlying VHS that transports heat via a circulating fluid from depth to the surface. In addition to heat, intrusions may supply magmatic volatiles to the VHS via both depressurization ('1^{st} degassing') as well as crystallization-driven degassing ('2^{nd} degassing')—exsolution of magmatic fluids driven by post-emplacement crystallization of an intrusion (Edmonds and Woods 2018; Fig. 4.4a). To estimate the contribution of intrusive degassing to the hydrothermal systems, we model the composition of the magmatic gas formed via depressurization degassing from a volatile-undersaturated batch of deep melt to higher crustal levels (Fig. 4.4; Table S3). As a starting composition, we assume parental melt volatile concentrations of 1 wt.% H_2O, 4000 ppm CO_2, 1400 ppm S and 350 ppm Cl, estimated for Kverkfjöll basalts (Supplementary Information). Using the MagmaSat model (Ghiorso and Gualda 2015) implemented in the VesiCal v1.01 software (Iacovino et al. 2021), a CO_2-H_2O saturation pressure of ~5 kbars (~18 km crustal depth) is computed for our model melt. Notably, the pressure below the thick crust of Central Iceland (~30-40 km; Jenkins et al. 2018) is likely to be sufficiently high to prevent direct degassing of mantle-level melts below Askja and Kverkfjöll. For pressures below 4 kbar, we use the SolEx 1.0 program (Witham et al. 2011), which calculates the equilibrium H_2O-CO_2-S-Cl composition of coexisting melt and gas for open and closed system behavior.

The most important parameters controlling the magmatic gas composition are the initial volatile concentrations of the melt and the intrusive depth. Approximately 70% of the primary CO_2 of our model melt is degassed upon ascent to a typical mid-crustal magma storage region at 2.5 kbars (~10 km depth; Fig. 4.4c; Neave and Putirka 2017, cf. Sigmundsson et al. 2021). In the same scenario, only minor degassing of about 0.3-0.6% H_2O, 2-5% S and 0.1-2% Cl is predicted. Further ascent to 0.5 kbars (~2 km), chosen as an approximate upper limit of intrusions, results in degassing of 95% CO_2, 0.6-4% H_2O, 6-16% S and 0.2-3% Cl of the initial volatile content of the melt (Fig. 4.4b).

Characteristically, intrusive magmatic gases have high molar ratios of CO_2/H_2O (~4-40) and $CO_2/\Sigma S$ (~12-160) (Fig. 4.4d) contrasting with low CO_2/H_2O (< 1) and $CO_2/\Sigma S$ (< 2) associated with *eruptive degassing* (e.g. Aiuppa et al. 2007). These differences between intrusive and eruptive magmatic gas compositions reflect the higher solubilities of H_2O and S at pressures >0.5 kbar relative to CO_2.

Degassing causes isotopic fractionation between the melt and the exsolving gas (Fig. 4.5). The $\delta^{13}C$ and $\delta^{34}S$ values of the magmatic gas are controlled by initial melt composition, the vapor-melt fractionation factors and the type of degassing (e.g., open or closed system). We model the $\delta^{13}C$ and $\delta^{34}S$ values for magmatic gases using conventional equations describing open and closed system equilibrium degassing (e.g., Macpherson and Mattey 1994) and previously established ($\Delta^{13}C_{v\text{-}m}$ = +4.3±0.5 ‰; Barry et al. 2014) and calculated ($\Delta^{34}S_{v\text{-}m}$ = –0.2 to +0.9 ‰; Ranta et al. 2021b) vapor-melt fractionation factors (Fig. 4.5). For the initial undegassed melt, a value of $\delta^{34}S$ = –1.4 ‰ was chosen based on averages of measured subglacial glass values for the Kverkfjöll basalts (Ranta et al. 2021b). For initial $\delta^{13}C$, the signature of the depleted MORB mantle (DMM) of –5±1 ‰ (rounded values from Marty and Zimmermann 1999) is used for the Icelandic mantle, as the two are indistinguishable based on available data (Barry et al. 2014). Combining the isotopic and elemental degassing models, the $\delta^{13}C$ and $\delta^{34}S$ composition of magmatic gases degassing from intrusions at different crustal depths can be estimated (Fig. 4.5).

The $\delta^{13}C$ of magmatic gas is initially more positive (as high as –0.2 ‰) relative to the source melt. During progressive ascent and closed system degassing, the $\delta^{13}C$ value of the gas approaches the initial melt value, reaching a value of –4.2 ‰ at 2.5 kbar and –4.8 ‰ at 0.5 kbar. Extensive open system degassing of CO_2 may lead to highly negative gas $\delta^{13}C$ values (< –10 ‰; Fig. S4) that are also observed in Icelandic subglacial glasses that are highly degassed with respect to CO_2 (Barry et al. 2014). The $\delta^{34}S(v)$ becomes either more negative or slightly more positive than initial melt depending on the melt and gas redox states (Mandeville et al. 2009). However, because only minor degassing of S occurs during melt ascent (~6-16 ‰ up to 0.5 kbar), the $\delta^{34}S$ values of both deep and shallow magmatic gases remain very close to the initial melt signatures (between –1.6 to –0.5 ‰; Fig. 4.5). Thus, $\delta^{13}C$ of magmatic gas is a more sensitive indicator of intrusion depth than $\delta^{34}S$ and could potentially be used as a tool to discriminate between deep and shallow magma sources.

A factor that complicates a simple interpretation of VHS volatile signatures is that a single geothermal area may simultaneously receive input of magmatic gases from intrusions at different depths and of different age. Thus, the observed gases at the surface may reflect juxtaposing chemical signals derived from both decompression and crystallization-driven degassing. Crystallization of water-poor minerals maintains a cooling intrusion at fluid saturation, leading to a "passive" supply of magmatic fluids to the hydrothermal domain. The temporal and compositional evolution of these secondary magmatic fluids is a subject of considerable complexity (e.g., Parmigiani et al. 2017) and outside the scope of the present work. For the further purposes of this study, we note that ageing intrusions will produce a magmatic gas with progressively lower CO_2/H_2O and CO_2/H_2S, leading eventually to the loss of virtually all of the CO_2, most of its original S and H_2O but will likely retain much of its Cl. Crystallization-driven degassing of intrusions may follow open system degassing paths, producing magmatic gases with much more negative $\delta^{13}C$ (and potentially $\delta^{34}S$) values relative to closed-system degassing (Fig. S4).

Further, we note that the small fraction of magmatic water in meteoric water-dominated VHSs, such as Askja and Kverkfjöll, prevents its detection in δD-$\delta^{18}O$ space: Assuming that CO_2 in fumaroles is derived from magmatic gas ($CO_2/H_2O \approx$ 6-10; Fig. 4.4d), the magmatic water contribution in the Askja and Kverkfjöll fumaroles (CO_2/H_2O = 0.002–0.03), is at maximum 0.3 mol.%. This would result in δD and $\delta^{18}O$ shifts of less than 0.4 ‰ and 0.1‰—smaller than the 2σ uncertainty of the δD-$\delta^{18}O$ measurements—assuming reasonable δD-$\delta^{18}O$ values for the magmatic water of –50 ‰ and +4‰, respectively. For this reason, trends toward magmatic water components seen in δD-$\delta^{18}O$ graphs at many subduction zone volcanoes (e.g., Giggenbach 1992, Taran et al. 2018), indicative of degassing of shallow, water-rich magma bodies, have not been observed at Icelandic VHSs.

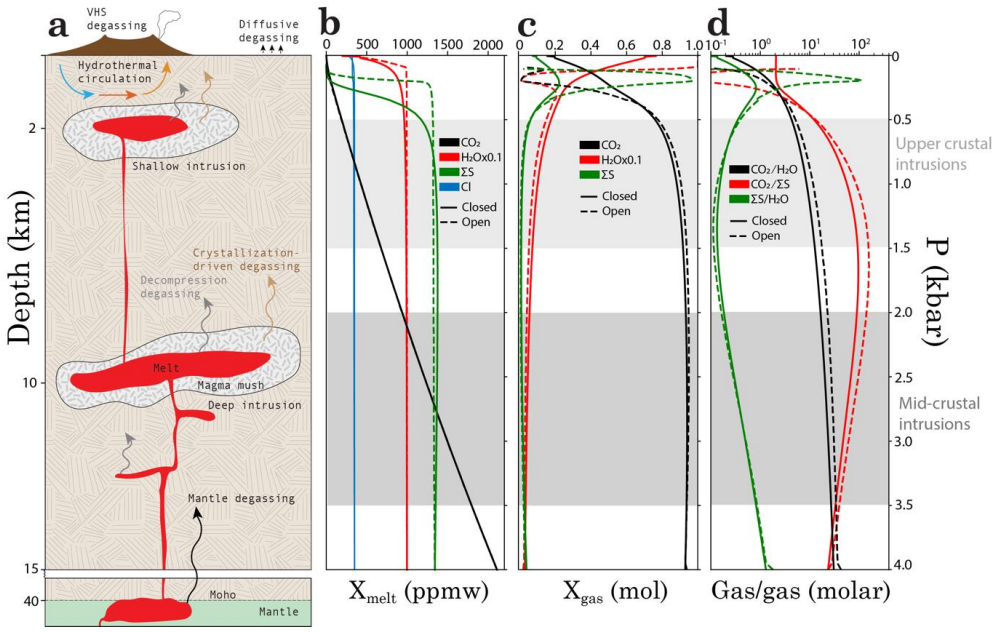

Figure 4.4 Deep and shallow melt degassing. (a) Cartoon representing a multi-tier magmatic system. Ascending melts exsolve magmatic gases via decompression degassing. Further degassing from stalled intrusions occurs via crystallization-driven degassing, as crystallization of dry minerals keeps residual melts volatile-saturated. The model curves show the composition of (b) melt and (c) magmatic gas during open and closed system degassing between pressures of 4 kbar to 1 bar. (d) The volatile ratios in the magmatic gas change depending on the intrusive pressures. Model curves for CO_2, H_2O, S and Cl were calculated using SolEx v1.0 (Witham et al. 2012). The Kverkfjöll sample KVK-169 (Chapter 5) major element composition was used for model calculations, with estimated undegassed volatile concentrations (Supplementary Information).

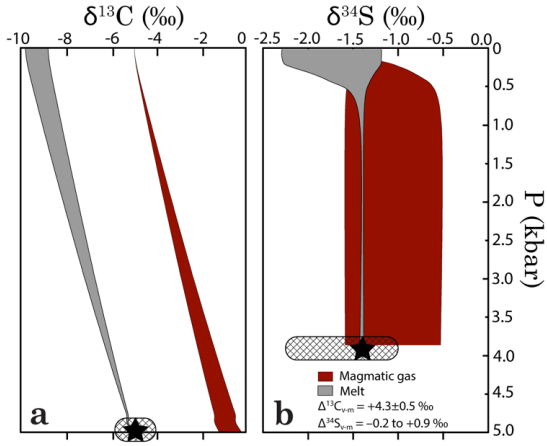

Figure 4.5 Isotopic composition of magmatic gas. (a) $\delta^{13}C$ and (c) $\delta^{34}S$ vs pressure. The isotopic compositions of an exsolved magmatic gas and the residual melt are shown for closed system degassing paths. The $\delta^{13}C$ value of magmatic gas is initially close to 0 ‰, but becomes lower with

decreasing intrusion depth, approaching the initial melt value of –5 ‰. The magmatic gas $\delta^{34}S$ value may be either slightly more positive or negative depending on the melt and gas redox states (Mandeville et al. 2009). However, because only minor degassing of H_2O and S occur during melt ascent to up to 0.5 kbar, all intrusions have similar $\delta^{34}S$ values. For $\delta^{13}C$, signature of the depleted MORB mantle (DMM) of –5±1 ‰ (Marty and Zimmermann 1999) is used as the initial melt value, as the $\delta^{13}C$ of the Icelandic mantle is indistinguishable from DMM (Barry et al. 2014). For CO_2 degassing, $\Delta^{13}C_{v\text{-}m}$ was chosen as +4.3±0.5 ‰ (Barry et al. 2014). The initial melting composition for $\delta^{34}S$ (–1.39 ‰) is the average Kverkfjöll glass values reported by Ranta et al. (2021b). A range of –0.2 to +0.9 ‰ was calculated for the vapor-melt fractionation factor $\Delta^{34}S_{v\text{-}m}$, assuming ranges of $[SO_2/(SO_2+H_2S)]_v$ = 0.25- 0.75 and $[S^{6+}/\Sigma S]_m$ = 0.1-0.2 (see Mandeville et al. 2009 and Ranta et al. 2021b for calculation details).

4.6.3 Volatile sources and secondary processes

Carbon sources

The $\delta^{13}C\text{-}CO_2$ and $CO_2/\Sigma S$ values of fumarolic gases can be used to discriminate between magmatic and crustal input of carbon into geothermal systems (Fig. 4.6). This is possible because the Icelandic crust has low $CO_2/\Sigma S$ of about 0.003 to 0.008 and highly negative $\delta^{13}C\text{-}CO_2$ (< –5 ‰; Barry et al. 2014), contrasting with intrusive magmatic gases that have high $CO_2/\Sigma S$ (>>1) and less negative $\delta^{13}C\text{-}CO_2$ (> –5 ‰) (Figs. 4.3d and 4.6).

The high-CO_2 fumaroles (> 10 mmol/mol) at both Askja and Kverkfjöll converge toward $CO_2/\Sigma S$ of ~13-25 (Figs. S2d and 4.6a), which we interpret as a primary $CO_2/\Sigma S$ range prior to shallow modifications by secondary processes. This range of $CO_2/\Sigma S$ is compatible with intrusive magmatic gas (Fig. 4.6a). Shallower processes in fumarole conduits may influence the $CO_2/\Sigma S$ ratio in low-flux fumaroles. For example, abnormally high $CO_2/\Sigma S$ seen in some low-gas flux Kverkfjöll fumaroles from Efri Hveradalur may result from sulfide fixation (Fig. S2b).

The average fumarolic $\delta^{13}C\text{-}CO_2$ in Askja is –3.7±0.4, close to the average of Icelandic VHSs of approximately –4 ‰ (Poreda et al. 1992, Barry et al. 2014). The $\delta^{13}C\text{-}CO_2$ values of the Kverkfjöll fumaroles (from –4.1 to –0.2‰) and the estimated reservoir fluid (–1.8 ± 1.6 ‰) are slightly higher, which could indicate that CO_2 in Kverkfjöll is sourced from deeper (> 4 kbar) intrusions (Fig. 4.6b). Thus, both $CO_2/\Sigma S$ and $\delta^{13}C\text{-}CO_2$ fumarole data suggest that the source of CO_2 (and S) at Askja and Kverkfjöll—and at Icelandic VHSs in general—is deep magmatic degassing from basaltic intrusions at various crustal levels from ~2 to 18 km.

The high concentrations of magmatic CO_2 and H_2S in Askja fumaroles relative to other Icelandic geothermal systems are consistent with a persistent lower crustal intrusive magmatism beneath the central volcano. Seismic tomographic imaging indicates that a semi-continuous series of magma storage zones underlies the volcano, with main melt reservoirs located at depths of 5 and 9 km (Mitchell et al. 2013, Greenfield et al. 2016). Deep (~20 km) and frequently occurring earthquake swarms beneath the Öskjuvatn caldera that coincide with a region of slow S-wave velocity indicate a continuous supply of deep magmatic injections to the lower crust (Greenfield and White 2015, Greenfield et al. 2016). Decompression degassing of deep-sourced melt injections in a multi-tier magma storage system could generate a near-continuous deep supply of CO_2-dominated magmatic gas to the geothermal system of Askja, which may be common at volcanoes that experience frequent deep intrusive activity.

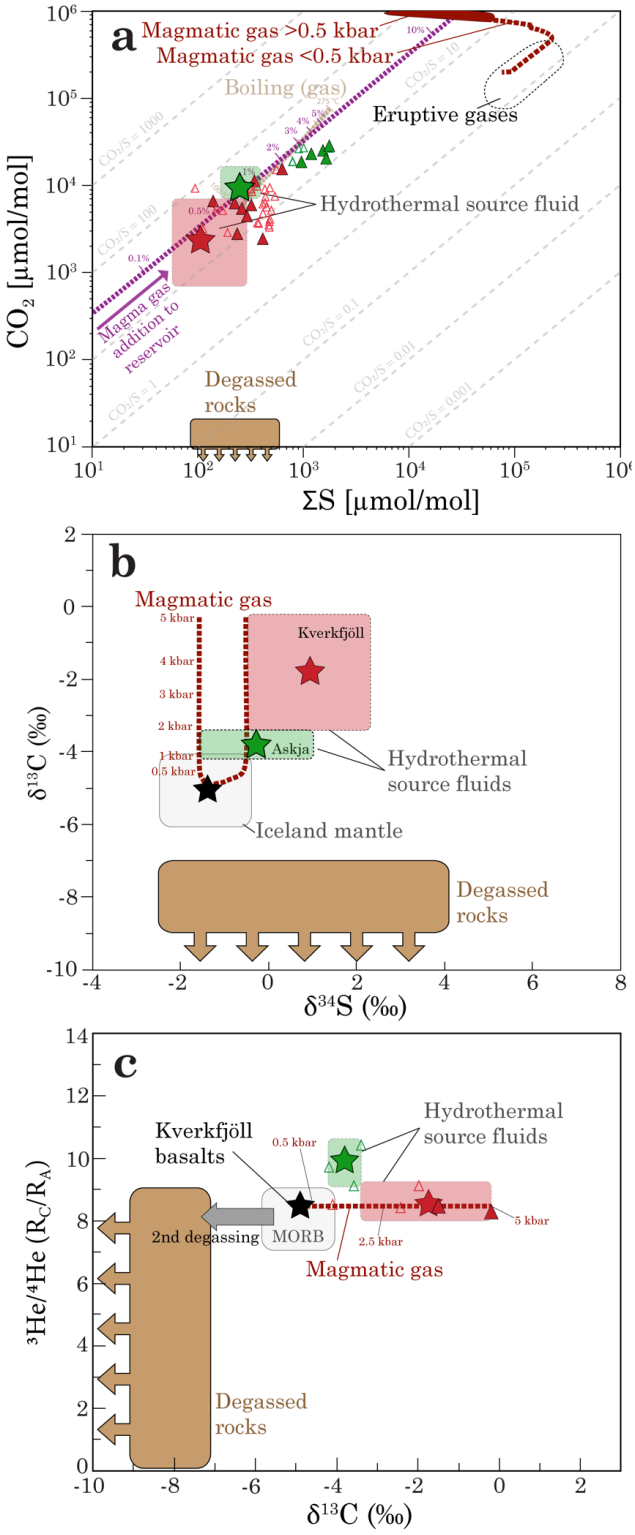
a
Magmatic gas >0.5 kbar
Magmatic gas <0.5 kbar
Boiling (gas)
Eruptive gases
Hydrothermal source fluid
Magma gas addition to reservoir
Degassed rocks
CO2/S = 1000
CO2/S = 100
CO2/S = 10
CO2/S = 1
CO2/S = 0.1
CO2/S = 0.01
CO2/S = 0.001
CO2 [µmol/mol]
ΣS [µmol/mol]
b
Magmatic gas
5 kbar
4 kbar
3 kbar
2 kbar
1 kbar
0.5 kbar
Kverkfjöll
Askja
Hydrothermal source fluids
Iceland mantle
Degassed rocks
δ13C (‰)
δ34S (‰)
c
Kverkfjöll basalts
0.5 kbar
Hydrothermal source fluids
2nd degassing
MORB
2.5 kbar
5 kbar
Magmatic gas
Degassed rocks
3He/4He (RC/RA)
δ13C (‰)

Figure 4.6 (previous page) Geochemical signatures of magmatic gases. (a) CO_2 versus H_2S. Measured fumarole and estimated reservoir compositions of Kverkfjöll and Askja (red and green stars, respectively) both display CO_2/S ratios that resemble deep (> 0.5 kbar) magmatic gases. A mixing line between a meteoric water component and magmatic gas (purple dashed line) implies ~0.5 to 3‰ input of magmatic gas to the reservoir fluid. The effect of depressurization boiling (light brown dashed line) on the CO_2/S ratio is small. (b) $\delta^{13}C$ versus $\delta^{34}S$. A field of magmatic gas compositions from closed-system degassing is shown in grey. Subfields show the estimated $\delta^{13}C$ of magmatic gases at a given intrusion pressure. The fields of degassed rocks (brown) are drawn after Torssander (1989), Füri et al. (2010) and Barry et al. (2014). (c) Measured $^3He/^4He$ versus $\delta^{13}C$. The $\delta^{13}C$-CO_2 values of both Askja and Kverkfjöll fumaroles are distributed between the estimated Iceland mantle value (taken as the MORB value of –5±1 ‰; Marty and Zimmermann 1999, Barry et al. 2014) and more positive $\delta^{13}C$ values estimated for magmatic gases from intrusions between 0.5 to 5 kbar (crimson dashed line), whereas the $^3He/^4He$ is not affected by degassing and is relatively invariable within each system. This observation is consistent with fumarole CO_2 being sourced from decompression degassing of intrusions at different crustal levels, rather than being derived from 2nd degassing or the host rocks, which are likely to have more negative $\delta^{13}C$ relative to source value.

Sulfur sources and reactions

Sulfur isotope ratios of hydrothermal fluids can help constrain the sources of S, and to identify secondary shallow processes that take place during the upflow (Ohmoto and Lasaga 1982, Ono et al. 2007, Marini et al. 2011, Gunnarsson-Robin et al. 2017, Kleine et al. 2021). Because of the small $\delta^{34}S$ fractionation associated with dissolution of magmatic gas into an aqueous hydrothermal reservoir liquid (Stefánsson et al. 2015), the $\delta^{34}S$ isotope value of the reservoir liquid is likely to closely reflect the signature of a source magmatic gas whereas the fumarole $\delta^{34}S$-H_2S can be shifted by up to +1.3 ‰ during decompression boiling upon fluid upflow (see section 4.6.2). The $\delta^{34}S$-H_2S values of Askja fumaroles (-1.5 to +1.3 ‰) are similar, or up to 2 ‰ more positive than basaltic, undegassed melts from the NRZ, which have $\delta^{34}S$ values of about -2.3 to -0.5 ‰ (Ranta et al. 2021b). These values are consistent with derivation of S from deep magmatic gas that experienced slight positive fractionation during adiabatic boiling. The Kverkfjöll fumarole $\delta^{34}S$-H_2S values (+1.1 to +4.8 ‰) are considerably more positive than undegassed, basaltic Kverkfjöll melts (-2.3 to -0.9 ‰), which indicates that significant fractionation must have taken place if S in the Kverkfjöll reservoir is sourced directly from magmatic gas. Positive $\delta^{34}S$ could be derived via leaching of degassed silicic host-rocks, which may have positive $\delta^{34}S$ of up to +4.2 ‰ (Torssander 1989, Ranta et al. 2021b). The highest $\delta^{34}S$ value in Kverkfjöll (+4.82 ‰) is found in a fumarole sample that also has the highest oxygen shift (d_O = +3.87 ‰), indicating extensive fluid-rock interaction, and low CO_2 (2800 µmol/mol), indicating low magmatic gas flux. Indeed, a weak negative correlation between $\delta^{34}S$-H_2S and ΣS in the Kverkfjöll fumaroles (Fig. 4.6c) suggests that the low-gas flux fumaroles experienced more $\delta^{34}S$ fractionation.

However, we note that previously measured $\delta^{34}S$-H_2S values in fumaroles at the Hveragerði and Krafla geothermal areas in Iceland span a wider range and are, on average, more positive relative to well discharges from same areas (Gunnarsson-Robin et al. 2017). We interpret these observations to reflect secondary effects imposed by unspecified shallow fumarole conduit processes on the measured $\delta^{34}S$-H_2S values. Thus, we consider the $\delta^{34}S$-H_2S signatures of fumaroles with higher gas-flux (> 10 mmol/mol CO_2) to better represent the reservoir fluid signature.

4.6.4 Magmatic volatile fluxes through hydrothermal systems

Several previous studies have attempted to quantify the mantle-to-atmosphere volatile fluxes associated with VHSs (Seward and Kerrick 1998, McGee et al. 2001, Barry et al. 2014, Stefánsson et al. 2016; Taran and Kalacheva 2018). Here, we apply a forward modeling approach, using the magmatic gas compositions that were estimated for intrusions at different crustal levels in Section 4.5.2 (Fig. 4.4). Then, using estimated magma extrusion rates (Thordarson and Larsen 2007, Thordarson and Höskuldsson 2008) and assuming intrusive/extrusive magmatism ratios of 4 to 8 (White et al. 2006) we calculate intrusive magmatic degassing potentials for Iceland for H_2O, CO_2, S and Cl (Table 4.3; Fig. 4.7; see Supplementary Information for calculation details). By comparing the magmatic degassing potential to observed volatile fluxes at geothermal systems and eruptions, it is possible to put semi-quantitative constraints on the deep volatile fluxes channeled via VHSs versus eruptions. Furthermore, this modeling approach allows us to place qualitative constraints on the relative contributions of decompression and crystallization-driven degassing and crustal leaching to the volatile fluxes in Icelandic VHSs.

Quantifying eruptive and intrusive volatile fluxes

Eruptive volatile flux. We estimate the eruptive CO_2 and S fluxes of 120-690 kt/yr and 70-170 kt/yr, respectively, based on estimated erupted basalt volumes from post-glacial (minimum value, 0.04-0.06 km^3/yr; Thordardson and Larsen 2007) and historic (last 1100 years; maximum value; 0.063 km^3/yr Thordarson and Höskuldsson 2008) eruptions (Fig. 4.7a).

Intrusive flux. The intrusive flux represents the total amount of volatiles carried by mantle-derived basaltic melts into the crust and atmosphere. This estimate does not differentiate between volatiles released to the atmosphere and volatiles sequestered by the crust. For CO_2 and S, the total intrusive flux is equal to the sum of volatiles lost through first and second boiling. We estimate an intrusive flux of 470 to 5520 kt/yr for CO_2 and 280 to 1380 kt/yr S, based on the eruptive fluxes and an intrusive/extrusive ratio for basaltic magmatism of 4 to 8 (Fig. 4.7a; White et al. 2006).

1^{st} degassing potential (= decompression degassing). The 1^{st} degassing potential is calculated by scaling the intrusive flux by the expected volatile release for two different intrusion pressures, 0.5 and 2.5 kbar (Table S3).

2^{nd} degassing potential (= crystallization-driven degassing). We make the assumption that most of the CO_2 and S remaining in magmatic intrusions after decompression degassing is lost via crystallization-driven degassing as the magmas cool and solidify. The validity of this assumption is supported by low concentrations of CO_2 (< 10 ppm) and S (< 200 ppm) in crystalline intrusions relative to undegassed melts (typically >1000 ppm for both CO_2 and S; Matthews et al. 2021, Ranta et al. 2021b). For CO_2 and S, the 2^{nd} degassing flux can thus be estimated by making the approximation

$$2^{nd}\text{ degassing flux} \approx \text{Intrusive flux} - 1^{st}\text{ degassing flux} \qquad (2)$$

Geothermal fluxes. A crude estimate of the flux of CO_2 and S emitted through geothermal systems to the atmosphere in Iceland can be made by multiplying a representative fumarole composition by the steam flux. We calculate a steam flux of 7600 kg/s using a total geothermal power estimate of 4000 MW for iceland (Björnsson 2006) and assuming a heat content of 1.9 kg/s/MW for pure water steam at 100°C (Stefánsson et al. 2011). This yields

a geothermal flux of 3360 kt/yr CO_2 and 220 kt/yr S. The same approach has been used previously to estimate geothermal gas fluxes for many individual Icelandic geothermal areas (Ármannsson 2016).

Kverkfjöll flux. The volatile fluxes emanating from the Kverkfjöll geothermal area was approximated similarly as above but using a geothermal heat output of 270±70 MW (Oddsson 2016), equivalent to a steam flux of 380-650 kg/s, and the average composition of 11 Hveratagl fumaroles (compositions from Ólafsson et al. 2000 and Byrne et al. 2021) that have relatively high gas flux and are assumed to be less affected by shallow S or C sequestration. This yields CO_2 and S fluxes of 290-500 kt/yr and 9-15 kt/yr, respectively.

Askja flux. Because the heat output or Askja is poorly constrained, we made a crude estimate of the geothermal volatile fluxes by assuming that (1) The high SO_4 concentrations (80-880 ppm, average 450 ppm; Ólafsson 1980, this study) of Lake Öskjuvatn are derived from quantitative condensation and oxidation of fumarolic H_2S that pass through the local aquifer (Fig. 4.8a), and that (2) the lake has a freshwater recharge of 48 Mt/yr (Ólafsson 1980). These values are used to calculate an average fumarolic S flux of 7 kt/yr. The flux of CO_2, which is not quantitatively scrubbed by the shallow aquifer (Ilyinskaya et al. 2015), cannot be estimated in the same way. Instead, if the average CO_2/H_2S of the Víti fumaroles is taken to be representative of the Askja hydrothermal fluids, the CO_2 flux can be estimated as 200 kt/yr. These yield a total steam flux of 103 kg/s or ≈ 3 Mt/yr, which correspond to 6.25% of the total inflow of freshwater into Lake Öskjuvatn, or an equivalent heat output of 196 MW.

Mantle to atmosphere CO_2 fluxes

Previous studies have estimated the total volcanic mantle-to-atmosphere CO_2 fluxes in Iceland at between 88 and 10,122 kt/yr (Barry et al. 2014) or 2200 and 4401 kt/yr (Stefánsson et al. 2016). These values are higher than our estimate for the eruptive CO_2 flux 120-690 kt/yr, but similar to our estimate of the intrusive CO_2 flux (470-5520 kt). The similarity between different CO_2 flux estimates suggests that (1) an intrusive/extrusive ratio of 4 to 8 is a reasonable estimate for Iceland, agreeing well with the ratio estimated by White et al (2006), and (2) the quiescent volcanic CO_2 degassing via VHSs is likely to account for >75 % of the total magmatic CO_2 flux, whereas CO_2 released during eruptions only accounts for a minor part (< 25%) of the total flux. Importantly, the independently calculated estimates for the flux of CO_2 through geothermal systems and the intrusive CO_2 flux roughly match (Fig. 4.7). The close match between the geothermal and intrusive CO_2 fluxes indicates that the basaltic intrusions vent a large part of their CO_2 load through geothermal systems (Fig. 4.8). The relative role between outgassing via VHSs and diffusive outlets is not well constrained. Existing estimates of diffusive CO_2 degassing in active Icelandic volcanoes vary from relatively low for Reykjanes (4-6 kt/yr; Fridriksson et al. 2006) and Hekla (16 kt/yr; Ilyinskaya et al. 2015) to extremely high for Katla (4380-8760 kt/yr; Ilyinskaya et al. 2018). The high estimate for Katla is anomalous, as it is similar to the entire estimated intrusive CO_2 flux of Iceland, and half of the CO_2 emissions rate of the 2014-15 Holuhraun eruption (12000-15600 kt/yr; Bali et al. 2018), which lasted for 180 days and was the largest basaltic eruption on Earth in the last > 200 years.

Table 4.4 Flux estimates

Type	Reference	Method	CO_2 (kt/year)			S (kt/yr)			H_2O (kt/yr)			Cl (kt/yr)		
			min	max	avg	min	max	avg	min	max	avg	min	max	avg
Iceland total flux														
Iceland (total CO2)	Barry2014	He flux and $CO_2/^3He$	88	10122	5105									
Iceland (total CO2)	Stefánsson2016	$\delta^{13}C$, heat output	2200	4401	3301									
Iceland (intrusive potential)[a]	Ármannsson2005	Magmatic flux			1300									
Iceland (intrusive potential)	*This study*	Magmatic flux	466	5328	2897	280	1332	806	932	13320	7126	47	466	256
Iceland eruptive flux[b]	*This study*	Magmatic flux	117	690	403	63	155	109	163	1208	685	1.2	6.0	3.6
Intrusive degassing fluxes														
1st degassing (2.5 kbar)	*This study*	Sol. model+mag.flx	326	3730	2028	5.6	67	36	2.8	80	41	0.0	9.3	4.7
1st degassing (0.5 kbar)	*This study*	Sol. model+mag.flx.	443	5062	2752	17	213	115	5.6	533	269	0.1	14.0	7.0
2nd degassing (2.5 kbar)	*This study*	Sol. model+mag.flx	140	1598	869	274	1265	770						
2nd degassing (0.5 kbar)	*This study*	Sol. model+mag.flx	23	266	145	263	1119	691						
Icelandic volcanoes														
Geldingadalir (estimate)	IES	Direct measurement			2192			1096						
Eyjafjallajökull 2010	Allard2010	Direct measurement			54788	1644	2192	1918			262980			708
Holuhraun 2014-15	Bali2018		11972	15625	13798			11477	45048					
Geothermal degassing														
Iceland geothermal	*This study*	Heat output			3365			220			236215	0.1		
Grímsvötn	Ágústsdóttir1994	Caldera lake composition			14	5.3	23	5.3						
Kverkfjöll	*This study*	Heat output	292	497	395	9.0	15	12	11688	19870	15779			
Askja geothermal	*This study*	Caldera lake composition	14	389	201	0.5	14	7.3						
Diffusive degassing														
Reykjanes	Fridriksson2006	Direct measurement	4.4	5.7	5.1									
Hekla	Ilyinskaya2015	Direct measurement			16			0.002						
Katla	Ilyinskaya2018	Airborne measurement	4380	8760	6570									

[a] Based on estimated magmatic flux of 5.8×10^{11} kg/yr with melt CO_2 concentration of 2000 ppm (Ármannsson 2005)
[b] Assuming degassing of 100% CO_2, 90% S, 70% H_2O and 10% Cl, based on decompression degassing to 1 bar

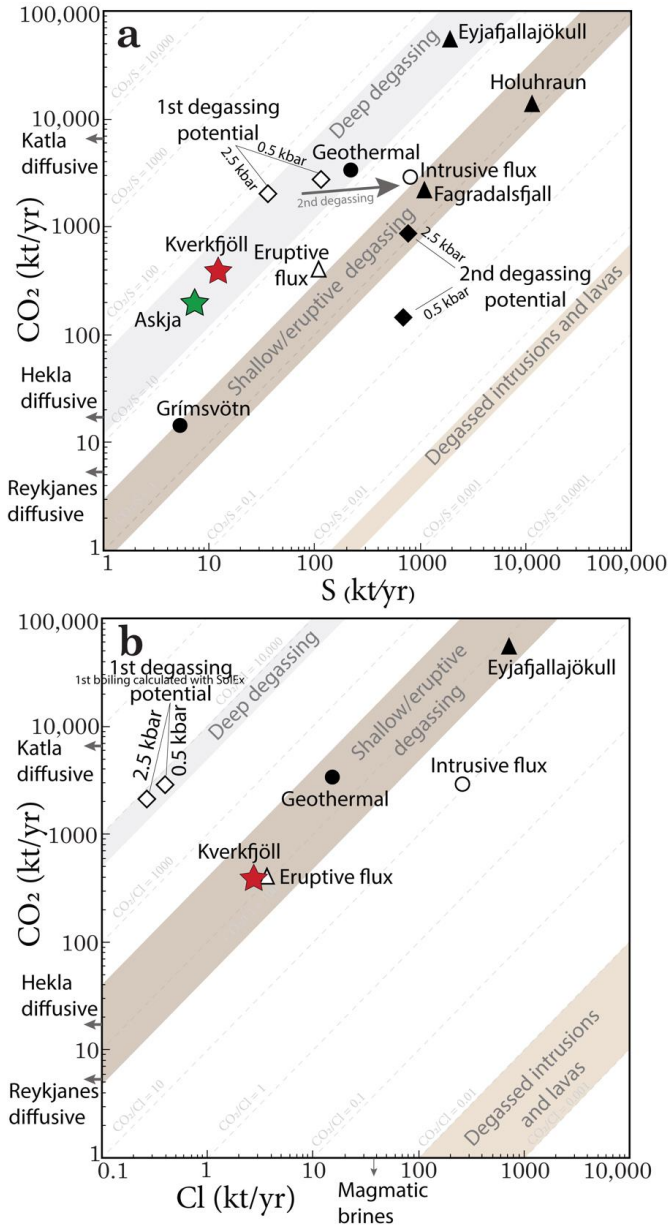

Figure 4.7 Volatile flux estimates for Icelandic volcanoes and VHSs. (a) Similar $CO_2/\Sigma S$ to between Icelandic VHSs and estimated magmatic gas compositions suggest that intrusive degassing is a plausible supplier of both CO_2 and S to VHSs in Iceland. Crustal leaching must play a minor role in the supply of CO_2 and S, because degassed intrusions and lavas that make up the upper Icelandic crust have very low $CO_2/\Sigma S$ (0.003-0.008). (b) By contrast, degassed crustal rocks retain most of their primary Cl content and are likely the main source of Cl in geothermal reservoir liquids.

Indeed, such high CO_2 flux, if maintained, would need to be sourced from an enormous inflow of deep-sourced melt corresponding to about 0.5 to 1 km^3/yr, assuming degassing of ~3000 ppm CO_2/kg melt with a density of 2700 kg/m^3. Such high melt production beneath Katla seems unrealistic (e.g., it would be noticed by the extensive GPS and seismic monitoring network at Katla). Thus, taken at face value, the extremely high CO_2 flux estimate for Katla could reflect either a transient phenomenon (a gas pulse or inflow of a fresh batch of magma) or a vastly higher CO_2 concentration in the Katla melts relative to our estimate, and is considered here to not be representative for typical quiescent CO_2 fluxes at active Icelandic volcanoes.

Importantly, a comparison between 1st degassing and total intrusive fluxes demonstrates that decompression degassing of basaltic intrusions is sufficient to account for the flux of CO_2 to Icelandic VHSs.

Mantle to atmosphere S fluxes

Whereas passive CO_2 degassing occurs through soils or via low-T groundwaters outside the realm of VHSs in Iceland (Gislason et al. 1992, Fridriksson et al. 2006, Ilyinskaya et al. 2016, Stefánsson et al. 2016), sulfur outgassing is typically negligible outside of geothermal areas. Thus, the flux of H_2S in fumaroles is a direct measure of quiescent magmatic sulfur fluxes to the atmosphere (McGee et al. 2001). Notably, this geothermal S flux estimated here (220kt/yr) is larger than the average atmospheric flux of S from eruptions (60-170 kt/yr).

For S, the gap between the magmatic 1st degassing flux (6-210 kt/yr S) and the total intrusive S flux potential (280-1380 kt/yr) is larger than for CO_2. (Fig. 8a) because of its higher solubility at intrusive pressures. Instead, most of the remaining intrusive S flux is expected to be lost from intrusions during 2nd degassing (the 2nd degassing potential is 270-1270 kt/yr). Cooling intrusions in a multi-tiered crustal plumbing system could provide a persistent flux of S to VHSs via 2nd degassing. However, the geothermal S flux estimated here is intermediate (220 kt/yr) between 1st and 2nd degassing fluxes, possibly suggesting that at least some S is sequestered naturally in the crust (see Gunnarsson-Robin et al. 2020), as is the case at submarine VHSs at mid-ocean ridges (Kleine et al. 2021). Another possible source of S to VHSs is leaching of host rocks (Gunnarsson-Robin et al. 2017), as the S concentration of basaltic lavas and intrusions (10-350 ppm, or up to 20% of the S in undegassed basaltic melts) is not negligible. Because the $\Delta^{34}S_{gas\text{-}melt}$ fractionation factor is poorly constrained (i.e., it may be either positive or negative), and due to possible $\delta^{34}S$ fractionation during shallow hydrothermal reactions, the $\delta^{34}S$ values of the fumarole gases cannot be conclusively used to separate between 2nd boiling and crustal leaching.

Mantle to atmosphere H_2O and Cl fluxes

Estimating the mantle fluxes for Cl and H_2O is more complicated than for CO_2 or S because of their higher solubility in basaltic melts and their potential sequestration in late-stage hydrous and chloride minerals and hydrosaline magmatic volatile phases (Webster 2004, Webster et al. 2015, Kleine et al. 2020, Ranta et al. 2021a). Mantle H_2O and Cl are transported by intrusions to the Icelandic crust at a rate of 930-13300 kt/yr and 50-470 kt/yr, respectively. However, only a small fraction of H_2O (3-530 kt/yr) and especially, of Cl (0.05 to 14 kt/yr), is lost during 1st degassing due to the high solubility of both volatiles at the chosen upper limit of intrusion pressures (0.5 kbar). Crystallization of magmas leads to exsolution of hydrosaline fluids or brines during late-stage evolution of silicic melts

(Webster 2004) amounting to approximately 2-32 kt/yr Cl in Iceland (Ranta et al. 2021a). However, because of their higher density relative to groundwater, brines are not easily incorporated into hydrothermal convection cells and may remain stagnant in the crust (Afanasyev et al. 2018). Instead, the estimated geothermal flux of Cl (0.1-31 kt/yr) is mainly due to remobilization of crustal Cl by high-T water-rock interaction (Stefánsson and Barnes 2016).

4.7 Summary and conclusions

This study demonstrates that the composition of natural geothermal fluids sampled at the surface can be used together with chemical, isotopic and volatile solubility modeling to recognize and quantify the contributions of magmatic volatile fluxes in volcanic hydrothermal systems. The results highlight the unique hydrogeology of Kverkfjöll, where a diluted and alkaline reservoir water flows out of the flank of the volcano, while the separated gas phase exits at a higher altitude producing an acid-sulfate geothermal area (Fig. 8b). Askja fumaroles are characterized by high gas content (2-3 mol.%) relative to other Icelandic VHSs (Fig. 4.8a). The $\delta^{13}C\text{-}CO_2$ and $\Delta^{33}S$ and $\delta^{34}S\text{-}H_2S$ signatures and $CO_2/\Sigma S$ measured in fumarole gases with high gas content are similar to estimated compositions of deep magmatic gases, suggesting that degassing from intrusive magmatism is the main source of CO_2 and S in Icelandic VHSs. Mass-balance calculations of estimated mantle CO_2 fluxes in Iceland show that most CO_2 degassed via VHSs (~3360 kt/yr) is derived from decompression degassing of basaltic magmas as they move from the mantle to the upper crust. However, decompression degassing of melts is probably insufficient to supply the observed VHS flux of S, amounting to about 50-100%; instead, leaching of host rock and crystallization-driven degassing of maturing intrusions below geothermal areas are suggested as additional sources of S to VHSs. By contrast, majority of the mantle flux of Cl (~50-470 kt/yr) is retained in the crust, as its high solubility in basalts leads to only minor intrusive (0-14 kt/yr) and eruptive (1-6 kt/yr) degassing. Instead, remobilization of crustal Cl by high-T water-rock interaction (0.1-31 kt/yr) and formation of magmatic brine (~9-23 kt/yr) are proposed as the main mechanisms that redistribute mantle-derived Cl in the crust.

4.8 Acknowledgements

ER gratefully acknowledges the Iceland Glaciological Society for field support during the 2019 Spring trip to Vatnajökull, and funding through multiple NordVulk Fellowships. Kate Gallagher and Karl Stefánsson were the best field assistants one could have hoped for in the occasionally harsh conditions during the sampling campaign in Hveradalur. Maja Bar Rasmussen and Matt Jackson are thanked for courageous field assistance at Askja. Ed Marshall, Dan Colman, Margaret Hartley, Maja and Guðmundur Guðmundsson are all thanked for joining various (failed) attempts at finding the source of the Hveragil river. Rósa Ólafsdóttir is thanked for ensuring superb water isotope data. Gareth Izon at MIT provided expert help during off-hours when the sulfur line was having hiccups.

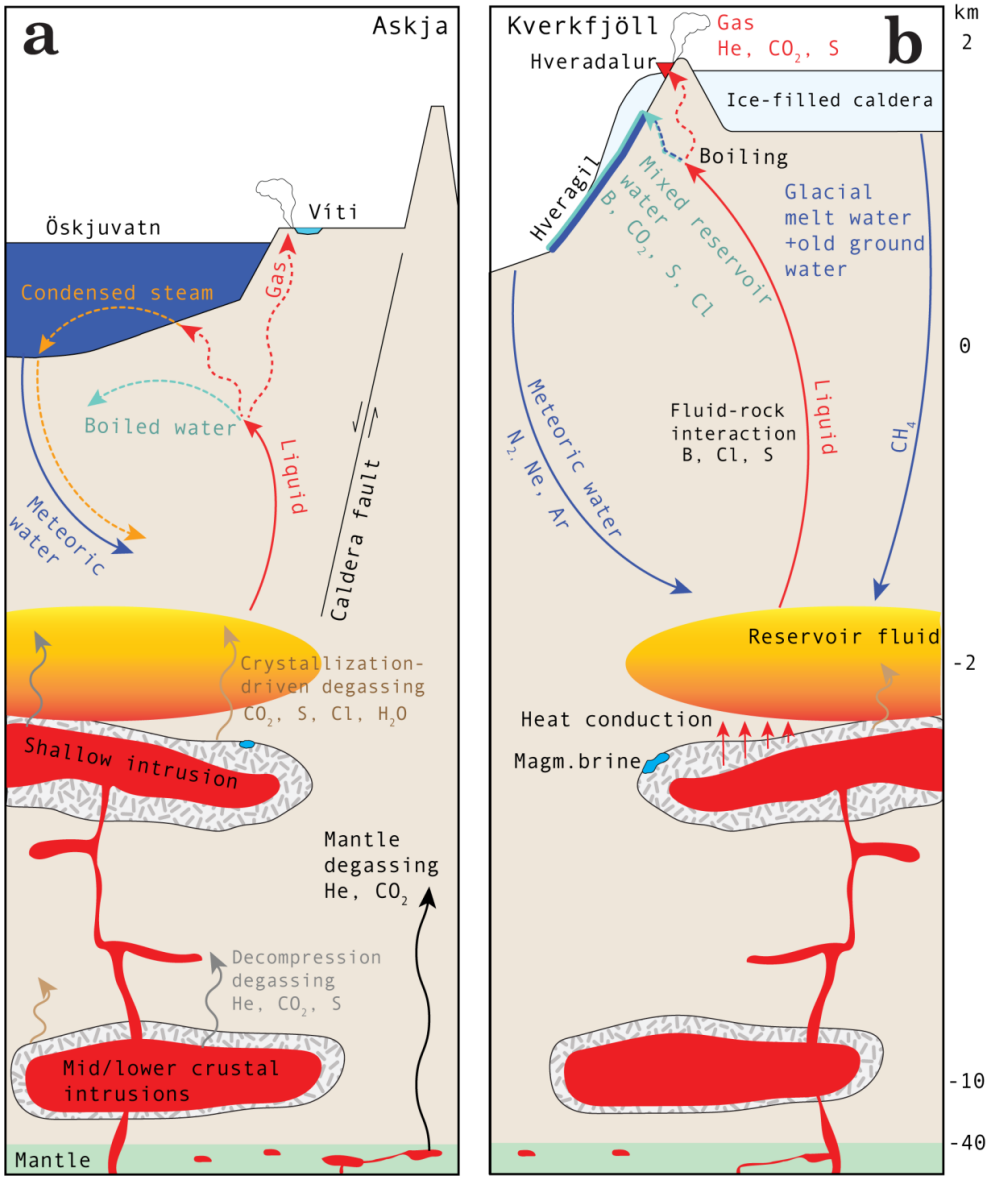

Figure 4.8 Summary figure illustrating the *volatile sources at the volcanic hydrothermal systems of (a) Askja and (b) Kverkfjöll. The differing thermal surface manifestations are largely dictated by the contrasting topography between Askja (flat) and Kverkfjöll (steep), whereas the magmatic roots underlying the hydrothermal reservoirs of the two systems are conceptually similar (see also Supplementary Information). Deep decompression degassing is the main source of He, CO_2 and S in the hydrothermal fluids. Crystallization-driven degassing and/or crustal leaching may be secondary sources of S, and provide small amounts of magmatic H_2O and Cl.*

4.9 References

Afanasyev, A., Blundy, J., Melnik, O., Sparks, S. (2018) Formation of magmatic brine lenses via focussed fluid-flow beneath volcanoes. Earth and Planetary Science Letters 486, 119–128.

Ágústsdóttir, A. M., & Brantley, S. L. (1994). Volatile fluxes integrated over four decades at Grímsvötn volcano, Iceland. Journal of Geophysical Research: Solid Earth, 99(B5), 9505-9522.

Aiuppa, A., Moretti, R., Federico, C., Giudice, G., Gurrieri, S., Liuzzo, M., Papale, P., Shinohara, H., & Valenza, M. (2007). Forecasting Etna eruptions by real-time observation of volcanic gas composition. *Geology*, *35*(12), 1115-1118.

Aiuppa, A., Fischer, T. P., Plank, T., & Bani, P. (2019). CO_2 flux emissions from the Earth's most actively degassing volcanoes, 2005–2015. *Scientific Reports*, *9*(1), 1-17.

Allard, P., Burton, M., Oskarsson, N., Michel, A., & Polacci, M. (2011). Magmatic gas composition and fluxes during the 2010 Eyjafjallajökull explosive eruption: implications for degassing magma volumes and volatile sources. In *Geophysical Research Abstracts*, Vol. 13.

Alt, J. C., & Shanks III, W. C. (1998). Sulfur in serpentinized oceanic peridotites: Serpentinization processes and microbial sulfate reduction. *Journal of Geophysical Research: Solid Earth*, *103*(B5), 9917-9929.

Andres, R. J., & Kasgnoc, A. D. (1998). A time-averaged inventory of subaerial volcanic sulfur emissions. *Journal of Geophysical Research: Atmospheres*, *103*(D19), 25251-25261.

Ármannsson, H. (2016). The fluid geochemistry of Icelandic high temperature geothermal areas. *Applied Geochemistry*, *66*, 14-64.

Árnason, B. Groundwater systems in Iceland traced by deuterium. *Publ. Soc. Sci. Isl.* **42,** 236 (1976)

Arnórsson, S., and Gunnlaugsson, E.: New gas geothermometers for geothermal exploration—calibration and application, Geochimica et Cosmochimica Acta, 49(6), (1985), 1307-1325.

Arnórsson, S., Bjarnason, J.Ö., Giroud, N., Gunnarsson, I., and Stefánsson, A.: Sampling and analysis of geothermal fluids. Geofluids, 6(3), (2006), 203-216.

Arnórsson, S., Stefánsson, A., & Bjarnason, J.O. (2007). Fluid-fluid interactions in geothermal systems, *Reviews in Mineralogy and Geochemistry*, *65(*1), 259-312.

Bali, E., Hartley, M. E., Halldórsson, S. A., Gudfinnsson, G. H., & Jakobsson, S. (2018). Melt inclusion constraints on volatile systematics and degassing history of the 2014–2015 Holuhraun eruption, Iceland. *Contributions to Mineralogy and Petrology*, *173*(2), 1-21.

Barry, P. H., Hilton, D. R., Füri, E., Halldórsson, S. A., & Grönvold, K. (2014). Carbon isotope and abundance systematics of Icelandic geothermal gases, fluids and subglacial basalts with implications for mantle plume-related CO2 fluxes. *Geochimica et Cosmochimica Acta*, *134*, 74-99.

Björnsson S. (2006) Geothermal power capacity. *Energy Conf.* 2006, 332–342 (in Icelandic).

Byrne, D. J., Broadley, M. W., Halldórsson, S. A., Ranta, E., Ricci, A., Tyne, R. L., Stefánsson, A., Ballentine, C.J., & Barry, P. H. (2021). The use of noble gas isotopes to trace subsurface boiling temperatures in Icelandic geothermal systems. *Earth and Planetary Science Letters*, *560*, 116805.

Craig, H. (1963). The isotopic geochemistry of water and carbon in geothermal areas. In: *Nuclear Geology on Geothermal Areas*, pp. 17-53, CNR, Pisa.

Edmonds, M., & Woods, A. W. (2018). Exsolved volatiles in magma reservoirs. *Journal of Volcanology and Geothermal Research*, *368*, 13-30.

Fiebig, J., Stefansson, A., Ricci, A., Tassi, F., Viveiros, F., Silva, S., Lopez, T.M., Schreiber, C., Hofmann, S. & Mountain, B.W. (2019). Abiogenesis not required to explain the origin of volcanic-hydrothermal hydrocarbons, *Geochemical Perspectives Letters*, 11, 23-27.

Fiebig, J. Woodland, A. B. Spangenberg, J., and Oschmann, W. (2007). Natural evidence for rapid abiogenic hydrothermal generation of CH_4. *Geochimica et Cosmochimica Acta*, 71, pp. 3028-3039.

Fiebig, J. Chiodini, G. Caliro, S. Rizzo, A. Spangenberg, J., and Hunziker, J. C. (2004). Chemical and isotopic equilibrium between CO_2 and CH_4 in fumarolic gas discharges: generation of CH_4 in arc magmatic-hydrothermal systems. *Geochimica et Cosmochimica Acta*, *68*.10, pp. 2321-2334.

Fischer, T. P. (2008). Fluxes of volatiles (H_2O, CO_2, N_2, Cl, F) from arc volcanoes. *Geochemical Journal*, *42*(1), 21-38.

Fischer, T. P., & Aiuppa, A. (2020). AGU Centennial Grand Challenge: Volcanoes and deep carbon global CO2 emissions from subaerial volcanism—Recent progress and future challenges. *Geochemistry, Geophysics, Geosystems*, *21*(3), e2019GC008690.

Fridriksson, T., Kristjánsson, B. R., Armannsson, H., Margrétardóttir, E., Ólafsdóttir, S., & Chiodini, G. (2006). CO_2 emissions and heat flow through soil, fumaroles, and steam heated mud pools at the Reykjanes geothermal area, SW Iceland. *Applied Geochemistry*, *21*(9), 1551-1569.

Füri, E., Hilton, D. R., Halldórsson, S. A., Barry, P. H., Hahm, D., Fischer, T. P., & Grönvold, K. (2010). Apparent decoupling of the He and Ne isotope systematics of the Icelandic mantle: The role of He

depletion, melt mixing, degassing fractionation and air interaction. *Geochimica et cosmochimica acta*, *74*(11), 3307-3332.
Gerlach, T. M. (1989). Degassing of carbon dioxide from basaltic magma at spreading centers: II. Mid-oceanic ridge basalts. *Journal of volcanology and geothermal research*, *39*(2-3), 221-232.
Gerlach, T. M. (1991). Present-day CO_2 emissions from volcanos. *Eos, Transactions American Geophysical Union*, *72*(23), 249-255.
Ghiorso, M. S. & Gualda, G. A. R. (2015). An H_2O–CO_2 mixed fluid saturation model compatible with rhyolite-MELTS. *Contributions to Mineralogy and Petrology*, *169*, 1–30.
Giggenbach, W. F. (1992). Isotopic shifts in waters from geothermal and volcanic systems along convergent plate boundaries and their origin. *Earth and planetary science letters*, *113*(4), 495-510.
Graham, D. W. (2002). Noble gas isotope geochemistry of mid-ocean ridge and ocean island basalts: Characterization of mantle source reservoirs. *Reviews in mineralogy and geochemistry*, *47*(1), 247-317.
Greenfield, T., & White, R. S. (2015). Building Icelandic igneous crust by repeated melt injections. *Journal of Geophysical Research: Solid Earth*, *120*(11), 7771-7788.
Greenfield, T., White, R. S., & Roecker, S. (2016). The magmatic plumbing system of the Askja central volcano, Iceland, as imaged by seismic tomography. *Journal of Geophysical Research: Solid Earth*, *121*(10), 7211-7229.
Gunnarsson-Robin, J., Stefánsson, A., Ono, S., & Torssander, P. (2017). Sulfur isotopes in Icelandic thermal fluids. *Journal of Volcanology and Geothermal Research*, *346*, 161-179.
Gunnarsson-Robin, J, Stefansson, A., Ono, S., Gunnarsson, I., & Aradottir, E. S. (2020). H_2S sequestration traced by sulfur isotopes at Hellisheiði geothermal system, Iceland. *Geothermics*, *83*, 101730.
Gylfadóttir, S.S., Kim, J., Helgason, J. K., Brynjólfsson, S., Höskuldsson, Á., Jóhannesson, T., Harbitz, C.B., & Løvholt, F. (2017). The 2014 Lake Askja rockslide-induced tsunami: Optimization of numerical tsunami model using observed data. *Journal of Geophysical Research: Oceans*, *122*(5), 4110-4122.
Harðardóttir, S., Halldórsson, S. A., & Hilton, D. R. (2018). Spatial distribution of helium isotopes in Icelandic geothermal fluids and volcanic materials with implications for location, upwelling and evolution of the Icelandic mantle plume. *Chemical Geology*, *480*, 12-27.
Hartley, M. E.,& Thordarson, T. (2012). Formation of Öskjuvatn caldera at Askja, North Iceland: Mechanism of caldera collapse and implications for the lateral flow hypothesis, Journal of Volcanology and Geothermal Research, *227*, 85-101.
Hilton, D. R. (1996). The helium and carbon isotope systematics of a continental geothermal system: results from monitoring studies at Long Valley caldera (California, USA). *Chemical Geology*, *127*(4), 269-295.
Horita, J., & Wesolowski, D. J. (1994). Liquid-vapor fractionation of oxygen and hydrogen isotopes of water from the freezing to the critical temperature. *Geochimica et Cosmochimica Acta*, *58*(16), 3425-3437.
Iacovino, K., Matthews, S., Wieser, P. E., Moore, G. M., & Bégué, F. (2021). VESIcal Part I: An open-source thermodynamic model engine for mixed volatile (H_2O-CO_2) solubility in silicate melts. *Earth and Space Science*, *8*(11), e2020EA001584.
Ilyinskaya, E., Aiuppa, A., Bergsson, B., Di Napoli, R., Fridriksson, T., Óladottir, A. A., Óskarsson, F., Grassa, F., Pfeffer, M., Lechner, K., Yeo, R., & Giudice, G. (2015). Degassing regime of Hekla volcano 2012–2013. *Geochimica et Cosmochimica Acta*, *159*, 80-99.
Ilyinskaya, E., Mobbs, S., Burton, R., Burton, M., Pardini, F., Pfeffer, M. A., Purvis, R., Lee, J., Bauguitte, S., Brooks, B., Colfescu, I., Petersen, G.N., Wellpott, A., & Bergsson, B. (2018). Globally significant CO_2 emissions from Katla, a subglacial volcano in Iceland. *Geophysical Research Letters*, *45*(19), 10-332.
Jackson, M. G., Blichert-Toft, J., Halldórsson, S. A., Mundl-Petermeier, A., Bizimis, M., Kurz, M. D., Price, A. A., Harðardóttir, S., Willhite, L. N. Breddam, K., Becker, T. W., & Fischer, R. A. (2020). Ancient helium and tungsten isotopic signatures preserved in mantle domains least modified by crustal recycling. *Proceedings of the National Academy of Sciences*, *117*(49), 30993-31001.
Jenkins, J., Maclennan, J., Green, R. G., Cottaar, S., Deuss, A. F., & White, R. S. (2018). Crustal formation on a spreading ridge above a mantle plume: receiver function imaging of the Icelandic crust. *Journal of Geophysical Research: Solid Earth*, *123*(6), 5190-5208.
Jónasson, K., & Einarsson, S. (2009) Jarðminjar á háhitasvæðum Íslands: jarðfræði, landmótun og yfirborðsummerki jarðhita. Icelandic Institute of Natural History, internal report, NÍ-09012, 151 pp.
Kleine, B. I., Stefansson, A., Halldórsson, S. A., & Barnes, J. D. (2020). Impact of fluid-rock interaction on water uptake of the Icelandic crust: Implications for the hydration of the oceanic crust and the subducted water flux. *Earth and Planetary Science Letters*, *538*, 116210.
Kleine, B. I., Gunnarsson-Robin, J., Kamunya, K. M., Ono, S., & Stefánsson, A. (2021). Source controls on sulfur abundance and isotope fractionation in hydrothermal fluids in the Olkaria geothermal field, Kenya. *Chemical Geology*, *582*, 120446.

Labidi, J., Barry, P. H., Bekaert, D. V., Broadley, M. W., Marty, B., Giunta, T., Warr., O, Sherwood Lollar, B., Fischer, T.P., Avice, G., Caracausi, A., Ballentine, C.J., Halldórsson, S.A., Stefánsson, A., Kurz, M.D., Kohl, I.E. & Young, E. D. (2020). Hydrothermal $^{15}N^{15}N$ abundances constrain the origins of mantle nitrogen. *Nature*, *580*(7803), 367-371.

Maclennan, J. (2019). Mafic tiers and transient mushes: evidence from Iceland. *Philosophical Transactions of the Royal Society A*, *377*(2139), 20180021.

Macpherson, C., & Mattey, D. (1994). Carbon isotope variations of CO2 in Central Lau Basin basalts and ferrobasalts. *Earth and planetary science letters*, *121*(3-4), 263-276.

Mandeville, C. W., Webster, J. D., Tappen, C., Taylor, B. E., Timbal, A., Sasaki, A., Hauri, E., & Bacon, C. R. (2009). Stable isotope and petrologic evidence for open-system degassing during the climactic and pre-climactic eruptions of Mt. Mazama, Crater Lake, Oregon. *Geochimica et Cosmochimica Acta*, *73*(10), 2978-3012.

Marini, L., Moretti, R., & Accornero, M. (2011). Sulfur isotopes in magmatic-hydrothermal systems, melts, and magmas. *Reviews in Mineralogy and Geochemistry*, *73*(1), 423-492.

Marty, B., & Giggenbach, W. F. (1990). Major and rare gases at White Island volcano, New Zealand: origin and flux of volatiles. *Geophysical Research Letters*, *17*(3), 247-250.

Marty, B., & Zimmermann, L. (1999). Volatiles (He, C, N, Ar) in mid-ocean ridge basalts: Assesment of shallow-level fractionation and characterization of source composition. *Geochimica et Cosmochimica Acta*, *63*(21), 3619-3633.

Matthews, S., Shorttle, O., Maclennan, J., & Rudge, J. F. (2021). The global melt inclusion C/Ba array: Mantle variability, melting process, or degassing?. *Geochimica et Cosmochimica Acta*, *293*, 525-543.

McGee, K. A., Doukas, M. P., & Gerlach, T. M. (2001). Quiescent hydrogen sulfide and carbon dioxide degassing from Mount Baker, Washington. *Geophysical Research Letters*, *28*(23), 4479-4482.

Mitchell, M. A., White, R. S., Roecker, S., & Greenfield, T. (2013). Tomographic image of melt storage beneath Askja Volcano, Iceland using local microseismicity. Geophysical Research Letters, 40(19), 5040-5046.

Montanaro, C., Scheu, B., Gudmundsson, M.T., Vogfjörd, K., Reynolds, H.I., Dürig, T., Strehlow, K., Rott, S., Reuschlé, T., & Dingwell, D.B. (2016). Multidisciplinary constraints of hydrothermal explosions based on the 2013 Gengissig lake events, Kverkfjöll volcano, Iceland. *Earth and Planetary Science Letters*, *434*, 308-319.

Neave, D. A., & Putirka, K. D. (2017). A new clinopyroxene-liquid barometer, and implications for magma storage pressures under Icelandic rift zones. *American Mineralogist*, *102*(4), 777-794.

Oddsson, B. (2016). Heat transfer in volcanic settings: Application to lava-ice interaction and geothermal areas. PhD dissertation, Faculty of Earth Science, University of Iceland, 106 pp.

Ohmoto, H., & Lasaga, A. C. (1982). Kinetics of reactions between aqueous sulfates and sulfides in hydrothermal systems. *Geochimica et Cosmochimica Acta*, *46*(10), 1727-1745.

Ohmoto, H., & Rye, R. O. (1979). Isotopes of sulfur of carbon. In: Barnes, H. L., ed., Geochemistry of hydrothermal ore deposits (2nd edition), New York, John Wiley & Sons, 509-569.

Óladóttir, B.A., Larsen, G., & Sigmarsson, O. (2011). Holocene volcanic activity at Grímsvötn, Bárdarbunga and Kverkfjöll subglacial centres beneath Vatnajökull, Iceland. *Bulletin of Volcanology*, *73*(9), 1187-1208.

Ólafsson, J. (1980). Temperature structure and water chemistry of the caldera Lake Öskjuvatn, Iceland. *Limnology and Oceanography*, *25*(5), 779-788.

Ólafsson, M., Torfason, H., & Grönvold, K. (2000). Surface exploration and monitoring of geothermal activity in the Kverkfjöll geothermal area, central Iceland. *Proceedings of the World Geothermal Congress*, Kyushu-Tohohu, Japan**,** 28, 1539-1545.

Ono, S., Shanks III, W. C., Rouxel, O. J., & Rumble, D. (2007). S-33 constraints on the seawater sulfate contribution in modern seafloor hydrothermal vent sulfides. *Geochimica et Cosmochimica Acta*, *71*(5), 1170-1182.

Ono, S., Keller, N. S., Rouxel, O., & Alt, J. C. (2012). Sulfur-33 constraints on the origin of secondary pyrite in altered oceanic basement. *Geochimica et Cosmochimica Acta*, *87*, 323-340.

Parkhurst, D. L., & Appelo, C. A. J. (1999). User's guide to PHREEQC (Version 2): A computer program for speciation, batch-reaction, one-dimensional transport, and inverse geochemical calculations. *Water-resources investigations report*, *99*(4259), 312.

Parmigiani, A., Degruyter, W., Leclaire, S., Huber, C., & Bachmann, O. (2017). The mechanics of shallow magma reservoir outgassing. *Geochemistry, Geophysics, Geosystems*, *18*(8), 2887-2905.

Poreda, R. J., Craig, H., Arnorsson, S., & Welhan, J. A. (1992). Helium isotopes in Icelandic geothermal systems: I. 3He, gas chemistry, and 13C relations. *Geochimica et Cosmochimica Acta*, *56*(12), 4221-4228.

Ranta, E., Barnes, J.D., Halldórsson, S.A., Jónasson, K., Stefánsson A. (2021a). Chlorine isotope ratios record magmatic brine assimilation during rhyolite genesis. *Geochemical Perspectives Letters*, *16*, 35-39.

Ranta, E., Gunnarsson-Robin, J., Halldórsson, S.A., Ono, S., Izon, G., Jackson, M.G., Reekie, C.D.J., Jenner, F.E., Guðfinnsson, G.H., Jónsson, O.P., Stefánsson, A. (2021b) Primordial and recycled sulfur sampled by the Iceland mantle plume. EartArXiv preprint, doi.org/10.31223/X5CD0Z

Sakai, H., & Matsubaya, O. (1977). Stable isotopic studies of Japanese geothermal systems. *Geothermics*, *5*(1-4), 97-124.

Sano, Y., & Marty, B. (1995). Origin of carbon in fumarolic gas from island arcs. *Chemical Geology*, *119*(1-4), 265-274.

Seward, T. M., & Kerrick, D. M. (1996). Hydrothermal CO_2 emission from the Taupo volcanic zone, New Zealand. *Earth and Planetary Science Letters*, *139*(1-2), 105-113.

Shinohara, H. (2013). Volatile flux from subduction zone volcanoes: Insights from a detailed evaluation of the fluxes from volcanoes in Japan. *Journal of Volcanology and Geothermal Research*, *268*, 46-63.

Sigmundsson, F., Pinel, V., Grapenthin, R., Hooper, A., Halldórsson, S. A., Einarsson, P., Ófeigsson, B. G., Heimisson, E. R., Jónsdóttir, K., Gudmundsson, M. T., Vogfjörd, K., Praks, M., Li, S., Drouin, V., Geirsson, H., Dumont, S., Frídriksdóttir, H. M., Gudmundsson, G. B., Wright, T. J., & Yamasaki, T. (2020). Unexpected large eruptions from buoyant magma bodies within viscoelastic crust. *Nature communications*, *11*(1), 1-11.

Sigurgeirsson, M.Á., Hjartarson, Á., Kaldal, I., Sæmundsson, K., Kristinsson, S.G., & Víkingsson, S. (2015). Geological Map of the Northern Volcanic Zone, Iceland. Southern Part. 1:100 000. Reykjavík: Iceland GeoSurvey.

Sparks, R. S. J., Wilson, L., & Sigurdsson, H. (1981). The pyroclastic deposits of the 1875 eruption of Askja, Iceland. *Philosophical Transactions of the Royal Society of London. Series A, Mathematical and Physical Sciences*, *299*(1447), 241-273.

Stefánsson, A., & Arnórsson, S. (2000). Feldspar saturation state in natural waters. *Geochimica et Cosmochimica Acta*, *64*(15), 2567-2584.

Stefánsson, A., & Arnórsson, S. (2002). Gas pressures and redox reactions in geothermal fluids in Iceland. *Chemical Geology*, *190*(1-4), 251-271.

Stefánsson, A., Arnórsson, S., Gunnarsson, I., Kaasalainen, H., & Gunnlaugsson, E. (2011). The geochemistry and sequestration of H2S into the geothermal system at Hellisheidi, Iceland. *Journal of Volcanology and Geothermal Research*, *202*(3-4), 179-188.

Stefánsson, A., & Barnes, J. D. (2016). Chlorine isotope geochemistry of Icelandic thermal fluids: Implications for geothermal system behavior at divergent plate boundaries. *Earth and Planetary Science Letters*, *449*, 69-78.

Stefánsson, A., Keller, N. S., Robin, J. G., & Ono, S. (2015). Multiple sulfur isotope systematics of Icelandic geothermal fluids and the source and reactions of sulfur in volcanic geothermal systems at divergent plate boundaries. *Geochimica et Cosmochimica Acta*, *165*, 307-323.

Stefánsson, A., Keller, N.S., Robin, J.G., Kaasalainen, H., Björnsdóttir, S., Pétursdóttir, S., Jóhannesson, H., & Hreggvidsson, G.Ó. (2016). Quantifying mixing, boiling, degassing, oxidation and reactivity of thermal waters at Vonarskard, Iceland. *Journal of Volcanology and Geothermal Research*, *309*, 53-62.

Stefánsson, A., Sveinbjörnsdóttir, Á. E., Heinemeier, J., Arnórsson, S., Kjartansdóttir, R., & Kristmannsdóttir, H. (2016). Mantle CO_2 degassing through the Icelandic crust: evidence from carbon isotopes in groundwater. *Geochimica et Cosmochimica Acta*, *191*, 300-319.

Stefánsson, A., Hilton, D. R., Sveinbjörnsdóttir, Á. E., Torssander, P., Heinemeier, J., Barnes, J. D., Ono, S., Halldórsson, S.A., Fiebig, J., & Arnórsson, S. (2017). Isotope systematics of Icelandic thermal fluids. *Journal of Volcanology and Geothermal Research*, *337*, 146-164.

Stefánsson, A. (2017). Gas chemistry of Icelandic thermal fluids. *Journal of Volcanology and Geothermal Research*, *346*, 81-94.

Taran, Y. A. (2009). Geochemistry of volcanic and hydrothermal fluids and volatile budget of the Kamchatka–Kuril subduction zone. *Geochimica et Cosmochimica acta*, *73*(4), 1067-1094.

Taran, Y., Zelenski, M., Chaplygin, I., Malik, N., Campion, R., Inguaggiato, S., Pokrovsky, B., Kalacheva, E., Melnikov, D., Kazahaya, R., & Fischer, T. (2018). Gas emissions from volcanoes of the Kuril Island arc (NW Pacific): geochemistry and fluxes. *Geochemistry, Geophysics, Geosystems*, *19*(6), 1859-1880.

Taran, Y., & Kalacheva, E. (2019). Role of hydrothermal flux in the volatile budget of a subduction zone: Kuril arc, northwest Pacific. *Geology*, *47*(1), 87-90.

Thode, H. G., Monster, J., & Dunford, H. B. (1961). Sulphur isotope geochemistry. *Geochimica et Cosmochimica Acta*, *25*(3), 159-174.

Thórarinsson, S. (1953). The Grímsvötn Expedition June-July 1953. *Jökull*, *3*, 6-22.

Thórarinsson, S. & Sigvaldason, G.E. (1962). The eruption in Askja, 1961; a preliminary report. *American Journal of Science*, 260(9), 641-651.
Thordarson, T., & Larsen, G. (2007). Volcanism in Iceland in historical time: Volcano types, eruption styles and eruptive history. *Journal of Geodynamics*, *43*(1), 118-152.
Thordarson, T., & Höskuldsson, Á. (2008). Postglacial volcanism in Iceland. *Jökull*, *58*(198), e228.
Torssander, P. (1989). Sulfur isotope ratios of Icelandic rocks. *Contributions to Mineralogy and Petrology*, *102*(1), 18-23.
Truesdell, A.H., & Fournier, R.O. (1977) Procedure for estimating the temperature of a hot-water component in a mixed water by using a plot of dissolved silica versus enthalpy. *USGS Journal of Research*, *5*, 49-52.
Webster, J. D. (2004). The exsolution of magmatic hydrosaline chloride liquids. *Chemical Geology*, *210*(1-4), 33-48.
Webster, J. D., Vetere, F., Botcharnikov, R. E., Goldoff, B., McBirney, A., & Doherty, A. L. (2015). Experimental and modeled chlorine solubilities in aluminosilicate melts at 1 to 7000 bars and 700 to 1250 C: Applications to magmas of Augustine Volcano, Alaska. *American Mineralogist*, *100*(2-3), 522-535.rner
White, S. M., Crisp, J. A., & Spera, F. J. (2006). Long-term volumetric eruption rates and magma budgets. *Geochemistry, Geophysics, Geosystems*, *7*(3).
Witham, F., Blundy, J., Kohn, S. C., Lesne, P., Dixon, J., Churakov, S. V., & Botcharnikov, R. (2012). SolEx: A model for mixed COHSCl-volatile solubilities and exsolved gas compositions in basalt. *Computers & Geosciences*, *45*, 87-97.

5 Paper IV

Geochemistry of basalts of the Kverkfjöll volcanic system, Iceland: Bridging the gap between rift and off-rift magmatism

Eemu Ranta[1], Sæmundur A. Halldórsson[1], Vesa Nykänen[2], Riina Kaikkonen[3], Guðmundur H. Guðfinnsson[1], Peter H. Barry[5], Hugh O'Brien[2], Maja Bar Rasmussen[1], Jóhann Gunnarsson-Robin[1], Edward W. Marshall[1], Andri Stefánsson[1], Enikő Bali[1], Matthew G. Jackson[6], Karl Grönvold[1]

[1]*Nordic Volcanological Center, Institute of Earth Sciences, University of Iceland, Iceland*
[2]*Geological Survey of Finland, Finland*
[3]*Oulu Mining School, University of Oulu, Finland*
[4]*Department of Geological Sciences , University of Texa at Austin, USA*
[5]*Marine Chemistry and Geochemistry Department, Woods Hole Oceanographic Institution, USA*
[6]*Department of Earth Science, University of California, Santa Barbara, USA*

Manuscript to be submitted to *Journal of Petrology* (or similar)

5.1 Abstract

Kverkfjöll is one of the major active volcanic systems in Iceland, accommodating a central stratovolcano and a fissure swarm that is characterized by subglacially erupted pillow basalt ridges. Located 30 km east of the main spreading axis of the Northern Rift Zone (NRZ), and 40 km to the west of the off-rift Öræfajökull Volcanic Belt (ÖVB), Kverkfjöll presents a unique and important, but sparsely studied example of Icelandic rift flank volcanism. Here, we present the first comprehensive petrochemical dataset of the Kverkfjöll magma suite, including major element concentrations of scoria and subglacial pillow rim glasses (n = 72), whole rock samples (n = 220) and minerals. In addition, select subglacial glasses were analyzed for trace element concentrations as well as noble gas (He-Ne-Ar), O and Pb isotope ratios. The Kverkfjöll magmas are almost exclusively basaltic tholeiites (95% of samples have MgO = 4-8 wt.%) and are characterised by high (enriched) K_2O (up to 1 wt.%), K_2O/TiO_2 (~0.19) and incompatible trace elements concentrations relative to the adjacent on-rift NRZ volcanic systems, but less enriched than the ÖVB. Steep, negatively sloping REE patterns with La/Yb of 4-6 and Dy/Yb of ~2, coupled to high Nb/Zr (0.10-0.13)—all intermediate between NRZ and ÖVB—indicate that the magmas are sourced as moderately low-degree partial melts of an enriched mantle source. Clinopyroxene-liquid barometry, microtextural observations and petrological modeling suggest that prior to eruption, the magmas evolve in a mid-crustal magma storage zone at ~3 kbar through fractional crystallization, receiving intermittent injections of more primitive magmas. Most (~80 %) sample compositions cluster at 4.0-5.5 wt.% MgO which coincides with a density maximum close to the onset of magnetite crystallisation at MgO of ~4.8 wt.%. The $\delta^{18}O_{glass}$ signature of Kverkfjöll glasses is +3.82±0.21 ‰ (1σ, n = 15, relative to VSMOW), which is lower than the composition of the depleted mantle source of mid-ocean ridge basalts (DMM; $\delta^{18}O_{glass}$ =+5.5‰). The $\delta^{18}O$ values of Kverkfjöll do not correlate with MgO but coincide with a broader Icelandic rift zone trend of decreasing $\delta^{18}O$ with decreasing MgO. The low $\delta^{18}O$ signature of Kverkfjöll is either an inherent feature of the Kverkfjöll mantle source, or is the result of earlier magmatic evolution deeper in the crust by assimilation of low-$\delta^{18}O$ crust. The Pb isotopic signatures of Kverkfjöll define a unique field among Icelandic volcanoes, with elevated $^{208}Pb/^{204}Pb$ and $^{207}Pb/^{204}Pb$ relative to $^{206}Pb/^{204}Pb$, that departs from the Iceland array toward the enriched mantle (EM2-type) signature of the ÖVB. We interpret the data to highlight the primary role of the lithospheric lid in controlling the degree of mantle melting in Iceland. The eastward-thickening lithosphere on the flank of the NRZ truncates the shallow end of the melting column, allowing preferential sampling of enriched mantle components seen in the trace element and radiogenic isotope chemistry of Kverkfjöll and ÖVB. The geochemical signature of the EM2 mantle component is only present to the east of the NRZ, and its absence to the west of the NRZ suggests it is either a peripheral component of the Iceland mantle plume or a local upper mantle anomaly, possibly reflecting DMM modified by both subduction fluids and subducted sediments.

5.2 Introduction

Among the presently active volcanic systems in Iceland, a dichotomy exists between the *on-rift* volcanic systems (e.g., Askja, Bárðarbunga, Krafla) that are characterized by tholeiitic basaltic eruptions along fissure swarms, and *off-rift* and *propagating rift* volcanoes (e.g. Snæfellsjökull, Heimaey, Öræfajökull, Snæfell, Hekla, Katla) that tend to lack well-developed fissure swarms and produce transitional to alkaline magmas

(Sigmarsson et al. 2008). These differences are thought to arise from the differing tectonic settings and melting regimes: Rift zones are characterized shallow average melt columns, high-degree decompression melting of the underlying mantle (e.g. Hardarson et al. 1997, Fitton et al. 2003, Schmeling and Marquart 2008) and subsequent melt homogenization in large crustal magma mush systems (Maclennan 2008a,b, Maclennan 2019, Caracciolo et al. 2020) that may be laterally widespread and transcend limits of individual volcanic systems (Gudmundsson and Andrew 2007, Sigmarsson and Halldórsson 2015). In contrast, the off-rift volcanoes represent shorter and deeper average melt columns that are truncated by a thicker lithosphere, producing lower-degree melts that preferentially sample enriched mantle components (Kokfelt et al. 2006, Martin and Sigmarsson 2010, Schattel et al. 2014, Kahl et al. 2021, van der Meer et al. 2021). Such melts migrate upwards in a colder crust in plumbing systems that are relatively isolated from crustal assimilation and magmatic input from neighbouring systems (Peate et al. 2010, Schattel et al. 2014, Banik et al. 2021, Kahl et al. 2021). Therefore, the trace element and isotopic signatures of the off-rift volcanoes potentially capture a fuller picture of the extent of mantle heterogeneity beneath Iceland (Kokfelt et al. 2006, Bo et al. 2018).

Indeed, the three volcanic regions outside the main rifts, where lower degree melting takes place, i.e., the Öræfajökull Volcanic Belt (ÖVB) and Snæfellsnes Peninsula (SNS) off-rift zones and the South Iceland Volcanic Zone (SIVZ) propagating rift (Fig. 5.1), all sample distinct and chemically enriched mantle (EM) components (e.g., Williams 2005; Kokfelt et al. 2006; Rasmussen et al. 2020). An enriched mantle 2 (EM2) type component (characterized by a distinct Sr-Nd-Pb isotopic signature; Zindler and Hart 1986) sampled by the ÖVB volcanoes is unique among Iceland's volcanoes (Sigmarsson et al. 1992, Prestvik et al. 2001, Williams 2005, Peate et al. 2010, Manning and Thirlwall 2014, Torsvik et al. 2015). Previous studies have attributed the origin of this signature to the presence of recycled marine sediments in the Icelandic mantle (Manning and Thirlwall 2014) or a block of continental crust belonging to the Jan Mayen Microcontinent buried beneath the basaltic crust of Iceland (Torsvik et al. 2015). Thus, the origin and the lateral extent of this mantle source are poorly constrained, in part because geochemical data from nearby volcanic formations (e.g., Kverkfjöll) are largely missing.

The active Kverkfjöll volcanic system lies on the eastern margin of the Northern Rift Zone (NRZ), partly covered by the Vatnajökull ice cap. Kverkfjöll is located in between the main rift axis of the NRZ and the ÖVB (Fig. 5.1), representing a unique intermediate member between on-rift and off-rift volcanism in Iceland—a so called rift flank volcanic system. As such, it is an ideal test ground for bridging models of melt generation at axial rift zones and off-rift volcanoes (e.g., Maccaferri et al. 2014, Haase et al. 2017) and to constrain the lateral extent of the ÖVB mantle domain. However, prior published geochemical data from Kverkfjöll are limited in terms of both basic and isotopic characterization.

The present work constitutes the first comprehensive geochemical study of the Kverkfjöll magma suite. We present major element data collected from a large sample set of glasses (n = 72) and whole-rocks (n = 220), that covers the spatial extent of the exposed northern part of the Kverkfjöll fissure swarm (the southern part of the volcanic system is covered by the Vatnajökull ice cap and is inaccessible for sampling; Fig. 5.1). In addition, trace element concentrations, noble gas isotope (He-Ne-Ar) and O and Pb isotope data, as well as mineral chemical data are presented for a subset of subglacially erupted pillow rim glasses. The goal of this study is three-fold: (1) To define the geochemical signature of the Kverkfjöll magma suite, (2) use this data to understand the crustal magmatic evolution and petrogenesis of the Kverkfjöll lavas, and (3) constrain the extent and nature of the EM2-type mantle component beneath Iceland.

5.3 Geological Setting

5.3.1 The Icelandic mantle plume and rift zone magmatism

Two fundamental geodynamic phenomena operate in Iceland: a divergent plate boundary marked by the Mid-Atlantic Ridge (MAR), and a mantle plume with Earth's highest buoyancy flux (Hoggard et al. 2020) that is currently centered beneath central Iceland (Wolfe et al. 1997, Rasmussen et al. 2020). As a result of this interaction, Iceland is one of the most volcanically active regions on Earth. Anomalously high melt production and thick crust in Iceland is attributed to a 100-200°C hotter (e.g. Schilling 1973, Ruedas et al. 2004, Matthews et al. 2016), and potentially wetter (Moore and Schilling, 1973, Nichols et al. 2002) Icelandic mantle compared to the depleted mantle source of mid-ocean ridge basalts (DMM). Excess heat and elevated water contents are associated with a hot upwelling mantle plume (i.e., the 'Iceland plume'), which appears to be rooted in an ultra-low seismic wave velocity zone (ULVZ) at the core-mantle boundary (Yuan and Romanowicz 2017).

Most postglacial (< ~14.5-10 ka; parts of Iceland became ice-free up to 5000 yrs before the Holocene; e.g., Patton et al. 2017) volcanism in Iceland is concentrated along actively deforming rift zones which mark the boundary between the North American and the Eurasian tectonic plates – the Western, Eastern and Northern Rift Zones (WRZ, ERZ and NRZ) and the Reykjanes Peninsula (RP), connecting to the submarine ridges Kolbeinsey (KR) and Reykjanes (RR) to the north and south, respectively (Fig. 1). Three active non-rifting volcanic zones are found outside the main rifts: The SIVZ is thought to represent an embryonic southward-extension of the ERZ; the SNVZ is located along an old rift segment in Snæfellsnes, with off-rift type magmatism since about 5.5 Ma (Martin and Sigmarsson 2010); and the ÖVB is defined by a row of the three stratovolcanoes Öræfajökull, Esjufjöll and Snæfell located east of the main ERZ and NRZ rift axes (Fig. 5.1). In contrast to the dominantly tholeiitic on-rift volcanism, these off-rift volcanoes are characterized by transitional to alkaline magmas that span a range from primitive basalts to rhyolites and trachytes (Jakobsson et al. 2008).

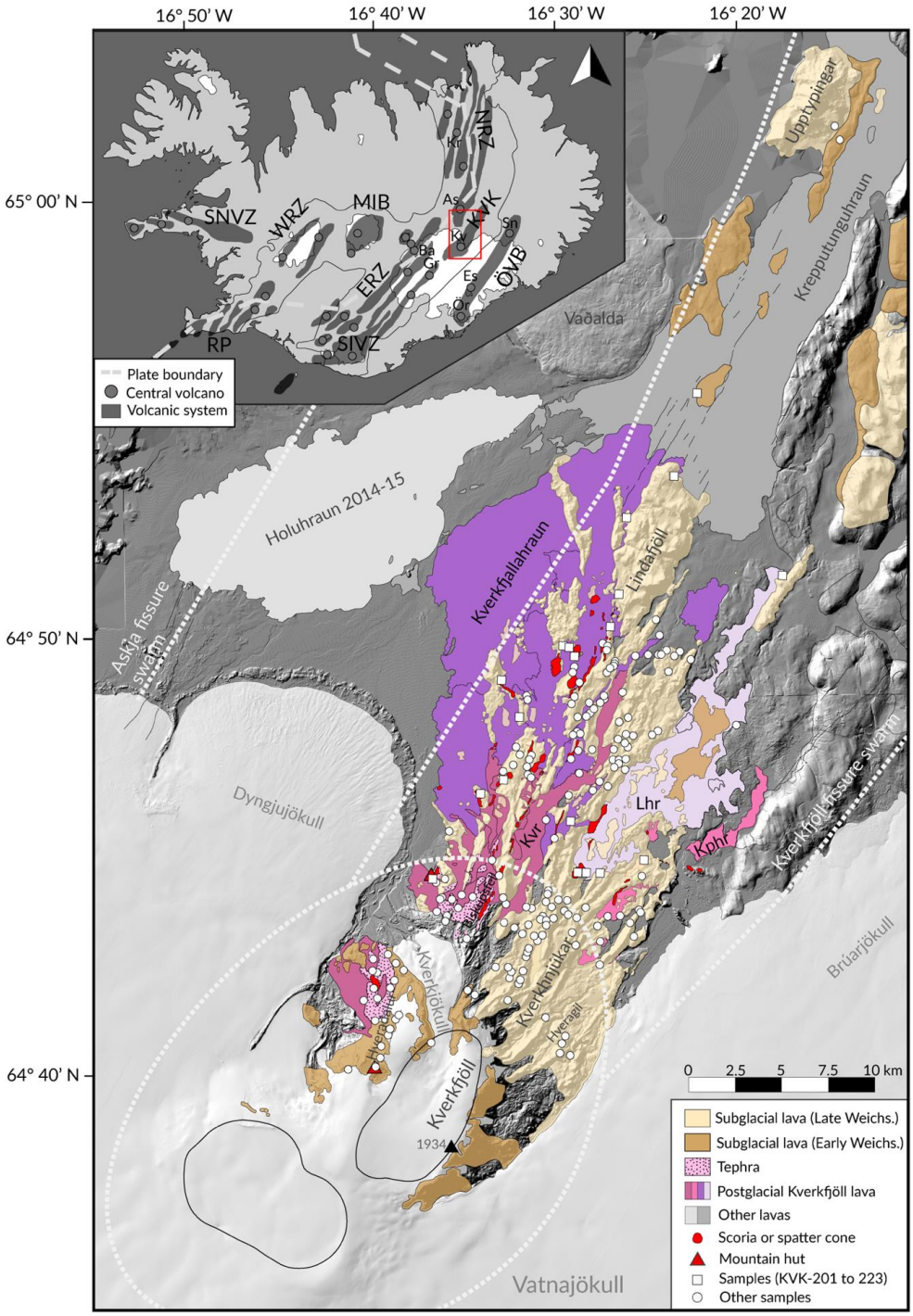

Figure 5.1 Overview map of Kverkfjöll. The inset shows the location of Kverkfjöll (KVK) and other active volcanic systems in Iceland. Dashed white lines indicate the approximate limits of the Askja and Kverkfjöll fissure swarms and the Kverkfjöll central volcano (after Hjartardóttir and Einarsson 2012). ERZ: Eastern Rift Zone. MIB: Mid-Iceland volcanic belt. NRZ: Northern Rift Zone. RP: Reykjanes Peninsula. SNVZ:

Snæfellsnes Volcanic Zone. SIVZ: South Iceland Volcanic Zone. WRZ: Western Rift Zone. ÖVB: Öræfajökull Volcanic Belt. The neighboring volcanoes Askja (As), Bárðarbunga (Ba), Esjufjöll (Es), Grímsvötn (Gr), Krafla (Kr), Öræfajökull (Ör), Snæfell (Sn) are labeled. Postglacial Kverkfjöll lava fields are abbreviated as follows: Lindahraun (Lhr), Kreppuhraun (Kphr), Kverkfjallaranahraun (kvr). Outlines and distinctions of the geological units are based on the map of Sigurgeirsson et al. (2015), reproduced with the permission of the Iceland GeoSurvey. Background digital elevation model is from the National Land Survey of Iceland.

5.3.2 The Kverkfjöll volcanic system

Geology

The Kverkfjöll volcanic system is situated in the central highlands of Iceland, ~30 km to the east of the main NRZ axis (Fig. 5.1). Its age is poorly constrained, but it is younger than the Brunhes-Matuyama magnetic field reversal (< 0.781 Ma; Sigurgeirsson et al. 2015). Together with Bárðarbunga-Vonarskarð and Grímsvötn, Kverkfjöll is one of the large volcanic systems in the Western Vatnajökull area and the 4th largest volcanic system in Iceland with an approximate area of 1600 km^2 (Thordarson and Höskuldsson 2008) and a fissure swarm with a total length of 100-130 km (Gudmundsson et al. 2013). Kverkfjöll sits on the eastern boundary of the NRZ, as defined by low gravity anomaly lineaments beneath Vatnajökull that likely mark a concentration of subglacial volcanic ridges (Gudmundsson and Högnadóttir 2007)

The volcanic system is centered around a mountain massif that rises to a maximum elevation of 1934 m.a.s.l., or about 1000-1200 m above its surroundings, and hosts two ovoidal, ~9x3 km glacier-filled calderas (Fig. 5.1; Sigurgeirsson et al. 2015). This mountain marks the central volcano of Kverkfjöll, an active stratovolcano built by dozens to hundreds of layers of stacked pillow basalts, hyaloclastites, tuffs and subaerial lavas. The 350 m deep 30 km^2 NE caldera is punctuated by the Kverkjökull outlet glacier, which has carved a valley through the partly exposed, steep-sided northern caldera rim (Gudmundsson et al. 2013). The 450 m deep 38 km^2 SW caldera is entirely ice-covered (Thórarinsson et al.1973, Gudmundsson et al. 2013). A significant positive gravity anomaly, centered at the SW caldera, likely represents a dense mafic intrusive complex, that was modeled by Gudmundsson and Högnadóttir (2007) as a gabbroic body in the uppermost 5 km of the crust with a volume of 200-300 km^3. Therefore, the SW caldera may have been the dominant locus of intrusive activity for a prolonged period of time.

Two fissure swarms connect to the central volcano in the NNE and SW. The NW fissure swarm is 15 km wide and extends at least 60 km to the NNE from the center of the central volcano to and including Mt. Upptyppingar (Hjartardóttir and Einarsson 2012), and possibly includes hyaloclastite formations even further to the north (Helgason 1989). The NW fissure swarm encompasses subglacially erupted pillow basalt and hyaloclastite ridges with a relief of up to 500 m, as well as post-glacial crater rows and lavas that typically occupy topographic lows. The eruptive fissure density is highest close to the central volcano and decreases abruptly north of Lindafjöll, while the non-eruptive fissures are relatively evenly distributed in the NE fissure swarm (Hjartardóttir and Einarsson 2012, Hjartardóttir et al. 2016). The Kverkfjöll fissure swarm terminates with atypically WNW oriented non-eruptive fissures between Mt. Upptyppingar and Mt. Herðubreið. This feature is interpreted by Hjartardóttir et al (2016) as a transform fault that accommodates the westward bend of the NRZ north of Kverkfjöll, by linking the northern end of Kverkfjöll fissure swarm all the way to the southern end of the Krafla fissure swarm. The Mt. Herðubreið region is known as one of the most earthquake-active regions in the area (Green et al. 2014). It is at present unknown whether the Fjallgarður province—a

voluminous hyaloclastite ridge formation defining a ~150 km long fissure system (Helgason 1989, Hjartardóttir and Einarsson 2012) running parallel, but off-set slightly to the east of Kverkfjöll—is related to the Kverkfjöll system.

A SW extension of the fissure swarm is inferred from the subglacial topography below Vatnajökull (Björnsson and Einarsson 1990, Björnsson and Pálsson 2020). The SW swarm extends, in the form of narrow ridges, about 10 km from the SW caldera toward, but terminating about 5 km short of Grímsvötn. These ridges can be assumed to be similar to the exposed subglacial hyaloclastite and pillow basalt ridges of the NW fissure swarm. A lack of associated gravity high might suggest that a corresponding sub-surface dike complex is too narrow to be resolved.

A 15 km long sinusoidal subglacial ridge south of the central volcano has an atypical N-S strike, extending towards the Esjufjöll volcanic system, which is a part of the ÖVB. This feature coincides with a weak positive gravity anomaly, but also with a magnetic anomaly that suggest that this subglacial ridge and/or underlying dikes were created before the Brunhes magnetic episode (i.e., prior to 0.781 Ma) (Jónsson et al. 1991, Gudmundsson and Högnadóttir 200). It is therefore unclear if this subglacial ridge is part of the Kverkfjöll system. This ridge is separated from Esjufjöll by a 500 m deep and 5 km wide subglacial canyon.

Magmas from rift volcanic systems in Iceland occasionally side-step and erupt toward, or through the fissures of their neighbouring volcanic system (Sigmarsson et al. 2000, Sigmarsson and Halldórsson 2015, Halldórsson et al. 2018). Whether magmas from neighbouring volcanic systems Bárðarbunga, Grímsvötn, Esjufjöll and Askja invade the Kverkfjöll fissure system is not known. The tensional stress field model of Gudmundsson and Andrew (2007) predicts only weak mechanical coupling between Kverkfjöll and Grímsvötn, and between Kverkfjöll and Bárðarbunga. Indeed, no spatial features connecting Kverkfjöll with its neighbouring volcanic systems have been observed in subglacial topography, gravity and magnetic mapping. Taken together, these observations suggest that Kverkfjöll is a relatively isolated volcanic system in the sense that it does not seem to share upper crustal magmatic pathways with its neighbours frequently.

A vigorous geothermal system at Kverkfjöll is manifested on the surface mainly as the two geothermally heated rivers Volga and Hveragil and a large geothermal area (25 km^2), centered along a fault on the northwestern rim of the NE caldera, with dozens of individual fumaroles, boiling pots and mud pools as well as two geothermal lakes (Friedman et al. 1974, Ólafsson 2000, Oddsson 2016). Hydrothermal explosions have occured at the ice-dammed lake Gengissig and its vicinity in 1959, 1968 and 2013 (Montanaro et al. 2015 and references therein).

Eruptive history

No historic (post-870 CE) eruptions are known, nor were any Kverkfjöll tephras found in ice cores from Vatnajökull spanning the last ~800 years (Larsen et al. 1998). About 12-15 post-glacial eruptive fissures and ~25 lava flows have been mapped, all in the southern part of the fissure swarm (Sigbjarnason 1996, Gudmundsson et al. 2013, Sigurgeirsson et al. 2015). Notable Holocene effusive eruptions include the Kreppuhraun and Lindahraun, which both produced approximately 0.1 km^3 of lava, an unnamed lava erupted from the flank of the central volcano, and Kverkfjallahraun, which represents the largest flow with an area of 80 km^2 and a likely volume of > 0.5 km^3 (Fig. 5.1; Larsen and Guðmundsson 2019). However, Kverkfjallahraun originates from five different fissures and it is unclear if these represent a single or several separate eruptions (Sigbjarnason 1996). Lindahraun

(~700 CE; Gudmunsson et al. 2013) is the latest post-glacial lava produced by Kverkfjöll. The basaltic Biskupsfell fissure eruption (~4-5 ka; Gudmundsson et al. 2013) is a volcanological peculiarity, being one of few known explosive fissure eruptions on Earth (Karhunen 1988). A detailed study by Karhunen (1988) shows that after an initial explosive phase, Biskupsfell eruption transformed to a more typical effusive phase including lava fountaining and gentle outpouring of lava, with a volume of 0.04 km^3 (Karhunen 1988). Similar eruptive sequences are probably characteristic of the other post-glacial eruptions at Kverkfjöll, although they typically erupt from distinct craters or crater rows. Post-glacial craters are often formed on top of older pillow basalt ridges, indicating that the magmas repeatedly use the same crustal pathways between their reservoirs and the surface. This results in frequent lava caps on top of the pillow ridges, a feature that is common in Iceland (*e.g.*, Pedersen et al. 2020). Three catastrophic Holocene pre-historic jökulhlaups with discharge rates of up to 10^5 m^3/s originating from Kverkfjöll have been identified by Carrivick et al. (2004). These cannot be tied to individual eruptions, but two of them pre-date, and one post-dates the Biskupsfell eruption. Such jökulhlaups are likely to be the main volcanic hazard posed by Kverkfjöll, as they can cause extensive flooding along the valley of the glacial river Jökulsá á Fjöllum even in distal areas over 100 km to the north.

The eruption frequency of Kverkfjöll during the last 7.5 ka was estimated by Óladóttir et al. (2011a), on the basis of tephra layers, to be on average one eruption per century, amounting to about 100 eruptions during the Holocene. The tephra layers associated with Kverkfjöll are mainly found along two distinct peaks at 6-5 ka and 3-2 ka, suggesting that Kverkfjöll experiences surges and lulls of eruptive activity (Óladóttir et al. 2011a).

Of pre-Holocene eruptions, few details are known. The most voluminous eruptive units of Kverkfjöll are the pillow- and hyaloclastite ridges that were erupted under up to 1.2-1.6 km thick ice during the latest glacial period (Höskuldsson et al. 2006), although several older pillow ridges are exposed (e.g. Rífnihnjúkur and eastern part of Mt. Upptyppingar; Fig. 5.1). Largest of these hyaloclastite-pillow ridge formations are Kverkhnjúkar and Lindafjöll (Fig. 5.2), each the result of multiple individual subglacial eruptions. Pre-Holocene tephra layers with Kverkfjöll-like compositions have been found in the North Atlantic region, including 17 layers from Greenlandic ice cores with ages between 35.7 and 28.5 ka (Bourne et al. 2015).

As a recent demonstration of ongoing magmatic activity at Kverkfjöll, a well-documented mid-crustal dyke injection event took place beneath Mt. Upptyppingar in 2007-2008 (White et al. 2011, Hooper et al. 2011). The associated seismicity and ground deformation are compatible with an injection of an inclined dyke from ~ 20 km to ~10 km depth, with an estimated volume of 0.04-0.05 km^3 (Hooper et al. 2011).

Geochemistry

Several previously published studies include geochemical data on the Kverkfjöll lavas (Sigvaldason et al. 1974, Sigvaldason and Óskarsson 1976, 1986, Nichols et al 2002, Macpherson et al. 2005, Höskuldsson et al. 2006, Füri et al. 2010, Pernet-Fisher 2012, Barry et al. 2014, Halldórsson et al. 2016a,b, Ranta et al. 2021, Marshall et al. 2022), but the datasets are incomplete. Major and trace element data have been published for tephra thought to originate from Kverkfjöll (Óladóttir et al. 2011a,b). The existing Kverkfjöll data suggest that its magma suite comprises dominantly evolved tholeiitic basalts, which are enriched in potassium (Sigvaldason et al. 1974), chlorine (Sigvaldason and Óskarsson, 1976) and water (Nichols et al. 2002; Höskuldsson et al. 2006) relative to most rift

tholeiites. Increasing K_2O contents from the off-shore Reykjanes Ridge (~0.1 wt.%) toward Kverkfjöll (up to 1 wt.%) was interpreted by Sigvaldason et al. (1974) as a sign that Kverkfjöll represents the center of the Iceland hotspot. Although the understanding of plume-ridge magmatism and the Iceland mantle plume has advanced greatly since (e.g., Sigmarsson and Steinthórsson 2007), the relationship between Kverkfjöll and the Iceland plume—now thought to be centered close to Bárðarbunga ~50 km west of Kverkfjöll (e.g., Wolfe et al. 1997)—is not yet clear.

Recent stable isotope studies suggest that Kverkfjöll represents a positive $\delta^{11}B$ (Marshall et al. 2022) and negative $\delta^{34}S$ (Ranta et al. 2021) endmember among Icelandic basalts, that have been interpreted as involvement of recycled and rehydrated oceanic crust (Marshall et al. 2022) and/or a subduction-fluid enriched mantle wedge-type material (Ranta et al. 2021) in its mantle source.

5.4 Samples and Methods

5.4.1 Samples

The sample set (Table S1) is compiled from four series that were collected from the Kverkfjöll area in multiple field campaigns between 1970 and 2017 under the auspices of the Nordic Volcanological Center (NordVulk; formerly Nordic Volcanological Institute) and the Institute of Earth Sciences (IES) at the University of Iceland. The KAL-series (n = 30) samples were collected in the early 1970's by K. Albertsson (Sigvaldason et al. 1974), focusing on the southern part of the volcanic system. The KFA-series (n = 40) were collected by K.Grönvold, G.E. Sigvaldason, P. Imsland and N. Óskarsson.. The most extensive series is represented by the KVK series, with KVK-1 to KVK-163 collected in expeditions from 1989 and onward lead by K. Grönvold and N. Óskarsson. The KVK series was extended in early 1990's by K. Grönvold and V. Nykänen from KVK-164 to KVK-193 and by E. Ranta, S.A. Halldórsson and M.B. Rasmussen from KVK-200 to KVK-223. In addition, four Kverkfjöll samples from the regional NAL-series (NAL-455, NAL-353 to NAL-358 and NAL-585; Macpherson et al. 2005) are included in this study.

5.4.2 Whole-rock analyses

For completeness, and to supplement the new data produced for this work, a previously unpublished NordVulk dataset comprising 220 whole-rock major and select trace element analyses from the KAL, KFA and KVK series from Kverkfjöll is included as a background dataset (Table S3). These data were collected from sample powders via inductively coupled plasma atomic emission spectroscopy (ICP-AES) at NordVulk. The full analytical protocol is described by Momme et al. (2003).

5.4.3 Electron probe microanalysis (EPMA) and melt inclusion post-entrapment correction

Major and minor element concentrations in glasses, minerals and melt inclusions were determined using a JEOL JXA-8230 SuperProbe electron probe microanalyser (EPMA) at the Institute of Earth Sciences (IES), University of Iceland, using wavelength-dispersive spectrometry (WDS). Reported data typically represent the average of 4-6 point analyses.

Analytical protocols follow those detailed by Bali et al. (2018), Caracciolo et al. (2020) and Ranta et al. (2021).
Olivine-hosted melt inclusions (MIs) were corrected for post-entrapment crystallization and diffusive re-equilibration (i.e., post-entrapment processes = PEP) using the Petrolog 3.1.1.3 program (Danyushevski and Plechov 2011). The FeO^* (estimated FeO content of melt at entrapment) of the MIs was estimated by calculating a FeO vs. TiO_2 regression line for the pillow rim glass data ($FeO^* = 7.041 + 2.304 \times TiO_2$; $R^2 = 0.89$). Both raw and PEP-corrected MI data are reported in Table S5, but only PEP-corrected data are plotted in the figures.

5.4.4 Laser ablation inductively coupled plasma mass spectrometry (LA-ICP-MS)

Trace element concentrations of 25 representative glasses were analysed *in-situ* by laser ablation inductively coupled plasma mass spetrometry (LA-ICP-MS) at the Finnish Geosciences Research Laboratory at the Geological Survey of Finland using an AttoM high-resolution ICP-MS instrument equipped with a 193 nm laser. The analytical protocol used was similar to the one outlined in Kaikkonen (2017) and Moilanen et al. (2020). The reported values for each sample represent averages of 6-12 spots. Spots were pre-ablated with 5 pulses to clean each spot prior to ablation, which was performed at an energy density of 2.5 J/cm^2 and a repetition rate of 10 Hz.

The BCR-2G reference material (Jochum et al. 2005) was used as an external standard for all elements. The Si concentration, as measured by EPMA-WDS, was used as an internal standard, matched with the intensity of the measured ^{27}Si signal. Beam diameters of 40-60 μm and 60 μm were used for samples and standards, respectively. The Ar auxiliary gas was set to 0.92 L/min. The measured isotopes were: ^{7}Li, ^{9}Be, ^{24}Mg, ^{29}Si, ^{43}Ca, ^{44}Ca, ^{45}Sc, ^{47}Ti, ^{49}Ti, ^{51}V, ^{52}Cr, ^{53}Cr, ^{55}Mn, ^{57}Fe, ^{59}Co, ^{60}Ni, ^{63}Cu, ^{66}Zn, ^{69}Ga, ^{72}Ge, ^{85}Rb, ^{88}Sr, ^{89}Y, ^{90}Zr, ^{93}Nb, ^{133}Cs, ^{137}Ba, ^{139}La, ^{140}Ce, ^{141}Pr, ^{146}Nd, ^{147}Sm, ^{153}Eu, ^{157}Gd, ^{159}Tb, ^{163}Dy, ^{165}Ho ^{166}Er, ^{169}Tm, ^{172}Yb, ^{175}Lu, ^{178}Hf, ^{181}Ta, ^{182}W, ^{208}Pb, ^{209}Bi, ^{232}Th and ^{238}U. The data were reduced with the SILLS software package (Guillong et al. 2008). Select major and trace element data from these sessions have been published previously by Ranta et al. (2021) and Marshall et al. (2022)

5.4.5 Iron redox state determination

The $Fe^{2+}/\Sigma Fe$ values of 5 hand-picked fresh pillow rim glass samples were analyzed by room-temperature Mössbauer spectrosopy (Helgason 2004) performed by prof. Örn Helgason, University of Iceland. Possible magnetite phenocrysts were removed by magnetic separation after crushing under propanol. The $Fe^{2+}/\Sigma Fe$ values of the same samples were also determined via Wilson-titration (Wilson, 1960). Of these, two samples were selected for low-temperature (70 K) Mössbauer spectroscopy performed by prof. Steen Morup, University of Copenhagen.

5.4.6 Noble gas isotope analysis

Helium, Ne and Ar isotopes were analyzed in three subglacial glasses (KVK-210, KVK-214, KVK-223) at the Woods Hole Oceanographic Institution, USA. The samples were chosen based on their high, undegassed S contents (Ranta et al. 2021). All samples were collected from lava flows that were not exposed and thus well-shielded from cosmic rays. Subglacial glasses chips free of visible alteration were handpicked from crushed and sieved

lavas, and then ultrasonically cleaned in ethanol. Glasses were then loaded and crushed under vacuum with a magnetically actuated metal ball. For He-Ne-Ar analyses, gases extracted from glasses were purified using a Ti sponge and Zr-Fe-Al getter pellets. He and Ne were sorbed/desorbed on a series of charcoal and nude stainless steel cryotraps, respectively, and were sequentially analyzed on a MAP 215-50 magnetic sector mass spectrometer. Procedural banks for ^{4}He were less than 5×10^{-12}. Procedural blanks for ^{20}Ne were less than 4×10^{-12} cm^3 STP. Ar isotopes were measured on a Hiden Triple Filter quadrupole mass spectrometer in ion counting mode with blanks less than 4×10^{-9} cm^3 STP. After applying blank corrections, all data were normalized to an in-house MORB glass and air standards, as described by Kurz et al. (2005, 2009) and Horton et al. (2021).

5.4.7 Oxygen isotope analysis

The $^{18}O/^{16}O$ ratios of 11 Kverkfjöll pillow rim glasses included in this study have been recently analysed at the High Temperature Stable Isotope Lab at Jackson School of Geosciences, University of Texas at Austin via laser fluorination isotope ratio mass spectroscopy (LF-IRMS). The method and data have been previously reported by Marshall et al. (2022).

Here, we report the $^{18}O/^{16}O$ ratios for additional 8 Kverkfjöll glasses that were measured by Geochron Laboratories, Inc., Cambridge, Mass., in 1996 with conventional methods. These data have an analytical uncertainty of $1\sigma = 0.2$ ‰. The data are reported in standard delta notation as $\delta^{18}O = (({}^{18}O/{}^{16}O)_{sample}/({}^{18}O/{}^{16}O)_{V\text{-}SMOW})\text{-}1)x1000$ ‰, where V-SMOW is refers to Vienna Standard Mean Ocean Water.

5.4.8 Multi-collector ICP-MS

Lead isotope ratios of 30 Kverkfjöll samples were analyzed at IES, University of Iceland, using a Nu Plasma multi collector ICP-MS (MC-ICP-MS). The analyses were made on hand-picked glass chips (N = 17) and whole-rock powders (N = 13). For glass chips, 300-500 mg of sample was leached twice with 6M HCl with a drop of concentrated HBr and subsequently twice in MQ-water (18.2 MΩ). All leaching steps took place in an ultrasonic bath over 30 min. The sample was rinsed twice with MQ water after each leaching step. Standard powders were not leached. Thus, the unleached reference values were used for evaluating accuracy of the analyses. Dissolution of samples and standards took place in a 4:1 mixture of concentrated double distilled HF and HNO_3 in Teflon vials. The vials were sonicated at 69°C for 90 minutes, then left on a hotplate at 140 °C for a minimum of 24 h. Following complete reaction, the sample was dried down, converted to HNO_3 by adding ~1-2 ml of HNO_3 and dried down again, then brought up in ~10 ml concentrated HNO_3, followed by sonication, heating and drying steps similarly to the previous dissolution step. In cases where dissolution was not complete, an additional dissolution step with aqua regia (3:1 solution of concentrated HCl:HNO_3) was applied. Fully dissolved samples were drier down and brought up in 4-8 ml 0.5M HBr. Pb was separated via ion chromatographic column chemistry, following the "HCl-method" of Kamber and Gladu (2009). The extracted Pb cut was converted to HNO_3 form and brought up in a 2% HNO_3 running solution. This solution was analyzed via MC-ICP-MS following the protocol described in Halldórsson et al. (2018). In short, Tl spiking (addition of SRM-997 with a known $^{205}Tl/^{203}Tl$ value) was used for correcting for instrumental mass fractionation. The SRM-981 reference material was used as a bracketing standard and was analyzed after every one or two unknowns. Procedural blanks contained up to 200 pg of Pb, which is considered negligible (~0.1 %) relative to the size of analyzed samples (100-300 ng Pb). Therefore no blank correction was performed. The analytical uncertainty (2 SE) is on average 0.0020 for $^{206}Pb/^{204}Pb$, 0.0019 for $^{207}Pb/^{204}Pb$ and 0.0045 for $^{208}Pb/^{204}Pb$ (Table S10).

5.5 Results

A summary of the petrographic observations, geochemical data (major and trace elements, mineral chemistry, noble gas, oxygen and lead isotopes) is presented below. The full dataset is provided in Tables S2-S14.

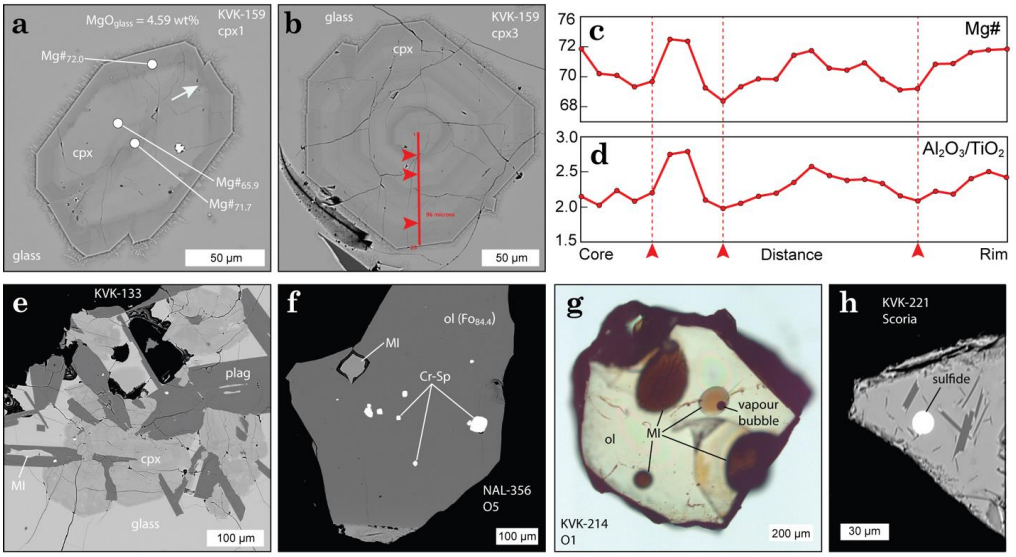

Figure 5.2 Petrography. (a) Clinopyroxene microphenocryst with reverse zoning. The contact between the interior and the more primitive rim has a partly resorbed contact (white arrow). (b) Clinopyroxene showing both short-wavelength (oscillatory) and long-wavelength zoning visible as lighter and darker bands. Red line shows the ~100 µm trajectory of an EPMA-WDS line scan with (c) Mg# and (d) Al_2O_3/TiO_2 (wt.%) shown against distance from the center of the crystal. Three red arrows in (b)-(d) indicate the locations of trend reversals in the crystal chemistry. Increasing Mg# during crystal growth implies arrival of more mafic melt into the proximity of the cpx, possibly following a recharge event in the magma storage zone. (e) A typical glomerocryst with intergrown clinopyroxene and plagioclase, sitting in glassy matrix of a subglacial pillow rim. (f) A relatively primitive olivine macrocryst ($Fo_{83.7}$) with inclusions of Cr-spinel and melt. (g) Double-polished olivine macrocryst with four visible (80-270 µm diameter) melt inclusions. The MI exposed on the surface has a vapor (or shrinkage) bubble. The remaining three MIs are exposed on the flip side of the crystal. (h) Sulfide globule in scoria from the Lindahraun crater.

5.5.1 Petrography

Based on point-counting, basaltic hand-samples from Kverkfjöll vary from almost aphyric (< 0.5 % macrocrysts, here defined as crystals larger than > 1 mm) to sparsely phyric (< 10 vol.% macrocryst; Table S2) to more rarely found plagioclase ultraphyric samples (> 25 vol.% plagioclase; e.g. sample NAL-455; Hansen and Grönvold 2000). The crystallinity of the pillow rim glasses is on average ~10 %. For both macro- and microphenocryst populations, the main minerals, in the order of decreasing abundance, are plagioclase, clinopyroxene, olivine and magnetite.

Most pillow rim glasses are vesicular; exceptions are the two most primitive samples NAL-356 and NAL-585 from Mt. Upptyppingar. The groundmass of the pillow rims is generally fresh and glassy, whereas the matrix glass in the scoria and hyaloclastite samples is rife with microlites.

Sub- to euhedral plagioclase laths of up to 30 mm are found in all samples and occur frequently in glomerocrysts together with clinopyroxene and/or olivine (Fig. 5.2e). Many plagioclase macrocrysts are euhedral to subhedral and have more An-rich or slightly resorbed cores that commonly display oscillatory and/or complex zoning (Figs. 5.2a-d). These cores are mantled by a compositionally homogeneous 10-100 μm wide rim of less An-rich composition that is typically similar to the composition of homogeneous plagioclase microcrysts (< 100 μm) in the matrix glass (cf. Kaikkonen 2017).

Olivine macro- and microphenocrysts vary from sub-to euhedral, but some have embayments or are visibly resorbed. Mineral inclusions of Cr-spinel are common in the more primitive (Fo > 83) olivine microphenocrysts (Fig. 5.3f), whereas magnetite is present only in groundmass of samples with less than ~4.8 wt.% MgO.

Both macro- and microphenocrysts of clinopyroxene typically display oscillatory and sector zoning. Reversely zoned clinopyroxenes are also common (Fig. 5.2a-b).

Glassy melt inclusions and embayments (10-300 μm) are found in the cores and rims of both plagioclase and olivine and, more rarely, in magnetite. Sulfide globules (2-20 μm) are found in the matrix glass of scoria samples, as inclusions in low-An plagioclase, and in glassy melt inclusions of low-An plagioclase.

5.5.2 Major and minor elements

Major and minor oxide compositions of whole-rocks, matrix glasses and MIs are reported in Tables S3-S5 and Fig. 5.3. The Kverkfjöll magma suite has a notably restricted compositional range with matrix glass compositions between 3.4-7.5 wt.% MgO and 47.7-52.9 wt.% SiO_2 (Fig. 5.3a). More primitive glass compositions are seen in olivine-hosted MIs, which have PEP-corrected MgO content of up to 9.6 wt.%. All matrix glass major oxide contents (e.g., CaO, K_2O) show tight correlations with MgO, that follow similar or parallel trends to the tholeiitic basalts of the NRZ and ERZ (Fig. 5.3a). The most notable differences between Kverkfjöll and NRZ/ERZ are the slightly lower SiO_2 concentrations of 48 wt.% (Fig. 5.3a) and relatively high K_2O concentrations of 0.4 wt.% at 7.5 wt.% MgO (Fig. 5.3c). The CaO content decreases with MgO owing to plagioclase and clinopyroxene crystallization (Fig. 5.3c). Both FeO_t and TiO_2 contents reach a peak at 15.5 wt% and 3.8 wt.% respectively at a MgO content of ~4.8 wt.% (Figs. 5.3d-e). At that point, titanomagnetite starts to crystallise and causes a depletion in both FeO_t and TiO_2 and an increase in SiO_2 in more evolved samples. The K_2O/TiO_2 (by weight) of Kverkfjöll, is between 0.16 and 0.20 for all glasses and MIs with MgO > 5 wt.% (Fig. 5.4f). At lower MgO, titanomagnetite crystallization causes an increase in K_2O/TiO_2. Kverkfjöll melts have a moderately enriched K_2O/TiO_2 signature that is intermediate between the K_2O/TiO_2 range of 0.03-0.16 seen in the rift zones and 0.27-0.40 of Snæfell (Fig. 5.4f).

Whole-rock compositions follow the trends defined by the matrix glass compositions, but show a somewhat larger variation of MgO (2.7-10.6 wt.%) and SiO_2 (47.3-55.5 wt.%; Fig. 5.3a). Anomalous whole-rock compositions with high MgO and low CaO contents relative to matrix glasses can be explained by olivine accumulation, whereas anomalously high CaO and low FeO contents result from plagioclase accumulation.

Almost all Kverkfjöll samples (WR and glass) are classified as tholeiitic basalts that are either quartz or olivine normative. Rare exceptions are two icelandite glasses (iron-rich basaltic andesites) and two andesitic whole rock samples from the NE caldera rim. The most primitive matrix glasses with MgO = 7.5 wt.% are found from Mt. Upptyppingar, at the northern part of the fissure swarm (Fig. 5.1), while several additional samples have moderately high MgO of 6-7 wt.%. However, 81% (N = 58) of the matrix

glasses have compositions between 4.0 and 5.5 wt.% MgO (Fig. 4). Although similar evolved basaltic compositions are common in eruptions within the nearby central volcano of Askja (Hartley and Thordarson 2013), the overwhelmingly evolved basaltic character of the Kverkfjöll fissure swarm makes the Kverkfjöll unusually homogeneous compared to most other Icelandic volcanic systems with central volcanoes, which generally display a wider spectrum of compositions. Notably, with the possible exception of a rhyolitic erratic (KFA-40) found south of the Kverkfjökull glacier, which may originate from Kverkfjöll (Gudmundsson et al. 2013), no dacitic or rhyolitic compositions are present in the dataset of 72 glasses and 220 whole rock samples.

5.5.3 Trace elements in glass

The LA-ICP-MS trace element data are reported in Table S6. Kverkfjöll basalts have incompatible trace element concentrations that are higher than the NRZ, but lower than the ÖVB basalts (Fig. 5.4a). The rare earth element (REE) pattern of Kverkföll is moderately steep, characterized by enrichment in lighter REEs (LREEs: La-Eu) and a depletion in the heavier REEs (HREEs: Sm-Lu) compared to the ERZ and NRZ tholeiites (Fig. 5.4b).

Partitioning coefficients for mineral-melt pairs for the Kverkfjöll magmas have been previously established by Kaikkonen (2017). The trace elements that are incompatible in all crystallising minerals, i.e. plagioclase, olivine, clinopyroxene and magnetite, are Li, Rb, Zn, Zr, Nb, REEs, Ba, Cs, Pb and Th. These incompatible elements increase systematically in concentration during melt evolution (Fig. S1). Vanadium, which is only compatible in magnetite, drops in concentration at the onset of magnetite crystallisation below 4.8 wt.% MgO (Fig. 5.5a). Copper, which is not compatible in any of the observed mineral phases, increases first from 140 ppm at MgO = 7.5 wt.% to 200 ppm at MgO = 6.0 wt.% and then decreases to 50 ppm at MgO = 4 wt.% (Fig. 5.5d). This sudden decrease in Cu concentrations signals the formation of immiscible sulfide melt, in which Cu is compatible (Fig. 5.5e-f; Ranta et al. 2021). Ni and Cr are strongly compatible in olivine and clinopyroxene and decrease from 100 to 10 ppm and from 250 to 2 ppm, respectively, between MgO = 7.5-4.0 wt% (Fig. S1). Strontium is moderately compatible in plagioclase ($K_d \approx 1.85$), but incompatible in olivine ($K_d \approx 0.0001$), clinopyroxene ($K_d \approx 0.08$) and magnetite (Kaikkonen 2017). The near-constant Sr concentrations throughout the Kverkfjöll magma evolution (Fig. S1) therefore indicate that plagioclase constitutes 50-70% of the bulk of crystallising minerals throughout the magmatic evolution, in accord with petrographic observations (cf. Kaikkonen 2017).

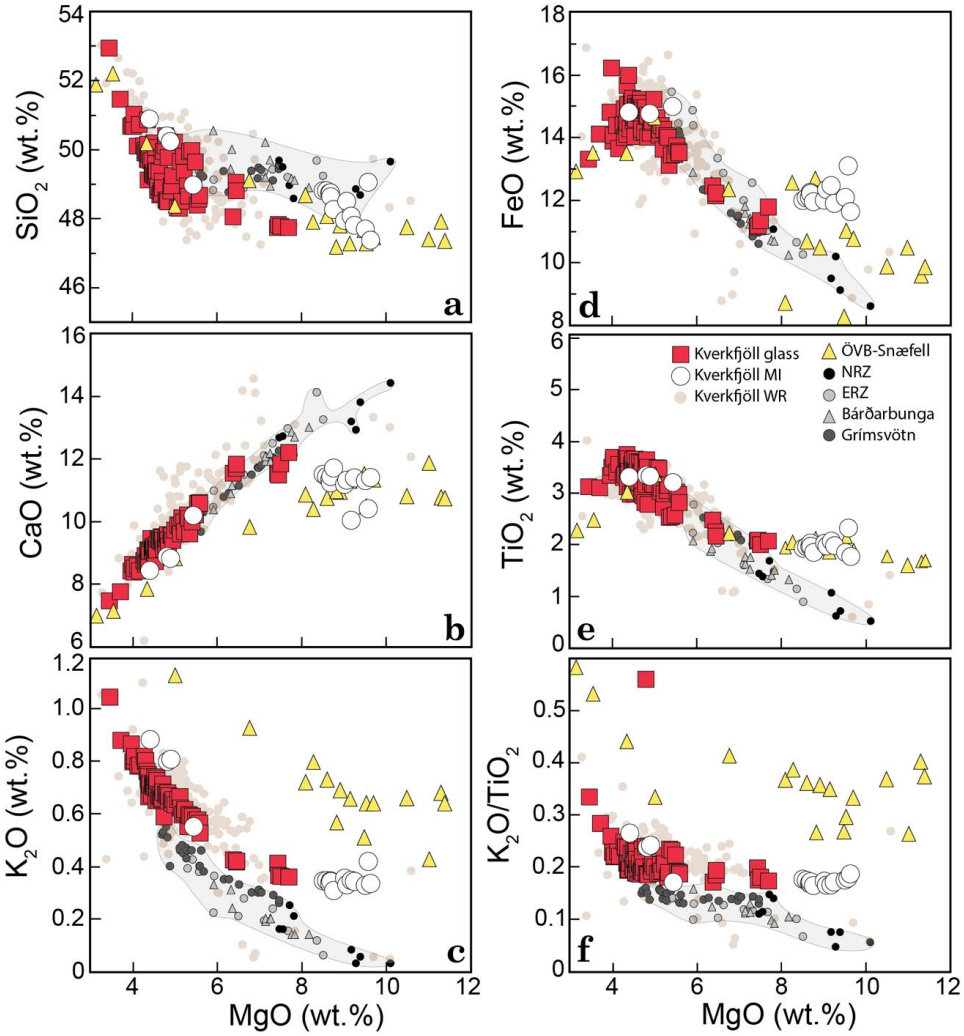

Figure 5.3 Major element variation diagrams. (a) SiO_2, (b) FeO, (c) CaO, (d) TiO_2, (e) K_2O and (e) K_2O/TiO_2 vs. MgO. The Kverkfjöll magma suite follows an evolution trend that is distinguished from the NRZ-ERZ basalts by its lower SiO_2 and higher K_2O and K_2O/TiO_2 at a given MgO. Notably, the K_2O and K_2O/TiO_2 of Kverkfjöll are intermediate between NRZ/ERZ and the off-rift Snæfell volcano. Whole-rock (WR) data from Kverkfjöll (n = 220; Table S3) overlaps with the glass data, apart from several samples with anomalously high CaO and low K_2O, FeO and TiO_2 concentrations resulting from plagioclase accumulation. Gray fields mark the range of non-Kverkfjöll NRZ and ERZ glass data. Comparative data from EVZ and NRZ from Ranta et al. (2021), tephra data for Grímsvötn and Bárdarbunga from Óladóttir et al. (2011). Melt inclusion (MI) data are corrected for post-entrapment processes. The ÖVB (Snæfell) (whole-rock) data are from Hards et al. (2000), Debaille et al. (2009) and Peate et al. (2010).

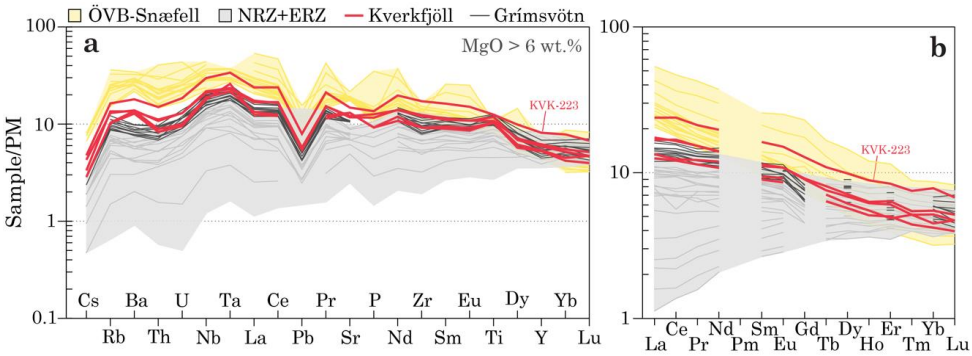

Figure 5.4 Trace elements. (a) Incompatible trace elements, in order of decreasing incompatibility and (b) rare-earth elements. Concentrations are normalized to the primitive mantle composition of McDonough and Sun (1995). In comparison with the NRZ-ERZ (including Bárdarbunga), Kverkfjöll and Snæfell basalts have higher concentrations of incompatible trace elements. Kverkfjöll and Snæfell are further distinguished by a positive Ba anomaly and a steeper REE pattern compared with NRZ-ERZ. Of the NRZ-ERZ volcanic systems, Grímsvötn has the most similar ITE pattern to Kverkfjöll, albeit lacking a positive Ba anomaly and with less steep HREE pattern. The most enriched Kverkfjöll sample, KVK-223, is labeled.

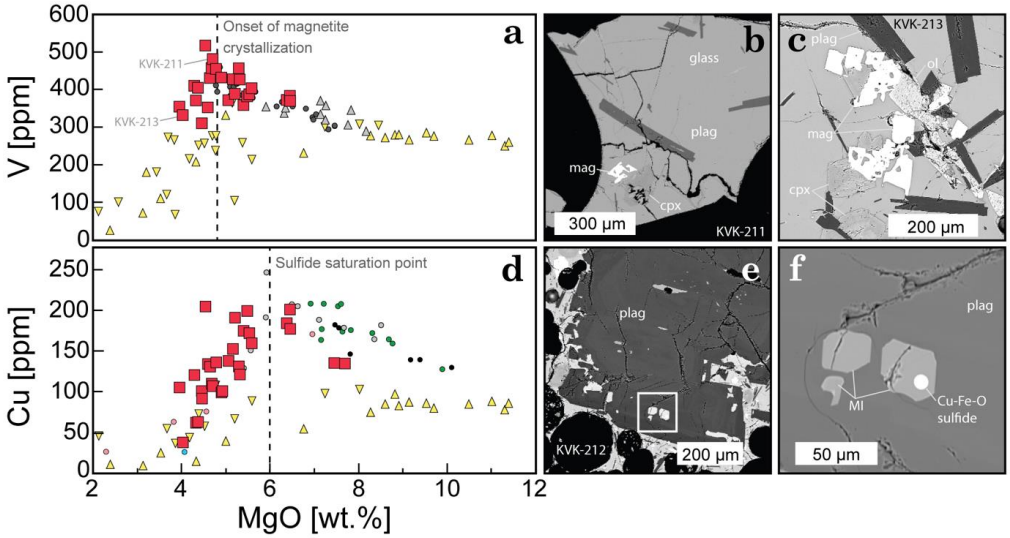

Figure 5.5 Sulfide and magnetite saturation. (a) Magnetite starts to form at melt MgO concentrations of less than 4.8 wt.%, tracked by decreasing V and FeO (Fig. 4d) concentrations. (b)-(c) Magnetite is only observed in samples with < 4.8 wt.% MgO, but is absent in more primitive samples. (d) Copper concentrations increase from 150 to 200 ppm during magmatic evolution between 7.5 and 6.0 wt% MgO but decrease at lower MgO contents (cf. Ranta et al. 2021). (e)-(f) Sulfide globules with Cu contents of up to 20 wt.% are found within plagioclase rims. The Kverkfjöll V and Cu vs. MgO trends are similar to Icelandic rift basalts. Whole-rock data from Snæfell and Öræfajökull follow a different, low-Cu trend, possibly suggesting that they reach sulfide saturation earlier during melt evolution. Symbols as in Fig. 5.3.

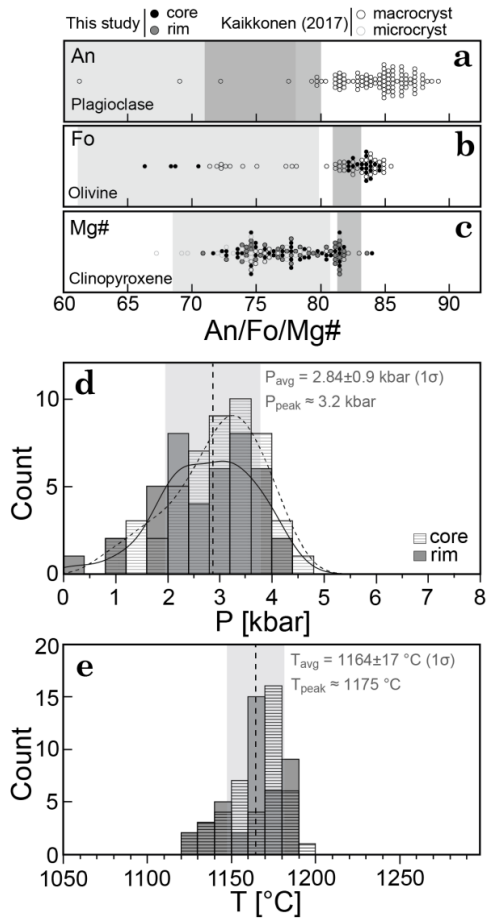

Figure 5.6 Mineral chemistry and thermobarometry (a)-(c) Compositions of plagioclase, olivine and clinopyroxene. Ranges of An, Fo and Mg#$_{cpx}$ compositions that are in equilibrium with matrix glasses (light grey) and primitive MIs (dark grey) are shown, calculated after Roeder and Emslie (1970; assuming Kd_{Fe-Mg}^{ol-liq} *= 0.3), Wood and Blundy (1997) and Namur et al. (2011; Eq. 33). Data from Kaikkonen (2017) are included (open symbols). (d)-(e) Magma pressures and temperatures were determined by clinopyroxene-melt thermobarometry (Neave and Putirka 2017). Clinopyroxene core compositions yield a single peak at ~3.2 kbar, whereas the cpx rims record a broader peak between c. 2 and 3.2 kbar.*

5.5.4 Iron oxidation state of glasses

An average glass $Fe^{2+}/\Sigma Fe$ value of 0.822±0.005 (n = 5) was derived from Mössbauer spectroscopy (Table S7). More scattered $Fe^{2+}/\Sigma Fe$ values of 0.78 to 0.84 were derived from the Wilson titrations. Low-temperature (70 K) Mössbauer spectroscopy showed existence of nanometer scale magnetites within the glasses, which may explain the larger scatter in the titration $Fe^{2+}/\Sigma Fe$ values relative to the Mössbauer results. Thus, the Mössbauer average $Fe^{2+}/\Sigma Fe$ of 0.822 for the glasses is considered to be representative for the pre-eruptive iron oxidation state of the basaltic Kverkfjöll melts (Kress and Carmichael 1991, O'Neill et al. 2018).

5.5.5 Mineral chemistry

Compositions of plagioclase, clinopyroxene, olivine and oxides (titanomagnetite and Cr-spinel) are given in Tables S11-14, including EPMA analyses from Kaikkonen (2017). Olivine, plagioclase (bytownite) and clinopyroxene (augite) have compositions with up to $Fo_{85.5}$, $An_{89.1}$ and $Mg\#_{84.0}$ (Figs. 5.6a-c). In general, macrocryst and microphenocryst cores are not in equilibrium with their host glasses; matrix glasses are in equilibrium with olivines only up to $Fo_{80.4}$, (assuming Kd_{Fe-Mg}^{ol-liq} = 0.3±0.01; Roeder and Emslie 1970), clinopyroxene with $Mg\#_{cpx}$ up to 80.7 (calculated after Wood and Blundy, 1997) and plagioclase with up to $An_{78.5}$ (Eq. 33 of Namur et al., 2012). By contrast, the most primitive melt inclusions are in equilibrium with their host olivines (by definition) and with clinopyroxenes with up to $Mg\#_{cpx}$ = 83.1 (Figs. 5.6b-c). However, most plagioclase cores are considerably more primitive than equilibrium plagioclase compositions for even the most primitive olivine-hosted melt inclusion ($An_{80.0}$; Fig. 5.6a).

5.5.6 Noble gas (He-Ne-Ar) isotopes

Noble gas isotope measurements are reported in Table S8. All three analyzed Kverkfjöll glasses yield moderate He concentrations ([^{4}He] between 1.4 x 10^{-9} and 1.3 x 10^{-8} cm^{3}STP/g). Atmospheric He contamination is considered minor based on ^{4}He/^{20}Ne values above 10, which can be used to calculate air-corrected values (R_C/R_A; Hilton 1996). Notably, air corrections are minor and within 0.2 R_A of the measured ^{3}He/^{4}He, which is smaller than the estimated 1σ uncertainty (±0.3 to 0.6 R_A). The two lowest [^{4}He] samples KVK-210 and KVK-214 have average ^{3}He/^{4}He values of 8.26±0.05 and 9.10±0.35 R_C/R_A, respectively (Fig. 5.7a). Duplicate measurements of these two samples agree within measurement uncertainty. The KVK-210 and KVK-214 values are similar to published ^{3}He/^{4}He of 7.9-8.8 R_C/R_A for Kverkfjöll glasses (Macpherson et al. 2005, Füri et al. 2010, Hardardóttir et al. 2018; Fig. 5.7a), and to ^{3}He/^{4}He of 8.3-9.1 R_C/R_A measured in Kverkfjöll hot spring and fumarole gases (Poreda et al. 1992, Füri et al. 2010, Byrne et al. 2021, Chapter 4). An anomalously high ^{3}He/^{4}He of 11.28 R_A was measured for sample KVK-223, which also has the highest [^{4}He] 1.3 x 10^{-8} cm^{3}STP/g. Apart from KVK-223, the ^{3}He/^{4}He signature of Kverkfjöll is the lowest of the NRZ lavas and is at the higher end of the well-constrained ^{3}He/^{4}He range of MORBs of 8±1 R_A (Fig. 5.7a; Graham 2002). The only volcanoes with lower ^{3}He/^{4}He values in Iceland are Snæfell (~7.1 R_A; Peate et al. 2010) and Öræfajökull (6.7 to 8.0 R_A; Hardardóttir et al. 2018).

The ^{20}Ne/^{22}Ne, ^{21}Ne/^{22}Ne values of KVK-210 and KVK-214 are indistinguishable from the Ne isotopic composition of air (9.8 and 0.028, respectively), whereas KVK-223 has an anomalously low ^{21}Ne/^{22}Ne value (Fig. 5.7b). However, this does not necessarily imply an air-like Ne isotopic mantle signature, as detection of non-air like neon isotope ratios on glasses typically requires highly undegassed material and high-precision in vacuo step-crushing (e.g. Trieloff et al. 2000). The ^{40}Ar/^{36}Ar values, between 300 and 314 are slightly higher than air (298.6; Lee et al. 2006), suggesting either a small mantle-derived or crustal component.

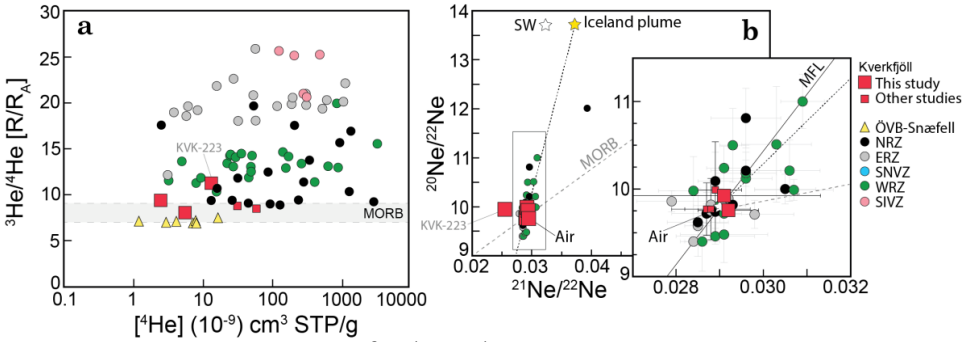

Figure 5.7 Helium and neon isotopes. (a) $^{3}He/^{4}He$ vs. ^{4}He (≈ ΣHe) concentration. Icelandic basalts from the ERZ, SIVZ, WRZ and most NRZ have elevated $^{3}He/^{4}He$ relative to MORBs (8±1 R_A; Graham 2002). Some NRZ, and all ÖVB and SNVZ (from the database of Hardardóttir et al. 2018) and Kverkfjöll basalts have MORB-like $^{3}He/^{4}He$ signatures. (b) Triple neon isotope plot. Icelandic samples tend to fall on a mixing line between air ($^{21}Ne/^{22}Ne$ = 0.029, $^{20}Ne/^{22}Ne$ = 9.8) and the Icelandic plume-endmember defined by step-crushing analyses of the DICE-1 and 2 samples from Miðfell in the WRZ (Trieloff et al. 2000, Mukhopadhyay 2012), which is similar to the solar wind (SW). The black rectangle is expanded in the inset. The Kverkfjöll samples are dominated by an air-like neon. The sample KVK-223 has anomalous elevated $^{3}He/^{4}He$ relative to other Kverkfjöll samples and low $^{21}Ne/^{22}Ne$. Comparative data from Macpherson et al. (2005) and Füri et al. (2010). Air-MORB mixing line after Moreira et al. (1998).

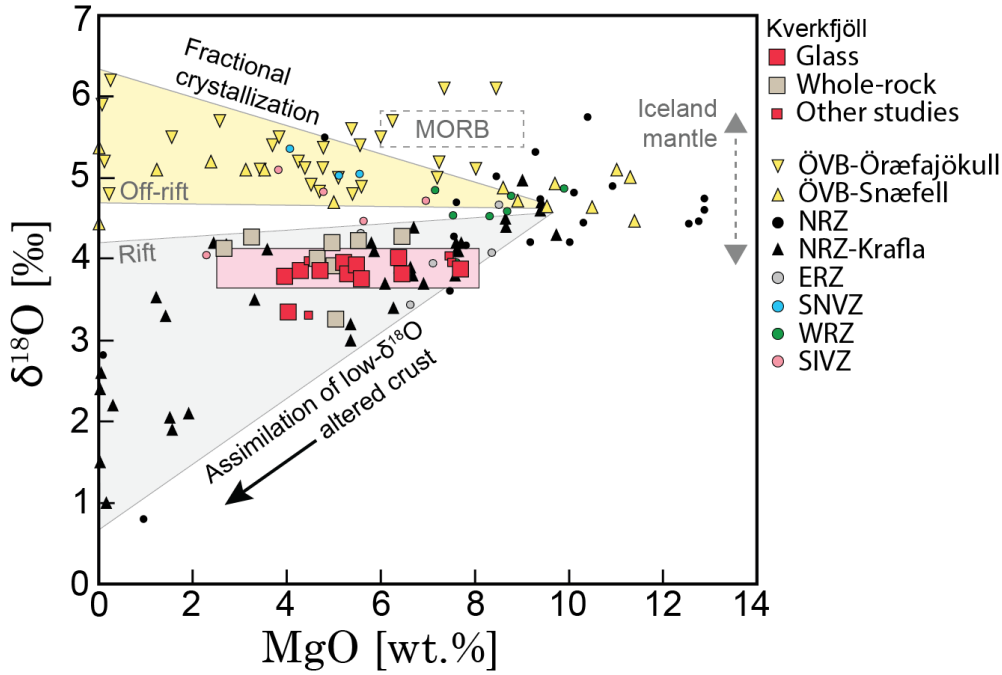

Figure 5.8 Oxygen isotopes vs. MgO. Comparative data were collected for Krafla from Nicholson et al. (1991), Hémond et al. (1993) and Jónasson (2005); for ÖVB from Hards et al. (2000), Prestvik et al. (2001), Peate et al. (2010), Manning et al. (2014); and for the remaining locations from Macpherson et al. (2005), Halldórsson et al. (2016), Caracciolo et al. (in review). The $\delta^{18}O_{olivine}$ values reported by Peate et al. (2010) and Manning et al. (2014) are shifted to estimated $\delta^{18}O_{melt}$ assuming $\Delta^{18}O_{melt\text{-}olivine}$ = +0.4 ‰, which within the range of melt-olivine pairs in Iceland (Thirlwall et al. 2006). The pink rectangle shows the average range of Kverkfjöll glasses.

5.5.7 Oxygen isotopes

The full oxygen isotope dataset is presented in Table S9. The $\delta^{18}O$ values of Kverkfjöll glasses vary between +3.25 to +4.28 ‰, with an average of +3.90±0.27 ‰ (n = 23, 1σ; Fig. 5.8). The average $\delta^{18}O$ value of laser fluorination glass analyses is slightly lower at 3.82±0.21 ‰ (N = 15, 1σ) than the value of +4.03±0.32 ‰ for conventional analyses (N = 8, 1σ). The $\delta^{18}O_{glass}$ values do not correlate with MgO (Fig. 5.8) but are significantly lower than N-MORBs ($\delta^{18}O_{glass}$ = +5.5±0.3‰; Eiler et al. 2000). Similar low $\delta^{18}O$ signatures, while rare in other hotspot lavas, are not uncommon in the Icelandic rift zone lavas (Muehlenbachs et al. 1974, Nicholson et al. 1991, Thirlwall et al. 2006; Fig. 5.8).

5.5.8 Lead isotopes

Measured Pb isotope ratios are reported in Table S10. Kverkfjöll has the most radiogenic Pb isotope ratios of the NRZ lavas, with well-confined ranges of $^{206}Pb/^{204}Pb$ = 18.4208-18.5194, $^{207}Pb/$ = 15.481-15.501 and $^{208}Pb/^{204}Pb$ = 38.222-38.352 (Fig. 5.9). The Kverkfjöll samples form a near-linear array in $^{206}Pb/^{204}Pb$ vs. $^{208}Pb/^{204}Pb$ space, that sits at an angle against the NHRL (Northern Hemisphere Reference Line; Hart 1984; Figs. 5.9b,d). Similar linear trends in multiple Pb isotope space identified at other locations in Iceland (e.g., among historical eruptions in Reykjanes; Peate et al. 2009) are generally interpreted to reflect binary mixing between less and more radiogenic mantle components, rather than secular evolution of a homogenous mantle. The Kverkfjöll lavas show distinct enrichment of ^{208}Pb and ^{207}Pb relative to the NHRL (Fig. 5.9b,d), here denoted as $\Delta^{208}Pb$ and $\Delta^{207}Pb$, (calculated according to Hart 1984). This is especially well-resolved in the $^{208}Pb/^{204}Pb$ vs. $^{206}Pb/^{204}Pb$ space where the field defined by the Kverkfjöll lavas does not overlap with any other Icelandic volcanic system (Fig. 5.9d). Similar enrichment of ^{208}Pb and ^{207}Pb relative to ^{206}Pb is in Iceland only known for the Snæfell and Öræfajökull volcanoes of the ÖVB belt (Prestvik et al. 2001, Peate et al. 2010, Manning et al. 2014; Fig. 5.10).

5.6 Discussion

5.6.1 Magmatic evolution and crustal plumbing system of Kverkfjöll

Crustal magma storage and evolution

The pre-eruptive storage pressures and temperatures of the Kverkfjöll magmas were calculated using the clinopyroxene-liquid thermobarometer of Putirka (2008) with the modifications outlined by Neave and Putirka (2017) (Table S15). As clinopyroxene phenocrysts are generally not in chemical equilibrium with adjacent glass, an equilibrium melt composition for each clinopyroxene analysis was selected from matrix glass and PEP-corrected MI analyses from Kverkfjöll using criteria outlined in Table S15.

The magma storage pressures are estimated as between 0.2 to 4.4 kbar, equivalent to a depth of approximately 0.7-16.6 km assuming an average Icelandic upper-mid crustal density of 2700-2740 kg/m^3 (Hartley and Maclennan 2018; Fig. 5.6d). The clinopyroxene-melt thermometer (Eq. 33 of Putirka 2008) yields an average temperature o 1164±17 °C (1σ, N = 97; Fig. 5.6e). The calculated pressures (including both cpx rims and cores) are distributed around a peak at ~3.2 kbar (~12 km), that is slightly lopsided toward higher

pressures, so that the average pressure is somewhat lower at 2.84±0.9 kbar (10.6±3.4 km) (Fig. 5.6d). Pressures recorded by cpx cores and rims are similar, although the rims have a broader distribution toward lower pressures (Fig. 5.6d). Magma storage pressures estimated previously for nearby rift volcanoes indicate a very similar pressure range: Bárðarbunga-Veiðivötn eruptions (including the 2014-15 Holuhraun eruption) typically have average cpx-liquid pressures from 1.9 to 3.0 kbar (Neave and Putirka 2017; Caracciolo et al. 2020); Grímsvötn tephras and the 1783 Laki eruption have cpx-melt pressures of 2.6 to 3.5 kbar (Neave and Putirka 2017).

The relatively narrow pressure interval of the Kverkfjöll magmas does not provide support for melt evolution in a vertically extensive transcrustal mush-dominated system (Cashman et al. 2017). Instead, the results agree with Maclennan (2019), who suggested that mush zones below Icelandic volcanoes are likely to be more transient and localized around sills in an otherwise mostly solid crust. However, it is important to note that cpx-liquid thermobarometry does not provide information about the storage pressures of more primitive melts if they did not crystallize clinopyroxene.

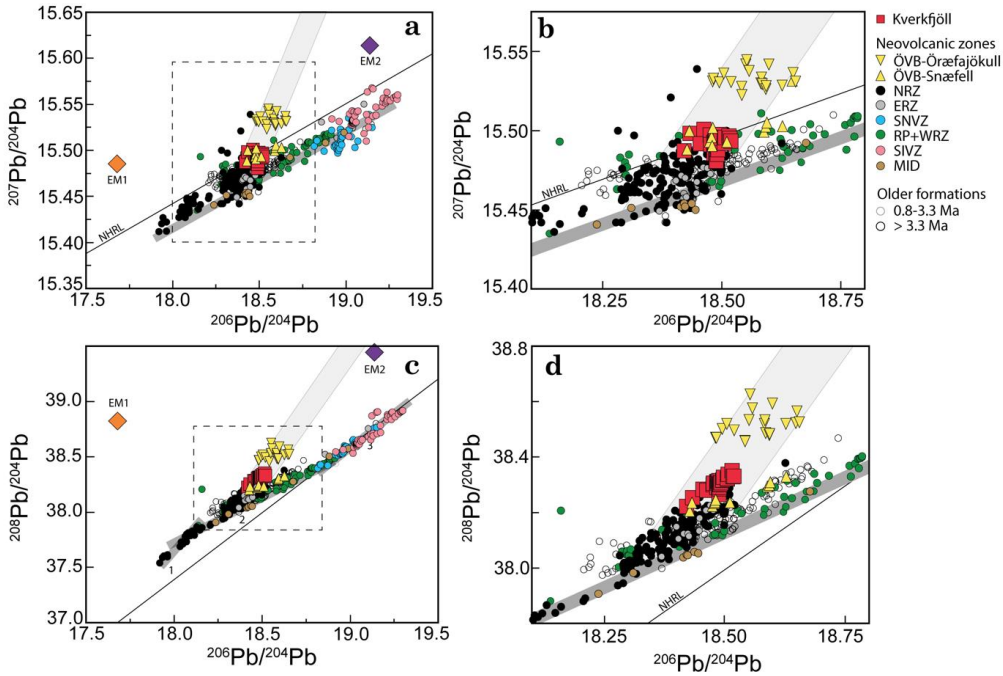

Figure 5.9 Pb and He isotopes. (a)-(b) $^{207}Pb/^{204}Pb$ vs. $^{206}Pb/^{204}Pb$. Area within the dashed box in (a) is expanded in (b). (c)-(d) $^{208}Pb/^{204}Pb$ vs. $^{206}Pb/^{204}Pb$. Area within the dashed box in (c) is expanded in (d). The NRZ, Kverkfjöll and ÖVB samples define an anomalous trend (light grey field) toward elevated $^{207}Pb/^{204}Pb$ and $^{208}Pb/^{204}Pb$ relative to $^{206}Pb/^{204}Pb$, which projects toward an intermediate composition between the EM1 and EM2 components (Jackson and Dasgupta 2008). Northern hemisphere reference line (NHRL) drawn after Hart (1984). The "baseline" Pb isotopic trend of Icelandic volcanoes can be defined by a single slope in $^{207}Pb/^{204}Pb$ vs. $^{206}Pb/^{204}Pb$ space but requires (at least) three segments in the $^{208}Pb/^{204}Pb$ vs. $^{206}Pb/^{204}Pb$ space (dark grey fields). Comparative data are from the IVID database (Hardardóttir 2020), which is filtered to only include high-quality, leached Tl-spiked MC-ICP-MS or double spiked TIMS analyses.

Microtextural evidence for melt mixing is frequently found as reversely zoned clinopyroxenes (Figs. 5.2a), which we interpret to form as a response to recharge of more mafic melt into a more evolved magma storage zone. Common observations of single clinopyroxene crystals with multiple reverse zones (Figs. 5.2b-d) suggest that multiple recharge events typically occur during the evolution of the magmas. Some evidence for mush mobilization in the Kverkfjöll melts is, however, present from frequently occurring glomerocrysts and high-An plagioclase ultraphyric samples, which is a common feature of Icelandic rift basalts (Hansen and Grönvold 2000, Halldórsson et al. 2008).

The most evolved rocks of Kverkfjöll are found on the caldera rim of the central volcano, while the most primitive rocks have erupted from Mt. Upptyppingar ~40 km NNE from the central volcano. In this respect, Kverkfjöll is consistent with a commonly invoked generic model of an Icelandic volcanic system, where most magma evolution takes place below a central volcano, while dikes along the fissure swarm are being fed through a more direct delivery line from deep-seated magma reservoirs. For example, the dike injection observed in 2007-2008 below Mt. Upptyppingar appeared to originate from ~20 km depth (Hooper et al. 2011), i.e., deeper than any cpx pressure estimates from the Kverkfjöll rocks. However, the dyke appeared to have stalled at ~10 km, i.e., approximately at the estimated main storage pressure of the Kverkfjöll melts. In light of the considerations above, the Mt. Upptyppingar dyke could be interpreted as a recharge injection of deep and primitive melt into the main mid-crustal magmatic storage zone.

Petrological modeling, performed with the Petrolog3 software (Danyushevsky and Plechov 2011), shows that the Kverkfjöll melt compositions (as inferred from glasses and MIs) follow an approximate fractional crystallization trajectory from the most primitive to the most evolved glasses, predicted for isobaric crystallization (3 kbar) at oxygen fugacity 0.5 log units above the fayalite-magnetite-quartz (FMQ) buffer (Fig. S2; cf. Kaikkonen 2017). However, the simple FC model does not fully replicate the late timing of the onset of magnetite crystallization at ~4.8 ‰, which in Petrolog3 would require reduced conditions (ΔFMQ < -1; Fig. S2) that are considered unrealistic given the moderately oxidized state ($Fe^{2+}/\Sigma Fe = 0.822$) of the Kverkfjöll lavas.

Taken together, the cpx-liquid thermobarometry, microtextural observations and major element trends suggest that prior to eruption, Kverkfjöll melts with MgO < 10 wt.% evolve mainly by fractional crystallization in a depth-constrained mid-crustal storage at ~3 kbar, that is frequently recharged by more primitive (and likely deep seated) melts.

Eruptibility of heavy, Fe-Ti rich melts

A striking feature of the Kverkfjöll magma suite is its narrow compositional range of MgO = 4.0-5.5 wt.% in ~80% of the samples (Fig. 5.10). The constricted range of erupted melt compositions suggests that more primitive melts are initially uneruptible, and only reach a narrow eruptibility window during magmatic evolution. The main physical parameter controlling the eruptibility of Icelandic basalts is the magma density (ρ) (e.g. Sigmundsson et al. 2020). Hartley and Maclennan (2018) showed that more than 85% of NRZ basalts (by volume) have $\rho < 2720$ kg/m^3, corresponding to a density (and viscosity) minimum occurring at ~7.5-8.5 wt.% MgO. Such melts are eruptible, because they are buoyant in the Icelandic upper crust ($\rho_{crust} \approx 2700$-$2740$ kg/m^3), i.e., their potentiometric surface is above ground level (Gudmundsson 2000).

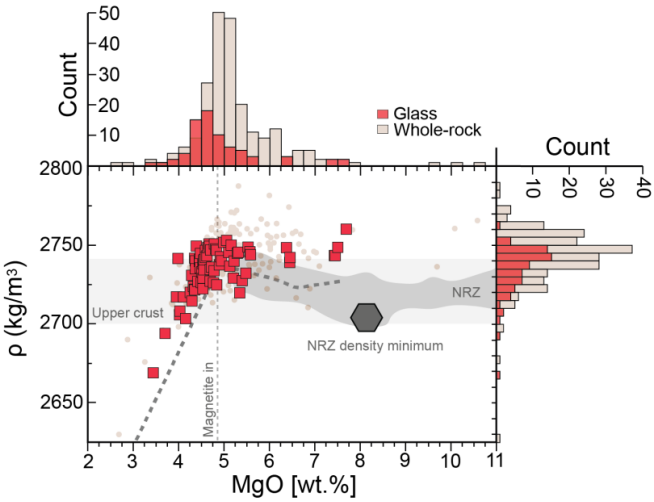

Figure 5.10 Melt density versus MgO content. Melt density was calculated using the DensityX script of Iacovino and Till (2019). Dashed line shows the melt density predicted by a fractional crystallization path modelled in rhy-MELTS using NAL-355 as a starting composition. The fields for Icelandic upper crust and the NRZ are drawn after Hartley and Maclennan (2018). The NRZ density minimum (Hartley and Maclennan 2018) is indicated with a dark grey hexagon. About 80% of NRZ eruptions, by volume, exploit this density minimum.

By contrast, the compositional peak of Kverkfjöll nearly coincides with a peak in model melt density (ρ_{melt}; calculated using the DensityX script of Iacovino and Till 2019) at ρ_{melt} of 2740-2750 kg/m^3 (Fig. 5.10), which is denser than the crust. Hartley and Maclennan (2018) showed that melts with $\Delta\rho_{melt\text{-}crust}$ above 15 kg/m^3 are unlikely to erupt. That eruptions repeatedly occur close to a density maximum is a characteristic but puzzling feature of the Kverkfjöll volcanic system.

An explanation could be related to magnetite crystallization; if magnetite is fractionated from the melt by crystal settling, melt density would be predicted to drop rapidly, which may render the remaining melt positively buoyant and thus eruptible. This effect is reflected in a drop in calculated melt densities at MgO < 4.8 wt.% to below 2720 kg/m^3 (Fig. 5.10).

Kverkfjöll may have a major subsurface volcanic complex

Due to the fact that Kverkfjöll are in general dense and must erupt through a constrained stress field at the flank of the main rift axis, it is likely that an unusually large portion of the Kverkfjöll magmas (compared to other rift basalts) do not reach the surface, but rather stall and solidify in the crust. Indeed, the 300 km^3 intrusive complex beneath the SE caldera of Kverkfjöll is comparable in size to the intrusive complex inferred beneath Bárðarbunga (Gudmunsson and Högnadóttir 2007), which is one of the most productive volcanoes in Iceland and has produced the largest Holocene lava flow on Earth, the >20 km^3 Thjórsárhraun (Halldórsson et al. 2008). Further, the evolved compositions that characterize most Kverkfjöll eruptions represent approximately 50% fractional crystallization from the most primitive glasses. Thus, erupted magmas must be balanced by at least a similar volume of melt that crystallizes in crustal magma storage zones and forms

mafic to ultramafic restites. Therefore, the magma supply (including both melts that stall in the crust and erupted melts) of the Kverkfjöll volcanic system may be comparable to on-rift volcanoes, despite the latter commonly having an order of magnitude higher eruptive frequency (Óladóttir et al. 2011a).

5.6.2 Assimilation of altered crust, low-$\delta^{18}O$ mantle or both?

Assimilation of low $\delta^{18}O$ hydrothermally altered crust within shallow crustal magma reservoirs is thought to produce lavas with unusually low $\delta^{18}O$ signatures (< 4 ‰) in Icelandic on-rift volcanic systems such as Askja, Krafla and Grímsvötn (Hattori and Muehlenbachs 1981, Nicholson et al. 2001, Gautason and Muehlenbachs 1998, Bindeman et al. 2006, 2008, Pope et al. 2013). This point is demonstrated by compiled $\delta^{18}O$ data from Icelandic volcanoes (Fig. 5.8), suggesting that crustal assimilation in Iceland (as tracked by a decrease in $\delta^{18}O$) is mostly restricted to evolved rift zones lavas (MgO < 8 wt.%), whereas magmatic suites from off-rift volcanoes instead show a trend of increasing $\delta^{18}O$ with decreasing MgO content (Fig. 5.8). The lack of low $\delta^{18}O$ in evolved glasses in the off-rift volcanoes further suggest that crustal assimilation does not play a large role during their evolution. Instead, increasingly positive $\delta^{18}O$ during magma evolution may be a result of dominant olivine crystallization, as the $\Delta^{18}O_{olivine\text{-}melt}$ fractionation factor is negative (-0.5 to -1.0 ‰), whereas $\Delta^{18}O_{cpx\text{-}melt} \approx 0$ and $\Delta^{18}O_{plag\text{-}melt} > 0$ (Zhao and Zheng 2003).

The large comparative dataset allows us to interpret the low-$\delta^{18}O$ signature of Kverkfjöll (+3.8±0.2 ‰) in a regional context. Before erupting, the Kverkfjöll magmas traverse and evolve within an unusually thick crust (> 30 km; Jenkins et al. 2018), which makes them susceptible to assimilation crustal materials. However, due to the fact that Kverkfjöll $\delta^{18}O$ values do not correlate with MgO, it seems implausible that the low $\delta^{18}O$ signature is derived via concurrent assimilation and fractional crystallization in the main magma storage zone, given the long evolutionary span (~50% fractional crystallization) between the most primitive (7.5 wt.% MgO) and evolved (4 wt.% MgO) melts. Instead, two end-member interpretations seem possible: (1) The low-$\delta^{18}O$ signature is derived by assimilation at an earlier stage of magma evolution, or (2) the Kverkfjöll mantle source has an unusually low $\delta^{18}O$ signature of ~4 ‰.

Several authors have argued that the Icelandic mantle has an isotopically lighter oxygen component than DMM, based on lower-than-MORB $\delta^{18}O$ values commonly found in primitive lavas and highly forsteritic olivines that lack other chemical indicators of crustal assimilation (e.g., Breddam et al. 2002, Macpherson et al. 2005, Thirlwall et al. 2006, Rasmussen et al. 2021). Indeed, a notable feature of Icelandic $\delta^{18}O$ data is that both the ÖVB and the rift magma suites seem to converge at the primitive end of melt compositions (MgO > 7 wt.%) at sub-DMM (+5.5±0.3 ‰ , Eiler et al. 2000) values of about +4.8±0.2 ‰ (Fig. 5.8). However, even for Iceland, the $\delta^{18}O$ signature of Kverkfjöll would represent an unusually low $\delta^{18}O$ mantle value.

Because the Kverkfjöll glasses lie within the general trend of decreasing $\delta^{18}O$ with decreasing MgO seen in the NRZ lavas (Fig. 5.8), we are inclined to interpret the low-$\delta^{18}O$ signature of Kverkfjöll to have been (at least partly) caused by crustal assimilation of low-$\delta^{18}O$ crust. However, because more primitive melts, that have a higher thermodynamic potential for assimilating crust (Bindeman et al. 2006, Heinonen et al. 2021), are not represented in the sample set, we cannot rule out either a low-$\delta^{18}O$ mantle source or assimilation of low-$\delta^{18}O$ basaltic crust by moderately primitive (i.e., more primitive that our most primitive glasses with 7.5 wt‰ MgO) Kverkfjöll melts.

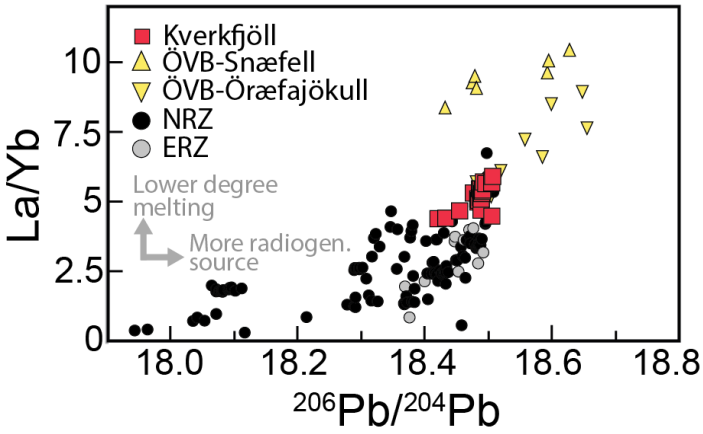

Figure 5.11 Trace element vs. isotopic enrichment. A positive correlation is seen between $^{206}Pb/^{204}Pb$ and La/Yb – an indicator of melt degree and prior trace element depletion. Individual volcanic systems (ÖVB, Snæfell, Kverkfjöll, Bárðarbunga-Veiðivötn (ERZ)) show tighter trends with slightly differing slopes. These correlations suggest that mixing takes place between a depleted source and another source that is enriched in both incompatible elements and radiogenic isotopes and preferentially tapped by lower-degree melts.

5.6.3 Petrogenesis of the Kverkfjöll magma suite

Radiogenic isotope enrichments (e.g. higher $^{206}Pb/^{204}Pb$ and $^{87}Sr/^{86}Sr$ and lower $^{143}Nd/^{144}Nd$) in Icelandic basalts correlate with trace element indicators of melt degree and enrichment, such as La/Yb, Dy/Yb and Nb/Zr (e.g., Zindler et al. 1979, Hémond et al. 1993, Chauvel and Hémond 2000, Shorttle and Maclennan 2011). These correlations cannot be explained by differences in the degree and depth of melting of a single source, but instead demonstrate the mixing of depleted and enriched components in the Icelandic mantle (Stracke et al. 2003, Koornneeff et al. 2012). At a regional scale, a broad positive correlation is seen between $^{206}Pb/^{204}Pb$ and La/Yb for for ERZ, NRZ, Kverkfjöll and ÖVB (Fig. 5.11). Individual volcanic systems (Öræfajökull, Snæfell, Kverkfjöll, Bárðarbunga-Veiðivötn (ERZ)) show tighter trends with slightly differing slopes (Fig. 5.11). These correlations suggest that mixing between melts derived from less radiogenic and more radiogenic Pb isotopic sources takes place both at regional and volcanic system length scales (Shorttle et al. 2013).

The observation that the geochemical enrichment (in terms of La/Yb, Dy/Yb, K_2O, K_2O/TiO_2; Figs. 5.3, 5.4 and 5.12) of the Kverkfjöll lavas is intermediate between the NRZ and ÖVB basalts, exactly echoing its intermediate geographical position, is consistent with the Kverkfjöll melts being sourced from a melting column directly beneath the volcano. Conversely, lateral transport of magma from a melt accumulation zone beneath the rift axis toward the rift flanks, which has been proposed as a model to explain rift flank volcanism at continental rifts (Maccaferri et al. 2014), is not compatible with Icelandic off-rift and rift flank volcanism, as such melts would be expected to be geochemically similar to high-degree melts found at Iceland's on-rift volcanoes.

Instead, the generation of increasingly incompatible trace element-enriched rocks away from the rift axis is compatible with the progressive suppression of shallow partial melting resulting from an eastward thickening lithospheric lid away from the axial rift zone (Fig. 5.14; Kokfelt et al. 2006, Peate et al. 2010). An unusually thick lithosphere (up to

>100 km) beneath East Iceland is also suggested by seismic imaging (Bjarnason and Schmeling 2008).

Due to the fact that Kverkfjöll melts are less diluted by high-degree shallow melting of a depleted (peridotitic) mantle sources than the on-rift basalts, they are able to retain a stronger chemical fingerprint of enriched mantle components that have lower solidus temperatures and thus melt at greater depths (e.g. Trønnes et al. 1999, Kokfelt et al. 2006). Another notable feature of Figs. 5.12a and 5.12c is that the ratios of Ba/La and La/Yb—which are similarly incompatible and should remain approximately constant during fractional crystallization—decrease and increase, respectively, with decreasing MgO. This implies that high-MgO melts with lower La/Yb (i.e., more depleted) and higher Ba/La mix with more enriched (higher La/Yb) melts with lower Ba/La during melt evolution. That mixing of melts derived from two slightly differing sources affects the Kverkfjöll melts is also implied by similar trends shown by $^{206}Pb/^{204}Pb$, $^{207}Pb/^{206}Pb$ and $^{208}Pb/^{206}Pb$ versus MgO (Fig. S3).

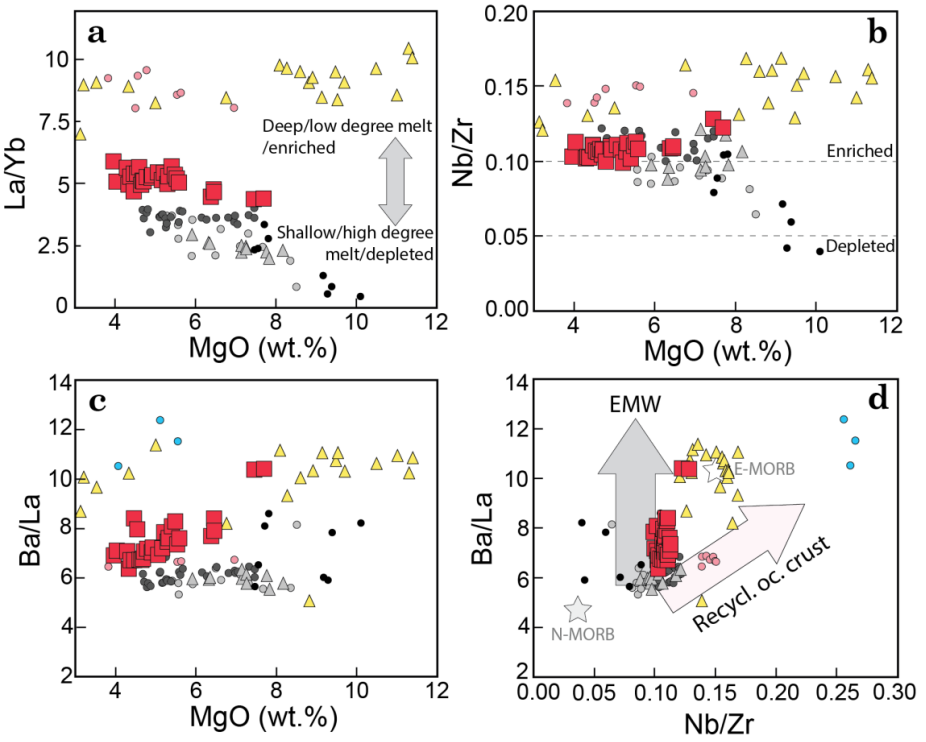

Figure 5.12 Trace element indicators of enriched sources. (a) La/Yb and (b) Nb/Zr vs. MgO diagrams show a wide gap between the rift zone lavas and the ÖVB and SIVZ rocks for high-MgO samples. This suggests that the primitive rift basalts are sourced from high-degree melting of trace element-depleted mantle. This gap narrows during melt evolution, suggesting concurrent crystallization melt mixing. (c) Ba/La vs. MgO shows a similar pattern. However, the otherwise trace element enriched SIVZ lavas do not have high Ba/La. Evidence of melt mixing is seen in the positive trend between Ba/La and MgO for the Kverkfjöll samples. (d) Ba/La vs. Nb/Zr plot can be used to distinguish between two separate enrichment trends. The high-Ba/La trend is most clearly defined by the Kverkfjöll and ÖVB rocks. The SIVZ samples define a low-Ba/La but high-Nb/Zr enrichment trend possibly related to recycled oceanic crust (Shorttle et al. 2011). Average normal (N-) and enriched (E-)MORB compositions are indicated by stars (Gale et al. 2013). Symbols are the same as in Fig. 5.8.

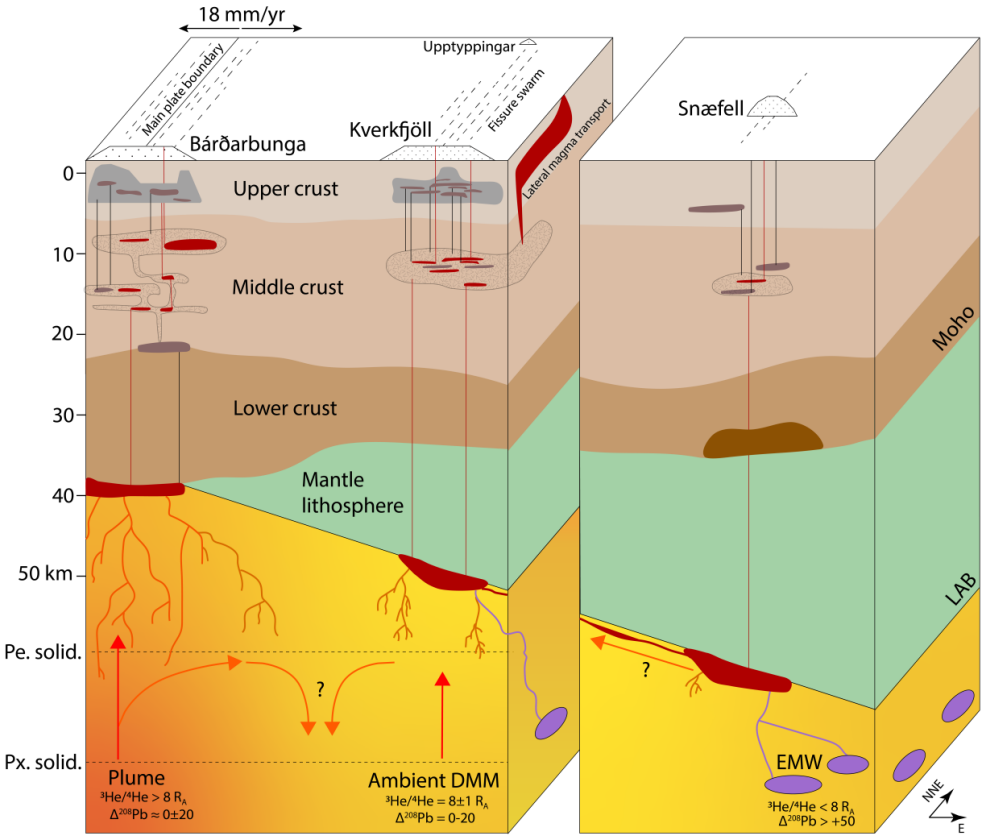

Figure 5.13 Lithospheric lid control on mantle melting beneath Central-East Iceland. Cross-section through crust (Jenkins et al. 2018) and lithosphere below rift (Bárdarbunga), flank (Kverkfjöll) and off-rift (Snæfell) volcanoes. Steep temperature gradient below the rift axis promotes formation of extensive mush zones and partial melting of altered crust. At the flank and off-rift region, the magmatic influx is lower and the crust is cooler. Such crustal and thermal structure is also suggested by seismic arrays, which reveal a west-to-east thickening of the lithosphere from ~40 km beneath the rift axis in Central Iceland to ~100 km in East Iceland (Bjarnason and Schmeling 2009). By contrast, the crustal thickness only decreases slightly from its thickest point of ~40 km at the main rift axis beneath Bárdarbunga to ~35 km below Kverkfjöll and Snæfell (Jenkins et al. 2018). Geochemical source tracers (Fig. 5.14) indicate that the Kverkfjöll melts are tapping a mixture between ambient DMM and an enriched mantle component (EMW, purple) with high $\Delta^{208}Pb$ that is only present in the mantle beneath East Iceland, whereas the high $^{3}He/^{4}He$ plume component appears to be virtually absent in volcanic systems to the east of the main rift. Red arrows indicate possible mantle flow paths. Probable upper crustal mafic complexes (grey) beneath Bárdarbunga and Kverkfjöll drawn after gravity model of Gudmundsson and Högnadóttir (2007). Plumbing system beneath Bárdarbunga drawn after Caracciolo et al. (2021). A hypothetical magma storage zone beneath Snæfell is drawn at ~13 km depth after Hards et al. (2000).

5.6.4 Icelandic EM2-type mantle component

Recipe for the Icelandic EM2 flavour

A striking feature of the Kverkfjöll magmas is their characteristic Pb isotopic fingerprint (with almost no overlap with other Icelandic volcanoes) with elevated $\Delta^{207}Pb$ and $\Delta^{208}Pb$ relative to the NRZ (Fig. 5.9). The Kverkfjöll Pb signature is clearly shifted from NRZ

toward that of Öræfajökull, the volcano that defines the endpoint of this trend in Iceland (Fig. 5.9).

We interpret the trend of sharply increasing $^{208}Pb/^{206}Pb$ relative to $^{206}Pb/^{204}Pb$, described by the NRZ, Kverkfjöll and ÖVB volcanoes, to represent a binary mixing trend that projects toward a component whose Pb isotopic signature resembles EM2 basalts from Samoa (Fig 5.9; Jackson and Dasgupta 2008). The elevated $\Delta^{208}Pb$ implies a mantle component with elevated Th/U (^{232}Th decays to ^{208}Pb; ^{206}Pb and ^{207}Pb are daughter isotopes of ^{238}U and ^{235}U, respectively). Öræfajökull also has radiogenic $^{87}Sr/^{86}Sr$ (high) and unradiogenic $^{143}Nd/^{144}Nd$ (low) relative to the DMM, similar to EM2 (Fig. S5; Zindler and Hart 1984, Jackson and Dasgupta 2008). Positive $\Delta^{207}Pb$, $\Delta^{208}Pb$, high $^{87}Sr/^{86}Sr$ and low $^{143}Nd/^{144}Nd$ signatures (Figs. S4 and S5) are all characteristic of mantle components derived from global subducted sediments (GLOSS) that are largely composed of weathering products of the upper continental crust (UCC; Hart 1988, Planck and Langmuir 1998, Jackson et al. 2007).

Helium isotope ratios are useful for categorizing mantle-derived basalt, as the DMM has a uniform $^{3}He/^{4}He$ signature of 8±1 R_A (Graham 2002), whereas higher $^{3}He/^{4}He$ in mantle-derived basalts are exclusively associated with mantle plumes that sample the lowermost mantle (Jackson et al. 2017, Williams et al. 2019). Notably, the $^{3}He/^{4}He$ signature of Kverkfjöll (~8.5 R_A) is indistinguishable from DMM (8±1 R_A, Graham 2002), apart from the sample KVK-223 with elevated $^{3}He/^{4}He$ (KVK-223 with 11.3 R_A). This suggests that Kverkfjöll only rarely receives input from the Icelandic high-$^{3}He/^{4}He$ plume component (Fig. 5.7a). The DMM-like $^{3}He/^{4}He$ in Kverkfjöll is noteworthy, as high $^{3}He/^{4}He$ values have been measured in the nearby Kistufell table mountain (16.8 R_A; Breddam 2002) located 20 km to the west of the Kverkfjöll central volcano, as well as Vaðalda, an interglacial shield only a few kilometers to the west of the Kverkfjöll fissure swarm, which has the highest measured $^{3}He/^{4}He$ in the neovolcanic zones (33.6 R_A; Jackson et al. 2020). This suggests a strong contrast between the mantle to the west and east of the NRZ (see following section).

An important feature of the Icelandic EM2 flavor is a pronounced positive Ba anomaly seen in Kverkfjöll and ÖVB basalts (Fig. 5.4a), which is not a general feature of EM2 basalts (Jackson et al. 2007). This Ba anomaly is absent in the NRZ-ERZ as well as in the otherwise enriched (high Nb/Zr and radiogenic $^{206}Pb/^{204}Pb$) SIVZ basalts (Fig. 5.4a). Thus, a Ba/La vs. Nb/Zr plot can be used to demarcate two distinct enrichment trends in Iceland represented by SIVZ (moderate-Ba/La, high-Nb/Zr) and ÖVB-Kverkfjöll (high-Ba/La, moderate Nb/Zr) trend (Fig. 5.12d). Intriguingly, Ba/La also correlates negatively with $^{3}He/^{4}He$ in Icelandic basalts (Ranta et al. 2021), with the high-Ba/La EM2-type component having a DMM-like $^{3}He/^{4}He$ signature of 7-8 R_A, and the moderate-Ba/La SIVZ lavas having a high $^{3}He/^{4}He$ of up to 26 R_A.

Elevated Ba/La, accompanied by DMM-like $^{3}He/^{4}He$ and low $\delta^{34}S$ in the Kverkfjöll rocks was suggested by Ranta et al. (2021) to be associated with an enriched, subduction-modified mantle wedge component (EMW). The EM2-flavored Pb-Pb signature of Kverkfjöll is consistent with this hypothesis, but requires the EMW component to also include material with elevated Th/U, such as GLOSS or UCC. It is feasible that a mantle component with multiple superimposed signals could be generated in the mantle wedge region of a subduction zone, which receives input from both devolatilizing fluids of the subducted slab, as well mélange diapirs that are likely to transport subducted sediments (GLOSS) to the mantle wedge region (Marschall and Schumacher 2012).

It should be noted that mixing of primary mantle melts, taking place in subcrustal magma reservoirs and melt extraction channels, acts to blunt the most extreme isotopic and

trace element signatures of the mantle endmembers (Maclennan 2008, Shorttle and Maclennan 2011, Halldórsson et al. in review). During the mixing process, signatures of enriched mantle components are better preserved because their higher incompatible trace element content (e.g. Stracke 2012, Neave et al. 2019). This preservation bias, along with the weak EM2-type signature in Iceland relative to the EM2 type locality, Samoa (Jackson et al. 2007), suggests that the EM2 component in the Iceland mantle must be volumetrically very minor.

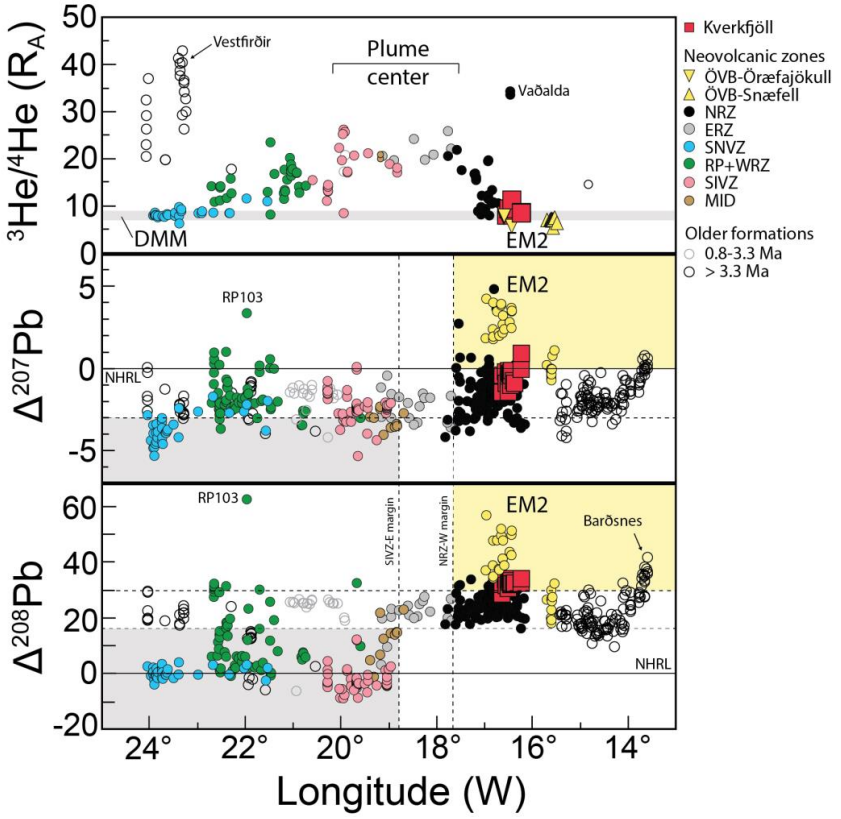

Figure 5.14 Longitudinal zonation of primordial and enriched components in the Iceland mantle. Different enriched mantle components sampled by the SNVZ, SIVZ and ÖVB basalts (Williams 2005) can be clearly distinguished based on their He and Pb isotope signatures. These show an asymmetric distribution across a longitudinal cross section of Iceland. Two components with DMM-like $^{3}He/^{4}He$ components are sampled by SNVZ in the west and ÖVB and Kverkfjöll in the east. However, the SNVZ enriched mantle is clearly distinct from ÖVB, with a negative $\Delta^{207}Pb$ and a circum-0 $\Delta^{208}Pb$ signature. Further, the SIVZ basalts have a similar $\Delta^{207}Pb$-$\Delta^{208}Pb$ signature as SNVZ, but are marked by high $^{3}He/^{4}He$ values indicative of plume involvement. Dashed vertical lines show the approximate eastern margin of SIVZ and western margin of NRZ, respectively. The lower dashed horizontal lines show approximate lower limits of $\Delta^{207}Pb$ and $\Delta^{208}Pb$ in modern day East Iceland. A dashed horizontal line in the bottom panel is set at $\Delta^{208}Pb = +30$ to highlight the ^{208}Pb-enriched signatures found in volcanoes in east Iceland. Comparative helium and Pb isotope data from the filtered $^{3}He/^{4}He$ data compilation of Hardardóttir et al. (2018) and the IVID database (Hardardóttir 2020), and Jackson et al. (2020). The anomalously high $^{3}He/^{4}He$ isotope value of the Vaðalda interglacial shield is highlighted (Macpherson et al. 2005, Jackson et al. 2020) as well as the outlier Pb isotopic composition of sample RP103 from the Reykjanes Peninsula (Thirlwall et al. 2006).

Spatial distribution of EM2-type signatures in Iceland

The longitudinal distribution of Δ^{208}Pb values of Icelandic lavas puts a strong constraint on the geographic limits of the EM2 component within the mantle beneath Iceland (Fig. 5.14). In particular, the lack of elevated Δ^{208}Pb west of the NRZ (apart from a single sample from the Reykjanes Peninsula, RP103; Thirlwall et al. 2006) or higher-than-DMM-^{3}He/^{4}He to the east of the NRZ shows that the EM2 component is mainly present in East Iceland (Figs. 5.13 and 5.14).

Conversely, the longitudinal distribution of ^{3}He/^{4}He in Icelandic lavas describes a broad peak to the west of NRZ, and a sharp decline to the east of the western margin of NRZ toward DMM-like (or lower) ^{3}He/^{4}He values (Fig. 5.14), Thus, the high-^{3}He/^{4}He plume component seems to only be present to the west of the NRZ.

In addition to Kverkfjöll, slightly elevated ^{208}Pb/^{204}Pb and ^{207}Pb/^{204}Pb versus ^{206}Pb/^{204}Pb signatures (relative to the local baseline) are also present in many other NRZ and some ERZ basalts (Fig. 5.9d). The Pb-Pb isotopic signatures that are closest to Kverkfjöll are seen in basalts from the volcanoes Askja, Mt. Herðubreið, Hrímalda, Grímsvötn, Gæsafjöll near Krafla, as well as the Thjórsá lava from the Bárðarbunga volcano (Kokfelt et al. 2006, Halldórsson et al. 2008, Sims et al. 2013, Shorttle et al. 2013). By contrast, samples from volcanoes located to the west of the NRZ completely lack the anomalous, elevated Δ^{208}Pb values; these include Hofsjökull, Hágöngur and Tungnafellsjökull, which are located about 100, 70 and 60 km west of Kverkfjöll, respectively (Kokfelt et al. 2006) as well the other volcanic zones of Iceland (SIVZ, RP, WRZ and SNVZ; Fig. 5.14). Kverkfjöll-like Pb-Pb signatures are also mostly lacking in the northernmost on-land NRZ volcano Theistareykir, which probably marks the northern boundary of the EM2-type component. Interestingly, lavas with elevated Δ^{208}Pb are also present in the easternmost lavas in Upper Tertiary lava pile in East Iceland that are older than 12 Ma (Fig. 5.14; Kitagawa et al. 2008, Askew 2020). This suggests that the EM2 component is a long-lived feature in the Icelandic mantle. The EM2 component is likely to be fusible, as it is most strongly expressed in lower melt degree lavas at the flank of the NRZ but suppressed in the rift magmas.

These observations are compatible with the focusing of partial mantle melts formed below the thicker off-rift lithosphere toward the rift axis by sublithospheric flow “up the bottom of the lithosphere” (Spiegelman 1993, Kelemen et al. 1997, Turner et al. 2017; Fig. 5.13). Melts that incorporate the EM2 component exclusively form beneath the eastern side of NRZ and flow westward toward the rift along the upward sloping base of the lithosphere that shallows to the west (Fig. 5.13). The relatively strong EM2 signal in Kverkfjöll basalts relative to on-rift NRZ volcanoes may partly reflect the fact that its fissure system is the first large-scale crustal structural weakness that the EM2-flavored melts encounter during their westward and upward flow along the base of the lithosphere.

Origin of the Icelandic EM2-type component

The origin of the Icelandic EM2-type component sampled by Öræfajökull has been a matter of debate. Torsvik et al. (2015) attribute the EM2-like isotopic signature of Öraefajökull to a fragment of continental crust located at depth, below Icelandic crust. Their argument is based on a plate reconstruction model of North Atlantic opening, which allows for a sub-crustal southward-extension of the Jan Mayen Microcontinent (JMM) beneath East Iceland, which may contain old continental material. This interpretation is at odds with earlier studies that instead ascribe the enriched radiogenic Pb signature of

Öraefajökull to an enriched, recycled mantle component inherent to the Iceland plume (Prestvik et al., 2001; Peate et al., 2010; Manning and Thirlwall, 2014).

Continental crust is a possible source of high Th/U material, which was used by Torsvik et al. (2015) to argue for a continental fragment beneath Öræfajökull. However, recycled sediments in general have elevated Th/U relative to DMM (Plank and Langmuir 1998) and will tend to generate high Δ^{208}Pb mantle components (Hart 1988). Further, no tendency toward lower Ce/Pb values that characterize the upper continental crust (~4; Rudnick and Gao 2003) is observed in Kverkfjöll (30-36) or Öræfajökull (28-35; Manning and Thirlwall 2014) lavas. Therefore, geochemical signals resembling continental crust cannot be ascribed unambiguously to submerged JMM fragments. Similar Δ^{208}Pb enrichments in the high Arctic slow-spreading ridges have been attributed to a local upper mantle anomaly that originates from subduction-modified mantle wedge (Richter et al. 2020) or delaminated sub-continental lithospheric mantle (Goldstein et al. 2008).

Given the MORB-like ^{3}He/^{4}He signature of most Kverkfjöll lavas (Fig. 5.8), the enriched component sampled by Kverkfjöll may also be a part of the local North Atlantic mantle (Ranta et al. 2021)—elevated H_2O-CO_2 contents of North Atlantic MORBs have been interpreted by previous workers to indicate subduction "pollution" remaining in the upper mantle (Dixon et al. 2017), possibly following Phanerozoic subduction events in the region (Hauri et al. 2018). However, in a strict sense, the available geochemical data alone cannot separate between a plume-sourced enriched component and an ambient upper mantle component.

The data presented here show that the Kverkfjöll component has a weak EM2-type flavor possibly derived from subducted sediments. The spatial disconnect between plume-like ^{3}He/^{4}He signals and small Δ^{208}Pb to the west of the NRZ, and MORB-like ^{3}He/^{4}He with elevated Δ^{208}Pb to the east of NRZ allows two interpretations: (1) Either the EM2 component sampled by ÖVB volcanoes and Kverkfjöll is derived from the local North Atlantic mantle, (2) the EM2 component is part of the Iceland plume. If the latter scenario is true, then the Iceland plume must be strongly zoned laterally, with a sharp boundary between a central high ^{3}He/^{4}He component and an eastern EMW-EM2-DMM-like component.

5.7 Conclusions

1. The Kverkfjöll magma suite has a limited compositional range of MgO = 3.7-7.6 wt.% (measured from subglacial pillow glasses) and is comprised almost exclusively of tholeiitic basalts. These basalts are enriched in incompatible elements compared to the tholeiitic rift volcanic systems, but not as enriched as the transitional and alkali basalts of the off-rift volcanoes.

2. The compositional range of the Kverkfjöll lavas is extremely narrow: About 80% of the eruptions fall in between MgO = 4-5.5 wt%. We propose that the concentration of eruptions at this compositional window—near a density maximum—is related to the onset of magnetite crystallization at c. 4.8 wt% MgO, which dramatically reduces the density of the melt.

3. Estimated crystallization pressures of clinopyroxene macrocrysts cluster around a single peak at ~3.2 kbar. The lack of significantly deeper recorded pressures indicates that most Kverkfjöll magma evolution takes place at about 12 km depth prior to eruption.

4. High Dy/Yb, high K_2O and low SiO_2 of the glasses indicate that the Kverkfjöll melts are derived from partial melting of the mantle that begins at the bottom of a deep-reaching melting column and is truncated by a lithospheric mantle that is considerably thicker than at the rift axis.

5. The $\delta^{18}O_{glass}$ signature of Kverkfjöll is distinct and low at 3.82±0.21%. If the low signature is due to assimilation of $\delta^{18}O$-depleted crust, assimilation must have occurred prior to the main evolution stage of the melts. Alternatively, the low $\delta^{18}O$ could be a feature of the Kverkfjöll mantle source.

6. Kverkfjöll basalts have a unique, enriched $^{208}Pb/^{204}Pb$ and $^{207}Pb/^{206}Pb$ signature among Icelandic volcanoes coupled to DMM-like $^{3}He/^{4}H$ of ~8.5 R_C/R_A. These signatures are off-set from other Icelandic basalts towards the EM2-type signature of the Öræfajökull volcano. Similar, but subdued off-set is seen in many ERZ and NRZ lavas and the Snæfell off-rift volcano, but is absent in elsewhere in the neovolcanic zones.

7. Longitudinal distribution of $^{3}He/^{4}He$ and $\Delta^{208}Pb$ signatures reveal a highly asymmetric distribution of enriched components in the Icelandic mantle, where the EM2-type mantle component is exclusively present in lavas to the east of the NRZ.

5.8 References

Askew, R. A. (2020). Breiðdalur Central Volcano. What came first: the central volcano or the fissure swarm? PhD thesis, University of Iceland.

Baker, J., Peate, D., Waight, T., & Meyzen, C. (2004). Pb isotopic analysis of standards and samples using a 207Pb–204Pb double spike and thallium to correct for mass bias with a double-focusing MC-ICP-MS. *Chemical Geology*, *211*(3-4), 275-303.

Bali, E., Hartley, M. E., Halldórsson, S. A., Gudfinnsson, G. H., & Jakobsson, S. (2018). Melt inclusion constraints on volatile systematics and degassing history of the 2014–2015 Holuhraun eruption, Iceland. *Contributions to Mineralogy and Petrology*, *173*(2), 9.

Banik, T. J., Carley, T. L., Coble, M. A., Hanchar, J. M., Dodd, J. P., Casale, G. M., & McGuire, S. P. (2021). Magmatic processes at Snæfell volcano, Iceland, constrained by zircon ages, isotopes, and trace elements. *Geochemistry, Geophysics, Geosystems*, *22*(3), e2020GC009255.

Barry, P. H., Hilton, D. R., Füri, E., Halldórsson, S. A., & Grönvold, K. (2014). Carbon isotope and abundance systematics of Icelandic geothermal gases, fluids and subglacial basalts with implications for mantle plume-related CO2 fluxes. *Geochimica et Cosmochimica Acta*, *134*, 74-99.

Bindeman, I. N., Sigmarsson, O., & Eiler, J. (2006). Time constraints on the origin of large volume basalts derived from O-isotope and trace element mineral zoning and U-series disequilibria in the Laki and Grímsvötn volcanic system. *Earth and Planetary Science Letters*, *245*(1-2), 245-259.

Bindeman, I., Gurenko, A., Sigmarsson, O., & Chaussidon, M. (2008). Oxygen isotope heterogeneity and disequilibria of olivine crystals in large volume Holocene basalts from Iceland: evidence for magmatic digestion and erosion of Pleistocene hyaloclastites. *Geochimica et Cosmochimica Acta*, *72*(17), 4397-4420.

Bjarnason, I. T., & Schmeling, H. (2009). The lithosphere and asthenosphere of the Iceland hotspot from surface waves. *Geophysical Journal International*, *178*(1), 394-418.

Björnsson, H., & Einarsson, P. (1990). Volcanoes beneath Vatnajökull, Iceland: Evidence from radio echo-sounding, earthquakes and jökulhlaups. *Jökull*, *40*, 147-168.

Björnsson, H., & Pálsson, F. (2020). Radio-echo soundings on Icelandic temperate glaciers: history of techniques and findings. *Annals of Glaciology*, *61*(81), 25-34.

Bo, T., Katz, R. F., Shorttle, O., & Rudge, J. F. (2018). The melting column as a filter of mantle trace-element heterogeneity. *Geochemistry, Geophysics, Geosystems*, *19*(12), 4694-4721.

Bourne, A. J., Cook, E., Abbott, P. M., Seierstad, I. K., Steffensen, J. P., Svensson, A., ... & Davies, S. M. (2015). A tephra lattice for Greenland and a reconstruction of volcanic events spanning 25–45 ka b2k. *Quaternary Science Reviews*, *118*, 122-141.

Breddam, K., Kurz, M. D., & Storey, M. (2000). Mapping out the conduit of the Iceland mantle plume with helium isotopes. *Earth and Planetary Science Letters*, *176*(1), 45-55.

Breddam, K. (2002). Kistufell: Primitive melt from the Iceland mantle plume. *Journal of Petrology*, *43*(2), 345-373.

Byrne, D. J., Broadley, M. W., Halldórsson, S. A., Ranta, E., Ricci, A., Tyne, R. L., Stefánsson, A., Ballentine, C.J., & Barry, P. H. (2021). The use of noble gas isotopes to trace subsurface boiling temperatures in Icelandic geothermal systems. *Earth and Planetary Science Letters*, *560*, 116805.

Caracciolo, A., Bali, E., Guðfinnsson, G. H., Kahl, M., Halldórsson, S. A., Hartley, M. E., & Gunnarsson, H. (2020). Temporal evolution of magma and crystal mush storage conditions in the Bárðarbunga-Veiðivötn volcanic system, Iceland. *Lithos*, *352*, 105234.

Carrivick, J. L., Russell, A. J., & Tweed, F. S. (2004). Geomorphological evidence for jökulhlaups from Kverkfjöll volcano, Iceland. *Geomorphology*, *63*(1-2), 81-102.

Cashman, K. V., Sparks, R. S. J., & Blundy, J. D. (2017). Vertically extensive and unstable magmatic systems: a unified view of igneous processes. *Science*, *355*(6331).

Chauvel, C., & Hémond, C. (2000). Melting of a complete section of recycled oceanic crust: Trace element and Pb isotopic evidence from Iceland. *Geochemistry, Geophysics, Geosystems*, *1*(2).

Danyushevsky, L. V., & Plechov, P. (2011). Petrolog3: Integrated software for modeling crystallization processes. *Geochemistry, Geophysics, Geosystems*, *12*(7).

Day, J.M.D. (2004). A helium, oxygen and rhenium-osmium isotope study of some intraplate magmatism (Doctoral dissertation, Durham University).

Debaille, V., Trønnes, R. G., Brandon, A. D., Waight, T. E., Graham, D. W., & Lee, C. T. A. (2009). Primitive off-rift basalts from Iceland and Jan Mayen: Os-isotopic evidence for a mantle source containing enriched subcontinental lithosphere. *Geochimica et Cosmochimica Acta*, *73*(11), 3423-3449.

Eiler, J. M., Schiano, P., Kitchen, N., & Stolper, E. M. (2000). Oxygen-isotope evidence for recycled crust in the sources of mid-ocean-ridge basalts. *Nature*, *403*(6769), 530-534.

Fitton, J. G., Saunders, A. D., Kempton, P. D., & Hardarson, B. S. (2003). Does depleted mantle form an intrinsic part of the Iceland plume?. *Geochemistry, Geophysics, Geosystems*, *4*(3).

Friedman, J. D., Williams, R. S., Thorarinsson, S., Pálmason, G. (1972). Infrared emission from Kverkfjöll subglacial volcanic and geothermal area, Iceland. *Jökull*, *22*, 27–43

Füri, E., Hilton, D. R., Halldórsson, S. A., Barry, P. H., Hahm, D., Fischer, T. P., & Grönvold, K. (2010). Apparent decoupling of the He and Ne isotope systematics of the Icelandic mantle: The role of He depletion, melt mixing, degassing fractionation and air interaction. Geochimica et Cosmochimica Acta, 74(11), 3307-3332.

Gale, A., Dalton, C. A., Langmuir, C. H., Su, Y., & Schilling, J. G. (2013). The mean composition of ocean ridge basalts. *Geochemistry, Geophysics, Geosystems*, *14*(3), 489-518.

Gautason, B., & Muehlenbachs, K. (1998). Oxygen isotopic fluxes associated with high-temperature processes in the rift zones of Iceland. *Chemical Geology*, *145*(3-4), 275-286.

Graham, D. W. (2002). Noble gas isotope geochemistry of mid-ocean ridge and ocean island basalts: Characterization of mantle source reservoirs. *Reviews in mineralogy and geochemistry*, *47*(1), 247-317.

Green, R. G., White, R. S., & Greenfield, T. (2014). Motion in the north Iceland volcanic rift zone accommodated by bookshelf faulting. *Nature Geoscience*, *7*(1), 29.

Gudmundsson, A. (2000). Dynamics of volcanic systems in Iceland: example of tectonism and volcanism at juxtaposed hot spot and mid-ocean ridge systems. *Annual Review of Earth and Planetary Sciences*, *28*(1), 107-140.

Gudmundsson, A., & Andrew, R. E. (2007). Mechanical interaction between active volcanoes in Iceland. *Geophysical Research Letters*, *34*(10).

Gudmundsson, M. T., & Högnadóttir, T. (2007). Volcanic systems and calderas in the Vatnajökull region, central Iceland: Constraints on crustal structure from gravity data. *Journal of Geodynamics*, *43*(1), 153-169.

Gudmundsson, M.T., Thordarson, T., Larsen, G., Einarsson, P., Höskuldsson, Á., Imsland, P. (2013) Undir vatnajökli. In: *Náttúruvá á Íslandi*,. Eds.: Sólnes, J., Sigmundsson, F., Bessason, B., Forlagið, Reykjavik, Iceland pp. 263-267

Larsen, G. & Guðmundsson, M.T. (2019). Kverkfjöll. In: Óladóttir, B., Larsen, G. & Guðmundsson, M. T. Catalogue of Icelandic Volcanoes. IMO, UI and CPD-NCIP. Retrieved from http://icelandicvolcanoes.is/?volcano=KVE

Guillong, M., Meier, D. L., Allan, M. M., Heinrich, C. A., & Yardley, B. W. (2008). Appendix A6: SILLS: A MATLAB-based program for the reduction of laser ablation ICP-MS data of homogeneous materials and inclusions. *Mineralogical Association of Canada Short Course*, *40*, 328-333.

Haase, K. M., Beier, C., Regelous, M., Rapprich, V., & Renno, A. (2017). Spatial variability of source composition and petrogenesis in rift and rift flank alkaline lavas from the Eger Rift, Central Europe. *Chemical Geology*, *455*, 304-314.

Hoggard, M. J., Parnell-Turner, R., & White, N. (2020). Hotspots and mantle plumes revisited: Towards reconciling the mantle heat transfer discrepancy. *Earth and Planetary Science Letters*, *542*, 116317.

Halldórsson, S. A., Oskarsson, N., Gronvold, K., Sigurdsson, G., Sverrisdottir, G., & Steinthorsson, S. (2008). Isotopic-heterogeneity of the Thjorsa lava—implications for mantle sources and crustal processes within the Eastern Rift Zone, Iceland. *Chemical Geology*, *255*(3-4), 305-316.

Halldórsson, S. A., Barnes, J. D., Stefánsson, A., Hilton, D. R., Hauri, E. H., & Marshall, E. W. (2016a). Subducted lithosphere controls halogen enrichments in the Iceland mantle plume source. Geology, 44(8), 679-682.

Halldórsson, S. A., Hilton, D. R., Barry, P. H., Füri, E., & Grönvold, K. (2016b). Recycling of crustal material by the Iceland mantle plume: New evidence from nitrogen elemental and isotope systematics of subglacial basalts. *Geochimica et Cosmochimica Acta*, *176*, 206-226.

Hanan, B. B., & Schilling, J. G. (1997). The dynamic evolution of the Iceland mantle plume: the lead isotope perspective. *Earth and Planetary Science Letters*, *151*(1-2), 43-60.

Hanan, B. B., Blichert-Toft, J., Kingsley, R., & Schilling, J. G. (2000). Depleted Iceland mantle plume geochemical signature: Artifact of multicomponent mixing?. *Geochemistry, Geophysics, Geosystems*, *1*(4).

Hansen, H., & Grönvold, K. (2000). Plagioclase ultraphyric basalts in Iceland: the mush of the rift. *Journal of Volcanology and Geothermal Research*, *98*(1-4), 1-32.

Harðardóttir, S., Halldórsson, S. A., & Hilton, D. R. (2018). Spatial distribution of helium isotopes in Icelandic geothermal fluids and volcanic materials with implications for location, upwelling and evolution of the Icelandic mantle plume. *Chemical Geology*, *480*, 12-27.

Harðarson, B. S., & Godfrey Fitton, J. (1997). Mechanisms of crustal accretion in Iceland. *Geology*, *25*(11), 1043-1046.

Hards, V. L., Kempton, P. D., & Thompson, R. N. (1995). The heterogeneous Iceland plume: new insights from the alkaline basalts of the Snaefell volcanic centre. *Journal of the Geological Society*, *152*(6), 1003-1009.

Hards, V. L., Kempton, P. D., Thompson, R. N., & Greenwood, P. B. (2000). The magmatic evolution of the Snaefell volcanic centre; an example of volcanism during incipient rifting in Iceland. *Journal of Volcanology and Geothermal Research*, *99*(1-4), 97-121.

Hart, S. R. (1984). A large-scale isotope anomaly in the Southern Hemisphere mantle. *Nature*, *309*(5971), 753-757.

Hart, S. R. (1988). Heterogeneous mantle domains: signatures, genesis and mixing chronologies. *Earth and Planetary Science Letters*, *90*(3), 273-296.

Hartley, M. E., & Thordarson, T. (2013). The 1874–1876 volcano-tectonic episode at Askja, North Iceland: Lateral flow revisited. *Geochemistry, Geophysics, Geosystems*, *14*(7), 2286-2309.

Hartley, M., & Maclennan, J. (2018). Magmatic densities control erupted volumes in Icelandic volcanic systems. *Frontiers in Earth Science*, *6*, 29.

Hattori, K., & Muehlenbachs, K. (1982). Oxygen isotope ratios of the Icelandic crust. *Journal of Geophysical Research: Solid Earth*, *87*(B8), 6559-6565.

Heinonen, J. S., Spera, F. J., & Bohrson, W. A. (2021). Thermodynamic limits for assimilation of silicate crust in primitive magmas. *Geology*.

Helgason, J. (1989). The Fjallgardur volcanic ridge in NE Iceland: an aborted early stage plate boundary or a volcanically dormant zone? In: A. D. Saunders and M. J. Norry, eds. Magmatism in the Ocean Basins. *Geological Society, Special Publications*, *42*, 201–213.

Hémond, C., Arndt, N. T., Lichtenstein, U., Hofmann, A. W., Oskarsson, N., & Steinthorsson, S. (1993). The heterogeneous Iceland plume: Nd-Sr-O isotopes and trace element constraints. *Journal of Geophysical Research: Solid Earth*, *98*(B9), 15833-15850.

Hilton, D. R. (1996). The helium and carbon isotope systematics of a continental geothermal system: results from monitoring studies at Long Valley caldera (California, USA). *Chemical Geology*, *127*(4), 269-295.

Hjartardóttir, Á. R., & Einarsson, P. (2012). The Kverkfjöll fissure swarm and the eastern boundary of the Northern Volcanic Rift Zone, Iceland. *Bulletin of volcanology*, *74*(1), 143-162.

Hjartardóttir, Á. R., Einarsson, Þ., Magnúsdóttir, S., Björnsdóttir, Þ., & Brandsdóttir, B. (2016). Fracture systems of the Northern Volcanic Rift Zone, Iceland: an onshore part of the Mid-Atlantic plate boundary. *Geological Society, London, Special Publications*, *420*(1), 297-314.

Horton, F., Curtice, J., Farley, K.A., Kurz, M.D., Asimow, P.D., Treffkorn, J. and Boyes, X.M. (2021) Primordial neon in high-^{3}He/^{4}He Baffin Island olivines. *Earth and Planetary Science Letters*, *558*, p.116762.

Hooper, A., Ófeigsson, B., Sigmundsson, F., Lund, B., Einarsson, P., Geirsson, H., & Sturkell, E. (2011). Increased capture of magma in the crust promoted by ice-cap retreat in Iceland. *Nature Geoscience*, *4*(11), 783-786.

Höskuldsson, A., Sparks, R. S., & Carroll, M. R. (2006). Constraints on the dynamics of subglacial basalt eruptions from geological and geochemical observations at Kverkfjöll, NE-Iceland. *Bulletin of Volcanology*, *68*(7-8), 689.

Iacovino, K., & Till, C. B. (2019). DensityX: A program for calculating the densities of magmatic liquids up to 1,627 C and 30 kbar. *Volcanica*, *2*(1), 1-10.

Jackson, M. G., Hart, S. R., Koppers, A. A., Staudigel, H., Konter, J., Blusztajn, J., Kurz, M., & Russell, J. A. (2007). The return of subducted continental crust in Samoan lavas. *Nature*, *448*(7154), 684-687.

Jackson, M. G., & Dasgupta, R. (2008). Compositions of HIMU, EM1, and EM2 from global trends between radiogenic isotopes and major elements in ocean island basalts. Earth and Planetary Science Letters, 276(1-2), 175-186.

Jackson, M. G., Konter, J. G., & Becker, T. W. (2017). Primordial helium entrained by the hottest mantle plumes. *Nature*, *542*(7641), 340-343.

Jackson, M. G., Blichert-Toft, J., Halldórsson, S. A., Mundl-Petermeier, A., Bizimis, M., Kurz, M. D., Price, A. A., Harðardóttir, S., Willhite, L. N. Breddam, K., Becker, T. W., & Fischer, R. A. (2020). Ancient helium and tungsten isotopic signatures preserved in mantle domains least modified by crustal recycling. *Proceedings of the National Academy of Sciences*, *117*(49), 30993-31001.

Jakobsson, S. P., Jónasson, K., & Sigurdsson, I. A. (2008). The three igneous rock series of Iceland. *Jökull*, *58*, 117-138.

Jenkins, J., Maclennan, J., Green, R. G., Cottaar, S., Deuss, A. F., & White, R. S. (2018). Crustal formation on a spreading ridge above a mantle plume: receiver function imaging of the Icelandic crust. *Journal of Geophysical Research: Solid Earth*, *123*(6), 5190-5208.

Jochum, K. P., Willbold, M., Raczek, I., Stoll, B., & Herwig, K. (2005). Chemical Characterisation of the USGS Reference Glasses GSA-1G, GSC-1G, GSD-1G, GSE-1G, BCR-2G, BHVO-2G and BIR-1G Using EPMA, ID-TIMS, ID-ICP-MS and LA-ICP-MS. *Geostandards and Geoanalytical Research*, *29*(3), 285-302.

Jónsson, G., Kristjánsson, L., & Sverrisson, M. (1991). Magnetic surveys of Iceland. *Tectonophysics*, *189*(1-4), 229-247.

Kahl, M., Bali, E., Guðfinnsson, G. H., Neave, D. A., Ubide, T., Van Der Meer, Q. H., & Matthews, S. (2021). Conditions and dynamics of magma storage in the Snæfellsnes volcanic zone, Western Iceland: insights from the Búðahraun and Berserkjahraun eruptions. *Journal of Petrology*.

Kaikkonen, R.M. (2017) Evolution of basaltic lavas of the Kverkfjöll volcanic system, Northern Volcanic Zone, Iceland: Evidence from in-situ LA-ICP-MS analyses. Unpublished MSc thesis, University of Oulu, pp. 87.

Kamber, B. S., & Gladu, A. H. (2009). Comparison of Pb purification by anion-exchange resin methods and assessment of long-term reproducibility of Th/U/Pb ratio measurements by quadrupole ICP-MS. *Geostandards and Geoanalytical Research*, *33*(2), 169-181.

Karhunen, R. (1988). Eruption mechanism and rheomorphism during the basaltic fissure eruption in Biskupsfell, Kverkfjöll, north-central Iceland. *Nordic Volcanological Institute Report*, 8802, 91 pp.

Kelemen, P. B., Hirth, G., Shimizu, N., Spiegelman, M., & Dick, H. J. (1997). A review of melt migration processes in the adiabatically upwelling mantle beneath oceanic spreading ridges. *Philosophical Transactions of the Royal Society of London. Series A: Mathematical, Physical and Engineering Sciences*, *355*(1723), 283-318.

Kitagawa, H., Kobayashi, K., Makishima, A., & Nakamura, E. (2008). Multiple pulses of the mantle plume: evidence from Tertiary Icelandic lavas. *Journal of Petrology*, *49*(7), 1365-1396.

Koornneef, J. M., Stracke, A., Bourdon, B., Meier, M. A., Jochum, K. P., Stoll, B., & Grönvold, K. (2011). Melting of a two-component source beneath Iceland. *Journal of Petrology*, *53*(1), 127-157.

Kokfelt, T. F., Hoernle, K. A. J., Hauff, F., Fiebig, J., Werner, R., & Garbe-Schoenberg, D. (2006). Combined trace element and Pb-Nd–Sr-O isotope evidence for recycled oceanic crust (upper and lower) in the Iceland mantle plume. Journal of Petrology, 47(9), 1705-1749.

Kress, V.C. & Carmichael, I.S.E. (1991). The compressibility of silicate liquids containing Fe_2O_3 and the effect of composition, temperature, oxygen fugacity and pressure on their redox states. Contib Mineral Petrol, 108: 82-92.

Kurz, M.D., Moreira, M., Curtice, J., Lott III, D.E., Mahoney, J.J. and Sinton, J.M. (2005). Correlated helium, neon, and melt production on the super-fast spreading East Pacific Rise near 17 S. *Earth and Planetary Science Letters*, *232*(1-2), pp.125-142.

Kurz, M.D., Curtice, J., Fornari, D., Geist, D. and Moreira, M. (2009). Primitive neon from the center of the Galápagos hotspot. *Earth and Planetary Science Letters*, *286*(1-2), pp.23-34

Larsen, G., Gudmundsson, M. T., & Bjornsson, H. (1998). Eight centuries of periodic volcanism at the center of the Iceland hotspot revealed by glacier tephrostratigraphy. *Geology*, *26*(10), 943-946.

Lee, J. Y., Marti, K., Severinghaus, J. P., Kawamura, K., Yoo, H. S., Lee, J. B., & Kim, J. S. (2006). A redetermination of the isotopic abundances of atmospheric Ar. *Geochimica et Cosmochimica Acta*, *70*(17), 4507-4512.

Maccaferri, F., Rivalta, E., Keir, D., & Acocella, V. (2014). Off-rift volcanism in rift zones determined by crustal unloading. *Nature Geoscience*, *7*(4), 297-300.

Maclennan, J. (2008a). Concurrent mixing and cooling of melts under Iceland. *Journal of Petrology*, *49*(11), 1931-1953.

Maclennan, J. (2008b). Lead isotope variability in olivine-hosted melt inclusions from Iceland. *Geochimica et Cosmochimica Acta*, *72*(16), 4159-4176.

Maclennan, J. (2019). Mafic tiers and transient mushes: evidence from Iceland. *Philosophical Transactions of the Royal Society A*, *377*(2139), 20180021.

Macpherson, C. G., Hilton, D. R., Day, J. M., Lowry, D., & Grönvold, K. (2005). High-$^{3}He/^{4}He$, depleted mantle and low-$\delta^{18}O$, recycled oceanic lithosphere in the source of central Iceland magmatism. Earth and Planetary Science Letters, 233(3), 411-427.

Manning, C. J., & Thirlwall, M. F. (2014). Isotopic evidence for interaction between Öræfajökull mantle and the Eastern Rift Zone, Iceland. Contributions to Mineralogy and Petrology,167(1), 959.

Marschall, H. R., & Schumacher, J. C. (2012). Arc magmas sourced from mélange diapirs in subduction zones. *Nature Geoscience*, *5*(12), 862-867.

Marshall, E. W., Ranta, E., Halldórsson, S. A., Caracciolo, A., Bali, E., Jeon, H., Whitehouse, M.J., Barnes, J.D., & Stefánsson, A. (2021). Boron isotope evidence for devolatilized and rehydrated recycled materials in the Icelandic mantle source. Accepted for publication in *Earth and Planetary Science Letters*.

Martin, E., & Sigmarsson, O. (2010). Thirteen million years of silicic magma production in Iceland: Links between petrogenesis and tectonic settings. *Lithos*, *116*(1-2), 129-144.

Matthews, S., Shorttle, O., & Maclennan, J. (2016). The temperature of the Icelandic mantle from olivine-spinel aluminum exchange thermometry. *Geochemistry, Geophysics, Geosystems*, *17*(11), 4725-4752.

Moilanen, M., Hanski, E., Konnunaho, J., Törmänen, T., Yang, S. H., Lahaye, Y., O´Brien, H., & Illikainen, J. (2020). Composition of iron oxides in Archean and Paleoproterozoic mafic-ultramafic hosted Ni-Cu-PGE deposits in northern Fennoscandia: application to mineral exploration. *Mineralium Deposita*, 1-20.

Momme, P., Óskarsson, N., & Keays, R. R. (2003). Platinum-group elements in the Icelandic rift system: melting processes and mantle sources beneath Iceland. *Chemical Geology*, *196*(1-4), 209-234.

Montanaro, C., Scheu, B., Gudmundsson, M. T., Vogfjörd, K., Reynolds, H. I., Dürig, T., Strehlow, K., Rott, S., Reuschlé, T., & Dingwell, D. B. (2016). Multidisciplinary constraints of hydrothermal explosions based on the 2013 Gengissig lake events, Kverkfjöll volcano, Iceland. *Earth and Planetary Science Letters*, *434*, 308-319.

Moore, J. G., & Schilling, J. G. (1973). Vesicles, water, and sulfur in Reykjanes Ridge basalts. *Contributions to Mineralogy and Petrology*, *41*(2), 105-118.

Moreira, M., Kunz, J., & Allegre, C. (1998). Rare gas systematics in popping rock: isotopic and elemental compositions in the upper mantle. *Science*, *279*(5354), 1178-1181.

Muehlenbachs, K., Anderson Jr, A.T., & Sigvaldason, G.E. (1974). Low-O^{18} basalts from Iceland. *Geochimica et Cosmochimica Acta*, *38*(4), 577-588.

Mukhopadhyay, S. (2012). Early differentiation and volatile accretion recorded in deep-mantle neon and xenon. Nature, 486(7401), 101.

Namur, O., Charlier, B., Toplis, M.J., & Vander Auwera, J. (2011). Prediction of plagioclase-melt equilibria in anhydrous silicate melts at 1-atm. *Contributions to Mineralogy and Petrology*, *163*, 133e150.

Neave, D. A., & Putirka, K. D. (2017). A new clinopyroxene-liquid barometer, and implications for magma storage pressures under Icelandic rift zones. *American Mineralogist*, *102*(4), 777-794.

Neave, D. A., Bali, E., Guðfinnsson, G. H., Halldórsson, S. A., Kahl, M., Schmidt, A. S., & Holtz, F. (2019). Clinopyroxene–liquid equilibria and geothermobarometry in natural and experimental tholeiites: the 2014–2015 Holuhraun eruption, Iceland. *Journal of Petrology*, *60*(8), 1653-1680.

Neave, D. A., Namur, O., Shorttle, O., & Holtz, F. (2019). Magmatic evolution biases basaltic records of mantle chemistry towards melts from recycled sources. *Earth and Planetary Science Letters*, *520*, 199-211.

Nicholson, H., Condomines, N., Fitton, J.G., Fallick, A. E., Grönvold, K., & Rogers, G. (1991). Geochemical and isotopic evidence for crustal assimilation beneath Krafla, Iceland. *Journal of Petrology*, *32*(5), 1005-1020.

Nichols, A. R. L., Carroll, M. R., & Höskuldsson, A. (2002). Is the Iceland hot spot also wet? Evidence from the water contents of undegassed submarine and subglacial pillow basalts. Earth and Planetary Science Letters, 202(1), 77-87.

Nikkola, P., Guðfinnsson, G. H., Bali, E., Rämö, O. T., Fusswinkel, T., & Thordarson, T. (2019). Signature of deep mantle melting in South Iceland olivine. *Contributions to Mineralogy and Petrology*, *174*(5), 1-19.

Oddsson, B. (2016). *Heat transfer in volcanic settings: Application to lava-ice interaction and geothermal areas* (Doctoral dissertation).

Óladóttir, B. A., Larsen, G., & Sigmarsson, O. (2011a). Holocene volcanic activity at Grímsvötn, Bárdarbunga and Kverkfjöll subglacial centres beneath Vatnajökull, Iceland. *Bulletin of Volcanology*, *73*(9), 1187-1208.

Óladóttir, B. A., Sigmarsson, O., Larsen, G., & Devidal, J. L. (2011b). Provenance of basaltic tephra from Vatnajökull subglacial volcanoes, Iceland, as determined by major-and trace-element analyses. *The Holocene*, *21*(7), 1037-1048.

Ólafsson, M., Torfason, H., & Grönvold, K. (2000). Surface exploration and monitoring of geothermal activity in the Kverkfjöll geothermal area, central Iceland. *World Geotherm. Congr*, *2000*, 1539-1545.

O'Neill, H.St.C., Berry, A.J. & Mallmann, G. (2018). The oxidation state of iron in Mid-Ocean Ridge Basaltic (MORB) glasses: Implications for their petrogenesis and oxygen fugacites. E*arth and Planetary Science Letters*, *504*, 152-162.

Patton, H., Hubbard, A., Bradwell, T., & Schomacker, A. (2017). The configuration, sensitivity and rapid retreat of the Late Weichselian Icelandic ice sheet. *Earth-Science Reviews*, *166*, 223-245.

Peate, D. W., Breddam, K., Baker, J. A., Kurz, M. D., Barker, A. K., Prestvik, T., Grassineau, N., & Skovgaard, A. C. (2010). Compositional characteristics and spatial distribution of enriched Icelandic mantle components. *Journal of Petrology*, *51*(7), 1447-1475.

Pedersen, G. B., Grosse, P., & Gudmundsson, M. T. (2020). Morphometry of glaciovolcanic edifices from Iceland: Types and evolution. *Geomorphology*, *370*, 107334.

Pernet-Fisher, J. F. (2012). *Petrochemistry of the Northern Rift Zone, NE Iceland: plumbing dyamics and source variations* (Doctoral dissertation, Royal Holloway, University of London).

Plank, T., & Langmuir, C. H. (1998). The chemical composition of subducting sediment and its consequences for the crust and mantle. *Chemical geology*, *145*(3-4), 325-394.

Pope, E. C., Bird, D. K., & Arnórsson, S. (2013). Evolution of low-18O Icelandic crust. *Earth and Planetary Science Letters*, *374*, 47-59.

Poreda, R. J., Craig, H., Arnorsson, S., & Welhan, J. A. (1992). Helium isotopes in Icelandic geothermal systems: I. 3He, gas chemistry, and 13C relations. *Geochimica et Cosmochimica Acta*, *56*(12), 4221-4228.

Prestvik, T., Goldberg, S., Karlsson, H., & Grönvold, K. (2001). Anomalous strontium and lead isotope signatures in the off-rift Öræfajökull central volcano in south-east Iceland: Evidence for enriched endmember (s) of the Iceland mantle plume?. *Earth and Planetary Science Letters*, *190*(3), 211-220.

Putirka, K. D. (2008). Thermometers and barometers for volcanic systems. *Reviews in mineralogy and geochemistry*, *69*(1), 61-120.

Ranta, E., Gunnarsson-Robin, J., Halldórsson, S.A., Ono, S., Izon, G., Jackson, M.G., Reekie, C.D.J., Jenner, F.E., Guðfinnsson, G.H., Jónsson, O.P., Stefánsson, A. (2021b) Primordial and recycled sulfur sampled by the Iceland mantle plume. EartArXiv preprint, doi.org/10.31223/X5CD0Z

Rasmussen, M. B., Halldórsson, S. A., Gibson, S. A., & Guðfinnsson, G. H. (2020). Olivine chemistry reveals compositional source heterogeneities within a tilted mantle plume beneath Iceland. *Earth and Planetary Science Letters*, *531*, 116008.

Rasmussen, M. B. (2021). Magmatic olivine as a tool to investigate geochemical mantle heterogeneities beneath Iceland. PhD thesis, University of Iceland, 127 pp.

Richter, M., Nebel, O., Maas, R., Mather, B., Nebel-Jacobsen, Y., Capitanio, F. A., Dick, H.J.B., & Cawood, P. A. (2020). An Early Cretaceous subduction-modified mantle underneath the ultraslow spreading Gakkel Ridge, Arctic Ocean. *Science advances*, *6*(44), eabb4340.

Roeder, P. L., & Emslie, R. (1970). Olivine-liquid equilibrium. *Contributions to mineralogy and petrology*, *29*(4), 275-289.

Ruedas, T., Schmeling, H., Marquart, G., Kreutzmann, A., & Junge, A. (2004). Temperature and melting of a ridge-centred plume with application to Iceland. Part I: Dynamics and crust production. *Geophysical Journal International*, *158*(2), 729-743.

Rudnick, R.L., & Gao, S. (2003) Composition of the continental crust. In: Rudnick, R.L. (ed.) *Treatise on Geochemistry*, Vol. 3, The Crust. Elsevier, Amsterdam, 1–64.

Schattel, N., Portnyagin, M., Golowin, R., Hoernle, K., & Bindeman, I. (2014). Contrasting conditions of rift and off-rift silicic magma origin on Iceland. *Geophysical Research Letters*, *41*(16), 5813-5820.

Schilling, J. G. (1973). Iceland mantle plume: geochemical study of Reykjanes Ridge. *Nature*, *242*(5400), 565-571.

Schmeling, H., & Marquart, G. (2008). Crustal accretion and dynamic feedback on mantle melting of a ridge centred plume: the Iceland case. *Tectonophysics*, *447*(1-4), 31-52.

Shorttle, O., & Maclennan, J. (2011). Compositional trends of Icelandic basalts: Implications for short–length scale lithological heterogeneity in mantle plumes. *Geochemistry, Geophysics, Geosystems*, *12*(11).

Shorttle, O., Maclennan, J., & Piotrowski, A. M. (2013). Geochemical provincialism in the Iceland plume. *Geochimica et Cosmochimica Acta*, *122*, 363-397.

Sigbjarnarson, G. (1996). Norðan Vatnajökuls III. Eldstöðvar og hraun frá nútíma. *Náttúrufræðingurinn 65*: 199-212.

Sigmarsson, O., Condomines, M., & Fourcade, S. (1992). Mantle and crustal contribution in the genesis of recent basalts from off-rift zones in Iceland: constraints from Th, Sr and O isotopes. *Earth and Planetary Science Letters*, *110*(1-4), 149-162.

Sigmarsson, O., Karlsson, H. R., & Larsen, G. (2000). The 1996 and 1998 subglacial eruptions beneath the Vatnajökull ice sheet in Iceland: contrasting geochemical and geophysical inferences on magma migration. *Bulletin of Volcanology*, *61*(7), 468-476.

Sigmarsson, O., & Steinthórsson, S. (2007). Origin of Icelandic basalts: A review of their petrology and geochemistry. *Journal of Geodynamics*, *43*(1), 87-100.

Sigmarsson, O., Maclennan, J., & Carpentier, M. (2008). Geochemistry of igneous rocks in Iceland: a review. *Jökull*, *58*, 139-160.

Sigmarsson, O., & Halldórsson, S. A. (2015). Delimiting Bárðarbunga and Askja volcanic systems with Sr- and Nd-isotope ratios. *Jökull*, *65*, 17-27.

Sigurgeirsson, M.Á., Hjartarson, Á., Kaldal, I., Sæmundsson, K., Kristinsson, S.G., & Víkingsson, S. (2015). Geological Map of the Northern Volcanic Zone, Iceland. Southern Part. 1:100 000. Reykjavík: Iceland GeoSurvey.

Sigvaldason, G. E., Steinthorsson, S., Oskarsson, N., & Imsland, P. (1974). Compositional variation in recent Icelandic tholeiites and the Kverkfjöll hot spot. *Nature*, *251*(5476), 579-582.

Sigvaldason, G. E., & Óskarsson, N. (1976). Chlorine in basalts from Iceland. Geochimica et Cosmochimica Acta,40(7), 777-789.

Sigvaldason, G. E., & Óskarsson, N. (1986). Fluorine in basalts from Iceland. *Contributions to Mineralogy and Petrology*, *94*(3), 263-271.

Spiegelman, M. (1993). Physics of melt extraction: Theory, implications and applications. *Philosophical Transactions of the Royal Society of London. Series A: Physical and Engineering Sciences*, *342*(1663), 23-41.

Stracke, A., Zindler, A., Salters, V. J., McKenzie, D., Blichert-Toft, J., Albarède, F., & Grönvold, K. (2003). Theistareykir revisited. *Geochemistry, Geophysics, Geosystems*, *4*(2).

Stracke, A. (2012). Earth's heterogeneous mantle: a product of convection-driven interaction between crust and mantle. *Chemical Geology*, *330*, 274-299.

Thirlwall, M. F., Gee, M. A. M., Taylor, R. N., & Murton, B. J. (2004). Mantle components in Iceland and adjacent ridges investigated using double-spike Pb isotope ratios. *Geochimica et Cosmochimica Acta*, *68*(2), 361-386.

Thirlwall, M. F., Gee, M. A. M., Lowry, D., Mattey, D. P., Murton, B. J., & Taylor, R. N. (2006). Low $\delta^{18}O$ in the Icelandic mantle and its origins: evidence from Reykjanes Ridge and Icelandic lavas. *Geochimica et Cosmochimica Acta*, *70*(4), 993-1019.

Thorarinsson, S. (1953). The Grímsvötn expedition June–July 1953 (Vatnajökulsferð 1953). *Jökull*, *3*, 6-22.

Thorarinsson, S., Saemundsson, K., & Williams, R.S. (1973). ERTS-1 image of Vatnajökull: Analysis of glaciological, structural and volcanic features. *Jökull*, *23*, 7–17.

Thordarson, T., & Höskuldsson, Á. (2008). Postglacial volcanism in Iceland. *Jökull*, *58*(198), e228.
Torsvik, T. H., Amundsen, H. E., Trønnes, R. G., Doubrovine, P. V., Gaina, C., Kusznir, N. J., Steinberger, B., Corfu, F., Ashwal, L.D., Griffin, W.L., Werner, S. C., & Jamtveit, B. (2015). Continental crust beneath southeast Iceland. *Proceedings of the National Academy of Sciences*, 201423099.
Trieloff, M., Kunz, J., Clague, D. A., Harrison, D., & Allègre, C. J. (2000). The nature of pristine noble gases in mantle plumes. *Science*, *288*(5468), 1036-1038.
Trønnes, R. G., Planke, S., Sundvoll, B., & Imsland, P. (1999). Recent volcanic rocks from Jan Mayen: Low-degree melt fractions of enriched northeast Atlantic mantle. *Journal of Geophysical Research: Solid Earth*, *104*(B4), 7153-7168.
Trautz, M. (1914) Die Kverkfjöll und die Kverkhnukaranar im Hochland von Island. Zeitschrift der Gesellschaft für Erdkunde zu Berlin 1914, 169–199.
Turner, A. J., Katz, R. F., Behn, M. D., & Keller, T. (2017). Magmatic focusing to mid-ocean ridges: The role of grain-size variability and non-newtonian viscosity. *Geochemistry, Geophysics, Geosystems*, *18*(12), 4342-4355.
Tyrrell, G. W. (1949). Petrography of Igneous Rocks from the Vatnajökull Region, Iceland. *Earth and Environmental Science Transactions of The Royal Society of Edinburgh*, *61*(3), 793-801.
van der Meer, Q. H., Bali, E., Guðfinnsson, G. H., Kahl, M., & Rasmussen, M. B. (2021). Warm and slightly reduced mantle under the off-rift Snæfellsnes Volcanic Zone, Iceland. *Journal of Petrology*.
White, R. S., Drew, J., Martens, H. R., Key, J., Soosalu, H., & Jakobsdóttir, S. S. (2011). Dynamics of dyke intrusion in the mid-crust of Iceland. *Earth and Planetary Science Letters*, *304*(3-4), 300-312.
Williams, A.J. (2005). *The nature of the chemically enriched components of the Iceland mantle plume* (Doctoral dissertation, University of Edinburgh).
Williams, C. D., Mukhopadhyay, S., Rudolph, M. L., & Romanowicz, B. (2019). Primitive helium is sourced from seismically slow regions in the lowermost mantle. *Geochemistry, Geophysics, Geosystems*, *20*(8), 4130-4145.
Wilson, A. D. (1960). The micro-determination of ferrous iron in silicate minerals by volumetric and colorimetric method. *Analyst*, *85*, 823–827.
Wolfe, C. J., Bjarnason, I. T., VanDecar, J. C., & Solomon, S. C. (1997). Seismic structure of the Iceland mantle plume. *Nature*, *385*(6613), 245-247.
Wood, B. J., & Blundy, J. D. (1997). A predictive model for rare earth element partitioning between clinopyroxene and anhydrous silicate melt. *Contributions to Mineralogy and Petrology*, *129*(2), 166-181.
Yuan K. & Romanowicz B. (2017) Seismic evidence for partial melting at the root of major hot spot plumes. *Science* 357, 393.
Zhao, Z. F., & Zheng, Y. F. (2003). Calculation of oxygen isotope fractionation in magmatic rocks. *Chemical Geology*, *193*(1-2), 59-80.
Zindler, A., Hart, S. R., Frey, F. A., & Jakobsson, S. P. (1979). Nd and Sr isotope ratios and rare earth element abundances in Reykjanes Peninsula basalts evidence for mantle heterogeneity beneath Iceland. *Earth and Planetary Science Letters*, *45*(2), 249-262.
Zindler, A., & Hart, S. (1986). Chemical geodynamics. Annual review of Earth and Planetary Sciences, 14(1), 493-571.

6 Paper V

A whiff of subduction fluids in the Iceland mantle

Eemu Ranta[1], Sæmundur A. Halldórsson[1], Jaime D. Barnes[2], Simon Matthews[1], Barbara I. Kleine[1], Edward W. Marshall[1], Matthew G. Jackson[3], Enikő Bali[1], Peter H. Barry[4], Andri Stefánsson[1], Guðmundur H. Guðfinnsson[1], Karl Grönvold[1]

[1]*Nordic Volcanological Center, Institute of Earth Sciences, University of Iceland, Iceland*
[2]*Department of Geological Sciences, University of Texas at Austin, USA*
[3]*Department of Earth Science, University of California, Santa Barbara, USA*
[4]*Marine Chemistry and Geochemistry Department, Woods Hole Oceanographic Institution, USA*

Manuscript to be submitted to *Earth and Planetary Science Letters* (or similar)

6.1 Abstract

Recent findings of subduction-related components in mid-ocean ridge basalts suggest that the impact of the so-called subduction factory is widespread in the upper mantle, reaching mid-ocean ridge regions that were canonically considered to be well-mixed and geochemically homogenized. However, such geochemical signals have not yet been extensively reported for hotspot magmatism. Here, we follow up on recent studies of basalts from the Iceland hotspot that highlight the unusual character of the mantle feeding the Kverkfjöll volcanic system in central Iceland. Kverkfjöll is underlain by an unusually thick crust and lithosphere that promote sampling of a fusible, high-$^{208}Pb/^{206}Pb$ mantle component. We report new volatile elemental abundance (H_2O, CO_2, S, Cl) data in subglacial pillow basalt glasses and olivine-hosted melt inclusions from Kverkfjöll. The δD and $\delta^{37}Cl$ compositions were analyzed for a subset (n = 11) of the subglacial glasses. Glass H_2O (0.4 to 1.2 wt.%) and Cl content (200-600 ppm), as well as Cl/K of up to 0.09 and H_2O/Ce of up to 290 are among the highest in Iceland, suggesting that the Kverkfjöll melts are sourced from a H_2O- and Cl-enriched mantle. The δD values of up to -51 ‰ define a high-δD endmember in Iceland, and the $\delta^{37}Cl$ signature is seawater-like at +0.1 ± 0.2 ‰. In addition, Kverkfjöll basalts have high $\delta^{11}B$ (-3.1 ± 1.2 ‰), low $\delta^{34}S$ (down to -2.3 ‰) and a MORB-like $^3He/^4He$ (~8.5 R_A) signature. These volatile abundance and isotope characteristics clearly distinguish Kverkfjöll from both the depleted North Atlantic mantle and the Icelandic high-$^3He/^4He$ plume component, instead resembling the volatile fingerprint of back-arc basin basalts. We ascribe this similarity to the presence of a subduction fluid enriched mantle wedge (EMW) type component in the Iceland mantle. These findings align with previously observed CO_2, H_2O and δD enrichments present in some North Atlantic and high-Arctic mid-ocean ridge basalts (MORBs), suggesting that the EMW component is not necessarily carried from the lower mantle by the Iceland plume, but rather, may be a North Atlantic mantle anomaly inherited from Phanerozoic subduction events. Importantly, the presence of the EMW component beneath Iceland may suggest that plume-ridge interaction hastens the resurfacing of subducted volatiles that are carried from arcs to the convecting upper mantle, promoting a faster turnover of Earth's volatiles through its interior.

6.2 Introduction

Abundances and stable isotope ratios of volatiles (H, He, B, C, N, S, Cl) in mid-ocean ridge and ocean island basalts (MORBs and OIBs) provide important constraints on the mode of deep Earth volatile cycles, and on the origin of primordial and recycled mantle components. Chemical heterogeneities present in mid-ocean ridge basalts (MORBs)—which sample the upper mantle—have been variably ascribed to incorporation of sub-continental lithospheric mantle (Goldstein et al. 2008), subducted continental or oceanic crust (Michael 1995, Shimizu et al. 2016), or subduction fluid-induced mantle metasomatism (Dixon et al. 2017, Hauri et al. 2018). Traces of past subduction events have been identified in the ambient upper mantle sampled at mid-ocean ridges in the high-Arctic, North Atlantic and Indian Oceans (Hauri et al. 2018, Richter et al. 2020, Yang et al. 2021, Cai et al. 2021), with the important implication that subducted volatiles that escape the subduction factory and enter the upper mantle may be sampled by mantle melting beneath mid-ocean ridges. Thus far, the mantle plume contribution to the deep Earth volatile cycle has been considered to be mostly limited to the delivery of primordial

volatiles from the lower mantle (e.g., Mukhopadhyay 2012), as well as recycling of subducted oceanic and continental crust and sediments (Dixon et al. 2002, Marty and Dauphas 2003, Workman et al. 2006, Jackson et al. 2007, Kendrick et al. 2012). In this respect, Iceland is a unique area as it owes its existence to a deep-rooted mantle plume that straddles the North Atlantic mid-ocean ridge, with both contributing to its magmatism (Schilling 1973, Hanan et al. 2000).

The existence of diverse volatile mantle domains of primordial and deeply recycled origin beneath Iceland has been well established from the isotope systematics of helium (Kurz et al. 1985, Breddam et al. 2000, Füri et al. 2010, Harðardóttir et al. 2018), and more recently using boron (Marshall et al. 2022), nitrogen (Halldórsson et al. 2016b), sulfur (Ranta et al. 2021b) and chlorine isotopes (Halldórsson et al. 2016a). The Iceland plume also appears to have elevated H_2O content relative to adjacent MORBs (Nichols et al. 2002). However, the origin of this volatile heterogeneity, and to what extent its origin can be constrained by additional geochemical tracers, is not well known.

The Kverkfjöll volcanic system is a high-$\delta^{11}B$ (Marshall et al. 2022) and a low-$\delta^{34}S$ (Ranta et al. 2021b) endmember in Iceland, carrying some of the highest dissolved H_2O (Nichols et al. 2002) and Cl (Sigvaldason and Óskarsson 1976) concentrations and anomalous high-$^{208}Pb/^{206}Pb$ signatures among Icelandic basalts. (Chapter 5). Kverkfjöll is located at the eastern flank of the Northern Rift Zone—a subaerial portion of the North mid-Atlantic ridge—and relatively close to the assumed center of the Iceland mantle plume (Wolfe et al.1997). The unique geographic position of Kverkfjöll, together with its unusual geochemical signatures, has prompted various hypotheses regarding its affiliation with either the plume (Sigvaldason 1973, Sigvaldason and Óskarsson 1976, Marshall et al. 2022) or ambient upper mantle (Ranta et al. 2021b).

To resolve this debate, we present new data on volatile concentrations (H_2O, CO_2, S, Cl) for well-characterized, subglacially erupted basaltic glasses and olivine-hosted melt inclusions (MIs), as well as stable isotope ratios of hydrogen and chlorine (δD, $\delta^{37}Cl$) for the subglacial glasses. Together with previously reported values for $^3He/^4He$ (Macpherson et al. 2005, Chapter 5), B-$\delta^{11}B$ (Marshall et al. 2022), $\Delta^{33}S$-$\delta^{34}S$ (Ranta et al. 2021b) from the same lavas, the dataset provides an unusually comprehensive volatile abundance and stable isotope characterization of the Kverkfjöll magmatic system. When paired with available major and trace element concentration and Pb isotope data (Chapter 5), the Kverkfjöll dataset provides an exceptional opportunity to tackle pressing questions about the origin of volatiles in mantle plumes and the convecting upper mantle.

6.3 Samples and Methods

Kverkfjöll is an active volcanic system in Central Iceland, hosting a central volcano and a 60 km long fissure swarm characterized by Holocene lava flows surrounding hyaloclastite and pillow basalt ridges that erupted below Pleistocene ice sheets. Kverkfjöll eruptions are almost exclusively tholeiitic basalts with MgO of 4-8 wt.%. For Icelandic rocks, the basalts have relatively high concentrations of K_2O (0.4-1.0 %) and incompatible trace elements, generated by lesser degree of melting below a slightly thickened lithosphere relative to axial rift basalts (Chapter 5).

Our sample set consists of post-glacial scoria and subglacially erupted hyaloclastite and pillow basalt glasses (n = 72) as well as olivine-hosted melt inclusions (MIs; n = 15). Subglacial pillow rim glasses from Kverkfjöll are well suited for volatile studies, as they were erupted under sufficient pressure to retain most of the pre-eruptive volatile content of

both H_2O and S (Fig. S3 and S4), and are not affected by seawater assimilation (Nichols et al. 2002, Ranta et al. 2021b). Major and trace element compositions of the glasses, and major element composition of the MIs were reported by Marshall et al. (2022) and Ranta et al. (2021b, Chapter 5). A subset of the samples was previously analyzed for B-δ^{11}B (Marshall et al. 2022) and S-Δ^{33}S-δ^{34}S (Ranta et al. 2021b).

Full analytical details are provided in Supplementary Information. Chlorine and S concentrations were determined for all samples via electron probe microanalysis (EPMA) at the Institute of Earth Sciences, University of Iceland (IES), using methods described in Bali et al. (2018) and Ranta et al. (2021b). The H_2O and CO_2 concentration of 15 subglacial glasses and 10 olivine-hosted melt inclusions (MIs) were determined via Fourier-transform infrared spectroscopy (FTIR) at IES. A subset of the glasses, chosen to accommodate the full chemical range of the Kverkfjöll magma suite, were targeted for analysis of stable H and Cl isotope ratios at the University of Texas in Austin, USA. Hydrogen isotope (D/H) measurements were performed in duplicate on ~10 mg of 0.5M HF-washed glass chips sieved to 63-125 μm fraction (Fig. S1), using a high-temperature conversion-elemental analyzer coupled to an isotope ratio mass spectrometer (TC/EA-IRMS). Chlorine isotope ratios (^{37}Cl/^{35}Cl) were obtained on 220-430 mg agate-milled glass powders via IRMS using a custom sample inlet and purification line setup involving pyrohydrolysis and conversion to CH_3Cl which was used as the analyte. Stable isotope ratios of H and Cl are reported in standard delta notation relative to the Vienna Standard Mean Ocean Water (VSMOW) and Standard Mean Ocean Chloride (SMOC), respectively, e.g., $\delta D = (D/H)_{sample}/(D/H)_{VSMOW})-1)x1000$ ‰. The accuracy of the measurements is < ±5 ‰ (1σ) for δD, based on reproducibility of samples, and ±0.2‰ (1σ) for δ^{37}Cl, based on long-term averages of internal standards.

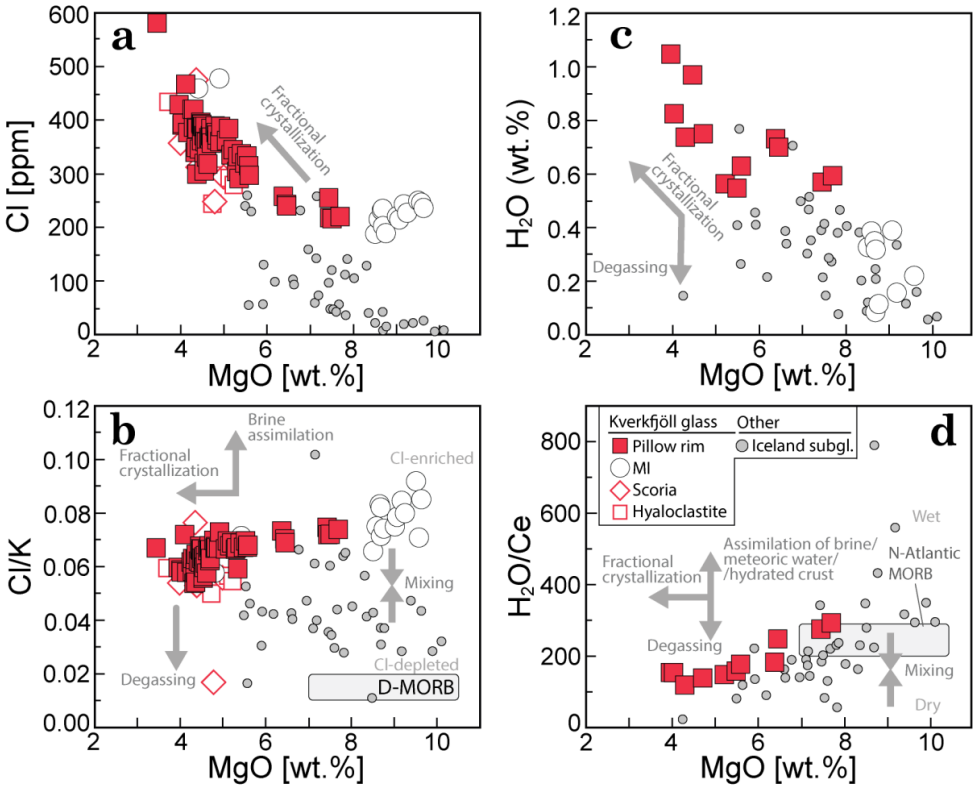

Figure 6.1 (a)-(b) Chlorine and (c)-(d) H_2O systematics. Major and trace element data from Ranta et al. (2021b) and Chapter 5. Cl and H_2O data for the non-Kverkfjöll Icelandic glasses from Matthews et al. (in prep.). Depleted MORB field in (b) as estimated by Shimizu et al. (2016). Depleted North Atlantic MORB field in (d) after H_2O/Ce range of 240±40 reported Dixon et al. (2017).

6.4 Results and discussion

6.4.1 Assessing the effects of degassing and assimilation

The Kverkfjöll glasses retain high dissolved Cl (200-600 ppm) and H_2O (0.6-1.1 wt.%) contents that are among the highest in Iceland (Fig. 6.1a,c; Table 1). These are coupled to Cl/K of 0.06 to 0.09 and H_2O/Ce of 120 to 290, with highest ratios seen in the MIs and the most primitive glasses (Figs. 6.1b and 6.1d). Chlorine and H_2O show well defined increasing trends with decreasing MgO, which confirm that Cl and H_2O behave as incompatible elements during the evolution of Kverkfjöll melts (Figs. 6.1a and 6.1c). The Cl and H_2O concentrations of the subglacial glasses and MIs fall on same melt evolution trends, and lack anomalously low Cl/K and H_2O/Ce ratios, indicating that the samples are relatively undegassed (Fig. 6.1), and that the MIs and host melts were quenched rapidly enough to prevent significant post-eruptive H_2O loss via H^+ diffusion. This suggestion is corroborated by relatively undegassed S contents (Fig. S4; Ranta et al. 2021b). By contrast, the subglacial glasses are strongly degassed with respect to CO_2, having low concentrations (below detection limit, i.e., less than approximately 20 ppm) relative to the MIs (up to 390 ppm). Low CO_2 concentrations are typical in subglacial eruptions, as the

cryostatic pressure (~90 bar for 1 km of glacier ice with a density of 920 kg/m^3) is typically not sufficient to keep more than ~40 ppm CO_2 in solution (cf. Barry et al. 2014). Relatively low CO_2 concentrations in the MIs seemingly suggest shallow trapping pressures (< 1 kbar; Fig. S4a-b) relative to previously established mid-crustal magma storage pressures of ~3 kbar (Chapter 5), but may also signal CO_2 loss to vapour bubbles (Aster et al. 2016) or decrepitation (Matthews et al. 2021). The lack of anomalously high Cl/K or H_2O/Ce values in the Kverkfjöll glassed suggests that they have not assimilated volatile-rich materials such as hydrothermally altered crust or seawater, a feature which they share with the majority of subglacial basalts in Iceland (Nichols et al. 2002, Halldórsson et al. 2016a) (Fig. 6.1). We interpret the decrease in Cl/K and H_2O/Ce with decreasing MgO to result from concurrent melt evolution and mixing of H_2O- and Cl-enriched and depleted melts, as these trends echo similar patterns seen for non-volatile incompatible trace element ratios (e.g. La/Yb and Ba/La) and Pb isotope ratios (Chapter 5).

The δD values of Kverkfjöll glasses range from –106 to –51 ‰ with an average of –68 ± 15 ‰ (1σ, n = 11; Fig. 6.2; Table 1) and are distinctly higher than other Icelandic basalts (–99 ± 10 ‰) and depleted North Atlantic MORBs (δD = –90 ± 20 ‰; Dixon et al. 2017; Fig. 6.2). The δ^{37}Cl signature of Kverkfjöll (0.0 ± 0.3 ‰, 1σ, n = 13) overlaps with the range identified in DMM (-0.1±0.3 ‰; Sharp et al. 2013) but is distinct from the positive δ^{37}Cl signature of up to +1.4 ‰ exhibited by samples with radiogenic Pb-isotopic signatures in Iceland (Halldórsson et al. 2016).

Degassing of H_2O generates residual melts with more negative δD values due to the positive sign of $\Delta D_{vapor\text{-}melt}$ (+25 ± 10 ‰; Pineau et al. 1998), and thus cannot explain the heavy δD signature of the Kverkfjöll glasses relative to other Icelandic subglacial glasses (Fig. S4). Further, due to the modest degassing experienced by the subglacial glasses, degassing-induced δD fractionation is estimated to be small (< –5 ‰; Fig. S4). Since the subglacial glasses effectively retain their pre-eruptive melt Cl and H_2O concentrations and show no signs of assimilation, we assume that Cl/K, H_2O/Ce, δD and δ^{37}Cl values directly reflect the signatures of their parental mantle melts. It is further assumed that primary mantle melts reflect the Cl/K, H_2O/Ce, δD and δ^{37}Cl signatures of their mantle sources, i.e., that no fractionation occurs during the melting process.

6.4.2 Defining the Icelandic volatile mantle end-members

A stand-out chemical characteristic of Kverkfjöll basalts is their high δD values and elevated Cl concentrations, expressed by a high Cl/K signature (0.06 to 0.09) relative to other Icelandic basalts (0.01-0.07; Fig. 6.2a). A positive correlation between Cl/K and δD shown by Icelandic subglacial glasses (Fig. 6.2a) suggests that Cl- and D-enrichments are controlled by a single Cl-enriched mantle endmember beneath Iceland, that is most clearly sampled by Kverkfjöll. Similar relationships between δD, Ba/La, δ^{11}B, δ^{34}S and ^{3}He/^{4}He require the existence of four separate volatile stable isotope mantle endmembers in the Iceland mantle (Figs. 6.2 and 6.3; Table S5):

(1) Plume 1 is a primordial high-^{3}He/^{4}He component (Jackson et al. 2021) that has the highest, approximately chondritic δ^{34}S values (~0 ‰; Ranta et al. 2021b), but lowest δD (Matthews et al., in prep) and Cl/K, and a DMM-like δ^{11}B signature (Marshall et al. 2022), and is mainly sampled by the Eastern Rift Zone basalts above the approximate center of the Iceland plume.

(2) Another plume-influenced component (Plume 2) with high ^{3}He/^{4}He is required to explain the signature of the South Iceland Volcanic Zone (SIVZ) basalts, which have a

more radiogenic Pb and enriched Nd-Sr isotopic signature (Jackson et al. 2021) and olivine compositions indicative of a recycled oceanic crust component in their source (Rasmussen et al. 2020). The SIVZ basalts have intermediate Cl/K and MORB-like δD-δ^{34}S, but higher-than-MORB δ^{11}B and δ^{37}Cl values.

(3) Ambient DMM is required as a mixing endmember explaining DMM-like ^{3}He/^{4}He-δD-δ^{11}B-δ^{34}S-δ^{37}Cl signature of many NRZ basalts.

(4) Kverkfjöll defines a second component with DMM-like ^{3}He/^{4}He values (~8.5 R_A), but has negative δ^{34}S signature (below values in DMM), which was proposed by Ranta et al. (2021b) to be related to sampling of a subduction fluid-enriched mantle wedge (EMW). The data presented here align with this hypothesis, because elevated Cl/K, δD and δ^{11}B of Kverkfjöll are all expected to be associated with EMW components, as discussed below.

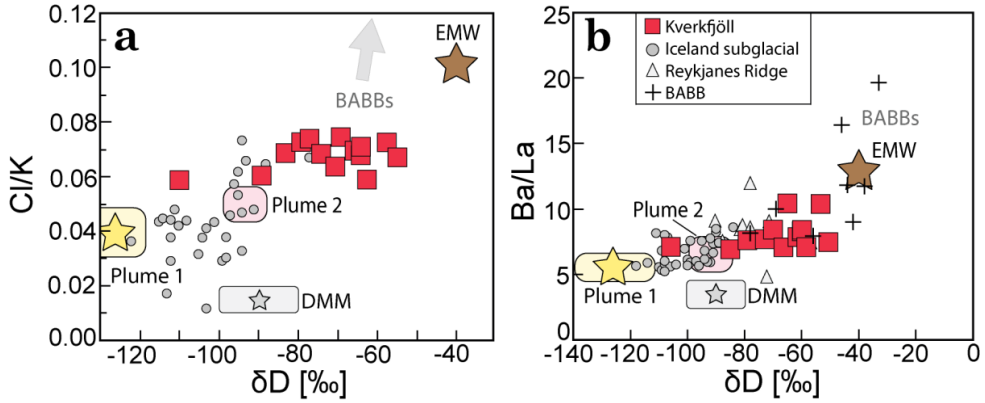

Figure 6.2 δD vs. (a) Cl/K and (b) Ba/La. Complementary Iceland data are from Matthews et al. (in prep.), where δD data were analyzed by IRMS using a similar setup as described here. Back-arc basin basalt (BABB; black crosses) data from Shaw et al. (2012). Reykjanes Ridge (light grey triangles) from Poreda et al. (1986) and Kelley et al. (2013). Stars and fields indicate estimated compositions of Icelandic mantle endmembers; Plume 1 (yellow), Plume 2 (pink), enriched mantle wedge (EMW; brown) and DMM (grey). The DMM field is drawn using the D-MORB Cl/K range of 0.01-0.02 (Shimizu et al. 2016) and the δD range of North Atlantic D-MORBs of -90±10 ‰ (Dixon et al. 2017). Symbols as in Fig. 6.1.

6.4.3 Origin of EMW: Drawing the link to BABBs

Mantle wedges are shallow mantle regions (30-150 km) that are fluxed with C-O-H-B-S-Cl-rich fluids emerging from a subducting slab. The fluids refertilize the mantle wedge—originally DMM in composition—with fluid-mobile elements, which becomes the source region of arc magmatism. Back-arc basin basalts (BABBs) are characterized by elevated concentrations of volatiles (H_2O-B-Cl) and fluid-mobile elements relative to less fluid-mobile elements, as expressed by elevated H_2O/Ce (> 500), Cl/K (> 0.2) and Ba/La (> 10; Fig. 6.2) (e.g., Shaw et al. 2012). Such trace element ratios in mantle-derived melts are indicative of derivation as partial melts of a subduction fluid-enriched mantle wedge (EMW).

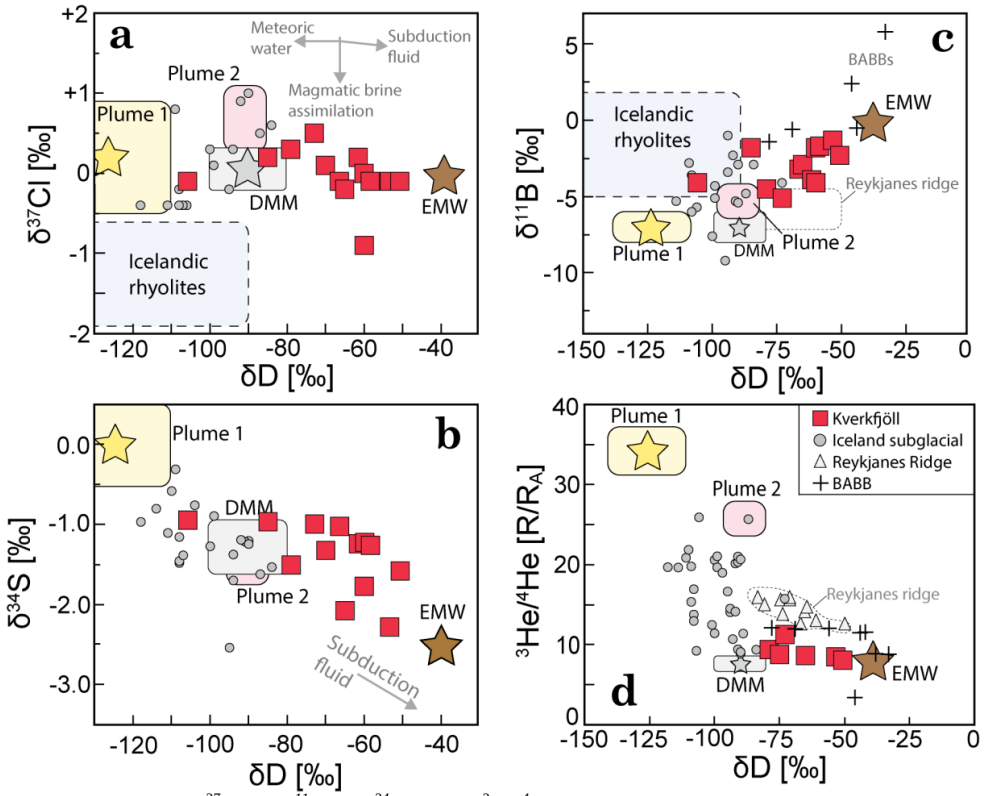

Figure 6.3 δD vs. (a) δ^{37}Cl, (b) δ^{11}B, (c) δ^{34}S, and (d) ^{3}He/^{4}He. The fields of Icelandic rhyolites in (a) and (c) are offset from the basalts toward lighter δD and δ^{37}Cl, and heavier δ^{11}B compositions. Thus, assimilation of Icelandic rhyolites, meteoric water or magmatic brine do not seemingly influence the δD-δ^{11}B-δ^{37}Cl values of Kverkfjöll melts, that are instead trending toward compositions similar to subduction fluids. Icelandic rhyolite data from Rose-Koga and Sigmarsson (2008), Halldórsson et al. (2016), Marshall et al. (2022) and Ranta et al. (2021a). Reykjanes Ridge (light grey triangles) from Poreda et al. (1986). The BABB data (black crosses) from Shaw et al. (2012). Additional δD and ^{3}He/^{4}He and data for Icelandic glasses from Macpherson et al. (2005), Füri et al. (2010) and Matthews et al. (in prep.). Symbols as in Fig. 6.1.

Slab fluids produce EMW-domains with more positive δD and δB (Fig. 6.3b), and similar or mildly negative δ^{37}Cl compared to the DMM, which are observed in both BABBs and arc magmas (Barnes et al. 2008, Shaw et al. 2008, 2012, John et al. 2010, Dixon et al. 2017). High Δ^{208}Pb (high time-integrated Th/U resulting in excess thorogenic Pb relative to northern hemisphere reference line; Hart 1984; Chapter 5) and elevated Ba/Nb (Fig S5) and Ba/La (Fig. 6.2b) characterize the Kverkfjöll lavas (Chapter 5). High Δ^{208}Pb signals in both OIBs and arc magmas can be explained by incorporation of subducted sediments and/or crustal material derived from subduction erosion of the fore-arc (Hart 1988, Plank and Langmuir 1998, Straub et al. 2020) and are thus not necessarily direct tracers of subduction fluids. A comparable coupling between elevated Δ^{208}Pb and enrichment in large-ion lithophile elements (e.g., elevated Ba/Nb and Ba/La; Fig. 6.2b, Fig. S5) have been previously observed in some MORBs at the Gakkel ridge (Richter et al. 2020), where these signals were interpreted to result from sampling of subduction-modified mantle components incorporated in the local depleted upper mantle.

Indeed, geochemical signals in EMW-type mantle regions expressed by the lithophile elements may be partly decoupled from the volatile systematics. This is due to the fact that

the mantle wedge region experiences a complex history of melt depletion, subduction erosion, slab melting and mélange diapirism in addition to subduction fluid-induced metasomatism (Marschall and Schumacher 2012, Dixon et al. 2017, Nielsen and Marschall 2017, Richter et al. 2020, Straub et al. 2020). Nonetheless, a clear enrichment in volatiles and concomitant isotopic signatures are evident in the Kverkfjöll lavas.

Notably, the volatile signatures of the EMW component and enriched mantle (EM) components are broadly expected to be complementary. This is due to the fact that H_2O, B and Cl devolatilize effectively at relatively shallow depths producing subduction fluids with high δD and $\delta^{11}B$ (e.g., Barnes et al. 2017, de Hood and Savov 2018), whereas recycled oceanic crust is dehydrated and depleted in B and Cl, with lowered H_2O/Ce, B/Ce and Cl/K and negative δD and $\delta^{11}B$ values relative to MORBs (Dixon et al. 2002, Workman et al. 2006, Kendrick et al. 2012, Dixon et al. 2017, Walowski et al. 2019). Further, EMW-type volatile signatures may partly overprint both incompatible trace element enriched *and* depleted mantle components, resulting from rehydration by subduction fluids (e.g., Marshall et al. 2022). Cai et al. (2021) suggested that IEDMORBs (isotopically enriched, incompatible element depleted MORBs) in the Gakkel ridge originated as EMW-type mantle that experienced prior low-degree melting. Indeed, the residual Kverkfjöll mantle could resemble the source of the Gakkel basalts.

Recent findings of subduction-modified components with EMW-type trace element, and δD signatures in MORBs, including in the North Atlantic demonstrate that EMW-type components that are not melted by arc or BABB magmatism can enter the convecting upper mantle to be incorporated at select segments of the global mid-ocean ridge system (Michael 1995, Dixon et al. 2017, Hauri et al. 2018, Richter et al. 2020, Yang et al. 2021, Cai et al. 2021). The striking affinity of the Kverkfjöll basalts to BABB-type volatile signatures extends to all studied volatile isotope systems (δD-^{3}He/^{4}He-δ^{11}B-δ^{34}S-δ^{37}Cl; Fig. 6.3), suggesting the presence of an EMW component in the Iceland mantle. Similar, heavy δD signatures in some North Atlantic MORBs have been attributed to subduction fluid-metasomatized components (Dixon et al. 2017); thus, we suggest that the Icelandic EMW component is derived from the North Atlantic upper mantle, rather than being sourced from a deep lower mantle plume component.

The relatively fast diffusivity of H in the mantle would result in smoothing out of mantle heterogeneities with respect to H_2O and δD over time (e.g., Shaw et al. 2012). This is especially true for short-length scale heterogeneities (<< 100 km). For example, partial re-equilibration between a 10 km thick dehydrated subducted slab (δD = –200 ‰) and the surrounding mantle (δD = –90 ‰) would reduce the maximum difference between the δD_{slab} and δD_{mantle} to a half of the original difference after 1 Gyr (Shaw et al. 2012). The survival of the anomalous Kverkfjöll δD signature in the Iceland mantle thus suggests either a relatively young age and/or relatively large initial size for the EMW component, and/or a large initial δD anomaly.

6.4.4 Why is the EMW beneath Iceland and what are the wider implications?

The tapping of the EMW component in Kverkjöll, only ~50 km east of the center of the plume (Wolfe et al. 1997), is puzzling. However, this finding aligns with an east-west asymmetry of the Iceland mantle defined by a drop in ^{3}He/^{4}He from a high-^{3}He/^{4}He plateau (Breddam et al. 2000, Harðardóttir et al. 2018) above the plume center to MORB-like values, and elevated Δ^{208}Pb signatures that are almost exclusively expressed by volcanoes to the east of the NRZ (Peate et al. 2010, Chapter 5).

Based on these previous observations, the Icelandic EMW component appears to be localized below eastern Iceland. Assuming that EMW is present in the ambient upper mantle, the preferential tapping of EMW in east Iceland may be related to the eastward movement of the Iceland plume center relative to the mid-Atlantic ridge, which has only recently activated melting in region. Furthermore, lower degree of melting below a the anomalously thick east Iceland lithosphere (Bjarnason and Schmeling 2009, Jenkins et al. 2018) may augment the geochemical expression of the EMW-type mantle, which we infer to be relatively fusible owing to its fluid-enrichment. Conversely, EMW components may become exhausted from regions of the mantle that experience prolonged melting or may be masked by extensive high-degree melting at shallow levels beneath the ridge axis. This may hinder the detection of EMW signatures in lavas even if it is relatively prevalent in the mantle.

The discovery of an EMW component adjacent to the Iceland mantle plume suggests that plume-ridge interaction may alleviate refluxing of non-plume-related EMW components in the ambient mantle, thus presenting a new mechanism by which plumes contribute to recycling of subducted materials back to Earth's surface.

6.5 References

Aster, E. M., Wallace, P. J., Moore, L. R., Watkins, J., Gazel, E., & Bodnar, R. J. (2016). Reconstructing CO_2 concentrations in basaltic melt inclusions using Raman analysis of vapor bubbles. *Journal of Volcanology and Geothermal Research*, *323*, 148-162.

Bali, E., Hartley, M. E., Halldórsson, S. A., Gudfinnsson, G. H., & Jakobsson, S. (2018). Melt inclusion constraints on volatile systematics and degassing history of the 2014–2015 Holuhraun eruption, Iceland. *Contributions to Mineralogy and Petrology*, *173*(2), 1-21.

Barry, P. H., Hilton, D. R., Füri, E., Halldórsson, S. A., & Grönvold, K. (2014). Carbon isotope and abundance systematics of Icelandic geothermal gases, fluids and subglacial basalts with implications for mantle plume-related CO2 fluxes. *Geochimica et Cosmochimica Acta*, *134*, 74

Barnes, J. D., Sharp, Z. D., & Fischer, T. P. (2008). Chlorine isotope variations across the Izu-Bonin-Mariana arc. *Geology*, *36*(11), 883-886.

Bjarnason, I. T., & Schmeling, H. (2009). The lithosphere and asthenosphere of the Iceland hotspot from surface waves. *Geophysical Journal International*, *178*(1), 394-418.

Breddam, K., Kurz, M. D., & Storey, M. (2000). Mapping out the conduit of the Iceland mantle plume with helium isotopes. *Earth and Planetary Science Letters*, *176*(1), 45-55.

Cai, Y., Yang, A. Y., Goldstein, S. L., Langmuir, C. H., Michael, P. J., Cochran, J. R., Zhang, W., Wang, D., & Bolge, L. (2021). Multi-stage melting of enriched mantle components along the eastern Gakkel Ridge. *Chemical Geology*, 120594.

Marty, B., & Dauphas, N. (2003). The nitrogen record of crust–mantle interaction and mantle convection from Archean to present. *Earth and Planetary Science Letters*, *206*(3-4), 397-410.

de Hoog, C. J., & Savov, I. P. (2017). Subduction zones, dehydration, metasomatism, mud and serpentinite volcanoes, and arc magmatism. *Boron isotopes—The fifth element, advances in isotope geochemistry*, *7*, 219-249.

Dixon, J. E., Leist, L., Langmuir, C., & Schilling, J. G. (2002). Recycled dehydrated lithosphere observed in plume-influenced mid-ocean-ridge basalt. *Nature*, *420*(6914), 385-389.

Dixon, J. E., Bindeman, I. N., Kingsley, R. H., Simons, K. K., Le Roux, P. J., Hajewski, T. R., Swart, P., Langmuir, C.H., Ryan, J.G., Walowski, K.J., Wada, I., & Wallace, P. J. (2017). Light stable isotopic compositions of enriched mantle sources: Resolving the dehydration paradox. *Geochemistry, Geophysics, Geosystems*, *18*(11), 3801-3839.

Füri, E., Hilton, D. R., Halldórsson, S. A., Barry, P. H., Hahm, D., Fischer, T. P., & Grönvold, K. (2010). Apparent decoupling of the He and Ne isotope systematics of the Icelandic mantle: The role of He depletion, melt mixing, degassing fractionation and air interaction. *Geochimica et cosmochimica acta*, *74*(11), 3307-3332.

Goldstein, S. L., Soffer, G., Langmuir, C. H., Lehnert, K. A., Graham, D. W., & Michael, P. J. (2008). Origin of a 'Southern Hemisphere'geochemical signature in the Arctic upper mantle. *Nature*, *453*(7191), 89-93.

Halldórsson, S. A., Barnes, J. D., Stefánsson, A., Hilton, D. R., Hauri, E. H., & Marshall, E. W. (2016a). Subducted lithosphere controls halogen enrichments in the Iceland mantle plume source. *Geology*, *44*(8), 679-682.

Halldórsson, S. A., Hilton, D. R., Barry, P. H., Füri, E., & Grönvold, K. (2016b). Recycling of crustal material by the Iceland mantle plume: new evidence from nitrogen elemental and isotope systematics of subglacial basalts. *Geochimica et Cosmochimica Acta*, *176*, 206-226.

Hanan, B. B., Blichert-Toft, J., Kingsley, R., & Schilling, J. G. (2000). Depleted Iceland mantle plume geochemical signature: Artifact of multicomponent mixing?. *Geochemistry, Geophysics, Geosystems*, *1*(4).

Harðardóttir, S., Halldórsson, S. A., & Hilton, D. R. (2018). Spatial distribution of helium isotopes in Icelandic geothermal fluids and volcanic materials with implications for location, upwelling and evolution of the Icelandic mantle plume. *Chemical Geology*, *480*, 12-27.

Hart, S. R. (1984). A large-scale isotope anomaly in the Southern Hemisphere mantle. *Nature*, *309*(5971), 753-757.

Hartley, M. E., De Hoog, J. C., & Shorttle, O. (2021). Boron isotopic signatures of melt inclusions from North Iceland reveal recycled material in the Icelandic mantle source. *Geochimica et Cosmochimica Acta*, *294*, 273-294.

Hauri, E. H., Maclennan, J., McKenzie, D., Gronvold, K., Oskarsson, N., & Shimizu, N. (2018). CO_2 content beneath northern Iceland and the variability of mantle carbon. *Geology*, *46*(1), 55-58.

Jackson, M. G., Hart, S. R., Koppers, A. A., Staudigel, H., Konter, J., Blusztajn, J., Kurz, M., & Russell, J. A. (2007). The return of subducted continental crust in Samoan lavas. *Nature*, *448*(7154), 684-687.

Jackson, M. G., Blichert-Toft, J., Halldórsson, S.A., Mundl-Petermeier, A., Bizimis, M., Kurz, M.D., Price, A.A., Harðardóttir, S. , Willhite, L.N.,. Breddam, K., Becker, T.W., Fischer, R.A. (2020) Ancient helium and tungsten isotopic signatures preserved in mantle domains least modified by crustal recycling. *Proceedings of the National Academy of Sciences*, *117*(49), 30993-31001.

Jenkins, J., Maclennan, J., Green, R. G., Cottaar, S., Deuss, A. F., & White, R. S. (2018). Crustal formation on a spreading ridge above a mantle plume: receiver function imaging of the Icelandic crust. *Journal of Geophysical Research: Solid Earth*, *123*(6), 5190-5208.

John, T., Layne, G. D., Haase, K. M., & Barnes, J. D. (2010). Chlorine isotope evidence for crustal recycling into the Earth's mantle. *Earth and Planetary Science Letters*, *298*(1-2), 175-182.

Kelley, K. A., Kingsley, R., & Schilling, J. G. (2013). Composition of plume-influenced mid-ocean ridge lavas and glasses from the Mid-Atlantic Ridge, East Pacific Rise, Galápagos Spreading Center, and Gulf of Aden. *Geochemistry, Geophysics, Geosystems*, *14*(1), 223-242.

Kendrick, M. A., Woodhead, J. D., & Kamenetsky, V. S. (2012). Tracking halogens through the subduction cycle. *Geology*, *40*(12), 1075-1078.

Kurz, M. D., Meyer, P. S., & Sigurdsson, H. (1985). Helium isotopic systematics within the neovolcanic zones of Iceland. *Earth and Planetary Science Letters*, *74*(4), 291-305.

Marschall, H. R., & Schumacher, J. C. (2012). Arc magmas sourced from mélange diapirs in subduction zones. *Nature Geoscience*, *5*(12), 862-867.

Marshall, E. W., Ranta, E., Halldórsson, S. A., Caracciolo, A., Bali, E., Jeon, H., Whitehouse, M.J., Barnes, J.D., & Stefánsson, A. (2022). Boron isotope evidence for devolatilized and rehydrated recycled materials in the Icelandic mantle source. *Earth and Planetary Science Letters*, *577*, 117229.

Matthews, S., Shorttle, O., Maclennan, J., & Rudge, J. F. (2021). The global melt inclusion C/Ba array: Mantle variability, melting process, or degassing?. *Geochimica et Cosmochimica Acta*, *293*, 525-543.

Michael, P. (1995). Regionally distinctive sources of depleted MORB: Evidence from trace elements and H_2O. *Earth and Planetary Science Letters*, *131*(3-4), 301-320.

Mukhopadhyay, S. (2012). Early differentiation and volatile accretion recorded in deep-mantle neon and xenon. *Nature*, *486*(7401), 101-104.

Nielsen, S. G., & Marschall, H. R. (2017). Geochemical evidence for mélange melting in global arcs. *Science advances*, *3*(4), e1602402.

Peate, D. W., Breddam, K., Baker, J. A., Kurz, M. D., Barker, A. K., Prestvik, T., Grassineau, N:, & Skovgaard, A. C. (2010). Compositional characteristics and spatial distribution of enriched Icelandic mantle components. *Journal of Petrology*, *51*(7), 1447-1475.

Pineau, F., Shilobreeva, S., Kadik, A., & Javoy, M. (1998). Water solubility and D/H fractionation in the system basaltic andesite–H_2O at 1250 C and between 0.5 and 3 kbars. *Chemical Geology*, *147*(1-2), 173-184.

Pope, E. C., Bird, D. K., & Arnórsson, S. (2013). Evolution of low-^{18}O Icelandic crust. *Earth and Planetary Science Letters*, *374*, 47-59.

Poreda, R., Schilling, J. G., & Craig, H. (1986). Helium and hydrogen isotopes in ocean-ridge basalts north and south of Iceland. *Earth and Planetary Science Letters*, *78*(1), 1-17.
Ranta, E., Barnes, J.D., Halldórsson, S.A., Jónasson, K., Stefánsson A. (2021a). Chlorine isotope ratios record magmatic brine assimilation during rhyolite genesis. *Geochemical Perspectives Letters*, *16*, 35-39.
Ranta, E., Gunnarsson-Robin, J., Halldórsson, S.A., Ono, S., Izon, G., Jackson, M.G., Reekie, C.D.J., Jenner, F.E., Guðfinnsson, G.H., Jónsson, O.P., Stefánsson, A. (2021b) Primordial and recycled sulfur sampled by the Iceland mantle plume. EartArXiv preprint, doi.org/10.31223/X5CD0Z
Rasmussen, M. B., Halldórsson, S. A., Gibson, S. A., & Guðfinnsson, G. H. (2020). Olivine chemistry reveals compositional source heterogeneities within a tilted mantle plume beneath Iceland. *Earth and Planetary Science Letters*, *531*, 116008.
Richter, M., Nebel, O., Maas, R., Mather, B., Nebel-Jacobsen, Y., Capitanio, F. A., Dick, H.J.B., & Cawood, P. A. (2020). An Early Cretaceous subduction-modified mantle underneath the ultraslow spreading Gakkel Ridge, Arctic Ocean. *Science advances*, *6*(44), eabb4340.
Schilling, J. G. (1973). Iceland mantle plume: geochemical study of Reykjanes Ridge. *Nature*, *242*(5400), 565-571.
Sharp, Z. D., Mercer, J. A., Jones, R. H., Brearley, A. J., Selverstone, J., Bekker, A., & Stachel, T. (2013). The chlorine isotope composition of chondrites and Earth. *Geochimica et Cosmochimica Acta*, *107*, 189-204.
Shaw, A. M., Hauri, E. H., Fischer, T. P., Hilton, D. R., & Kelley, K. A. (2008). Hydrogen isotopes in Mariana arc melt inclusions: Implications for subduction dehydration and the deep-Earth water cycle. *Earth and Planetary Science Letters*, *275*(1-2), 138-145.
Shaw, A. M., Hauri, E. H., Behn, M. D., Hilton, D. R., Macpherson, C. G., & Sinton, J. M. (2012). Long-term preservation of slab signatures in the mantle inferred from hydrogen isotopes. *Nature Geoscience*, *5*(3), 224-228.
Shimizu, K., Saal, A. E., Myers, C. E., Nagle, A. N., Hauri, E. H., Forsyth, D. W., Kamenetsky, V. S., & Niu, Y. (2016). Two-component mantle melting-mixing model for the generation of mid-ocean ridge basalts: implications for the volatile content of the Pacific upper mantle. *Geochimica et Cosmochimica Acta*, *176*, 44-80.
Sigvaldason, G. E., & Óskarsson, N. (1976). Chlorine in basalts from Iceland. Geochimica et Cosmochimica Acta,40(7), 777-789.
Straub, S. M., Gómez-Tuena, A., & Vannucchi, P. (2020). Subduction erosion and arc volcanism. *Nature Reviews Earth & Environment*, *1*(11), 574-589.
Torsvik, T. H., Amundsen, H. E., Trønnes, R. G., Doubrovine, P. V., Gaina, C., Kusznir, N. J., Steinberger, B., Corfu, F., Ashwal, L.D., Griffin, W.L., Werner, S. C., & Jamtveit, B. (2015). Continental crust beneath southeast Iceland. *Proceedings of the National Academy of Sciences*, 201423099.
Yang, A. Y., Langmuir, C. H., Cai, Y., Michael, P., Goldstein, S. L., & Chen, Z. (2021). A subduction influence on ocean ridge basalts outside the Pacific subduction shield. *Nature communications*, *12*(1), 1-10.
Wolfe, C. J., Bjarnason, I. T., VanDecar, J. C., & Solomon, S. C. (1997). Seismic structure of the Iceland mantle plume. *Nature*, *385*(6613), 245-247.
Workman, R. K., Hauri, E., Hart, S. R., Wang, J., & Blusztajn, J. (2006). Volatile and trace elements in basaltic glasses from Samoa: Implications for water distribution in the mantle. *Earth and Planetary Science Letters*, *241*(3).

Appendix A: Supplementary information for Paper I

Reprinted under Creative Commons License CC BY-NC-ND 4.0

Geochemical Perspectives Letters

© 2021 The Authors
Published by the European Association of Geochemistry

Chlorine isotope ratios record magmatic brine assimilation during rhyolite genesis

E. Ranta, S.A. Halldórsson, J.D. Barnes, K. Jónasson, A. Stefánsson

Supplementary Information

The Supplementary Information includes:

- S-1: Samples and Methods
- S-2: Geological Setting
- S-3: Chlorine Contents in Icelandic Melt Inclusions
- S-4: Bulk Assimilation Model
- S-5: Quantifying Magmatic Brine Formation in the Crust
- Tables S-1 to S-3
- Figures S-1 to S-5
- Supplementary Information References

S-1: Samples and Methods

A total of 16 volcanic rocks from Iceland were analysed in this study (Tables S-1, S-2). New $\delta^{37}Cl$ data are reported for 14 of these samples (Table S-2). Together with the samples analysed by Halldórsson *et al.* (2016), they cover the main neovolcanic zones of Iceland, *i.e.*, the rift, propagating rift and rift zones, as well as the full geochemical range within these zones, *i.e.*, tholeiitic, transitional and alkaline magma suites (Fig. S-1, S-2). The basaltic (n = 3) and intermediate (n = 4) rocks are subglacial (HNAUS-1) or subaerial lavas. The silicic samples from this study (n = 8) and Halldórsson et al. (2016) (n = 3) are tephras (n = 5) and obsidians (n = 6). All material extracted from the samples for chemical analysis was chosen to be as fresh as possible and free from visible alteration. Therefore, any secondary low-T chlorine isotopic fractionation induced by hydrothermal or surface alteration of the rocks is considered unlikely. For all samples,

except for HNAUS-1, ASD1L and ASD14L, major element data has been published previously; by Óskarsson *et al.* (1982) for samples A-THO, A-ALK, B-ALK, D28a (same as SNS-32), I-DAC, I-ICE and SAL-76; by Jónasson (2007) for KER-3 and H-6; by Sverrisdóttir (2007) for H3a, H4 and H5. The samples are Holocene (< 10 ka) in age except for A-THO, D28a, KER-3, H-6, SAL-74 and SAL-76 that are Upper Pleistocene (< 0.8 Ma).

Major element, Cl and S concentrations for the obsidian glasses A-THO, A-ALK, D28a, H-6 and KER-3 were analysed at the Institute of Earth Sciences (IES), University of Iceland using a JEOL JXA-8230 SuperProbe electron probe microanalyser (EPMA). Major elements for the subglacial glass HNAUS-1 were determined with an ARL-SEMQ EPMA at IES, University of Iceland, using a setup described in Halldórsson *et al.* (2008). For this sample, the chlorine concentrations were analysed by secondary ion mass spectroscopy (SIMS) at the Department of Terrestrial Magnetism, Carnegie Institution of Washington, using methods described in Hauri *et al.* (2002). Major element composition of samples ASD1L and ASD14L were analysed at IES by inductively coupled plasma optical emission spectrometry (ICP-OES) using methods described in Momme *et al.* (2003), and the Cl concentrations with X-Ray fluoresence spectrometry (XRF) with analytical details described in Sigvaldason and Óskarsson (1976). For the five obsidians (A-THO, A-ALK, H-6, KER-3, D28a), the H_2O and CO_2 concentrations were determined by Fourier transform infrared spectroscopy (FTIR) at IES on 50-380 um thick, doubly polished glass wafers. The H_2O and CO_2 concentrations were calculated with Beer-Lambert's law

$$C = \frac{100MA}{\rho h \varepsilon} \qquad \text{Eq. S-1}$$

where M is the molar weight of the species [g/mol], A is the absorbance, ρ is density [g/L], h is the thickness of the glass wafer [cm] and ε is the absorptivity coefficient [L $mol^{-1}cm^{-1}$]. For the H_2O peak at 3500 cm^{-1}, a value of ε = 93.1 L $mol^{-1}cm^{-1}$ was used, determined experimentally for an Icelandic tholeiitic series rhyolite sample (KRA-045-2; McIntosh *et al.*, 2017). The CO_2 concentrations were below detection limit (c. 10 ppm) for all samples.

Chlorine and oxygen isotope ratios were measured at the University of Texas at Austin using methods described in the supplement of Halldórsson *et al.* (2016). For chlorine isotope analysis, 200-600 mg of sample powder was washed five times in 18 MΩ deionised water. Chloride ions were released by pyrohydrolysis, trapped in an aqueous solution and converted to AgCl. The AgCl was reacted with CH_3I to produce CH_3Cl. The CH_3Cl was purified on-line in a series of cryogenic traps and a gas chromatograph before introduction into a ThermoElectron MAT 253 isotope ratio mass spectrometer (IRMS). The reported error of 1σ = 0.2 ‰ is based on a long-term average of internal standards.

Oxygen isotope ratios for samples D28a, H-6, HNAUS-1, KER-3, and SAL-76 were determined on chips of ≈ 2 mg of sample by laser fluorination-IRMS using a CO_2 laser in a BF_5 atmosphere. The extracted O_2 was purified in a series of cryogenic traps before introduction into a ThermoElectron MAT 253 IRMS. Full methodology is described by Sharp (1990). An error of 1σ = 0.07 ‰ is based on the long-term reproducibility of $\delta^{18}O$ values of the San Carlos olivine ($\delta^{18}O$ = 5.25 ‰), Lausanne-1 quartz ($\delta^{18}O$ = 18.1 ‰) and UWG-2 garnet ($\delta^{18}O$ = 5.8 ‰) (Valley *et al.*, 1995) standards.

Oxygen isotope ratios for ASD1L, ASD14L, H3a, H4 and H5 were analysed from whole rock samples by Geochron Laboratories, Inc., Cambridge, Mass., in 1996 with conventional methods and have an analytical uncertainty of 1σ = 0.2 ‰.

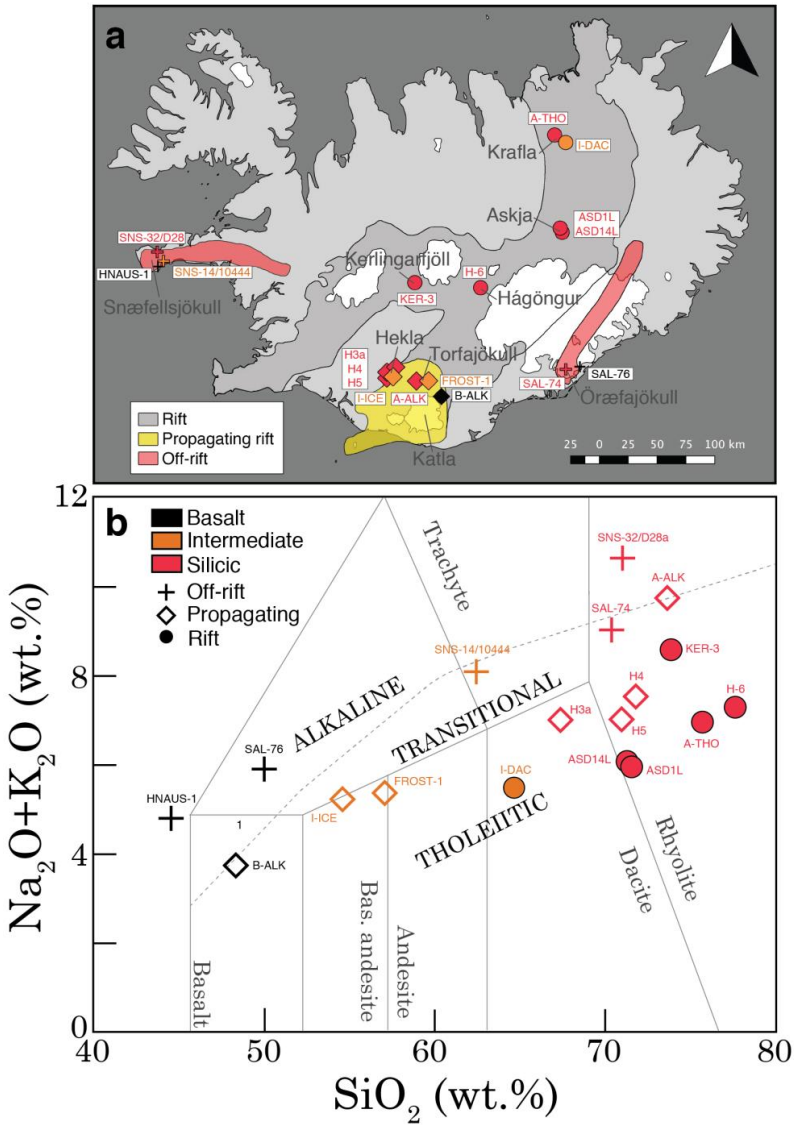

Figure S-1 **(a)** Sample map and classification. The neovolcanic zones in Iceland are indicated by grey field. Locations of samples used in this study are indicated by black (basalts), orange (intermediate) and red (silicic) circles (rift), diamonds (propagating rift) and crosses (off-rift). **(b)** Total alkali vs. SiO_2 diagram showing the geochemical range of the samples. The samples cover the Icelandic alkaline, transitional and tholeiitic magmatic suites.

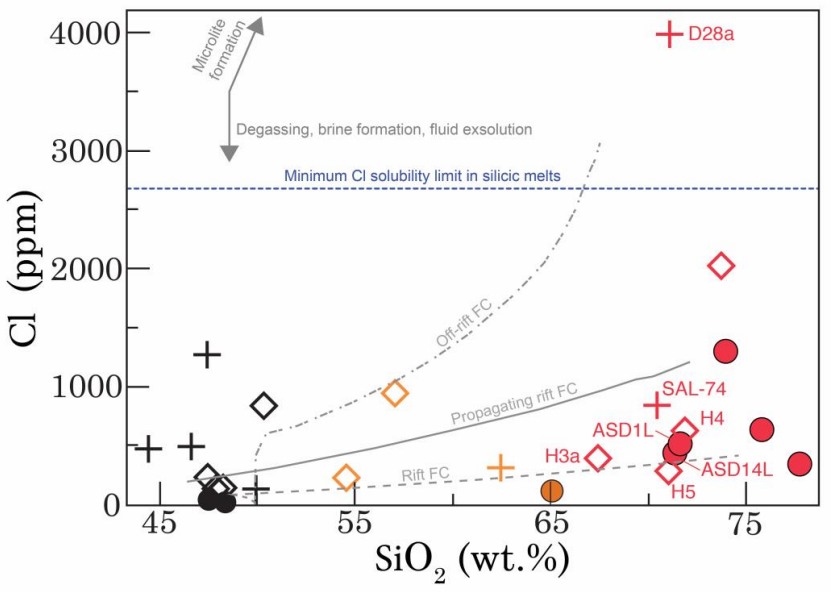

Figure S-2 Chlorine concentrations show an overall increase from low to high concentrations with increasing SiO_2 contents, compatible with isobaric fractional crystallisation models (using MELTS, c.f. Fig. S-3) for the different volcano-tectonic settings. Propagating rift and off-rift samples have generally higher Cl concentrations than the rift samples. However, the large spread in chlorine concentrations at a given SiO_2 content even within similar settings probably indicates the combined effect of different source concentrations, chlorine loss by degassing and fluid exsolution, increase during microlite formation upon cooling, and chlorine addition by assimilation of magmatic brines. Notably, all except one sample (D28a) plot below the estimated minimum Cl solubility limit in silicic melts (Metrich and Rutherford, 1992; Webster, 1997). Symbols as in Figure S-1.

S-2: Geological Setting

Rhyolites are rare in most oceanic islands but constitute up to 10 % of the crust of Iceland (Jónasson, 2007). Genesis of rhyolites in Iceland is favored by prolonged melt evolution in long-lived magmatic reservoirs beneath central volcanoes that sit on top of an unusually thick, up to 40 km, oceanic-type crust, which in turn is the result of excessive melt generation beneath Iceland. Icelandic rhyolite genesis is often seen as a modern analogue for how the first silicic continental crust on the planet may have emerged before the onset of plate tectonics (Willbold *et al.*, 2009; Reimink *et al.*, 2014).

Prevailing ideas suggest that silicic melts in Iceland have been created by (1) partial melting of hydrated basaltic crust, (2) fractional crystallisation of mantle-derived basaltic melts or (3) a combination of (1) and (2) (Nicholson *et al.*, 1991; Sigmarsson *et al.*, 1992; Gunnarsson *et al.*, 1998; Martin and Sigmarsson, 2010; Schattel *et al.*, 2014). Moreover, (1) and (2) are generally thought to dominate at two end-member volcano-tectonic settings: partial melting is favored at rift

zones where the geothermal gradient is high (*e.g.*, Askja, Krafla) (Martin and Sigmarsson, 2007; Kuritani *et al.*, 2011; Schattel *et al.*, 2014), whereas fractional crystallisation from basaltic parental melts seems to the dominant rhyolite forming process at the off-rift volcanoes (Snæfellsjökull, Öræfajökull) that are situated on top of colder crust (Prestvik *et al.*, 2001; Martin and Sigmarsson, 2010). An intermediate setting is represented by the non-rifting South Iceland Volcanic Zone (*e.g.*, Hekla, Torfajökull), which is the southward-propagating tip of the Eastern Rift Zone and is marked by high magma production rates and high frequency of rhyolitic eruptions, whose genesis is likely a combination of (1) and (2) (Gunnarsson *et al.*, 1998; Martin and Sigmarsson, 2010; Chekol *et al.*, 2011).

Possible correlation between volcano-tectonic setting and δ^{37}Cl – implications for magmatic brine formation

The negative δ^{37}Cl shifts in silicic rocks observed in this study seem to be larger at propagating rift and rift settings, but smaller or absent at off-rift settings (Figs. 1b and 2). This apparent correlation may be explained by considering how the volcano-tectonic setting is likely to influence how magmatic brine formation and assimilation take place. Silicic magma genesis below rift and propagating rift central volcanoes in Iceland takes place in hot (Martin and Sigmarsson, 2010; Schattel *et al.*, 2014) and dynamic mush systems that are maintained by frequent injections of fresh basaltic magma from underlying mafic domain or impinging rift dikes, which stimulate partial melting of wall rock and remobilisation of previously formed silicic segregations (Gunnarsson *et al.*, 1998; Jónasson 2007; Gurenko *et al.*, 2015). Such conditions promote magmatic brine formation. The off-rift systems reside in a colder crust, experience longer intervals without activity and are characterised by silicic magma generation that more closely resembles closed-system fractional crystallisation (Martin and Sigmarsson, 2010; Schattel *et al.*, 2014). In such environment, mushes are likely to be less developed, melts interact less with their surroundings, and the conditions for magmatic brine assimilation are suboptimal.

S-3: Chlorine Contents in Icelandic Melt Inclusions

Glassy melt inclusions (MI) potentially record the pre-eruptive volatile contents of the melts from which they crystallised and may hold information about the de- and regassing history of Cl within the crustal magma storage domain (Webster *et al.*, 2019). We compiled volatile concentration data in melt inclusions (MIs) in olivine, clinopyroxene and plagioclase in Icelandic basalts and rhyolites published before July 2020 with the aim of assessing degassing relationships between H_2O and Cl (Fig. S-3; Table S-3). Where available, the database includes data for paired matrix glass (MG) or whole-rock analyses, as well as MI major and trace element data. Values corrected for post-entrapment crystallisation are plotted as published.

MI and matrix glass Cl concentrations in Icelandic silicic rocks are similar (Fig. S-3a), suggesting that insignificant amount of syn-eruptive Cl degassing takes place, presumably caused by the slow diffusion of Cl compared to H_2O from melt into vapor bubbles (Baker and Balcone-Boissard, 2009; Barnes *et al.*, 2014). Chlorine concentrations in the silicic MIs are generally lower than predicted by fractional crystallisation (Fig. S-3b), and the wide range of Cl concentrations in silicic MIs suggests that Cl is affected by other pre-eruptive processes. In the case of rift and propagating rift samples, low and variable Cl concentrations may be explained by their formation mechanism which involves partial melting of

altered crust with low Cl contents. Melt Cl concentrations can also increase through assimilation of Cl-rich material such as brines (Webster *et al.*, 2019) and decrease by exsolution of hydrosaline fluids or assimilation of Cl poor material. Exsolution of a Cl-rich brine is not indicated by the MI data, because the Cl concentrations are lower than the solubility limit of Cl at the pressure range of the model of Webster *et al.* (2015) (up to 7 kbar) and below the lower end of solubility limits of Cl in rhyolitic melts in general of 2200-2700 ppm at 1 bar (Metrich and Rutherford, 1992; Webster, 1997). Chlorine may also be lost by partitioning to an aqueous vapor phase (Shinohara, 2009). Essentially, the Cl/H_2O ratio of the melt controls whether a melt will exsolve a hydrosaline fluid or a Cl-bearing aqueous vapor upon reaching saturation (Webster, 2004) . About half of the silicic Icelandic MIs record Cl/H_2O ratios above 0.05, which is the approximate threshold for hydrosaline liquid exsolution in granitic melts (Webster, 2004).

In conclusion, the published MI and matrix glass volatile data available for Icelandic volcanic systems demonstrates that Cl concentrations in MIs are highly variable and indistinguishable from the matrix glasses (Fig. S-3a). Furthermore, Cl concentrations are also decoupled from the MI H_2O concentrations (Fig. S-3e), which in turn are essentially controlled by magma storage depths and degassing during eruptions (Schattel *et al.*, 2014). The pre- and syn-eruptive processes that affect Cl systematics of silicic rocks in Iceland and elsewhere, *e.g.*, at Mono Craters, USA (Barnes *et al.*, 2014) seem to be complex compared to H_2O and not fully understood at present (Webster *et al.*, 2019).

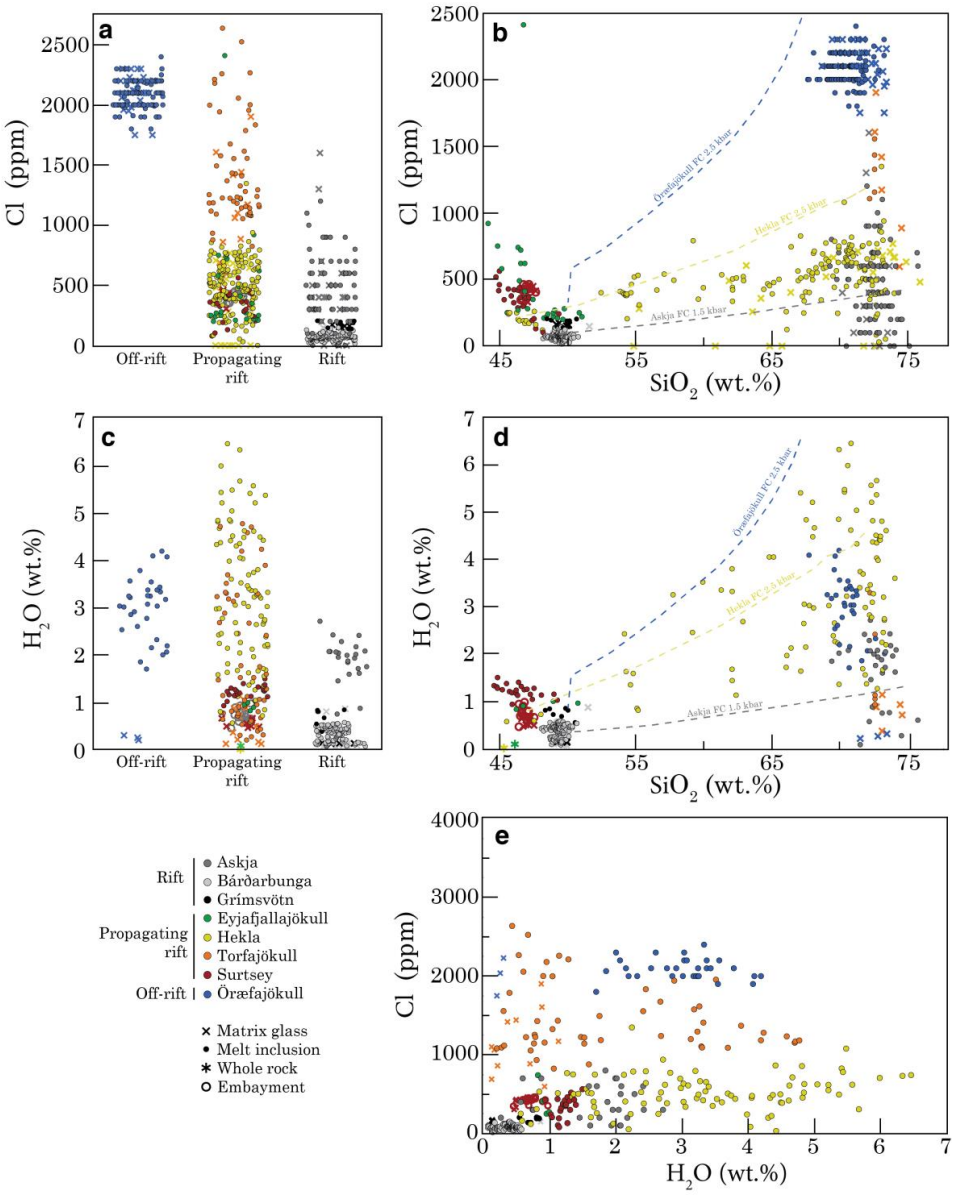

Figure S-3 **(a)-(e)** Compilation of published melt inclusion H_2O and Cl data from Iceland. The basaltic samples from different volcanic systems have variable Cl and H_2O concentrations depending on the degree of partial melting and, possibly, source volatile concentrations (Nichols *et al*., 2002). This results in rift basalts with relatively low Cl and H_2O concentrations (Bárdarbunga, Grímsvötn) compared to alkaline basalts of Surtsey. Fractional crystallisation paths were calculated with the rhyolite-MELTS software (Gualda *et al.,* 2012; Ghiorso and Gualda, 2015). The total range in Cl conents of rhyolitic MIs from rift and propagating rift settings is large (< 50 to 2600 ppm) compared to Öræfajökull (1700-2400 ppm), the only rhyolitic off-rift volcano with available MI data. We take this difference to reflect the two different modes of rhyolite genesis in Iceland: at off-rift settings the pre-eruptive volatile history with respect to Cl is

seemingly simple and controlled by fractional crystallisation (Martin and Sigmarsson, 2010), while partial melting, assimilation as well as fluid exsolution and resorption processes at rift and propagating rift settings amount to a complex volatile history. The data was compiled from Moune *et al*. (2007), Sharma *et al*. (2008), Brounce *et al*. (2012), Moune *et al*. (2012), Portnyagin *et al*. (2012), Owen *et al*. (2013), Schattel et al. (2014), Lucic *et al*. (2016), Schipper *et al*. (2016) and Bali *et al*. (2018).

S-4: Bulk Assimilation Model

Bulk assimilation can be simulated with a binary mixing model (*e.g.*, Albarède, 1995). A binary mixture of a melt and an assimilant will attain the concentration C of element A of

$$C^A_{mix} = C^A_{assimilant} f_{assimilant} + C^A_{melt}(1-f_{assimilant}) \quad \text{Eq. S-2}$$

where $f_{assimilant}$ is the fraction of the assimilant. The mixture will have an isotopic ratio R of

$$R^A_{mix} = \rho^A_{melt} R^A_{melt} + \rho^A_{assimilant} R^A_{assimilant} \quad \text{Eq. S-3}$$

where the mixing parameters ρ^A_{melt} and $\rho^A_{assimilant}$ are defined as

$$\rho^A_{melt} = \frac{C^A_{melt}(1-f_{assimilant})}{C^A_{assimilant} f_{assimilant} + C^A_{melt}(1-f_{assimilant})} \quad \text{Eq. S-4}$$

$$\rho^A_{assimilant} = \frac{C^A_{assimilant} f_{assimilant}}{C^A_{melt}(1-f_{assimilant}) + C^A_{assimilant} f_{assimilant})} \quad \text{Eq. S-5}$$

For chlorine and oxygen, the isotopic ratios are converted to standard delta notation as

$$\delta^A = \frac{R^A_{mix} - R^A_{standard}}{R^A_{standard}} \times 1000\ ‰ \quad \text{Eq. S-6}$$

The isotopic ratios used for the international standards for chlorine (SMOC = Standard Mean Ocean Chloride) and oxygen (VSMOW = Vienna Standard Mean Ocean Water) were

$$R^{Cl}_{SMOC} = (^{37}Cl/^{35}Cl)_{SMOC} = 0.3188962681$$

$$R^{O}_{VSMOW} = (^{18}O/^{16}O)_{VSMOW} = 0.002005171$$

We performed assimilation modeling using the following hypothetical end-member compositions:

(1) Pristine rhyolite melt: Cl = 200 ppm, O = 48 wt.%, $\delta^{37}Cl$ = 0 ‰, $\delta^{18}O$ = 6.0 ‰ (the low Cl concentrations and the basalt-like $\delta^{18}O$ values are typical for Hekla rhyolites; Table S-2).

(2) Saline pore water (*e.g.*, mix of magmatic brine and meteoric-derived hydrothermal water): Cl = 20,000 ppm (NaCl equivalent = 3.3 wt.%), O = 83.1 wt.%, $\delta^{18}O$ = -10 ‰, $\delta^{37}Cl$ = -4.0 ‰ (the low $\delta^{18}O$ value representing high-latitude precipitation (Árnason, 1976)).

(3) Magmatic brine: Cl = 100,000 ppm ($NaCl_{equivalent}$ = 16.5 wt.%), O = 62.2 wt.%, $\delta^{18}O$ = 6.0 ‰, $\delta^{37}Cl$ = -4.0 ‰ (the $\delta^{18}O$ is assumed to be similar to pristine rhyolite melt).

(4) Hydrothermally altered crust: Cl = 500 ppm, O = 48 wt.%, $\delta^{18}O$ = -10.0 ‰, $\delta^{37}Cl$ = -4.0 ‰ (the Cl concentration is at the upper end of altered oceanic crust (Barnes and Cisneros, 2012) and the $\delta^{18}O$ value is at the lower end of altered crust in Iceland (Gautason and Muehlenbachs, 1998)).

Our choice of $\delta^{37}Cl$ = -4 ‰ for magmatic brine and saline pore fluid is less negative than the possible $\delta^{37}Cl$ = -5 ‰ demonstrated by Fortin *et al.* (2017). The model demonstrates that assimilation of hydrothermally altered basalt, even if ascribed a relatively high Cl concentration (500 ppm; Barnes and Cisneros, 2012) and an unrealistically low $\delta^{37}Cl$ value of -4 ‰ (see main text), is unable to explain the observed data (Fig. S-4) because unrealistically high degrees of assimilation (> 40 wt.%) would be required to explain the observed negative $\Delta^{37}Cl_{rhyolite\text{-}basalt}$ shifts.

Other globally known materials with distinctly negative $\delta^{37}Cl$ values include marine sediments (-3.0 to +0.7 ‰; Barnes and Sharp, 2017) and marine pore fluids (-7.8 to +0.3 ‰; Ransom *et al.*, 1995; Bonifacie *et al.*, 2007), but are not widespread in the Icelandic crust, which has not significantly interacted with seawater (Halldórsson *et al.*, 2016). Potential assimilation of clays with negative $\delta^{37}Cl$ values cannot readily explain the negative $\Delta^{37}Cl_{rhyolite\text{-}basalt}$ shifts as their Cl concentrations are generally similar to rhyolites (< 2000 ppm; Barnes *et al.*, 2008). Negative $\delta^{37}Cl$ values found in arc basalts (Barnes and Straub, 2010; Chiaradia *et al.*, 2014; Manzini *et al.*, 2017; Bouvier *et al.*, 2019) and some recycled mantle components (John *et al.*, 2010) are most likely related to Cl sourced from subducted slabs. While incorporation of recycled sediments in the Icelandic mantle has been suggested to explain the $\delta^{37}Cl$ variability of Icelandic basalts (Halldórsson *et al.*, 2016), it can not explain the negative $\delta^{37}Cl$ values of silicic rocks relative to the basalts.

Instead, all negative $\delta^{37}Cl$ values in this study can be explained by up to 0.5 wt.% assimilation of a magmatic brine (Fig. S-4). Notably, the $\delta^{18}O_{rhyolite}$ values resulting from fluid assimilation are relatively unsensitive to the $\delta^{18}O$ value of the assimilant, because only low degrees of assimilation are required, and because the oxygen concentrations of melts and fluids are of the same order (Fig. S-4b). For example, 2.5 wt.% assimilation of the saline pore fluid end member required for the maximum $\delta^{37}Cl$ shift of -2.9 ‰ leads only to a minor (-0.7 ‰) shift of the $\delta^{18}O$ value of the silicic melts despite a very low hypothetical $\delta^{18}O$ = -10 ‰ (Fig S-4b).

Lowered K/Cl ratios have been used to trace brine assimilation in mid-ocean ridge basalts (e.g. Kendrick et al. 2013, 2017) as K/Cl ratios are low in saline fluids and brines (<< 1) compared to the pristine basaltic melts (c. 10-100), and because the K/Cl ratio is not fractionated during fractional crystallisation of basalts. Compared to basaltic MIs (K/Cl ≈ 5-50), silicic MIs in Iceland show a considerably larger variation of K/Cl ratios at the propagating rift volcano Hekla (13-755) and the rift volcano Askja (16-291). This large variation is caused by the complicated controls on Cl concentrations in silicic melts (see section S-3). Because of the large variability in K/Cl ratios in silicic melts, assimilation of small amounts (< 1 wt.%) of magmatic brine is difficult to demonstrate using K/Cl (Fig. S-5). Figure S-5 demonstrates that δ^{37}Cl is a much more sensitive tracer of magmatic brine assimilation in silicic rocks than K/Cl.

Furthermore, we consider a fluid assimilant the most likely candidate for controlling the δ^{37}Cl signatures of silicic rocks because isotopes of non-volatile elements show that (1) rhyolites in Iceland generally preserve the long-lived radiogenic isotopic (Sr-Nd-Hf-Pb) signatures of corresponding basalts confirming that the source material of the refractory elements is ultimately basalt from the same system (Sigmarsson *et al.*, 1992 ; Kuritani *et al.*, 2011), and (2) extensive previous work on multiple non-volatile stable isotopes in Hekla samples, where the largest $\Delta^{37}Cl_{rhyolite\text{-}basalt}$ shifts are seen, conclude that the δ^{7}Li, δ^{41}K, δ^{66}Zn, δ^{98}Mo and ε^{205}Tl systematics show no difference between rhyolites and basalts from Hekla (Schuessler *et al.*, 2009; Chen *et al.*, 2013; Yang *et al.*, 2015; Prytulak *et al.*, 2017; Tuller-Ross, 2019), or that, in the case of δ^{30}Si, δ^{49}Ti, δ^{51}V, $\delta^{56/54}$Fe and $\delta^{94/90}$Zr, can be fully explained by fractional crystallisation (Schuessler *et al.*, 2009; Savage *et al.*, 2011; Prytulak *et al.*, 2016; Deng *et al.*, 2019; Inglis *et al.*, 2019).

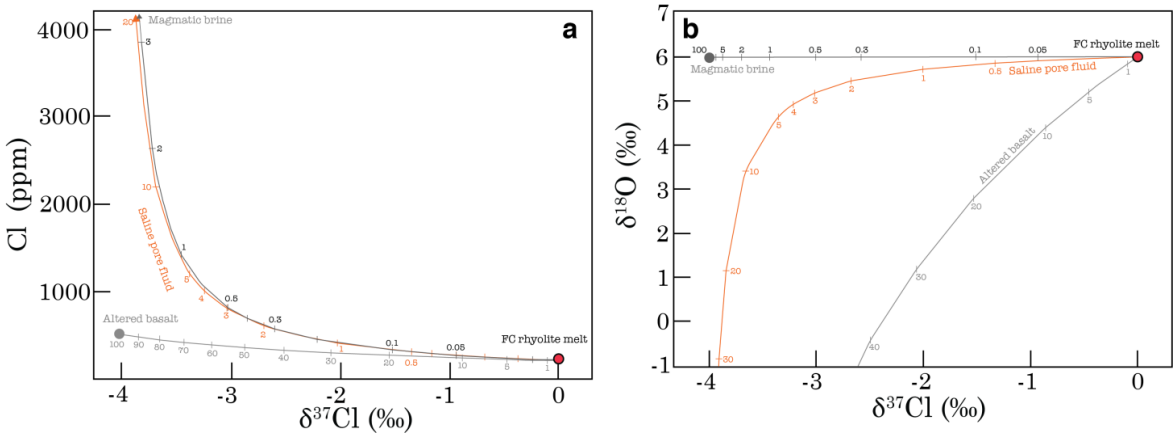

Figure S-4 **(a)-(b)** The effects of bulk assimilation of magmatic brine, saline pore fluid and hydrothermally altered crust on Cl, δ^{18}O and δ^{37}Cl values on pristine (unaffected by assimilation) rhyolite melt. See text for the used assimilant compositions.

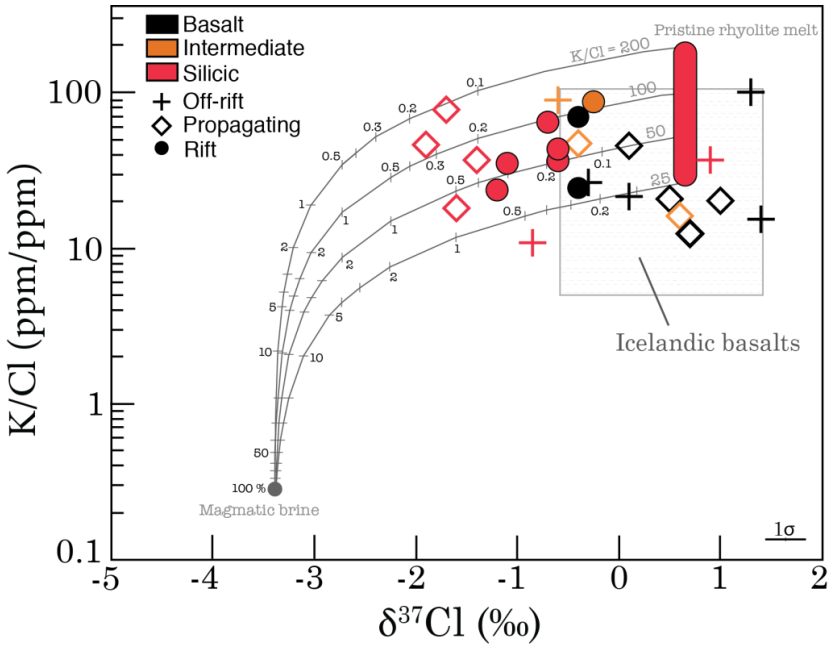

Figure S-5 The effect of bulk assimilation of magmatic brine on K/Cl and δ^{37}Cl values of rhyolitic melt. Small amount of magmatic brine assimilation does not generate K/Cl ratios subceeding the K/Cl range of basalts. Grey curves show binary mixing curves between magmatic brine with K/Cl = 0.28 (calculated for a brine with 10 wt.% Cl dissolved as $Na_{0.5}K_{0.5}Cl$, comparable to brine inclusions analysed by Audétat and Pettke (2003)) and pristine rhyolite melts with variable K/Cl ratios (25-200), K = 20,000 ppm. The δ^{37}Cl compositions of magmatic brine and pristine rhyolite melt are shifted by +0.7 ‰ compared to the end-member compositions defined in section S-4, so that the value of pristine rhyolite melts reflects the average δ^{37}Cl value of +0.7 ‰ of the propagating rift basalts. Note that binary mixing curves in K/Cl-δ^{37}Cl space are linear, but are here plotted on a logarithmic y-axis.

S-5: Quantifying Magmatic Brine Formation in the Crust

In the following, we assess (1) how much magmatic brine is expected to exsolve from magmatic intrusions, and (2) whether this production would be enough to sustain assimilation of 0.3 wt.% brine in extrusive silicic rocks, which is enough to explain most negative δ^{37}Cl shifts in rhyolites in this study (Fig. S-5).

Our estimate for brine assimilation, A = 0.3 wt.% (mass of assimilated brine/mass of erupted rhyolite), with salinity of Cl = 10 wt.% or NaCl = 16.5 wt.% (see previous section), corresponds to a volume ratio for brine/melt of about 0.006 (using densities of ρ_{melt} = 2260 kg/m^3 and ρ_{brine} = 1200 kg/m^3). For a hypothetical cylindrical silicic magma chamber with a thickness of 50 m, this corresponds to an overlaying brine layer with a thickness of c. 0.3 m, or equivalently, a 6 m thick mush layer with 5% porosity that is occupied by brine. This estimate can be compared to a > 1 km thick low-resistivity layer below the Merapi volcano, Indonesia, interpreted as saline fluids of possible magmatic origin residing

in host rock of 15% porosity (Müller and Haak, 2004). To convert A to a maximum brine assimilation rate B_a (kg of brine assimilated/yr) in Iceland, we use a silicic extrusion rate of $R_e = 0.004$ km^3/yr estimated for silicic historic eruptions (Thordarson and Larsen, 2007). Thus,

$$B_a = \rho_{melt} \times R_e \times A \approx 27 \times 10^6 \text{ kg/yr} \quad \text{Eq. S-7}$$

To estimate how much brine can be produced by magmatic intrusions, R_b (kg brine/yr) *i.e.*, magma that stalls and crystallises in the crust without erupting, we use

$$R_b = \rho_{melt} \times R_i \times F \quad \text{Eq. S-8}$$

where F is the mass ratio of exsolved brine/intrusive melt and R_i is derived from the magmatic intrusion/extrusion production ratio X,

$$X = R_i/R_e \quad \text{Eq. S-9}$$

We choose a value of X = 5, which is considered plausible for Iceland (White *et al.*, 2006), yielding a silicic intrusion rate for Iceland of $R_i = 0.02$ km^3/yr. The most difficult parameter to estimate in Eq. S-8 is F. An effort to estimate fluid/melt ratios and the salinities of exsolved fluids from a global compilation of silicic MIs was recently undertaken by Webster *et al.* (2019). The Cl contents of fluids exsolved from magmas range from 0.3 to up towards 70 wt. % for low fluid/melt ratios of F = 2 x 10^{-3} (by mass) and 0.3-11 wt.% for a higher fluid/melt estimate of F = 4.7 x 10^{-2}, *i.e.*, lower fluid/melt ratios generate higher salinity fluids (Webster *et al.*, 2019). A brine can alternatively be created from a supersolvus fluid with moderate NaCl concentrations by unmixing to a low-NaCl vapor and a high-NaCl liquid upon hitting a solvus curve at 1.3-1.5 kbar (Webster and Mandeville, 2007; Audétat *et al.*, 2008), or alternatively, by vapor condensation (Audétat *et al.*, 2008; Giggenbach *et al.*, 2003). For example, a supersolvus fluid exsolved from a melt with a relatively high fluid/melt ratio of 2 x 10^{-2} but a relatively low salinity of NaCl = 2 wt.% would unmix upon decompression from 1.5 kbar to 1 kbar to form vapor with about NaCl = 1 wt.% and a liquid with NaCl = 11 wt.% with vapor/liquid mass proportions of 10. In this case, the effective brine/melt ratio with respect to original melt would be 2 x 10^{-3}. In the following calculations we use a range of brine/melt ratios of F = 2 x 10^{-3} to 5 x 10^{-3}, which we consider to be a realistic estimate for generating a brine with an average $NaCl_{equivalent}$ = 16.5 wt.% from crystallising intrusions (the concentration used in our assimilation model).

Using these estimates, Eq. S-8 yields magmatic brine production rates of 90-226 x 10^6 kg/yr from silicic intrusions in Iceland. Thus, the supply of brines from crystallizing intrusions is likely to exceed the amount of brine assimilation required to explain the observed δ^{37}Cl signatures in Icelandic rhyolites by a factor of 3 to 8.

Supplementary Tables

Table S-1 Sample information.

Sample	Volcanic system	Location/eruption	Rock type	Class	Setting	Type
ASD1L	Askja	1875 eruption	Rhyolite	Silicic	Rift	Tephra
ASD14L	Askja	1875 eruption	Rhyolite	Silicic	Rift	Tephra
A-THO[a]	Krafla	Hrafntinnuhryggur	Rhyolite	Silicic	Rift	Obsidian
I-DAC	Krafla	Hraunbunga	Dacite	Intermediate	Rift	Lava
KER-3	Kerlingarfjöll	Ögmundur	Rhyolite	Silicic	Rift	Obsidian
H-6	Hágöngur	Hágöngur	Rhyolite	Silicic	Rift	Obsidian
SNS-32/D28a	Snæfellsjökull	Mælifell	Rhyolite	Silicic	Off-rift	Obsidian
SNS-14/10444	Snæfellsjökull	Háahraun	Dacite	Intermediate	Off-rift	Lava
HNAUS-1	Snæfellsjökull	Hnausagil	Basanite	Basalt	Off-rift	Subglacial
SAL-74[a]	Öræfajökull	Kvísker	Rhyolite	Silicic	Off-rift	Obsidian
SAL-76	Öræfajökull	Kálfafellsdalur	Trachybasalt	Basalt	Off-rift	Lava
A-ALK[a]	Torfajökull	Hrafntinnusker	Alkali rhyolite	Silicic	Propag. rift	Obsidian
H3a	Hekla	H3	Dacite	Silicic	Propag. rift	Tephra
H4	Hekla	H4	Rhyolite	Silicic	Propag. rift	Tephra
H5	Hekla	H5	Rhyolite	Silicic	Propag. rift	Tephra
I-ICE	Hekla	Hekla 1970	Icelandite	Intermediate	Propag. rift	Lava
B-ALK	Katla	Eldgjá	Fe-Ti Basalt	Basalt	Propag. rift	Lava

[a]Halldórsson *et al.* (2016)

Table S-2 Sample data.

Sample	$\delta^{37}Cl$ ‰	$\delta^{18}O$ ‰	SiO_2 wt.%	TiO_2 wt.%	Al_2O_3 wt.%	FeO_{tot} wt.%	MnO wt.%	MgO wt.%	CaO wt.%	Na_2O wt.%	K_2O wt.%	P_2O_5 wt.%	Total wt.%	n (EPMA)	H_2O wt.%	± 1σ (n=6)	CO_2 ppm
ASD1L[b]	-0.6	-0.50	71.62	0.85	12.83	4.32	0.11	0.99	2.96	3.70	2.26	0.20			0.51		
ASD14L[b]	-0.9	0.70	71.35	0.87	12.85	4.30	0.10	0.91	3.11	3.80	2.28	0.25			0.14		
duplicate	-0.3																
A-THO[a]	-1.1	2.82	75.80	0.23	12.19	3.20	0.09	0.09	1.68	4.28	2.68	0.02	100.36	6	0.08	0.01	b.d.
I-DAC[c]	-0.1	4.20	64.68	0.88	15.26	6.02	0.12	1.46	4.83	4.12	1.37	0.21			0.45		
duplicate	-0.4																
KER-3	-1.2	4.40	73.95	0.18	13.13	2.54	0.07	0.06	0.92	4.89	3.71	0.02	99.60	6	0.13	0.004	b.d.
H-6	-0.7	4.74	77.74	0.15	11.57	2.17	0.05	0.00	0.92	4.64	2.66	0.02	99.96	6	0.10	0.02	b.d.
SNS-32/D28a	-0.6	5.37	71.09	0.16	14.06	2.58	0.14	0.05	0.45	5.45	5.21	0.01	99.60	6	0.08	0.02	b.d.
duplicate	-1.1	5.67															
SNS-14/10444[d]	-0.5	5.3	62.45	0.90	16.15	6.96	0.18	0.70	3.28	4.75	3.35	0.20			0.18		
duplicate	-0.7																
HNAUS-1	-0.3	5.05	44.43	4.23	12.22	14.07	0.30	5.20	10.47	3.30	1.50	0.84			0.12		10
SAL-74[a]	0.9	6.10	70.44	0.19	14.10	2.93	0.08	0.10	1.14	5.30	3.74	0.01			0.84		
SAL-76	1.2	4.35	49.93	2.56	16.36	11.45	0.22	4.15	7.00	4.33	1.58	0.84			0.48		
duplicate	1.4																
A-ALK[a]	-1.6	4.08	73.72	0.20	12.41	3.08	0.07	0.05	0.39	5.35	4.42	0.02	99.89	6	0.08	0.01	b.d.
H3a[b]	-1.9	5.76	67.42	0.39	14.57	5.07	0.16	0.30	2.95	4.84	2.17	0.07			1.28		
H4[b]	-1.4	5.70	71.86	0.18	13.02	2.33	0.09	0.07	1.55	4.77	2.78	0.00			2.53		
H5[b]	-1.7	5.57	71.03	0.47	13.97	4.14	0.12	0.42	2.57	4.38	2.64	0.12					
I-ICE[d]	-0.4	4.8	54.55	2.02	14.50	11.69	0.27	2.95	6.96	3.95	1.28	1.02			0.29		
B-ALK[d]	0.1	4.3	48.25	4.22	12.38	14.52	0.22	5.35	10.00	2.97	0.77	0.56			0.25		

Table S-2 (Continued)

Sample	F	Cl	S	Reference for major and volatile element concentrations
ASD1L[b]	466	513		this study
ASD14L[b]	382	435		this study
duplicate				
A-THO[a]		634	41	this study
I-DAC[a]	350	130		Óskarsson *et al.* (1982)
duplicate				
KER-3		1298	24	this study
H-6		342	26	this study
SNS-32/D28a		3988	28	this study
duplicate				
SNS-14/10444[d]	1260	310		Óskarsson *et al.* (1982)
duplicate				
HNAUS-1	1101	470	52	this study
SAL-74[a]	1080	840		Óskarsson *et al.* (1982)
SAL-76	752	130		Óskarsson *et al.* (1982)
duplicate				
A-ALK[a]		2024	23	this study
H3a[b]	1084	390		Sverrisdóttir (2007)
H4[b]	1424	624		Sverrisdóttir (2007)
H5[b]		282[c]		Sverrisdóttir (2007)
I-ICE[d]	1230	225		Óskarsson *et al.* (1982)
B-ALK[d]	443	140		Óskarsson *et al.* (1982)

[a]$\delta^{18}O$ and $\delta^{37}Cl$ data from Halldórsson *et al.* (2016) except for the $\delta^{18}O$ value of SAL-74, which is from Condomines *et al.* (1983)

[b]$\delta^{18}O$ values measured on whole rock by Geochron Laboratories, Inc., Cambridge, Mass.

[c]$\delta^{18}O$ value from Jónasson (2005)

[d]$\delta^{18}O$ value from Óskarsson *et al.* (1982)

[e]Cl concentration was determined based on the IRMS peak area and calibrated with internal standards of known Cl concentration.

Supplementary Data Table

A compilation of published melt inclusion H_2O and Cl data from Iceland (n = 725) is presented in Table S-3, which can be downloaded as a separate Excel file at http://www.geochemicalperspectivesletters.org/article2101. The data was compiled from Moune *et al*. (2007), Sharma *et al*. (2008), Brounce *et al*. (2012), Moune *et al*. (2012), Portnyagin *et al*. (2012), Owen *et al*. (2013), Schattel *et al*. (2014), Lucic *et al*. (2016), Schipper *et al.* (2016) and Bali *et al.* (2018).

Supplementary Information References

Albarède, F. (1995) *Introduction to geochemical modeling*. Cambridge University Press, New York.

Audétat, A., Pettke, T. (2003) The magmatic-hydrothermal evolution of two barren granites: A melt and fluid inclusion study of the Rito del Medio and Canada Pinabete plutons in northern New Mexico (USA). *Geochimica et Cosmochimica Acta* 67, 97–121.

Baker, D.R., Balcone-Boissard, H. (2009) Halogen diffusion in magmatic systems: Our current state of knowledge. *Chemical Geology* 263, 82–88.

Barnes, J.D., Straub, S.M. (2010) Chorine stable isotope variations in Izu Bonin tephra: implications for serpentinite subduction. *Chemical Geology* 272, 62–74.

Barnes, J.D., Cisneros, M. (2012) Mineralogical control on the chlorine isotope composition of altered oceanic crust. *Chemical Geology* 326, 51–60.

Bali, E., Hartley, M.E., Halldórsson, S.A., Gudfinnsson, G.H., Jakobsson, S. (2018) Melt inclusion constraints on volatile systematics and degassing history of the 2014–2015 Holuhraun eruption, Iceland. *Contributions to Mineralogy and Petrology* 173, 9.

Bouvier, A.S., Manzini, M., Rose-Koga, E.F., Nichols, A.R., Baumgartner, L.P. (2019) Tracing of Cl input into the sub-arc mantle through the combined analysis of B, O and Cl isotopes in melt inclusions. *Earth and Planetary Science Letters 507*, 30–39.

Brounce, M., Feineman, M., LaFemina, P., Gurenko, A. (2012) Insights into crustal assimilation by Icelandic basalts from boron isotopes in melt inclusions from the 1783–1784 Lakagígar eruption. *Geochimica et Cosmochimica Acta* 94, 164–180.

Chen, H., Savage, P.S., Teng, F.Z., Helz, R.T., Moynier, F. (2013) Zinc isotope fractionation during magmatic differentiation and the isotopic composition of the bulk Earth. *Earth and Planetary Science Letters* 369, 34–42.

Chekol, T.A., Kobayashi, K., Yokoyama, T., Sakaguchi, C., Nakamura, E. (2011) Timescales of magma differentiation from basalt to andesite beneath Hekla volcano, Iceland: constraints from U-series disequilibria in lavas from the last quarter-millennium flows. *Geochimica et Cosmochimica Acta* 75, 256–283.

Chiaradia, M., Barnes, J.D., Cadet-Voisin, S. (2014) Chlorine stable isotope variations across the Quaternary volcanic arc of Ecuador. *Earth and Planetary Science Letters* 396, 22–33.

Condomines, M., Grönvold, K., Hooker, P.J., Muehlenbachs, K., O'Nions, R.K., Oskarsson, N., Oxburgh, E.R. (1983) Helium, oxygen, strontium and neodymium isotopic relationships in Icelandic volcanics. *Earth and Planetary Science Letters* 66, 125–136.

Deng, Z. Chaussidon, M., Savage, P., Robert, F., Pik, R., Moynier, F. (2019) Titanium isotopes as a tracer for the plume or island arc affinity of felsic rocks. *Proceedings of the National Academy of Sciences USA* 116, 1132–1135.

Giggenbach, W.F., Shinohara, H., Kusakabe, M., Ohba, T. (2003) Formation of acid volcanic brines through interaction of magmatic gases, seawater, and rock within the White Island volcanic-hydrothermal system, New Zealand. *The Society of Economic Geologists Special Pubication* 10, 19-40.

Gualda, G.A., Ghiorso, M.S., Lemons, R.V., Carley, T.L. (2012) Rhyolite-MELTS: a modified calibration of MELTS optimized for silica-rich, fluid-bearing magmatic systems. *Journal of Petrology* 53, 875–890.

Gunnarsson, B., Marsh, B.D., Taylor Jr., H.P. (1998) Generation of Icelandic rhyolites: silicic lavas from the Torfajökull central volcano. *Journal of Volcanology and Geothermal Research* 83, 1–45.

Gurenko, A.A., Bindeman, I.N., Sigurdsson, I.A. (2015) To the origin of Icelandic rhyolites: insights from partially melted leucocratic xenoliths. *Contributions to Mineralogy and Petrology* 169, 49.

Ghiorso, M.S., Gualda, G.A. (2015) An H_2O–CO_2 mixed fluid saturation model compatible with rhyolite-MELTS. *Contributions to Mineralogy and Petrology* 169, 53.

Halldórsson, S.A., Óskarsson, N., Grönvold, K., Sigurdsson, G., Sverrisdóttir, G., Steinthórsson, S. (2008) Isotopic-heterogeneity of the Thjorsa lava—implications for mantle sources and crustal processes within the Eastern Rift Zone, Iceland. *Chemical Geology* 255, 305–316.

Hauri, E., Wang, J., Dixon, J.E., King, P.L., Mandeville, C., Newman, S. (2002) SIMS analysis of volatiles in silicate glasses: 1. Calibration, matrix effects and comparisons with FTIR. *Chemical Geology* 183, 99–114.

Inglis, E.C., Moynier, F., Creech, J., Deng, Z., Day, J.M.D., Teng, F.Z., Bizzarro, M., Jackson, M., Savage, P. (2019) Isotopic fractionation of zirconium during magmatic differentiation and the stable isotope composition of the silicate Earth. *Geochimica et Cosmochimica Acta* 250, 311–323.

Jónasson, K. (2005) Magmatic evolution of the Heiðarsporður ridge, NE-Iceland. *Journal of Volcanology and Geothermal Research* 147, 109–124.

Kendrick, M. A., Hémond, C., Kamenetsky, V. S., Danyushevsky, L., Devey, C. W., Rodemann, T., Jackson, M.G., Perfit, M. R. (2017) Seawater cycled throughout Earth's mantle in partially serpentinized lithosphere. *Nature Geoscience* 10, 222–228.

Kuritani, T., Yokoyama, T., Kitagawa, H., Kobayashi, K., Nakamura, E. (2011) Geochemical evolution of historical lavas from Askja Volcano, Iceland: implications for mechanisms and timescales of magmatic differentiation. *Geochimica et Cosmochimica Acta* 75, 570–587.

Lucic, G., Berg, A.S., Stix, J. (2016) Water-rich and volatile-undersaturated magmas at Hekla volcano, Iceland. *Geochemistry, Geophysics, Geosystems* 17, 3111–3130.

Manzini, M., Bouvier, A., Barnes, J.D., Bonifacie, M., Rose-Koga, E.F., Ulmer, P., Métrich, N., Bardoux, G., Williams, J., Layne, G.D., Straub, S., Baumgartner, L.P., John, T. (2017) SIMS chlorine isotope analyses in melt inclusions from arc settings. *Chemical Geology* 449, 112–122.

Martin, E., Sigmarsson, O. (2007) Crustal thermal state and origin of silicic magma in Iceland: the case of Torfajökull, Ljósufjöll and Snæfellsjökull volcanoes. *Contributions to Mineralogy and Petrology* 153, 593-605.

Martin, E., Sigmarsson, O. (2010) Thirteen million years of silicic magma production in Iceland: Links between petrogenesis and tectonic settings. *Lithos* 116, 129–144.

McIntosh, I.M., Nichols, A.R., Tani, K., Llewellin, E.W. (2017) Accounting for the species-dependence of the 3500 cm^{-1} $H2O_t$ infrared molar absorptivity coefficient: Implications for hydrated volcanic glasses. *American Mineralogist* 102, 1677-1689.

Metrich, N., Rutherford, M.J. (1992) Experimental study of chlorine behavior in hydrous silicic melts. *Geochimica et Cosmochimica Acta* 56, 607–616.

Momme, P., Óskarsson, N. & Keays, R.R. (2003) Platinum-group elements in the Icelandic rift system: melting processes and mantle sources beneath Iceland. *Chemical Geology* 196, 209–234.

Moune, S., Sigmarsson, O., Thordarson, T., Gauthier, P.J. (2007) Recent volatile evolution in the magmatic system of Hekla volcano, Iceland. *Earth and Planetary Science Letters* 255, 373–389.

Moune, S., Sigmarsson, O., Schiano, P., Thordarson, T., Keiding, J.K. (2012) Melt inclusion constraints on the magma source of Eyjafjallajökull 2010 flank eruption. *Journal of Geophysical Research* 117, B00C07.

Müller, A, Haak, V. (2004) 3-D modeling of the deep electrical conductivity of Merapi volcano (Central Java): integrating magnetotellurics, induction vectors and the effects of steep topography. *Journal of Volcanology and Geothermal Research* 138, 205–222.

Nichols, A.R. L., Carroll, M.R., Höskuldsson, A. (2002) Is the Iceland hot spot also wet? Evidence from the water contents of undegassed submarine and subglacial pillow basalts. *Earth and Planetary Science Letters* 202, 77–87.

Nicholson, H., Condomines, M., Fitton, J.G., Fallick, A.E., Grönvold, K., Rogers, G. (1991) Geochemical and isotopic evidence for crustal assimilation beneath Krafla, Iceland. *Journal of Petrology* 32, 1005–1020.

Óskarsson, N., Sigvaldason, G.E., Steinthorsson, S.A (1982) dynamic model of rift zone petrogenesis and the regional petrology of Iceland. *Journal of Petrology* 23, 28–74.

Owen, J., Tuffen, H., McGarvie, D.W. (2013) Explosive subglacial rhyolitic eruptions in Iceland are fuelled by high magmatic H_2O and closed-system degassing. *Geology* 41, 251–254.

Portnyagin, M., Hoernle, K., Storm., S., Mironov, N., van den Bogaard, C., Botcharnikov, R. (2012) H_2O-rich melt inclusions in fayalitic olivine from Hekla volcano: Implications for phase relationships in silicic systems and driving forces of explosive volcanism on Iceland. *Earth and Planetary Science Letters* 357, 337–346.

Prestvik, T., Goldberg, S., Karlsson, H., Grönvold, K. (2001) Anomalous strontium and lead isotope signatures in the off-rift Öræfajökull central volcano in south-east Iceland: evidence for enriched endmember (s) of the Iceland mantle plume? *Earth and Planetary Science Letters* 190, 211–220.

Prytulak, J., Sossi, P.A., Halliday, A.N., Plank, T., Savage, P.S., Woodhead, J.D. (2016) Stable vanadium isotopes as a redox proxy in magmatic systems? *Geochemical Perspectives Letters* 3, 75–84.

Prytulak, J., Brett, A., Webb, A., Plank, T., Rehkämper, M., Savage, P.S., Woodhead, J. (2017) Thallium elemental behavior and stable isotope fractionation during magmatic processes. *Chemical Geology* 448, 71–83.

Ransom, B., Spivack, A.J., Kastner, M. (1995) Stable Cl isotopes in subduction-zone pore waters: Implications for fluid-rock reactions and the cycling of chlorine. *Geology* 23**,** 715–718.

Reimink, J. R., Chacko, T., Stern, R.A., Heaman, L.M. (2014) Earth's earliest evolved crust generated in an Iceland-like setting. *Nature Geoscience* 7, 529.

Savage, P.S., Georg, R.B., Williams, H.M., Burton, K.W., Halliday, A.N. (2011) Silicon isotope fractionation during magmatic differentiation. *Geochimica et Cosmochimica Acta* 75, 6124–6139.

Schattel, N., Portnyagin, M., Golowin, R., Hoernle, K., Bindeman, I. (2014) Contrasting conditions of rift and off-rift silicic magma origin on Iceland. *Geophysical Research Letters* 41, 5813–5820.

Schipper, C.I., Le Voyer, M., Moussallam, Y., White, J.D.L., Thordarson, T., Kimura, J., Chang, Q. (2016) Degassing and magma mixing during the eruption of Surtsey Volcano (Iceland, 1963–1967): the signatures of a dynamic and discrete rift propagation event. *Bulletin of Volcanology* 78, 33.

Schuessler, J.A., Schoenberg, R., Sigmarsson, O. (2009) Iron and lithium isotope systematics of the Hekla volcano, Iceland—

evidence for Fe isotope fractionation during magma differentiation. *Chemical Geology* 258, 78–91.

Sharma, K., Self, S., Blake, S., Thordarson, T., Larsen, G. (2008) The AD 1362 Öræfajökull eruption, SE Iceland: Physical volcanology and volatile release. *Journal of Volcanology and Geothermal Research* 178, 719–739.

Sharp, Z.D. (1990) A laser-based microanalytical method for the in situ determination of oxygen isotope ratios of silicates and oxides. *Geochimica et Cosmochimica Acta* 54, 1353–1357.

Shinohara, H. (2009) A missing link between volcanic degassing and experimental studies on chloride partitioning. *Chemical Geology* 263, 51–59.

Sigmarsson, O., Condomines, M., Fourcade, S. (1992) A detailed Th, Sr and O isotope study of Hekla: differentiation processes in an Icelandic volcano. *Contributions to Mineralogy and Petrology* 112, 20–34.

Sigvaldason, G.E., Óskarsson, N. (1976) Chlorine in basalts from Iceland. *Geochimica et Cosmochimica Acta* 40, 777–789.

Sverrisdottir, G. (2007) Hybrid magma generation preceding Plinian silicic eruptions at Hekla, Iceland: evidence from mineralogy and chemistry of two zoned deposits. *Geological Magazine* 14, 643–659.

Thordarson, T., Larsen, G. (2007) Volcanism in Iceland in historical time: Volcano types, eruption styles and eruptive history. *Journal of Geodynamics 43*, 118–152.

Tuller-Ross, B., Savage, P.S., Chen, H., Wang, K. (2019) Potassium isotope fractionation during magmatic differentiation of basalt to rhyolite. *Chemical Geology* 525, 37–45.

Valley, J.W., Kitchen, N., Kohn, M.J., Niendorf, C.R., Spicuzza, M.J. (1995) UWG-2, a garnet standard for oxygen isotope ratios: strategies for high precision and accuracy with laser heating. *Geochimica et Cosmochimica Acta* 59, 5223–5231.

Webster, J.D. (1997) Chloride solubility in felsic melts and the role of chloride in magmatic degassing. *Journal of Petrology* 38, 1793–1807.

Webster, J.D. Vetere, F., Botcharnikov, R.E., Goldoff, B., McBirney, A., Doherty, A.L. (2015) Experimental and modeled chlorine solubilities in aluminosilicate melts at 1 to 7000 bars and 700 to 1250 C: Applications to magmas of Augustine Volcano, Alaska. *American Mineralogist* 100, 522–535.

White, S.M., Crisp, J.A., Spera, F.J. (2006) Long-term volumetric eruption rates and magma budgets. *Geochemistry, Geophysics, Geosystems* 7.

Willbold, M., Hegner, E., Stracke, A., Rocholl, A. (2009) Continental geochemical signatures in dacites from Iceland and implications for models of early Archaean crust formation. *Earth and Planetary Science Letters* 279, 44–52.

Yang, J., Siebert, C., Barling, J., Savage, P., Liang, Y., Halliday, A.N. (2015) Absence of molybdenum isotope fractionation during magmatic differentiation at Hekla volcano, Iceland. *Geochimica et Cosmochimica Acta* 162, 126–136.

Appendix B: Supplementary information for Paper II

1. Analytical details

1.1 Inductively coupled plasma mass spectrometry (ICP-MS)

Trace element concentrations were determined from dissolved glass powders by inductively coupled plasma mass spectrometry (ICP-MS) at the Scripps Institution of Oceanography using a Thermo-Fischer Element-2 ICP-MS following the method described in Halldórsson et al. (2016a). Copper concentrations were determined by laser ablation ICP-MS (LA-ICP-MS) at the Research School of Earth Sciences, Australian National University, following the methods of Jenner and O'Neill (2012), for all samples with the exception of the KVK-2xx series. Trace elements (including Cu) for the KVK-2xx samples were analyzed at the Geological Survey of Finland, Espoo, by LA-ICP-MS using a Nu AttoM instrument. The analytical protocol used was similar to the one outlined in Moilanen et al. (2020), except BCR-2G was used as a calibrating standard. Reported values are based on the average of 6-11 point analyses. Trace element data for the KVK-2xx glasses were reduced using the SILLS software package (Guillong et al. 2008).

1.2 Accuracy and precision of S isotope measurements

We estimate the long-term reproducibility of our $\delta^{34}S$, $\Delta^{33}S$ and $\Delta^{36}S$ measurements via replicate measurements of IAEA-S-1 Ag_2S standard and an in-house Ag_2S standard (Ono-Ag_2S, Sigma Aldrich), fluorinated and measured alongside our samples during 7 measurement sessions that span four years (2016-2020). The long-term average $\delta^{34}S$, $\Delta^{33}S$ and $\Delta^{36}S$ values of IAEA-S-1 relative to our laboratory reference gas (SG1) were –1.19±0.17 ‰, 0.100±0.004 ‰ and –0.669±0.028 ‰, respectively (1σ, n = 10). The $\delta^{34}S_{S\text{-}1/SG1}$ value of IAEA-S-1 is used to convert measured isotope ratios to V-CDT notation using the certified value for IAEA-S-1 of $\delta^{34}S_{S\text{-}1/V\text{-}CDT}$ = -0.3 ‰ (Coplen and Krouse 1998). The long-term average values for $\delta^{34}S$, $\Delta^{33}S$ and $\Delta^{36}S$ of our lab Ag_2S standard relative to SG1 are 0.97±0.12 ‰, 0.020±0.004 ‰ and -0.029±0.086 ‰, respectively (1σ, n = 18; Fig. S1). The reproducibilities of these standards are similar, reflecting the uncertainty associated with fluorination and mass spectrometry. Given the higher number of analyses, we conservatively adopt the standard deviation calculated from replicate analyses of Ono-Ag_2S as the estimate of our long-term reproducibility for $\delta^{34}S$, $\Delta^{33}S$ and $\Delta^{36}S$.

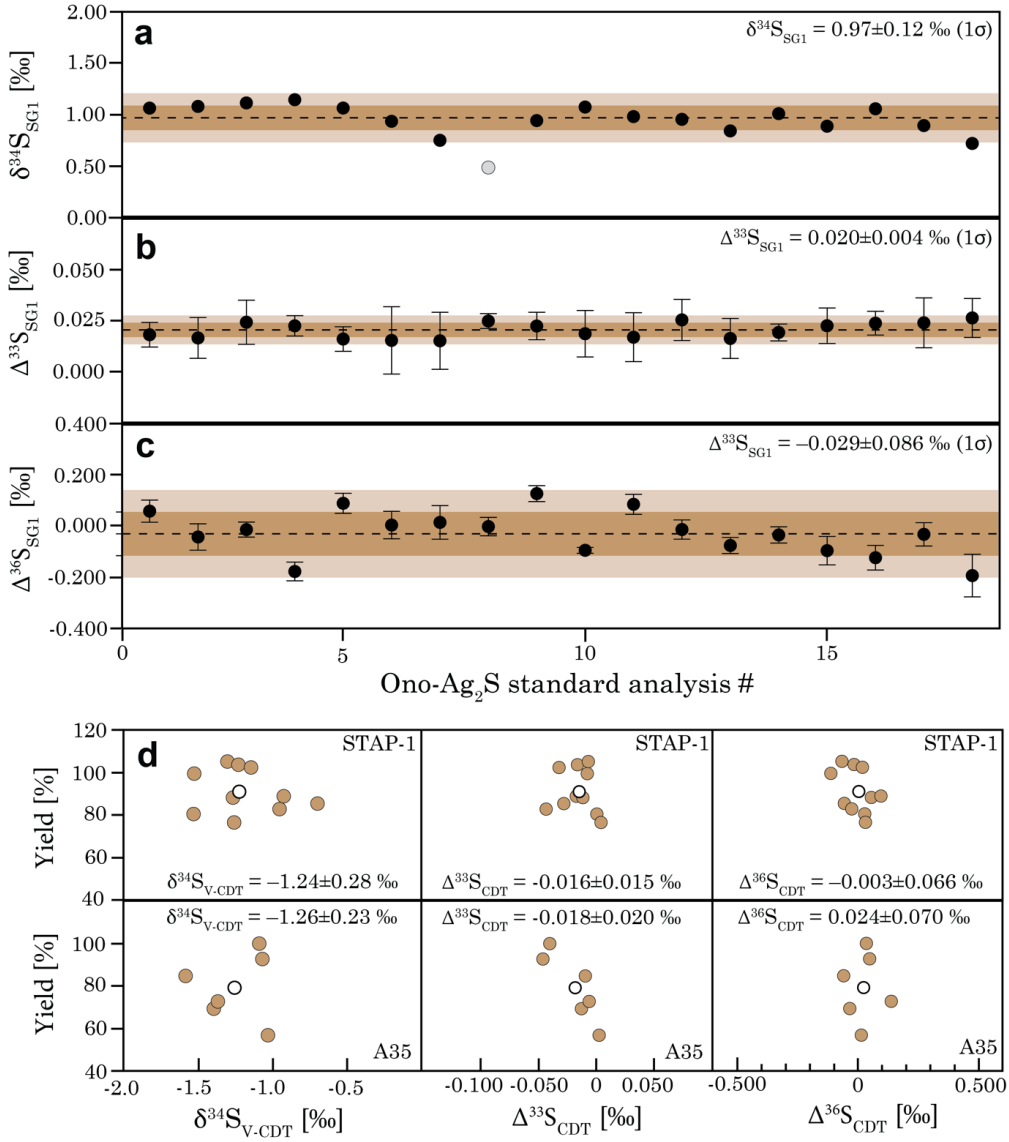

Figure S1 (a)-(c) Evaluation of analytical uncertainty associated with S isotope measurements. Data is shown for the Ono-Ag_2S standard (n = 18), which was analyzed during all 7 sessions. Shaded show respective 1 and 2σ of the average. Error bars indicate 2 standard errors based on 6 measurement cycles. For $\delta^{34}S$, the instrumental error is smaller than the size of the symbols. One measurement (grey circle) is excluded from the $\delta^{34}S$ average, as it falls outside 3σ uncertainty. (d) Replicate standard glass analyses for STAP-1 and A35 show that measured S isotope compositions do not correlate with yields. Data is reported in Tables S1 and S2.

To estimate errors related to S extraction and glass heterogeneity, two Icelandic subglacial glasses STAP-1 (n = 11) and A35 (n = 6) were repeatedly extracted and measured (Fig. S1d; Table S2). Compared with the Ag_2S standards, replicate analyses of these sample glasses returned larger standard deviations (Fig. S1d). The source of the larger 1σ uncertainty suggests either minor intra-sample S isotopic heterogeneity, or an additional uncertainty related to the extraction process. Individual extractions of the glasses produced variable yields (57–105 %). Low yields may have resulted from incomplete extractions, lower-than-expected S^{2-} concentration in the dissolved sample (because of high crystal content or high $S^{6+}/\Sigma S$), or weighing error. Experimental processing of known quantities of sulfide limits mechanical Ag_2S losses to less than 8%. While incomplete extractions could yield artificially high measured $\delta^{34}S$ values because of the positive fractionation factor associated with the conversion of dissolved S^{2-} to H_2S gas at 300 °C ($1000 \ln a_{H_2S-S^{2-}} \approx 3$ ‰; Supplementary Information section 5), the lack of correlation between yields and isotopic composition (Fig. S1) renders this unlikely. Consequently, we consider the variable yields to reflect variable glass/crystal content of the extracted material and thus we conclude that the larger isotopic variability associated with measurements of STAP-1 and A35 likely reflects isotopic heterogeneity present in the subglacial glasses.

1.3 Definition of the $\Delta^{33}S$ and $\Delta^{36}S$ scales relative to CDT

Given the small $\Delta^{33}S$ variability in basaltic glasses, a well-defined reference scale is paramount to make comparisons between $\Delta^{33}S$ datasets produced at different laboratories. While IAEA-S-1 is the certified reference material that anchors $\delta^{34}S$ to the V-CDT-scale (Coplen and Krouse, 1998), as yet, it lacks certified values for $\delta^{33}S$ and $\delta^{36}S$. Consequently, $\Delta^{33}S$ and $\Delta^{36}S$ values are either reported relative to a laboratory reference gas (e.g. Labidi et al. 2012), which conceivably has different S isotopic compositions at different labs, or are anchored to the CDT-scale via coupled measurements of IAEA-S-1 and CDT (Ono et al. 2006, Labidi et al. 2016, Antonelli et al. 2014).

We compiled coupled IAEA-S-1 and CDT measurements that have been used to anchor the former to the $\Delta^{33}S_{CDT}$ scale in studies conducted at the University of Maryland (Antonelli et al. 2014, Labidi et al. 2017), the Geophysical Laboratory, Carnegie Institute of Washington (Ono et al. 2006, Ono et al. 2007) and the Laboratoire de Géochimie des Isotopes Stables, Institut de Physique du Globe de Paris (Labidi et al. 2012, Labidi et al., 2014, Defouilloy et al. 2016) and calculated the associated standard deviations (Table S-3, Fig. S3). In these studies, the definitions of the $\Delta^{33}S_{CDT}$ scale vary from IAEA-S-1 values of $\Delta^{33}S_{CDT} = 0.093 \pm 0.013$ ‰ (GL: Ono et al. 2007; based on 3 laser fluorinations of CDT) to $\Delta^{33}S_{CDT} = 0.118 \pm 0.006$ ‰ (UMD: Labidi et al. 2017). It is not known with certainty whether the slight differences reflect analytical differences between laboratories or heterogeneities within CDT itself.

The average IAEA-S-1 definitions based on 8 studies are $\Delta^{33}S_{CDT} = 0.109 \pm 0.006$ ‰ and $\Delta^{36}S_{CDT} = -0.730 \pm 0.153$ ‰ (both errors reflect 95% confidence intervals; Fig. S3). As CDT has not been measured at the MIT, we use these average definitions of $\Delta^{33}S_{CDT}$ and $\Delta^{36}S_{CDT}$ to anchor our data to the CDT scale, allowing direct comparison between $\Delta^{33}S$ data reported herein and those published from MORBs and OIBs (Figs. 4-8)

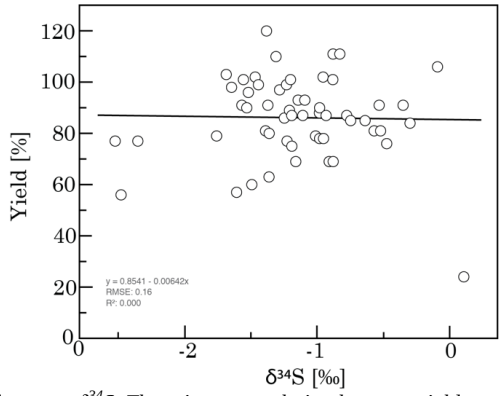

Figure S2 Extraction yields versus $\delta^{34}S$. There is no correlation between yields and $\delta^{34}S$. This indicates that the $\delta^{34}S$ data is not biased by incomplete extractions.

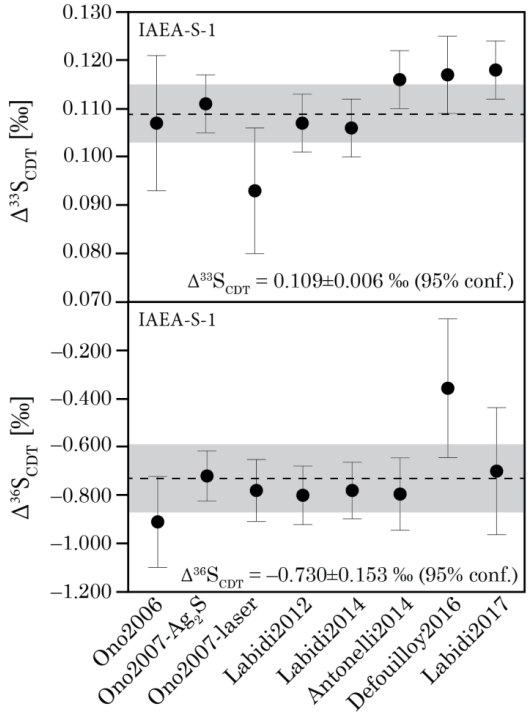

Figure S3 Published $\Delta^{3x}S_{CDT}$ values of the IAEA-S-1 Ag_2S standard material. The $\Delta^{33}S_{CDT}$ value of IAEA-S-1 used to define the CDT scale for $\Delta^{33}S$. All $\Delta^{33}S_{CDT}$ values are based on measurements of IAEA-S-1 and CDT extracted as Ag_2S, except for the lowest $\Delta^{33}S_{CDT}$ = 0.093±0.013 estimate, which is based on three in situ KBr laser fluorination analyses of CDT (Ono et al. 2007). All estimates overlap within 2σ. Error bars represent the propagated 1σ error from the IAEA-S-1 and CDT measurements reported in each study. The grey field reflects the 95% confidence interval surrounding the average value of 8 reported IAEA-S-1 versus CDT definitions (Ono et al. (2006, 2007; Labidi et al. 2012, 2014, 2017; Antonelli et al. 2014; Defouilloy et al. 2016).

2. Evaluation of magmatic S degassing

Sulfur degasses from melts dominantly as SO_2 and H_2S, with $SO_2/H_2S(g)$ determined primarily by the degassing pressure and oxygen fugacity of the melt (Gaillard et al. 2011, Burgisser et al. 2015). The SO_2/H_2S ratio of the degassing magmatic gas is expected to be > 10 in ascending Icelandic basalts (Fig. S5).

According to experimental data on S solubility, degassing of S in H_2O-poor tholeiitic basalts starts already at c. 150 MPa (~6 km crustal depth; Wallace and Edmonds 2011). However, relatively little degassing takes place above pressures of ~10 MPa (Wallace and Edmonds 2011). Therefore, high sulfur contents are preserved in subglacial pillow rim glasses if emplacement takes place under sufficient pressure, and if quenching occurs before microlite crystallization (Moore and Calk 1991). The observation that matrix glasses in subaerial lavas that were emplaced at 1 atm have relatively high sulfur contents between 300-1600 ppm (0-80% degassing relative to the initial S content; Fig 2a) implies that decompression degassing in rapidly quenched glasses is kinetically limited. Therefore, degassing estimates based on experimental S solubility limits probably overestimate the degree of degassing in subglacial glasses. In comparison, microcrystalline subaerial lavas (B-ALK, I-ICE) and the obsidian glass A-THO have low bulk S concentrations (< 100 ppm), indicating degassing of > 90 % of their primary S content.

We identify degassing in the subglacial glasses using the S vs. MgO trends (Fig. 2a). Compiled S data from Icelandic melt inclusions (Ranta et al. 2021) define a trend of rising S concentrations in Phase 1 followed by a decreasing trend in Phase 2 (Fig. 2a). Most subglacial glasses plot subparallel to these trends (Fig. 2a), which implies that they haven't experienced significant S degassing. This is expected for basalts that erupt below an ice cover thicker than ~200-350 m, corresponding to a threshold pressure of ~2-3 MPa above which extensive S degassing is inhibited (Moore and Calk 1991). Fourteen samples that clearly deviate from the S vs. MgO trends toward lower S concentrations are interpreted to be partly degassed with respect to S (A1, A3, A6, A32, THOR-1, STORID-1, SELJA-1, SAL-601, BOTN-1, HNAUS-1, OLAF-1, NAL-460, KVK-202, KVK-205). These samples were likely erupted below a thinner ice cover.

3. Model I: Quantification of sulfide melt formation

The weight fraction X_{sulf} of the forming sulfide melt can be quantified independently using [S] or [Cu] (or other chalcophile elements) using the relationship

$$D_i^{min-liq} = X_{sulf} D_i^{sulf-liq} + (1 - X_{sulf}) D_i^{sil-liq} \qquad \text{Eq. 5}$$

where $D_i^{sulf-liq}$ and $D_i^{sil-liq}$ are the distribution coefficients of i = S or Cu between silicate minerals and melt, and sulfides and melt, respectively (c.f. Labidi et al. 2014). $D_i^{min-liq}$,

the empirical bulk distribution coefficient, is calculated from concentrations of i at the beginning ($C_{i,0}$) and end ($C_{i,1}$) of a phase as

$$D_i^{min-liq} = \frac{\log(C_{i,1}/C_{i,0})}{\log F} + 1 \quad \text{Eq. 6}$$

where F is the fraction of remaining melt/crystallized minerals. Assuming fractional distillation, the Rayleigh fractionation equation can be used to estimate F:

$$F = \left(\frac{C_{j,1}}{C_{j,0}}\right)^{\frac{1}{D_j^{min-liq}-1}} \quad \text{Eq. 7}$$

where $C_{j,1}$ and $C_{j,0}$ are the initial and final concentrations of an incompatible element and $D_j^{min-liq}$ is the bulk distribution coefficient of j. We use j = Th to calculate F. Thorium is incompatible in both silicate minerals and sulfide melts as well as in Fe-Ti oxides, with a bulk distribution coefficient of $D_{Th}^{min-liq} = 0.007$ estimated for the Kverkfjöll suite (Kaikkonen 2017). Similar results for F within ±0.05 are derived using other incompatible elements such Ce ($D_{Ce}^{min-liq} = 0.07$) and Zr ($D_{Zr}^{min-liq} = 0.06$) (Kaikkonen 2017). X_{sulf} can be then calculated by solving Eq. 3.

A similar computation can be undertaken for concentration ratios of elements j and i, that change with fractional crystallization according to

$$\frac{C_{i,1}}{C_{j,1}} = \frac{C_{i,0}}{C_{j,0}} F^{\left(D_i^{min-liq} - D_j^{min-liq}\right)} \quad \text{Eq. 8}$$

If $D_i^{sil-liq} = D_j^{sil-liq}$ and $D_j^{sulf-liq} \approx 0$, Eq. 8 can be rewritten as

$$\frac{C_{i,1}}{C_{j,1}} = \frac{C_{i,0}}{C_{j,0}} F^{\left(D_i^{sulf-liq} - D_j^{sil-liq}\right)} \quad \text{Eq. 9}$$

Eq. 3 can then be used to determine X_{sulf} using element pairs such as Cu/Y (Labidi et al. 2015).

4. Bulk $\delta^{34}S$ value of Icelandic melts

Assuming isotopic equilibrium between dissolved sulfide and sulfate in undegassed melts and extrapolating the experimental results of Miyoshi et al. (1984) to 1250 °C using their Eq (3), we use a fractionation factor of

$$\Delta^{34}S_{sulfate-sulfide} = \delta^{34}S_{sulfate} - \delta^{34}S_{sulfide} = 7.4 \times 10^6/T^2 - 0.19 \qquad \text{Eq. 10}$$

where T is temperature in K. Eq. 10 gives $\Delta^{34}S_{sulfate-sulfide} \approx +3$ ‰ for T = 1250 °C. If all the sulfur in the melt is dissolved as S^{6+} and S^{2-}, we can state that

$$\delta^{34}S_{\Sigma S} = f_{sulfate} \times \delta^{34}S_{sulfate} + (1 - f_{sulfate}) \times \delta^{34}S_{sulfide} \qquad \text{Eq. 11}$$

where $f_{sulfate} = S^{6+}/\Sigma S$. Combining Eqs. 10 and 11, $\delta^{34}S_{\Sigma S}$ can be estimated using

$$\delta^{34}S_{\Sigma S} = f_{sulfate} \times \Delta^{34}S_{sulfate-sulfide} + \delta^{34}S_{sulfide} \qquad \text{Eq. 12}$$

if $f_{sulfate}$ is known. The size of the correction term $f_{sulfate} \times \Delta^{34}S_{sulfate-sulfide}$ varies with $S^{6+}/\Sigma S$ and T. Based on an approximate range of $S^{6+}/\Sigma S \approx 0.05$ to 0.4 (Fig. S6), we estimate that $\delta^{34}S_{\Sigma S}$ values of Icelandic melts could be between 0.15 and 1.2‰ more positive than the measured $\delta^{34}S_{S^{2-}}$ values (Table S2). However, it is unclear if equilibrium between sulfate and sulfide species is always attained. For example, $\Delta^{34}S_{sulfate-sulfide}$ in Icelandic rocks, where both $\delta^{34}S_{S^{2-}}$ and $\delta^{34}S_{S^{6+}}$ have been determined, varies between +0.4 to +6.3 ‰ (Torssander 1989). A deviation from equilibrium $\Delta^{34}S_{sulfate-sulfide}$ values toward more positive values measured in Samoan and Hawaiian basalts have been attributed to kinetic fractionation during shallow sulfur degassing, which favors partitioning of the $^{32}SO_2$ ions to the vapor phase (Sakai et al. 1982; Labidi et al. 2015) from the sulfate fraction of the melt. The implication is that SO_2 degassing takes place rapidly at shallow depths and does not impose fractionation on the measured $\delta^{34}S_{S^{2-}}$ values (Labidi et al. 2015). However, isotopic equilibrium between S species is more likely to be attained in undegassed melts during their considerably longer residence time in high-T magmatic reservoirs.

5. Model II: $\delta^{34}S$ fractionation during degassing

S isotope fractionation during degassing can be modelled by estimating a bulk $a_{gas-melt}$ fractionation constant, defined by

$$\varepsilon^{34}S_{gas-melt} = \delta^{34}S_{gas} - \delta^{34}S_{melt} \approx 1000 \ln a_{gas-melt} \qquad \text{Eq. 13}$$

Following Mandeville et al. (2009), we estimate $1000 \ln a_{gas-melt}$ by assuming isotopic equilibrium between the main S species in the gas (SO_2 and H_2S) and melt (S^{6+} and S^{2-}). Then,

$$1000 \ln a_{gas-melt} =$$
$$f_{SO_2} \times f_{S^{6+}} \times 1000 \ln a_{SO_2-S^{6+}} + f_{SO_2} \times (1 - f_{S^{6+}}) \times 1000 \ln a_{SO_2-S^{2-}} + (1 - f_{SO_2}) \times$$
$$f_{S^{6+}} \times 1000 \ln a_{H_2S-S^{6+}} + (1 - f_{SO_2})(1 - f_{S^{6+}}) 1000 \ln a_{H_2S-S^{2-}} \qquad \text{Eq. 14}$$

where $f_{SO_2} = SO_2/(SO_2 + H_2S)$ of the gas phase and $f_{S^{6+}} = S^{6+}/(S^{6+} + S^{2-})$ of the melt. Equilibrium fractionation factors for the pairs SO_2(g)-H_2S(g), H_2S(g)-S^{2-}(m), S^{6+}(m)-H_2S(g) and S^{6+}(m)-S^{2-}(m) have been determined experimentally as

$$1000 \ln a_{SO_2-H_2S} = -0.42 \times \frac{10^9}{T^3} + 4.367 \times \frac{10^6}{T^2} - 0.105 \times \frac{10^3}{T} - 0.41 \text{ (Taylor 1986)} \quad \text{Eq. 15}$$

$$1000 \ln a_{H_2S-S^{2-}} = 1.1 \times \frac{10^6}{T^2} - 0.19 \text{ (Taylor 1986)} \quad \text{Eq. 16}$$

$$1000 \ln a_{S^{6+}-S^{2-}} = 7.4 \times \frac{10^6}{T^2} - 0.19 \text{ (Miyoshi et al. 1984)} \quad \text{Eq. 17}$$

$$1000 \ln a_{S^{6+}-H_2S} = 6.5 \times \frac{10^6}{T^2} \text{ (Miyoshi et al. 1984)} \quad \text{Eq. 18}$$

The fractionation factors for the pairs SO_2(g)-S^{6+}(m) and SO_2(g)-S^{2-}(m) can be expressed as

$$1000 \ln a_{SO_2-S^{6+}} = 1000 \ln a_{SO_2-H_2S} - 1000 \ln a_{S^{6+}-H_2S} \quad \text{Eq. 19}$$

$$1000 \ln a_{SO_2-S^{2-}} = 1000 \ln a_{SO_2-S^{6+}} + 1000 \ln a_{S^{6+}-S^{2-}} \quad \text{Eq. 20}$$

For reference, the fractionation constants calculated with Eqs. 15-20 are $a_{SO_2-S^{6+}} \approx 0.9984$, $a_{SO_2-S^{2-}} \approx 1.0016$, $a_{H_2S-S^{6+}} \approx 0.9970$ and $a_{H_2S-S^{2-}} \approx 1.0003$ at T = 1200 °C, and $a_{SO_2-S^{6+}} \approx 0.9973$, $a_{SO_2-S^{2-}} \approx 1.0035$, $a_{H_2S-S^{6+}} \approx 0.9944$ and $a_{H_2S-S^{2-}} \approx 1.00076$ at T = 800 °C. The largest fractionation is seen for degassing of H_2S(g) from the S^{6+}(m) pool, because of the large difference in S oxidation state from 6+ to 2- (Marini et al. 2011). For the same reason, the redox-neutral degassing of H_2S(g) from the S^{2-}(m) pool is only associated with minor $\delta^{34}S$ fractionation and the associated term in Eq (16) is frequently ignored (Mandeville et al. 2009, Marini et al. 2011).

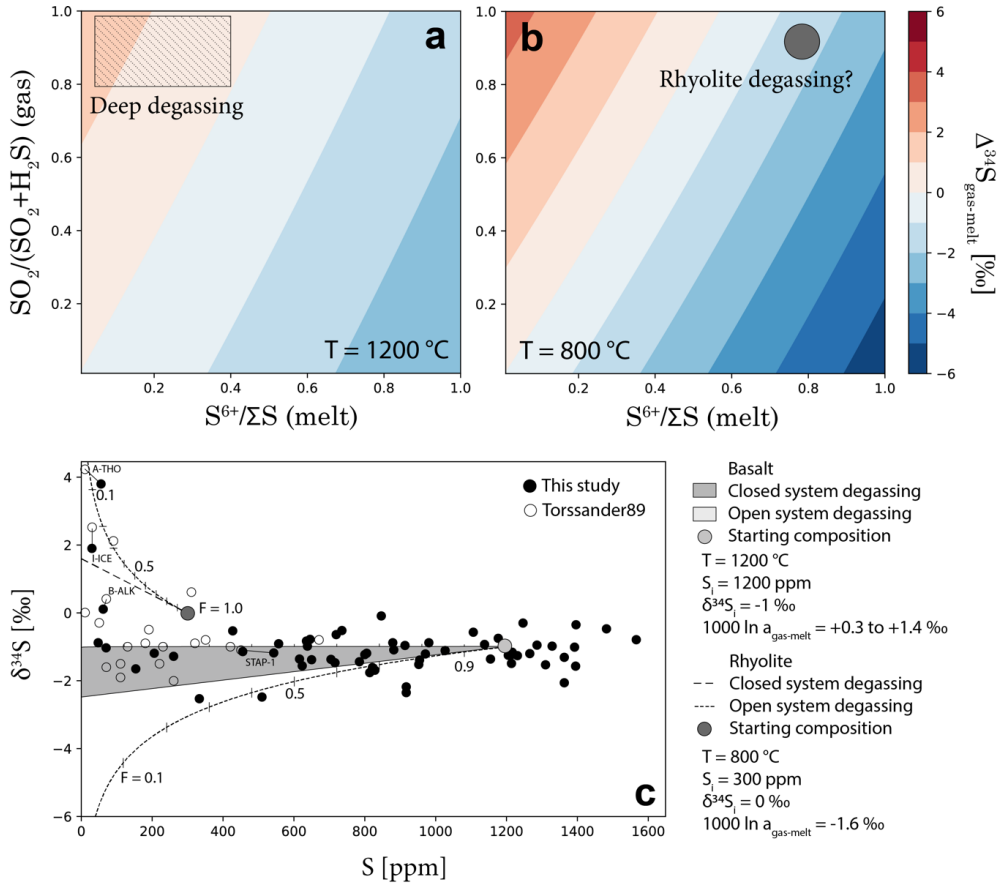

Figure S4 Effect of S speciation of gas and melt on $\Delta^{34}S_{gas-melt}$ fractionation at (a) 1200 °C and (b) 800 °C. (c) Open- and closed-system degassing models for basalts and rhyolites. A starting value of S_i = 300 ppm was used for the rhyolite model, as S concentrations in rhyolitic melt inclusions rarely exceed 300 ppm in Iceland (Fig. 2a).

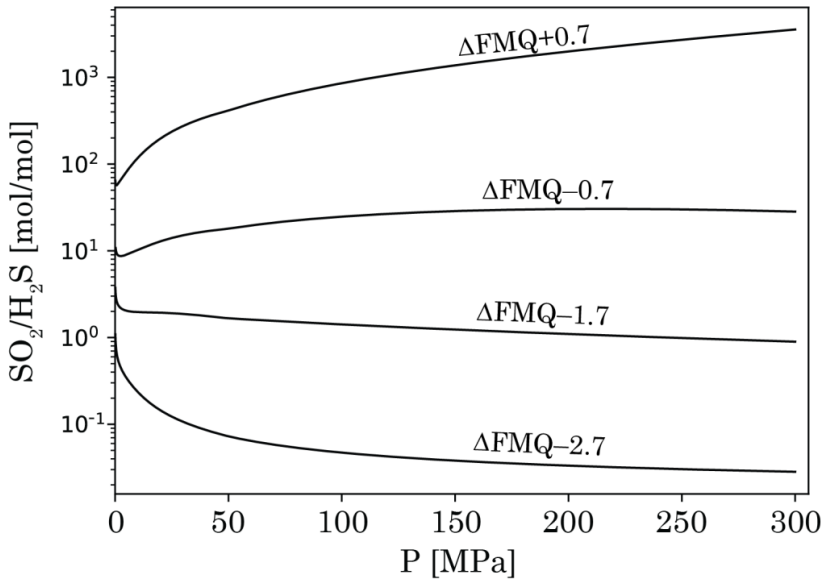

Figure S5 Sulfur speciation of magmatic gas during degassing. The black curves show SO_2/H_2S of the exsolved gas phase during decompressional degassing, modelled at different oxygen fugacities using the D-Compress program (Burgisser et al. 2015). Icelandic melts are moderately oxidized at approximately ΔFMQ between -0.2 and +0.7 (Hartley et al. 2017, Novella et al. 2020), implying that degassing produces a gas with SO_2/H_2S of more than 10 and up to several thousand at all pressures. The major element composition of the sample KVK-169 was used as input, with H_2O and CO_2 concentrations of 0.5 wt.% and 300 ppm, respectively.

6. Relationship between melt $S^{6+}/\Sigma S$ and oxygen fugacity

Buffering of melt $S^{6+}/\Sigma S$ may occur through electron-exchange equilibrium with either dissolved Fe or H_2O (Métrich et al. 2009, Jugo et al. 2010, Nash et al. 2019). Experimental data of Nash et al. (2019) supports the redox coupling between Fe and S according to Eq. (4). This buffer reaction hinders an unchecked increase in the $S^{6+}/\Sigma S$ of the melt during sequestration of S^{2-} by a sulfide melt. Instead, the resulting increase in oxidation potential of the melt is accommodated by an increasing Fe^{3+}/Fe^{2+} according to the empirical linear relationship between $\log(S^{6+}/S^{2-})$ and $\log(Fe^{3+}/Fe^{2+})$ reported in Eq. (11) of Nash et al. (2019):

$$\log\frac{S^{6+}}{S^{2-}} = 8\log\frac{Fe^{3+}}{Fe^{2+}} + \frac{8.743\times10^{6}}{T^{2}} - \frac{27703}{T} \qquad \text{Eq. 21}$$

An almost complete turnover from $S^{6+}/\Sigma S \approx 0$ to $S^{6+}/\Sigma S \approx 1$ takes place over a relatively narrow interval of $Fe^{3+}/\Sigma Fe$ values (between 0.1 and 0.3 at 1200 °C; Fig. S6a), approximately equivalent to a change from ΔFMQ = 0 to +1. The T dependence Eq. (21) means that at constant $Fe^{3+}/\Sigma Fe$, hotter melts have higher $S^{6+}/\Sigma S$ (Fig. S6b). Icelandic basalts are hotter (Matthews et al. 2016) and more oxidized than MORBs (Hartley et al. 2017, Novella et al. 2020) and are thus expected to have higher $S^{6+}/\Sigma S$ than MORBs, where the sulfur is almost entirely dissolved as S^{2-} (e.g., Jugo et al. 20210, Labidi et al. 2014).

Notably, the T dependence of Eq. 21 predicts that $S^{6+}/\Sigma S$ of Icelandic and other moderately oxidized melts will, somewhat counterintuitively, decrease during magma evolution from MgO = 10 to 6 wt.% (Fig. S6c), while simultaneously, Fe^{3+}/Fe^{2+} stay roughly constant or increase because of preferential Fe^{2+} sequestration by olivine ($D_{Ol}^{Fe_2O_3} < 0.1$) and clinopyroxene ($D_{cpx}^{Fe_2O_3} = 0.45$) (Mallmann and O'Neill 2009, Shorttle et al. 2015).

Figure S6 illustrates different scenarios for how $S^{6+}/\Sigma S$ is expected to vary during magma evolution and associated changes in $Fe^{3+}/\Sigma Fe$, T and MgO content. The modeled decrease in $S^{6+}/\Sigma S$ during magma shows that melt $S^{6+}/\Sigma S$ is mainly controlled by melt T above MgO = 6 wt.% (Fig. S6c). Below 6 wt.% MgO, sequestration of S^{2-} by immiscible sulfide melts becomes the dominant control on $S^{6+}/\Sigma S$, leading to a reversal of the $S^{6+}/\Sigma S$ vs. MgO trend (Fig. S6c).

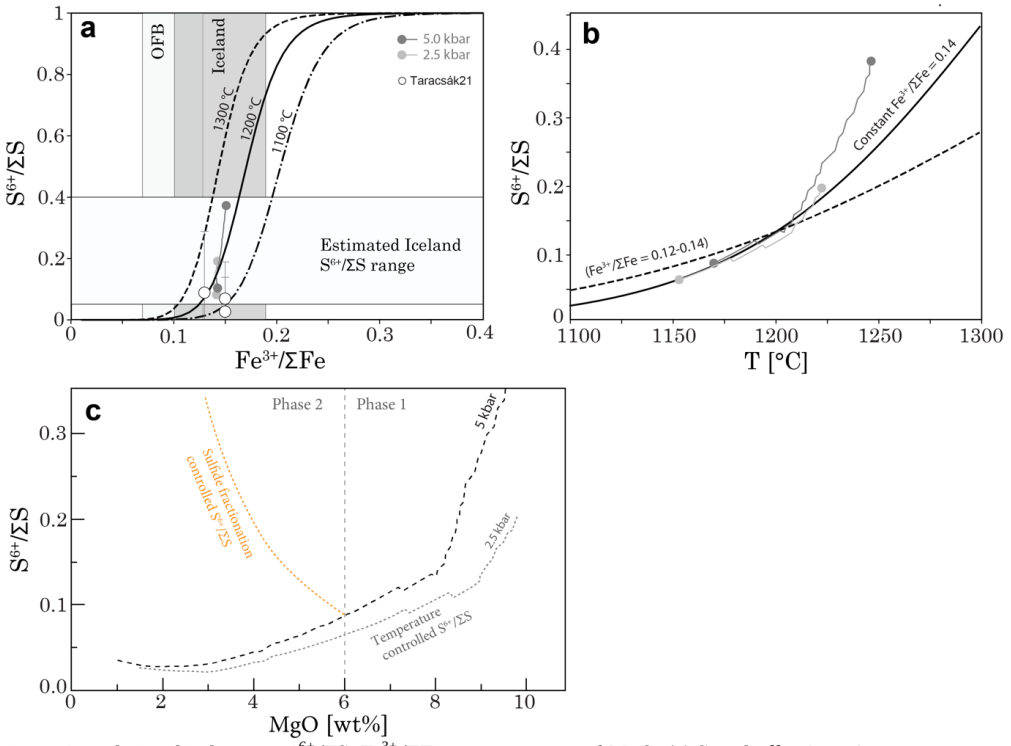

Figure S6 Relationship between $S^{6+}/\Sigma S$, $Fe^{3+}/\Sigma Fe$, temperature and MgO. (a) S-Fe buffer (Eq. 4) curves are shown for T = 1100, 1200 and 1300 °C, calculated using Eq. (21). 95% of published $Fe^{3+}/\Sigma Fe$ values for ocean floor basalts (OFBs) fall within the light gray shaded field (O'Neill 2020). Published range of $Fe^{3+}/\Sigma Fe$ for Icelandic and Reykjanes Ridge pillow rim glasses (Óskarsson et al. 1994, Novella et al. 2020) is more oxidized (dark grey field). Coupled data for samples A35, A36 and STAP-1are shown with 2σ error bars (Taracsák et al. 2021). (b) The temperature dependence of $S^{6+}/\Sigma S$ is calculated using Eq. (15). Solid curve shows the solution for constant $Fe^{3+}/\Sigma Fe = 0.14$ scenario. Dashed line shows a hypothetical scenario with linearly increasing $Fe^{3+}/\Sigma Fe$ from 0.10 at T = 1300 °C to 0.12 at T = 1100 °C, showing that S can become reduced even during moderate oxidation of Fe. In (a) and (b), the effect of fractional crystallization on $S^{6+}/\Sigma S$ is modelled with COMAGMAT v3.72 (Ariskin et al. 2018) using sample NAL-688 as starting composition, buffered at FMQ+0.2 in isobaric conditions at 2.5 kbar (light grey circle-ended line) and 5 kbar (dark grey circle-ended line) to MgO = 6 wt.%. The controlling factor on $S^{6+}/\Sigma S$ is the drop in liquidus temperature of 69-80 °C accompanying fractional crystallization from 9.8 to 6.0 wt. MgO, that has a net effect of $\Delta S^{6+}/\Sigma S = -0.14$ and -0.30 at 2.5 and 5 kbar, respectively. Although limited, the three data points in (a) seem compatible with the modelled FC curves. (c) Modelled sulfur speciation versus MgO. Above MgO >

6 wt.%, decreasing $S^{6+}/\Sigma S$ during fractional crystallization is controlled by temperature (Eq. 21). Below 6 wt.% MgO, sulfide precipitation causes an increase in $S^{6+}/\Sigma S$. Non-buffered $S^{6+}/\Sigma S$ evolution trend (orange) was calculated based on measured/expected S, estimated assuming loss of S^{2-} to a sulfide phase below 6 wt.% MgO. Two model trajectories are shown for 2.5 kbar (grey dotted) and 5 kbar (black dashed), calculated from Eq. 21, with $Fe^{3+}/\Sigma Fe$ and T vs. MgO for the model derived from the isobaric fractional crystallization in (a) and (b).

7. Model III: Effect of sulfide fractionation on $\delta^{34}S$

In MORBs, sulfide melt fractionation only has a tangential effect on the $\delta^{34}S_{S^{2-}}$ values because virtually all sulfur is dissolved as S^{2-} (Labidi et al. 2014). This is not necessarily case for more oxidized melts, if the $S^{6+}/\Sigma S$ is buffered (Labidi et al. 2015). The effects of sulfide fractionation and $S^{6+}/\Sigma S$ buffering on melt $\delta^{34}S_{\Sigma S}$ and $\delta^{34}S_{S^{2-}}$values can be quantified separately for non-buffered (7.1) and buffered (7.2) scenarios (Fig. S7).

7.1 Non-buffered system

The initial $S^{6+}/\Sigma S$ ratio of the melt is defined as

$$X_0 = [S^{6+}/\Sigma S]_0 = \frac{S_0^{6+}}{S_0^{2-}+S_0^{6+}} \quad \text{Eq. 22}$$

If $\delta^{34}S_0^{6+}$ and $\delta^{34}S_0^{2-}$ denote the initial $\delta^{34}S$ values of the sulfate and sulfide pools, respectively, the initial bulk $\delta^{34}S$ value is

$$\delta^{34}S_0^{\Sigma S} = X_0 \times \delta^{34}S_0^{6+} + (1 - X_0) \times \delta^{34}S_0^{2-} \quad \text{Eq. 23}$$

Assuming that the sulfide melt only taps the S^{2-} pool of the silicate melt, sulfide fractionation in a non-buffered system leads to an increase in $S^{6+}/\Sigma S$, so that

$$X_1 = [S^{6+}/\Sigma S]_1 = \frac{S_0^{6+}}{S_0^{2-}-x_{sulf}+S_0^{6+}} \quad \text{Eq. 24}$$

where x_{sulf} is the weight fraction of S^{2-} sequestered by sulfide melt. Because $\Delta^{34}S_{\text{sulfide}-S^{2-}(m)} \approx 0$, the isotopic values of the sulfate and sulfide pools in the silicate melt remain the same, so that

$$\delta^{34}S_0^{6+} = \delta^{34}S_1^{6+} \quad \text{Eq. 25}$$
$$\delta^{34}S_0^{2-} = \delta^{34}S_1^{2-} \quad \text{Eq. 26}$$

However, the bulk $\delta^{34}S$ value

$$\delta^{34}S_1^{\Sigma S} = X_1 \times \delta^{34}S_1^{6+} + (1 - X_1) \times \delta^{34}S_1^{2-} = \\ = X_1 \times \delta^{34}S_0^{6+} + (1 - X_1) \times \delta^{34}S_0^{2-} \quad \text{Eq. 27}$$

will increase because the proportion of isotopically heavier S^{6+} increases.

7.2 Redox buffered system

In a system where the $S^{6+}/\Sigma S$ is buffered, subsequent conversion of S^{6+} to S^{2-} by some amount a will take place, so that

$$S_2^{2-} = S_0^{2-} - x_{sulf} + a \quad \text{Eq. 28}$$

$$S_2^{6+} = S_0^{6+} - a \quad \text{Eq. 29}$$

$$X_2 = \frac{S_0^{6+} - a}{S_0^{2-} - x_{sulf} + S_0^{6+}} \quad \text{Eq. 30}$$

The conversion of S^{6+} to S^{2-} will not change the bulk $\delta^{34}S$ value, so that

$$\delta^{34}S_2^{\Sigma S} = X_2 \times \delta^{34}S_2^{6+} + (1 - X_2) \times \delta^{34}S_2^{2-} = \delta^{34}S_1^{\Sigma S} \quad \text{Eq. 31}$$

However, buffering will impose a change on $\delta^{34}S^{6+}$ and $\delta^{34}S^{2-}$. For an end-member scenario where $S^{6+}/\Sigma S$ is buffered to its original value, i.e., $X_0 = X_2$, assuming isotopic equilibrium between S^{2-} and S^{6+} and combining Eqs. 13, 25, 26 and 31, we can state that

$$\begin{cases} X_0 \times \delta^{34}S_2^{6+} + (1 - X_0) \times \delta^{34}S_2^{2-} = X_1 \times \delta^{34}S_0^{6+} + (1 - X_1) \times \delta^{34}S_0^{2-} \\ \delta^{34}S_2^{6+} = \delta^{34}S_2^{2-} + \varepsilon^{34}S_{S^{6+}-S^{2-}} \end{cases} \quad \text{Eq. 32}$$

We can then solve for $\delta^{34}S_2^{6+}$ and $\delta^{34}S_2^{2-}$ to get

$$\delta^{34}S_2^{6+} = X_1 \times \delta^{34}S_0^{6+} + (1 - X_1) \times \delta^{34}S_0^{2-} + \varepsilon^{34}S_{S^{6+}-S^{2-}} \times (1 - X_0) \quad \text{Eq. 33}$$

$$\delta^{34}S_2^{2-} = X_1 \times \delta^{34}S_0^{6+} + (1 - X_1) \times \delta^{34}S_0^{2-} - \varepsilon^{34}S_{S^{6+}-S^{2-}} \times X_0 \quad \text{Eq. 34}$$

Alternatively, we note that with the given assumptions, the change Δ^{34} in $\delta^{34}S$ is the same for both $\delta^{34}S_{S^{2-}}$, $\delta^{34}S_{S^{6+}}$ and $\delta^{34}S_{\Sigma S}$ (Fig. S7c) so that

$$\Delta_1^{34} = \Delta_2^{34} = \delta^{34}S_1^{bulk} - \delta^{34}S_0^{bulk} = (X_1 - X_0) \times \varepsilon^{34}S_{S^{6+}-S^{2-}} \quad \text{Eq. 35}$$

which yields the expressions

$$\delta^{34}S_2^{6+} = \delta^{34}S_0^{6+} + \Delta_1^{34} \quad \text{Eq. 36}$$

$$\delta^{34}S_2^{2-} = \delta^{34}S_0^{2-} + \Delta_1^{34} \quad \text{Eq. 37}$$

that are equivalent to Eqs. 33 and 34. For this scenario, the amount of converted sulfur a can be expressed as

$$a = S_0^{6+} - X_0(S_0^{2-} - x_{sulf} + S_0^{6+}) \quad \text{Eq. 38}$$

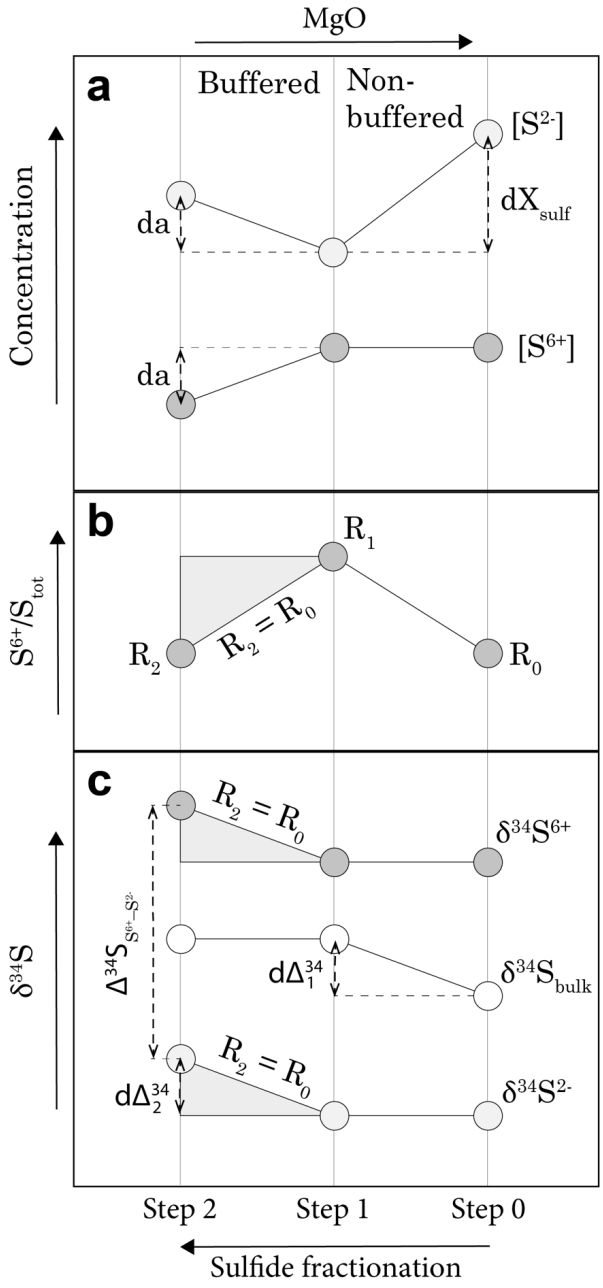

Figure S7 Schematic representation of the effects of sulfide fractionation on melt (a) S^{2-} and S^{6+} concentrations, (b) $S^{6+}/\Sigma S$, and (c) $\delta^{34}S$. Step 0 shows the initial state, step 1 after sulfide fractionation with no redox buffering, and step 2 after redox buffering. The magnitude of da, the amount of S^{6+} to S^{2-} conversion, depends on the redox buffer, and can assume values between 0 (no buffering) and da_{max}, which occurs when $S^{6+}/\Sigma S$ is fully buffered so that $R_2 = R_0$. This condition limits the maximum effect of sulfide fractionation on $\delta^{34}S_{S^{2-}}$ and $\delta^{34}S_{S^{6+}}$ so that $\Delta^{34}_{2,max} = \Delta^{34}_1$.

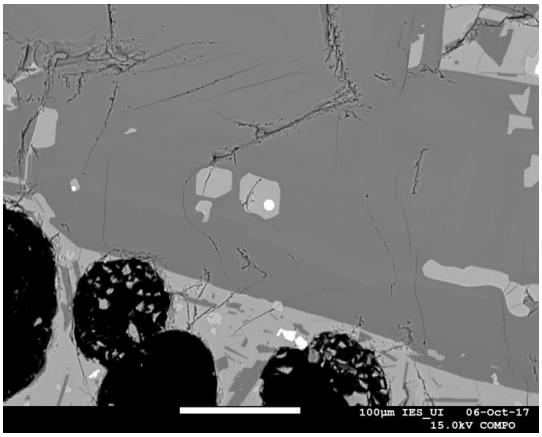

Figure S8 Sulfide globules (bright) in plagioclase-hosted melt inclusions in a Kverkfjöll scoria sample (KVK-212). This sample was not analyzed in this study.

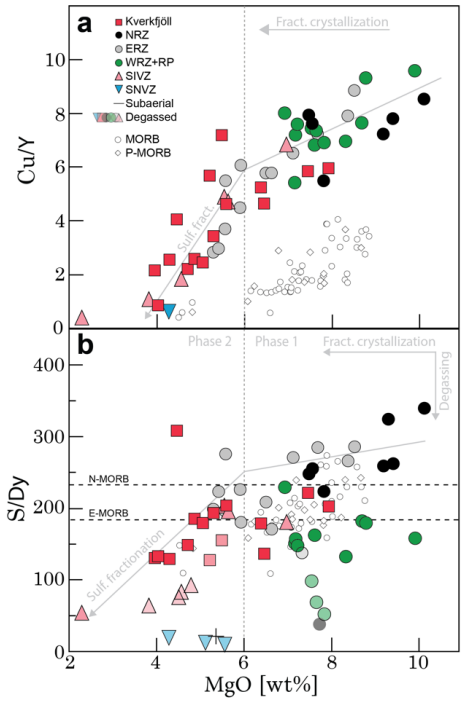

Figure S9 Effect of sulfide melt immiscibility (a) Cu/Y versus MgO. Because $D_{Cu}^{sil-liq} \approx D_{Y}^{sil-liq}$, decreasing Cu/Y may indicate slight fractionation of sulfide during Phase 1. (b) S/Dy versus MgO. The S/Dy variability in undegassed, primitive (MgO > 6 wt.%) samples suggest either lower S/Dy in the WRZ and Kverkfjöll mantle compared to NRZ and ERZ, or, alternatively, buffering of primitive melt S concentrations during partial melting by mantle sulfides (Ding and Dasgupta 2018).

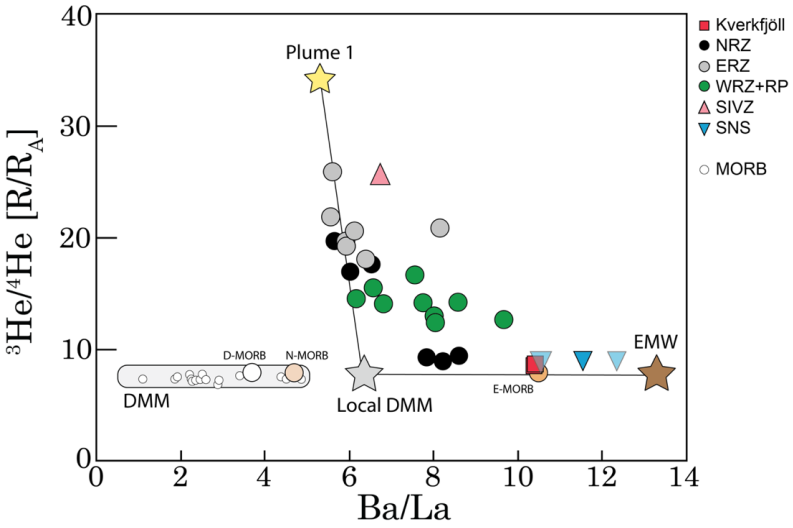

Figure S10 $^3He/^4He$ versus Ba/La. Subduction fluids have elevated Ba/La compared to DMM. We thus assume that the enriched mantle wedge component (EMW) has a high Ba/La (~13.5). Highest Ba/La in Iceland are observed in the Kverkfjöll and Snæfellsnes samples that both have MORB-like $^3He/^4He$. Kverkfjöll plots close to the estimated composition of E-MORB (Gale et al. 2013). The $^3He/^4He$ vs. Ba/La systematics are compatible with the subduction fluid origin of low $\delta^{34}S$ and $\Delta^{33}S$ signatures in the Icelandic mantle (Fig. 7). Symbols and MORB data as in Figs. 2 and 7.

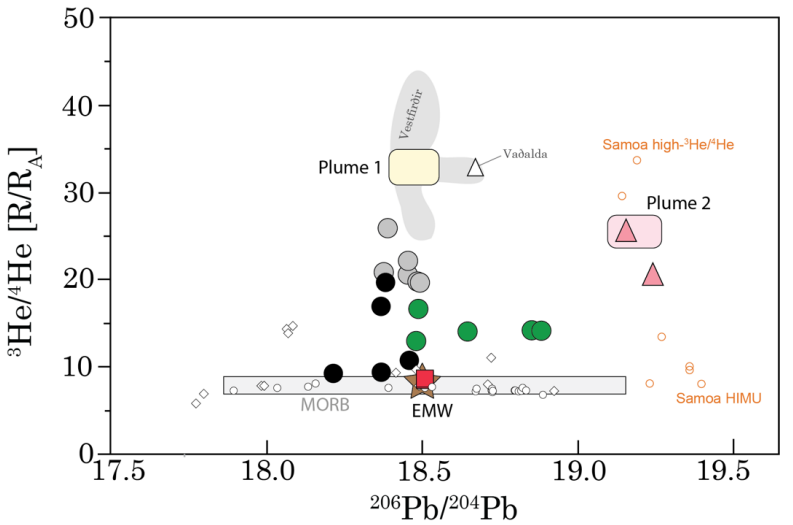

Figure S11 $^3He/^4He$ versus $^{206}Pb/^{204}Pb$. High-$^3He/^4He$-samples in Iceland seem to have a binary $^{206}Pb/^{204}Pb$ distribution (Jackson et al. 2020). The less-radiogenic Plume 1 component is sampled by the ERZ-NRZ lavas and is similar to the Miocene Vestfirðir lavas and the interglacial shield volcano Vaðalda in the NRZ (Jackson et al. 2020). The high-$^3He/^4He$ SIVZ lavas sample a more radiogenic component, Plume 2, which has a similar $^3He/^4He$-$^{206}Pb/^{204}Pb$ signature as the Samoan high-$^3He/^4He$ component. The EMW component has MORB-like $^3He/^4He$ and a $^{206}Pb/^{204}Pb$ signature similar to Plume 1. Symbols, MORB and Samoa data as in Figs. 2 and 7.

8. Supplementary references

Antonelli, M. A., Kim, S. T., Peters, M., Labidi, J., Cartigny, P., Walker, R. J., Lyons, J.R., Hoek, J., & Farquhar, J. (2014). Early inner solar system origin for anomalous sulfur isotopes in differentiated protoplanets. *Proceedings of the National Academy of Sciences*, *111*(50), 17749-17754.

Ariskin, A. A., Bychkov, K. A., Nikolaev, G. S., & Barmina, G. S. (2018). The Comagmat-5: modeling the effect of Fe–Ni sulfide immiscibility in crystallizing magmas and cumulates. *Journal of Petrology*, *59*(2), 283-298.

Bali, E., Hartley, M. E., Halldórsson, S. A., Gudfinnsson, G. H., & Jakobsson, S. (2018). Melt inclusion constraints on volatile systematics and degassing history of the 2014–2015 Holuhraun eruption, Iceland. *Contributions to Mineralogy and Petrology*, *173*(2), 1-21.

Carroll M. R., & Rutherford M. J. (1988). Sulfur speciation in hydrous experimental glasses of varying oxidation state: results from measured wavelength shifts of sulfur X-rays. *American Mineralogist, 73*, 845–849.

Defouilloy, C., Cartigny, P., Assayag, N., Moynier, F., & Barrat, J. A. (2016). High-precision sulfur isotope composition of enstatite meteorites and implications of the formation and evolution of their parent bodies. *Geochimica et Cosmochimica Acta*, *172*, 393-409.

Ding, S., & Dasgupta, R. (2018). Sulfur inventory of ocean island basalt source regions constrained by modeling the fate of sulfide during decompression melting of a heterogeneous mantle. *Journal of Petrology*, *59*(7), 1281-1308.

Gaillard, F., Scaillet, B., & Arndt, N. T. (2011). Atmospheric oxygenation caused by a change in volcanic degassing pressure. *Nature*, *478*(7368), 229-232.

Gale, A., Dalton, C. A., Langmuir, C. H., Su, Y., & Schilling, J. G. (2013). The mean composition of ocean ridge basalts. *Geochemistry, Geophysics, Geosystems*, *14*(3), 489-518.

Guillong M, Meier D.L, Allan M.M., Heinrich C.A., & Yardley B.W. (2008) SILLS: a MATLAB-based program for the reduction of laser ablation ICP–MS data of homogeneous materials and inclusions. *Mineralogical Association of Canada Short Course, v. 40*, 328–333

Hauri, E. H., J. Wang, J. E. Dixon, P. L. King, C. Mandeville, & S. Newman. 2002. SIMS Investigations of volatiles in silicate glasses, 1: Calibration, matrix effects and comparisons with FTIR. *Chemical Geology, 183*, 99-114.

Hartley, M. E., Shorttle, O., Maclennan, J., Moussallam, Y., & Edmonds, M. (2017). Olivine-hosted melt inclusions as an archive of redox heterogeneity in magmatic systems. *Earth and Planetary Science Letters*, *479*, 192-205.

Kaikkonen, R.M. (2017) Evolution of basaltic lavas of the Kverkfjöll volcanic system, Northern Volcanic Zone, Iceland: Evidence from in-situ LA-ICP-MS analyses. Unpublished MSc thesis, University of Oulu, pp. 87.

Labidi, J., Farquhar, J., Alexander, C. O. D., Eldridge, D. L., & Oduro, H. (2017). Mass independent sulfur isotope signatures in CMs: Implications for sulfur chemistry in the early solar system. *Geochimica et Cosmochimica Acta, 196*, 326-350.

Mallmann, G., & O'Neill, H. S. C. (2009). The crystal/melt partitioning of V during mantle melting as a function of oxygen fugacity compared with some other elements (Al, P, Ca, Sc, Ti, Cr, Fe, Ga, Y, Zr and Nb). *Journal of Petrology*, *50*(9), 1765-1794.

Mandeville, C. W., Webster, J. D., Tappen, C., Taylor, B. E., Timbal, A., Sasaki, A., Hauri, E., & Bacon, C. R. (2009). Stable isotope and petrologic evidence for open-system degassing during the climactic and pre-climactic eruptions of Mt. Mazama, Crater Lake, Oregon. *Geochimica et Cosmochimica Acta*, *73*(10), 2978-3012.

Marini, L., Moretti, R., & Accornero, M. (2011) Sulfur isotopes in magmatic-hydrothermal systems, melts, and magmas. *Reviews in Mineralogy and Geochemistry*, *73*, 423–492.

Matthews, S., Shorttle, O., & Maclennan, J. (2016). The temperature of the I celandic mantle from olivine-spinel aluminum exchange thermometry. *Geochemistry, Geophysics, Geosystems*, *17*(11), 4725-4752.

Métrich N., Berry A. J., O'Neill H. St. C., & Susini J. (2009) The oxidation state of sulfur in synthetic and natural glasses determined by X-ray absorption spectroscopy. *Geochimica et Cosmochimica Acta, 73*, 2382–2399.

Miyoshi, T., Sakai, H., & Chiba, H. (1984). Experimental study of sulfur isotope fractionation factors between sulfate and sulfide in high temperature melts. *Geochemical Journal, 18*(2), 75-84.

Moilanen, M., Hanski, E., Konnunaho, J., Törmänen, T., Yang, S.H., Lahaye, Y., O'Brien, H., & Illikainen, J. (2020). Composition of iron oxides in Archean and Paleoproterozoic mafic-ultramafic hosted Ni-Cu-

PGE deposits in northern Fennoscandia: application to mineral exploration: *Mineralium Deposita*, *55(8)*. 1515–1534.
Moore, J. G., & Calk, L. C. (1991). Degassing and differentiation in subglacial volcanoes, Iceland. *Journal of Volcanology and Geothermal Research*, *46*(1-2), 157-180.
Nash, W. M., Smythe, D. J., & Wood, B. J. (2019). Compositional and temperature effects on sulfur speciation and solubility in silicate melts. *Earth and Planetary Science Letters*, *507*, 187-198.
Newman, S., & Lowenstern, J. B. (2002). VolatileCalc: a silicate melt–H_2O–CO_2 solution model written in Visual Basic for excel. *Computers & Geosciences*, *28*(5), 597-604.
Novella, D., Maclennan, J., Shorttle, O., Prytulak, J., & Murton, B. J. (2020). A multi-proxy investigation of mantle oxygen fugacity along the Reykjanes Ridge. *Earth and Planetary Science Letters*, *531*, 115973
O'Neill, H. St.C. (2021). The thermodynamic controls on sulfide saturation in silicate melts with application to Ocean Floor Basalts. In: R. Moretti and D. R. Neuville, ed., *Magma Redox Geochemistry*, John Wiley & Sons.
Ono, S., Shanks III, W. C., Rouxel, O. J., & Rumble, D. (2007). S-33 constraints on the seawater sulfate contribution in modern seafloor hydrothermal vent sulfides. *Geochimica et Cosmochimica Acta*, *71(5)*, 1170-1182.
Óskarsson, N., Helgason, Ö., & Steinthórsson, S. (1994). Oxidation state of iron in mantle-derived magmas of the Icelandic rift zone. *Hyperfine Interactions*, *91*(1), 733-737.
Sakai, H., Casadevall, T. J., & Moore, J. G. (1982). Chemistry and isotope ratios of sulfur in basalts and volcanic gases at Kilauea Volcano, Hawaii. *Geochimica et Cosmochimica Acta*, *46*(5), 729-738.
Schattel, N., Portnyagin, M., Golowin, R., Hoernle, K., & Bindeman, I. (2014). Contrasting conditions of rift and off-rift silicic magma origin on Iceland. *Geophysical Research Letters*, *41*(16), 5813-5820.
Taylor Jr, H. P. (1986). Igneous rocks: I. Process of isotopic fractionation and isotope systematics. Stable isotopes in high temperature geological processes. *Reviews in Mineralogy and Geochemistry*, 16, pp. 185-225

Appendix C: Supplementary information for Paper III

1 Hydrogeology of Askja and Kverkfjöll

The steep topography of the Kverkfjöll central volcano results in a steeply dipping groundwater table, that flows out along numerous rivers on the flanks of the mountain massif. The Hveragil river flows out at ~1100 m, roughly at the estimated elevation of the initiation of boiling of the rising reservoir fluid (900-1200 m.a.s.l.). Mixing of the slightly boiled, or even unboiled reservoir water at ~300 °C and cold groundwater takes place at depth, preventing further boiling upon ascent, making it a rare natural example of a diluted reservoir liquid. The mixing allows the Hveragil water to retain high dissolved CO_2 concentrations (c.f. Arnórsson and Barnes, 1983; Fig. 4.4a). Following boiling, the vapour phase rises above the ground water table to Hveradalur, which is dominated by acid-sulfate type geothermal activity and CO_2-H_2S rich fumarole discharge. Thus, the reservoir fluid is largely preserved in a diluted form in Hveragil, whereas only the gas phase is sampled at Hveradalur. Sampling the waters at Hveragil and the steam at Hveradalur can be seen a natural analogue to sampling of two-phase wells drilled into geothermal reservoirs.
In contrast to the steep groundwater table at Kverkfjöll, at Askja, the groundwater table is relatively flat, marked by the surface of Lake Öskjuvatn at 1050 m.a.s.l. Here, an upwelling, hot one-phase reservoir fluid boils at an estimated depth of ~300 m below the floor of Lake Öskjuvatn. Above this depth, the vapour phase rises towards the surface along caldera faults and either escapes in fumaroles or condensates and dissolves into shallow groundwater. The boiled reservoir fraction may the dissipate laterally and mix with local groundwater before reaching the surface. The lack of upwellings of the boiled liquid phase may also indicate a younger age for the geothermal system at Askja (Hermanska et al. 2019). No limiting condition at Askja, such as the topographic gradient in Kverkfjöll, blocks the backflow of steam-heated water to the aquifer to form a mixed local groundwater reservoir (Fig. 4.5a). The generation of a mixed geothermal reservoir is also compounded by the lack of outflow for Lake Öskjuvatn. Hence, Lake Öskjuvatn and adjacent springs all seem to reflect various mixtures of non-thermal water, condensed steam and boiled reservoir water which contrasts with the solute-poor chemistry of a local cold stream. The contrasting hydrogeology of Kverkfjöll and Askja demonstrate the influence of topography on both the surface expressions and surface chemistry of VHSs. Notably, however, these differences are expressed mainly in the compositions of the thermal springs, whereas the compositions of high-flux fumarole vapors mainly reflect deeper processes in the system.

2. Reconstructing the Reservoir Liquid Composition and Temperature

The temperature and composition of the reservoir liquid of Kverkfjöll, i.e., the deep parental hydrothermal fluid prior to phase separation and shallow modifications, was reconstructed from the chemistry of the hot spring waters and fumaroles using techniques outlined below.

2.1 Reservoir fluid temperatures

To estimate reservoir fluid temperatures, three types of gas geothermometers were applied: Silica-enthalpy mixing model (Fig. S1; Truesdell and Fournier 1977), noble gas thermometer (reported previously in Byrne et al. 2021) as well as various gas

thermometers (Árnorsson and Gunnlaugsson, 1985, Arnórsson (1998). The silica-enthalpy mixing model yields a reservoir liquid temperature of ~280 °C for Kverkfjöll (Fig. S1). The noble gas $T_{Ar\text{-}Kr}$ and $T_{Ar\text{-}Ne}$ thermometers yield temperatures of 263 to 332 °C for Kverkfjöll and 337 to 345 °C for Askja (Byrne et al. 2021). The H_2, H_2S, H_2S/H_2, CO_2, CO_2/N_2, H_2S/Ar and H_2/Ar gas thermometers of Árnorsson (2000) give a mean reservoir temperature of 300±20°C for Kverkfjöll and 320±20 °C for Askja (Table. S1).

The general agreement between the major gas (with the exception of CO_2), silica-enthalpy and noble gas thermometers is notable, given that they are based on entirely independent underlying assumptions: The major gas thermometers assume *chemical* mineral-fluid equilibrium in the reservoir, whereas the noble gas thermometer is based on the elemental fractionation during the *physical* process of boiling. The high temperature (c. 280°C) estimated for the thermal source fluid of the Hveragil river suggests that mixing of reservoir liquid and cold groundwater likely takes place at depth after minimal amount of boiling. Mixing taking place above the decompression boiling pressure would prevent further boiling during the upflow (c.f. Arnórsson and Barnes, 1983).

2.3 Reservoir fluid compositions

The linear trends shown by the Hveragil thermal water samples for most major, minor and trace elements vs. temperature (Figs. S1, S2a) show that it represents a rare natural example of a binary mixture of nearly unboiled reservoir liquid and shallow groundwater of local meteoric water origin. Silica-enthalpy mixing thermometer (Truesdell and Fournier 1977) can thus be applied to yield both a reservoir liquid temperature of ~280 °C as well as a meteoric/reservoir water mixing ratio or mixing proportion for a given sample. Then, the concentration of a conservative element i in the reservoir fluid ($C_{i,res}$) can be calculated using the concentrations i in meteoric water ($C_{i,cold}$; average of three Hveragil cold streams) and the Hveragil sample H-4 ($C_{i.hve}$) with a binary mixing equation

$$C_{i.res} = [C_{i.hve} - C_{i,cold}(1 - f)]/f \quad (3)$$

The reconstructed reservoir fluid composition of Kverkfjöll is presented in Table 3. A simple mixing model cannot be applied to reconstruct the reservoir fluid composition at Askja samples, because there are no surface outflows of the reservoir or boiled reservoir liquid. Instead, all surface springs at Askja, as well as Lake Öskjuvatn, have a high component of condensed fumarolic vapour, as reflected by their high SO_4 contents (Fig. S2a) and the the poorly defined mixing trajectory in Fig. S1.

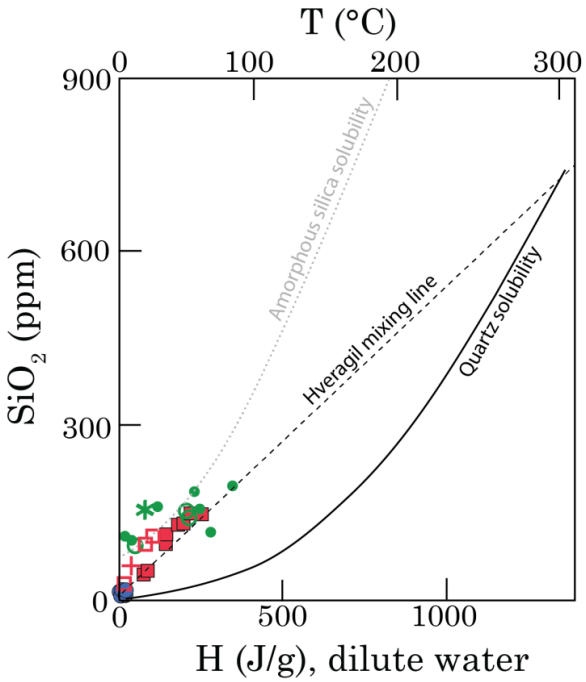

Figure S1: Silica-enthalpy mixing model. The quartz solubility model of Arnórsson et al. (1983) was used together with the silica-enthalpy mixing model of Truesdell and Fournier (1977) to estimate the reservoir fluid composition (section 4.2). Solubility curves for amorphous silica, chalcedony and quartz from Fournier (1977) and Fournier and Potter (1982) are plotted for reference. Symbols as in Fig. 4.3.

.

2.3 Reservoir fluid composition: fumaroles

The reservoir fluid concentrations of volatile species can be estimated from the fumarole chemistry. We make the assumption that the fumarole vapors form by closed system adiabatic boiling of a dilute, one-phase reservoir liquid. Then, because of the conservation of enthalpy, the vapor fraction, x_v, can be calculated by

$$x_v = \frac{h_{liq,res-T} - h_{liq,bp}}{h_{v,bp} - h_{liq,bp}} \quad (4)$$

where $h_{liq,res}$ is the enthalpy of the dilute reservoir liquid at the estimated reservoir temperature, and $h_{liq,bp}$ and $h_{v,bp}$ are the enthalpies of water liquid and vapor at the sampling temperatures, which can be acquired from standard steam tables. Then, the reservoir liquid concentration of a volatile element i can be calculated by

$$C_{i,res} = x_v \times C_{i,.v} + (1 - x_v) \times C_{i,lq} \times B_i \quad (5)$$

where B_i is a modified distribution coefficient accounting for the dissociation of gas species in the liquid, (Arnórsson and Sigurdsson 1982). $C_{i,res}$, $C_{i,liq}$ and B_i are solved using the WATCH 2.4 software (Bjarnason 2010). For average S and CO_2 concentrations of the Kverkfjöll fumaroles, and assuming degassing of ΣS^{2-} and CO_2 from the reservoir liquid

between 280°C to the fumaroles at 100°C using Eqs. (4) and (5), the reservoir ΣS and CO_2 concentrations are estimated at ~200 ppm and 5400 ppm, respectively.

The isotope compositions of the Kverkfjöll reservoir liquid (δD and $\delta^{18}O$-H_2O, $\delta^{13}C$-ΣCO_2, $\Delta^{33}S$-$\delta^{34}S$) were estimated by iteratively finding a starting composition that matches the average fumarole isotope values after taking account adiabatic boiling between 280°C and 100 °C. The used fractionations factors and calculation details are outlined in Stefánsson et al. 2015, 2016, 2017). In short, the effects of boiling on the speciation of S and C in the liquid and vapor phases were computed first with WATCH. These were then used together with available equilibrium isotope fractionation factors to calculate $\delta^{13}C$ and $\delta^{34}S$ fractionation during boiling (Table S1). For δD and $\delta^{18}O$-H_2O, the effects of boiling were calculated using Eq.(4) and vapor-liquid fractionation factors for δD and $\delta^{18}O$ from Horita and Wesolowski (1984).

3 Constraining Water-Rock Interaction

The dissolution of basalt and formation of secondary minerals is modelled using the PHREEQC program (Parkhurst and Appelo 1999). The solutions are calculated at 300 °C using the composition of the sample KVK-168 (Ranta et al. 2021b) with degassed S (300 ppm) and CO_2 (1 ppm) concentrations. The output of the model is used for isotopic modelling of δD-$\delta^{18}O(H_2O)$ (Table S2; Fig. 4.3a) using a compilation of mineral-water fractionation factors from Kleine et al. (2020).

4 Sulfur isotopes of sulfate in thermal waters

When the reservoir liquid cools as a result of adiabatic boiling or mixing with cold groundwater, $\Sigma S^{2-}(lq)$ oxidizes to $SO_4(lq)$ (Stefánsson et al. 2015). Similar oxidation may take place when fumarole gases pass a shallow aquifer, which likely occurs at Lake Öskjuvatn at Askja, which is characterized by high SO_4 concentrations (Fig. S2a). In this case, oxidation can be represented by the reaction

$$H_2S(g) + 4H_2O(lq) \leftrightarrow SO_4^{2-}(lq) + 2H^+ + 4H_2 \quad (6)$$

Assuming that oxidation takes place under closed system conditions, S isotope fractionation can be calculated following Ono et al. (2007, 2012):

$$\delta^x S(SO_4^{2-}) = [\delta^x S(H_2S) + 1] \times \frac{1-f^{\,x\alpha}}{1-f} - 1 \quad (7)$$

where f is the fraction of sulfide remaining, x is 33, 34 or 36 and α is the fractionation factor of S between sulfate and sulfide. Value for $^{34}\alpha$ is estimated using Eq. 11 of Ono et al. (2012), whereas $^{34}\alpha$ is related to $^{33}\alpha$ through

$$^{33}\alpha = {}^{34}\alpha^{\theta} \quad (8)$$

where θ is the triple fractionation coefficient calculated with Eq. (12) of Ono et al. (2012). The S-$\Delta^{33}S$-$\delta^{34}S$ values of the Öskjuvatn springs are consistent with sulfate being derived from >90% closed-system oxidation of Askja fumarole H_2S at 200-300 °C (Fig. S3). The

$\Delta^{33}S$-$\delta^{34}S$ values of Hveragil and Volga waters can be explained by similar amount of oxidation of the reservoir liquid sulfide, and a minor effect from mixing with a low-S (0.55 ppm) meteoric water component (Fig. 4.3c).

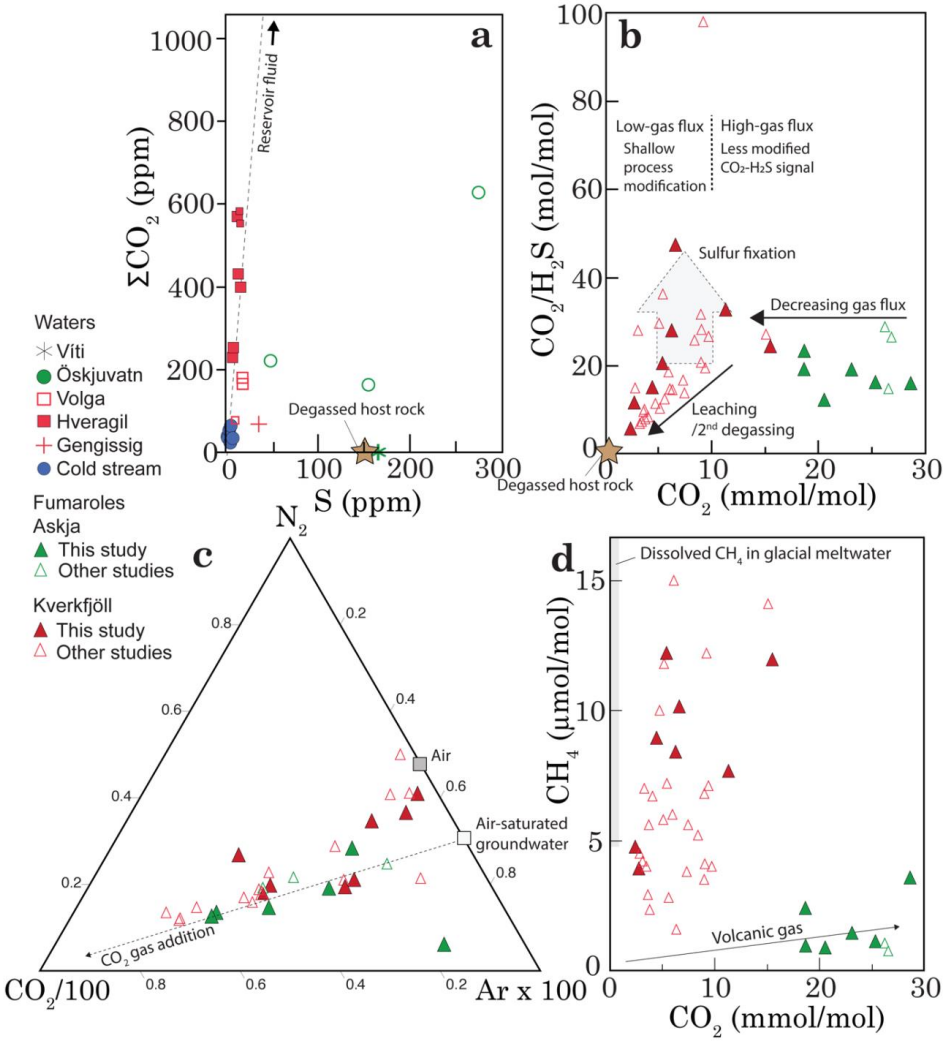

Figure S2. Water and gas chemistry. (a) CO_2 versus. ΣS in thermal and non-thermal waters. (b) CO_2/H_2S versus CO_2 in fumaroles. (c) N_2-CO_2-Ar ternary diagram. Fumarole vapors record N_2/Ar ratios between air and air-saturated groundwater, but require external addition of CO_2. (d) CH_4 versus CO_2. The CH_4 concentrations are higher in Kverkfjöll fumaroles. High CH_4 could be derived from glacial meltwater, which can have high CH_4 concentrations (Burns et al. 2018).

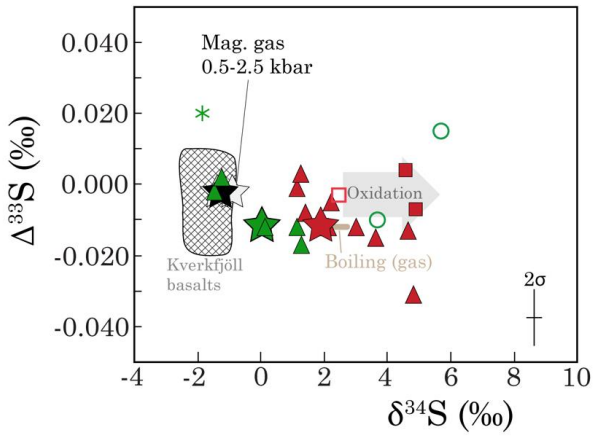

Figure S3. $\Delta^{33}S$ vs $\delta^{34}S$ of H_2S (in fumaroles) and SO_4 (in water samples) from Askja and Kverkfjöll. Symbols as in Fig. 4.3.

5 Flux Calculations

5.1 Eruptive volatile flux potential

Eruptive fluxes (volatiles released from melts during volcanic eruptions) are calculated as

$$F_{erup,i} = f_{erup,i} \times C_{i,.0} \times M_{erup} \quad (9)$$

Where $F_{erup,i}$ (kg/s) is the eruptive flux of volatile i (= H_2O, CO_2, S, Cl), M_{erup} is the eruptive mass flux of basalts (kg/s) and f_i is the fraction of i that is degassed relative to its mass concentration $C_{i,.0}$ in the undegassed melt, i.e.,

$$f_{erup,i} = 1 - C_{erup,i}/C_{i,0} \quad (10)$$

where $C_{erup,i}$ is the concentration of volatile i in the melt after degassing at P = 1 bar.

5.2 Total intrusive volatile flux potential

We estimate the total intrusive volatile flux by calculating

$$F_{tot,i} = C_{i,.0} \times M_{erup} \times X \quad (11)$$

where X is the intrusion/extrusion production ratio. We assume an X value of 4-8, suggested for Iceland by White et al. (2006). The calculated $F_{tot,i}$ is an estimate for the total transport of mantle volatiles by crust-forming basaltic melts and does not differentiate between volatiles that remain in the crust and volatiles that are degassed into the atmosphere.

5.3 Intrusive fluxes from decompression degassing

The intrusive volatile fluxes that exsolve from ascending melts via decompression degassing, $F_{intr,i}$, are calculated as

$$F_{intr,i} = f_{intr,i} \times C_{i,.0} \times M_{erup} \times X \quad (12)$$

where $f_{intr,i}$ is the fraction of volatile i that is degassed by decompression degassing, given by

$$f_{intr,i} = 1 - C_{intr,i}/C_{i,0} \quad (13)$$

The concentration of volatile i remaining in the melt after decompression degassing ($C_{intr,i}$) of an originally volatile-undersaturated melt (with concentration of i $C_{i,0}$) is calculated using the SolEx 1.0 program (Witham et al. 2012; see section S2.4)

5.4 Pre-eruptive volatile concentrations

We model closed and open system decompression degassing to 0.5 and 2.5 kbar using a range of estimated undersaturated H_2O-CO_2-S-Cl concentration of typical tholeiitic melts ($C_{i,0}$) with MgO = 5-8 wt.%. This MgO interval approximately represents the bulk of erupted basalts in Iceland (Hartley and Maclennan 2018). Composition of the modeled volatile content of the melt is shown in Fig. 9a. For the flux calculations, the undegassed concentrations are estimated at 0.2 to 1 wt.% H_2O, 100-350 ppm Cl and 600-1000 ppm S and 0.1-0.4 wt.% CO_2. For H_2O, Cl and S, these values are based on typical ranges of previously established pre-eruptive concentrations of these volatiles measured in melt inclusions and subglacial glasses (Sigvaldason and Óskarsson 1976, Nichols et al. 2002, Halldórsson et al. 2016, Bali et al. 2018, Hauri et al. 2018, Miller et al. 2019), which are assumed to represent undersaturated concentrations due to the relatively high solubility of these volatiles at magma storage depths (> ~1 kbar). For CO_2, which is less soluble and because CO_2-undersaturated MIs for high CO_2-melts are unlikely to form at crustal pressures, the higher concentration estimate (4000 ppm) is deemed to be representative based on inferred mantle ratios of C/Ba of 10-35 (equivalent to CO_2/Ba = 37-130; Matthews et al. 2021) and typical Ba concentrations of 10-150 ppm in rift basalts (Ranta et al. 2021b). However, because of the complexities related to the mantle C/Ba estimates (Matthews et al. 2021), the upper estimate of the undersaturated melt CO_2 concentrations is the least well constrained of the above values.

6 Non-magmatic volatile sources

In addition to direct magma degassing, VHSs in Iceland may receive volatiles from the groundwater, atmosphere or crustal rocks. The H_2O—the bulk of the hydrothermal fluids—is almost exclusively of non-magmatic origin (i.e., meteoric or seawater; see section 4.6.5). Fumarolic H_2 is derived from H_2O reduction via fluid-rock reactions (Ricci et al. *in press*). Noble gases heavier than He as well as N in hydrothermal fluids are mainly of atmospheric origin and derived from air or air-saturated groundwater recharge (Fig. S2c;

Füri et al. 2010, Labidi et al. 2020, Byrne et al. 2021). Crustal rocks may contribute to the volatile budget of hydrothermal fluids via fluid-rock interaction. The Icelandic crust comprises mostly subaerially and subglacially erupted basaltic lava flows and intrusions (e.g., Óskarsson et al. 1982). Due to the low melt solubility of CO_2 and S at low pressures (Fig. 4.4b) and crystallization-driven fluid exsolution following lava or intrusion emplacement (Edmonds and Woods 2018), both lavas and intrusions tend to be poor in CO_2 (< 10 ppm; Barry et al. 2014) and S (~90 ppmw; average of 9 lava flows; Torssander 1989). Thus, the igneous crust is likely to be only a minor source of C—supported by the magma gas-like $\delta^{13}C$ signature of hydrothermal source fluids (Fig. 4.3d)—-whereas small amounts of S may be leached from the crust. Crustal sedimentary sources of C or S are almost absent kn the Icelandic crust, although CH_4, which is a minor component in fumarole gases (1-13 μmol/mol), may have a biogenic origin along with other trace hydrocarbons (Fiebig et al. 2020). Basalt-like Cl/B (Stefánsson et al. 2019) and $\delta^{37}Cl$ compositions of Icelandic thermal fluids, as well as excess Cl concentration relative to source waters point to rock dissolution as the main source of Cl and B in Icelandic meteoric water-fed VHSs, whereas higher Cl concentrations measured in coastal VHSs result from seawater input (Stefánsson and Barnes 2016, Stefánsson et al. 2017, Gunnarsson-Robin et al. 2017).

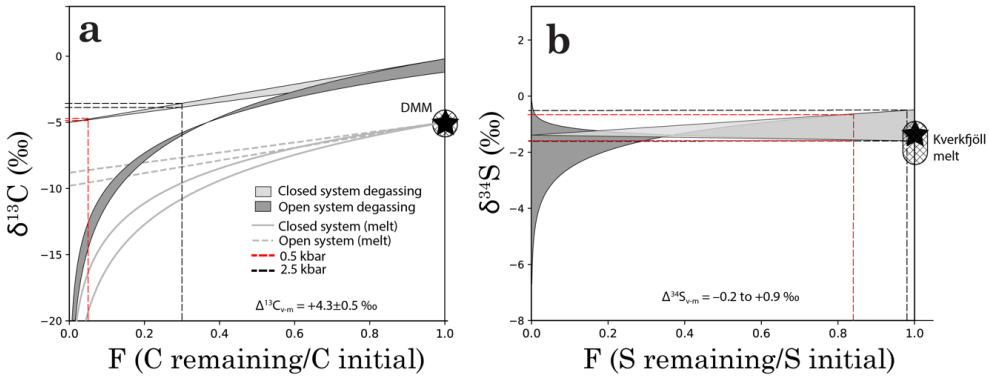

Figure S4. Isotopic composition of magmatic gas. (a) $\delta^{13}C$ and (c) $\delta^{34}S$ vs F. The isotopic composition of an exsolved magmatic gas is shown for open- and closed system degassing paths. Black and red dashed lines mark the isotopic composition of the gas at F (fraction of C or S remaining in the melt) and corresponding to closed system degassing of intrusions to 2.5 and 0.5 kbar, respectively. The $\delta^{13}C$ values of magmatic gas become progressively lower during degassing of a basaltic melt, whereas $\delta^{34}S$ may become either slightly more positive or negative depending on the melt and gas redox states (Mandeville et al. 2009). However, because only minor degassing of S occurs during melt ascent to 2.5 kbar or even 0.5 kbar, the $\delta^{34}S$ values of both deep and relatively shallow magmatic gases are indistinguishable from the initial melt signatures. By contrast deep degassing may yield gas with up to 4.8 ‰ more positive $\delta^{13}C$ values relative to initial melt. Crystallization-driven degassing of intrusions would follow the closed- or open system degassing paths toward lower F. Initial melt $\delta^{13}C$ and (c) $\delta^{34}S$ signatures as in Fig. 4.5.

Supplementary References

Arnórsson, S., & Barnes, I. (1983). The nature of carbon dioxide waters in Snaefellsnes, western Iceland. *Geothermics*, *12*(2-3), 171-176.

Arnórsson, S., Gunnlaugsson, E., and Svavarsson, H. (1983). The chemistry of geothermal waters in Iceland. III, Chemical geothermometry in geothermal investigations. *Geochimica et Cosmochimica Acta*, *47*(3), 567-577.

Arnorsson, S., Sigurdsson, S., & Svavarsson, H. (1982). The chemistry of geothermal waters in Iceland. I. Calculation of aqueous speciation from 0 to 370 C. *Geochimica et Cosmochimica Acta*, *46*(9), 1513-1532.

Arnórsson, S. (ed.) (2000), Isotopic and chemical techniques in geothermal exploration, development and use. Sampling methods, data handling, interpretation. International Atomic Energy Agency, Vienna, 267-308.

Bjarnason, J.Ö. (2010). The Speciation Program WATCH Version 2.4, User's Guide. Iceland water chemistry group, Reykjavik, 9 pp.

Fournier, R.O. (1977) Chemical geothermometers and mixing models for geothermal systems, *Geothermics*, *5*(1-4), 41-50,

Fournier, R.O., &Potter, R.W. (1982) Revised and expanded silica (quartz) geothermometer. *Geothermal Resources Council Bulletin*, *11*(10).

Hartley, M., & Maclennan, J. (2018). Magmatic densities control erupted volumes in Icelandic volcanic systems. *Frontiers in Earth Science*, *6*, 29.

Hauri, E. H., Maclennan, J., McKenzie, D., Gronvold, K., Oskarsson, N., & Shimizu, N. (2018). CO_2 content beneath northern Iceland and the variability of mantle carbon. *Geology*, *46*(1), 55-58.

Heřmanská, M., Stefánsson, A., & Scott, S. (2019). Supercritical fluids around magmatic intrusions: IDDP-1 at Krafla, Iceland. *Geothermics*, *78*, 101-110.

Miller, W. G., Maclennan, J., Shorttle, O., Gaetani, G. A., Le Roux, V., & Klein, F. (2019). Estimating the carbon content of the deep mantle with Icelandic melt inclusions. *Earth and Planetary Science Letters*, *523*, 115699.

Stefánsson, A., Arnórsson, S., Sveinbjörnsdóttir, Á. E., Heinemaier, J., & Kristmannsdóttir, H. (2019). Isotope (δD, $\delta^{18}O$, ^{3}H, $\delta^{13}C$, ^{14}C) and chemical (B, Cl) Constrains on water origin, mixing, water-rock interaction and age of low-temperature geothermal water. *Applied Geochemistry*, *108*, 104380.

Appendix D: Supplementary information for Paper IV

Figures S1-S5

Table S1: Sample information

Table S2: Summary of point counting and least square mixing

Table S3: Whole-rock ICP-OES data

Table S4: Glass major element EPMA data

Table S5: Melt inclusion data

Table S6: Glass trace element LA-ICP-MS and ICP-MS data

Table S7: Glass $Fe^{2+}/\Sigma Fe$ Mössbauer and titration measurements

Table S8: Noble gas isotope measurements

Table S9: Oxygen isotopes

Table S10: Lead isotope ratios

Table S11: Olivine EPMA analyses

Table S12: Plagioclase EPMA analyses

Table S13: Clinopyroxene EPMA analyses

Table S14: Spinel and magnetite EPMA analyses

Table S15: Clinopyroxene-liquid thermobarometry

Table S16: Melt density and viscosity

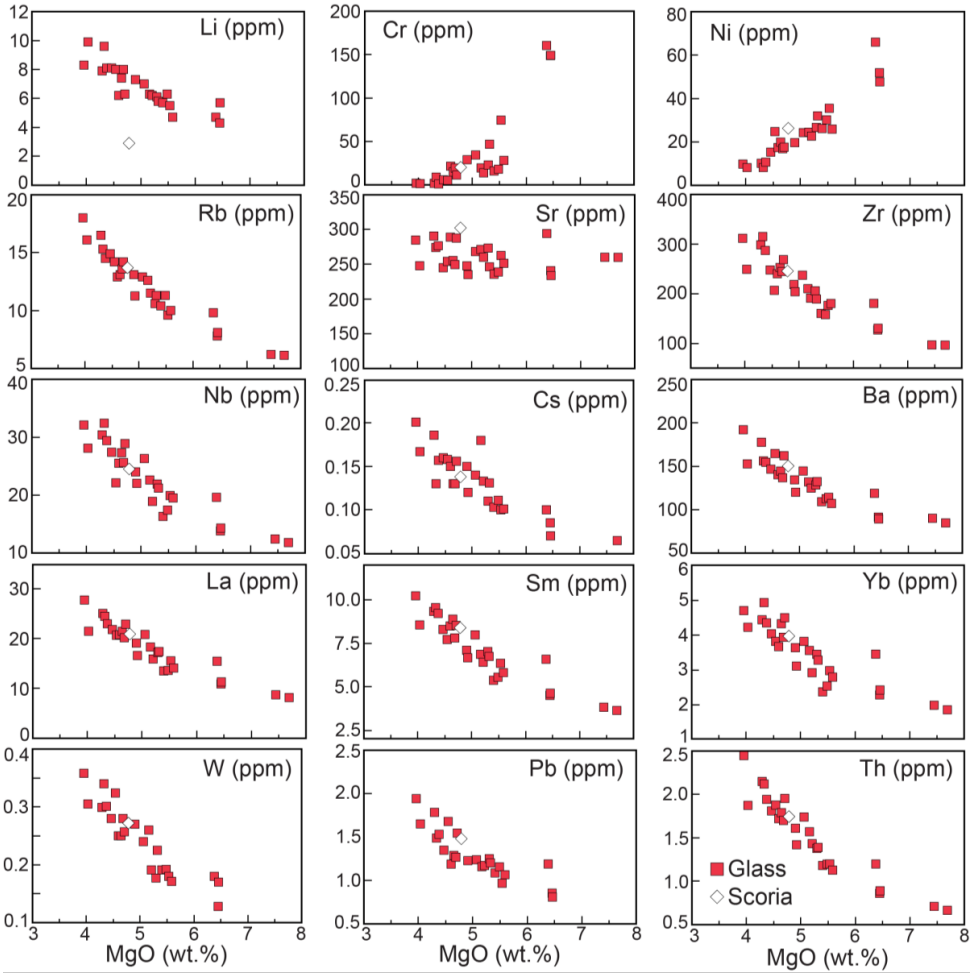

Figure S1. Trace element concentrations vs. MgO. Both LA-ICP-MS (this study) and ICP-MS data (Ranta et al. 2021) are included.

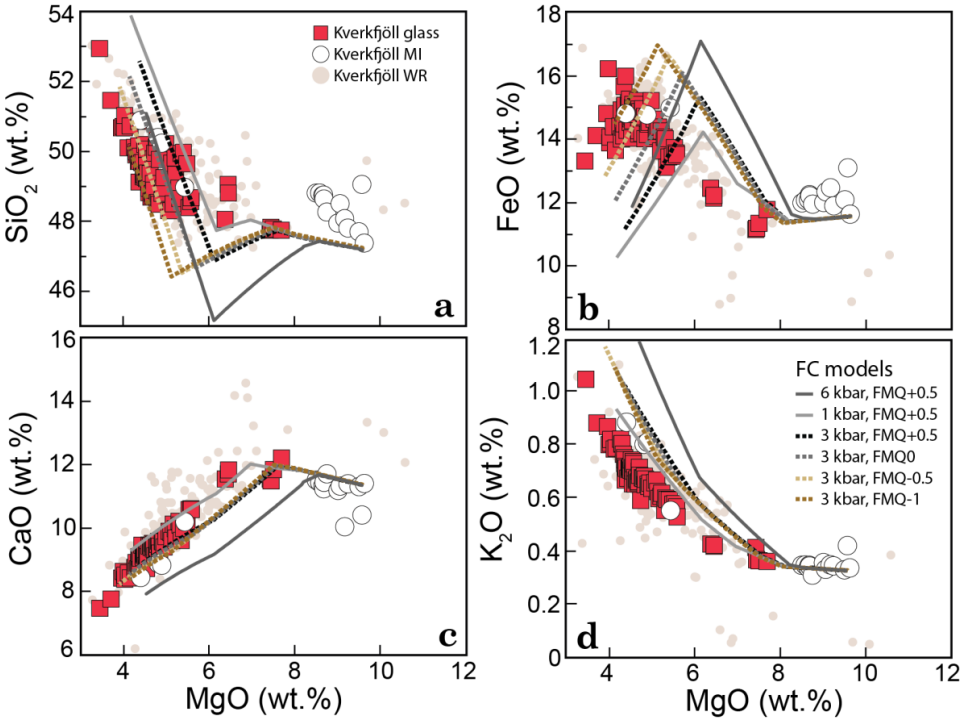

Figure S2. Fractional crystallization models. Fractional crystallization (FC) trajectories were modelled using the Petrolog3 program (Danyushevsky and Plechov 2011). The PEP-corrected composition of the MI glass NAL-356-O5 was used as starting composition for all models. The models were calculated for isobaric fractional crystallization at different pressures (1 kbar, 3 kbar, 6 kbar) and oxygen buffers (FMQ-1, FMQ-0.5, FMQ0, FMQ+0.5). The most realistic pressure-fO_2 conditions are assumed to be 3 kbar and QFM+0.5 (black dashed line), estimated via cpx-liquid barometry and the moderately oxidized $Fe^{2+}/\Sigma Fe \approx 0.822$ of the glasses (see main text). The models regenerate – although not perfectly – the general patterns observed in the measured glass, MI and WR compositions that result from changing proportions of olivine-cpx-plagioclase-magnetite crystallization. Notably, all models fail to recreate the late timing of the onset of magnetite crystallization, even at unrealistically reduced conditions.

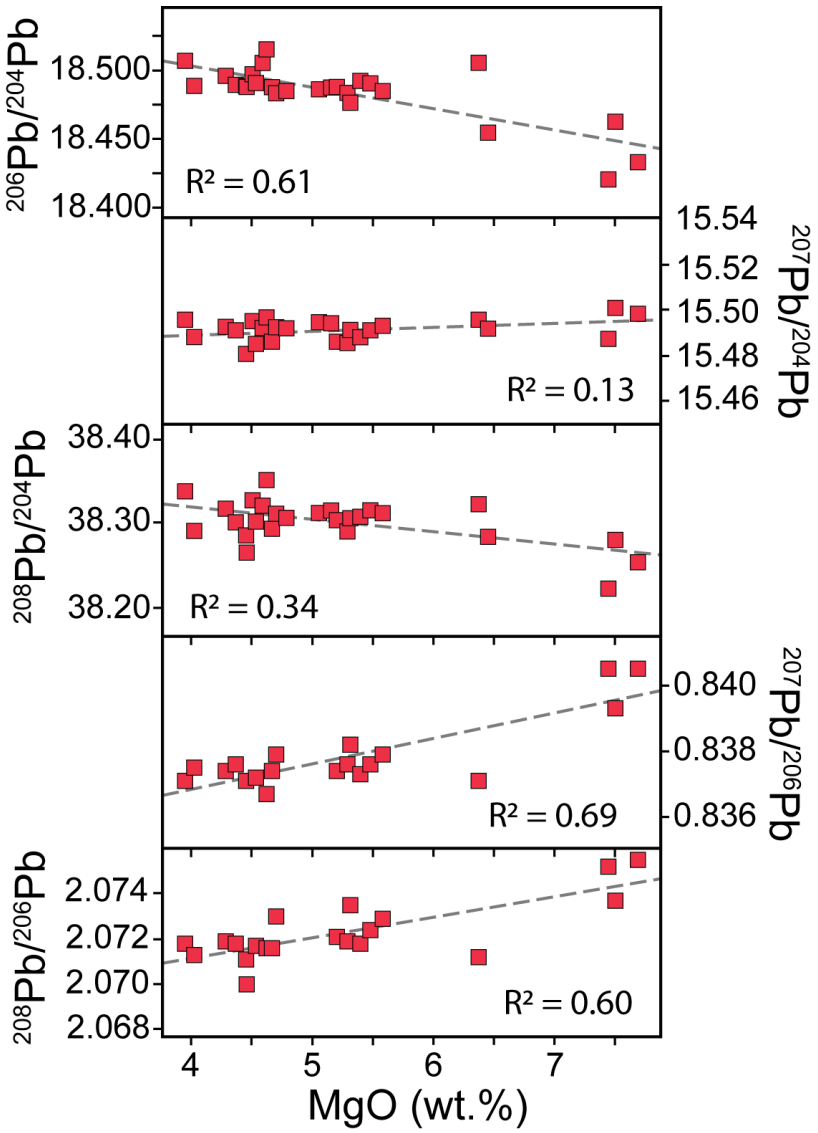

Figure S3. Pb isotope ratios versus MgO of Kverkfjöll glasses. The $^{206}Pb/^{204}Pb$ ratios increase, whereas the $^{208}Pb/^{206}Pb$ and $^{207}Pb/^{206}Pb$ ratios decrease during melt evolution (decreasing MgO). This suggests concurrent melt mixing with progressive melt evolution (Maclennan 2008a) between two isotopically distinct melts. No significant change in $^{207}Pb/^{204}Pb$ or $\Delta^{208}Pb$ (not shown) versus MgO is observed. Regression lines (grey dashed lines) are plotted with their respective R^2 values. The measurement uncertainty is smaller than the size of the symbols.

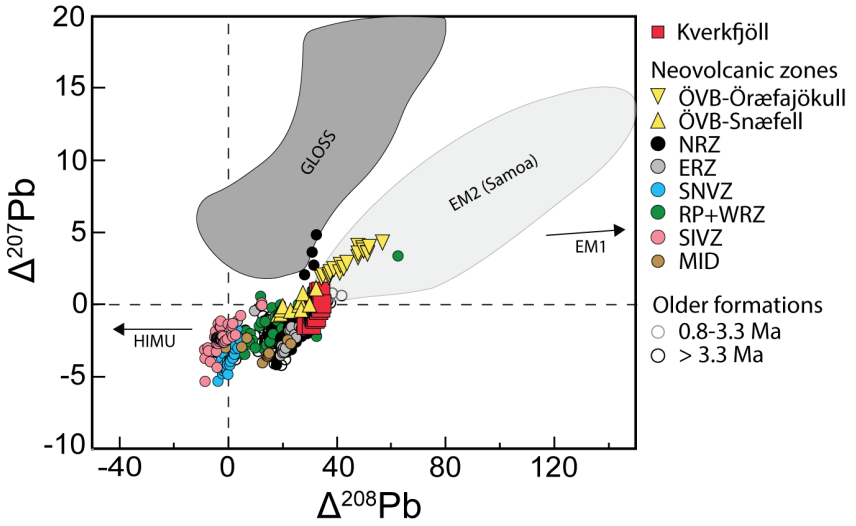

Figure S4. $\Delta^{207}Pb$ versus $\Delta^{208}Pb$. The global subducting sediments field (GLOSS) after Plank and Langmuir (1998). EM2 (Samoa), EM1 and HIMU after Jackson et al. (2007). Other Iceland data from sources given in Fig. 5.8.

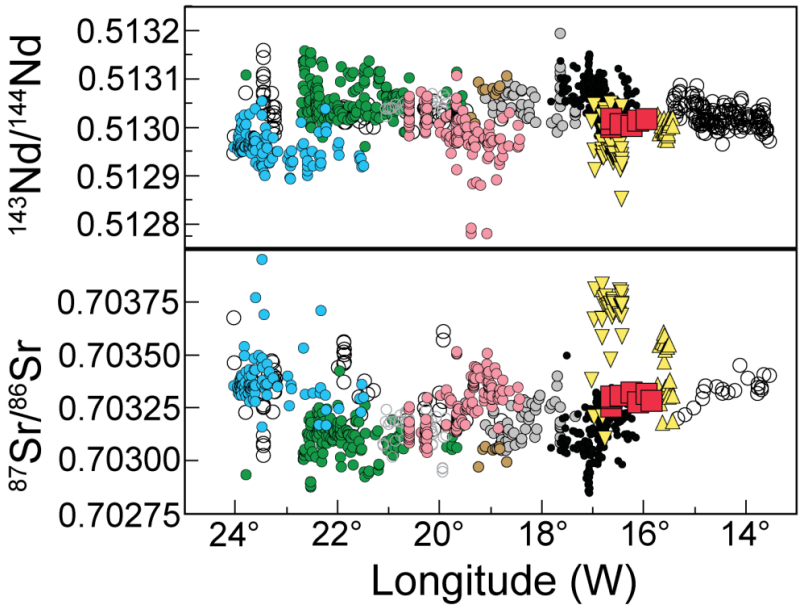

Figure S5. Sr and Nd isotope ratios versus longitude.The relatively low $^{143}Nd/^{144}Nd$ (~0.5130) and high $^{87}Sr/^{88}Sr$ values (~0.7033) of Kverkfjöll are intermediate between the NRZ and Öræfajökull. Symbols as in Fig. S4. Kverkfjöll data are from Pernet-Fisher (2012) and Day (2004). Other Iceland data from sources given in Fig. 5.8.

Appendix E: Supplementary information for Paper V

1. Analytical details

1.1 Fourier transform infrared spectroscopy (FTIR)

The H_2O and CO_2 concentration of 15 subglacial glasses from and 10 olivine-hosted melt inclusions (MIs) from Kverkfjöll were determined via Fourier-transform infrared spectroscopy (FTIR) at IES using a Bruker IFS 66 FTIR spectrometer with a spectral resolution of 4 cm^{-1}. Samples were double polished to a thickness of 30-180 μm, which was measured with a Mitutoyo digital micrometer, with a nominal precision of ±0.1 μm. Only the largest MIs were double exposed; smaller MIs were only exposed on one side. In these cases, adjacent olivine was also measured, and the host-crystal signal was substracted from the mixed signal. The H_2O and CO_2 concentrations were calculated from the measured absorbance (A) with Beer-Lambert's law

$C = 100MA/\rho h\varepsilon$ Eq. S-1

where C is the concentration of H_2O or CO_2, M is the molar weight of the species [g/mol], A is the absorbance, ρ is density [g/L], h is the thickness of the glass wafer [cm] and ε is the absorption coefficient [L $mol^{-1}cm^{-1}$]. Densities were approximated for each melt composition using the parametrization of Silver et al. (1990). H_2O+OH^- and CO_3^{2-} bands were fitted with a straight base line between 2650-3740 and 1362-1553 cm^{-1}, respectively. The H_2O concentrations were calculated based on height of the the $H2O+OH^-$ absorbance band at ~3500 cm^{-1}, using an absorption coefficient of ε = 59.2 L $mol^{-1}cm^{-1}$ (Shishkina et al. 2014). The CO_2 concentrations were determined using the CO_3^{2-} absorbance band at 1430 cm^{-1}, for which an ε of 359 L $mol^{-1}cm^{-1}$ was used (Shishkina et al 2014).

Some of the MIs host either vapour or shrinkage bubbles. Thus, the measured CO_2 concentrations should be taken as minimum estimates (e.g. Aster et al. 2016, Rasmussen et al. 2020). Measured volatile concentrations in MIs were corrected for post-entrapment crystallization using a Rayleigh distillation equation.

1.2 Hydrogen isotope analysis

Fresh glass fragments of basaltic subglacial pillow rims were picked for hydrogen isotope analysis. Only pristine glass fragments with no visible signs of secondary clays or carbonates were accepted (Fig. S1). However, for a few samples, grains with occasional rust or pale white coloured thin coating on vesicle walls was accepted because of lack of completely fresh-looking material. Larger crystals were avoided, but microcrysts of plagioclase, olivine and clinopyroxene and magnetite are unavoidable and vary in abundance from sample to sample (crystallinity of the pillow rim glasses is estimated at 10% based on point-counting; Chapter 5). The picked material (c. 0.3 to 2 mm glass grains) was split into three roughly equal batches of ~30 mg, which were prepared individually with the following methods to test how sample treatment affects the δD measurements:

Method 1 (untreated): Quickly washed with ethanol (20-30s) to remove surface dust, excess ethanol removed with pipette, dried in room temperature.

Method 2 (sonicated): Ultrasonicated in DI water for 60 min, excess water removed with pipette, dried in 60°C oven, washed in ethanol as above.

Method 3 (HF abrasion): This is a modified version of the acid abrasion method of Cassel and Breecker (2017). Glasses were first washed 3x in 10% concentrated HCl at room temperature for 30-40 s, and rinsed thoroughly in DI water after each wash. Following this, the samples were washed 3x in 1% concentrated HF at room temperature for 30-40 s. Glasses were rinsed thoroughly in DI water after each wash, and finally dried in the oven at 60°C.

Following the different initial preparations, all samples were hand-crushed in an agate mortar and sieved in steel sieves. Only the 63-125 μm fraction was used for analysis, as a similar size fraction is known to be optimal for TC/EA-IRMS analysis of δD (Cassel and Breecker 2017).

The hydrogen isotope ratios of the samples were analyzed by continuous-flow mass spectrometry at the University of Texas at Austin, using a ThermoElectron TC/EA (high temperature conversion elemental analyzer), coupled to a ThermoElectron MAT 253 isotope ratio mass spectrometer (IRMS). Analytical methods follow those outlined in Sharp et al. (2001). Approximately 5-15 mg of glass sample were enclosed into silver foil capsules, dried under vacuum at 70°C for 24 h and then immediately transferred to the a Costech zero-blank autosampler and flushed with helium gas. Five internationally referenced and certified standard materials (IAEA-CH7, NBS-22, NBS-30, USGS-57, USGS-58) and one in-house working glass standard were analyzed along with the samples. The raw δD values were then corrected for instrumental drift and then the unknowns were normalized to the VSMOW scale using the standards IAEA-CH7, NBS-22, USGS-57, and USGS-58. Measured δD values of standards did not vary with sample size and the total peak areas of all unknowns were within the linear range of this IRMS. Error based on reproducibility of standards and samples in the analytical runs was < ±5‰. Sample water contents (wt.% H_2O) were calculated using the sample weight and peak area in the mass spectrometer, based on the standards USGS-57 and USGS-58.

Comparison between TC/EA-IRMS analyses of the untreated, sonicated and HF-washed samples shows that, on average, the HF abrated samples have lower TC/EA-H_2O concentrations that match the H_2O concentrations analyzed via FTIR (Fig. S2) or SIMS (secondary ion mass spectrometry; unpublished data). The HF abrated samples also typically have more positive δD values (Fig. S2). The results of the experiment are interpreted to indicate the success of the HF abrasion method in removing minor hydrated low-δD surface layers that may have been present in some of the glasses. A similar conclusion was reached by Cassel and Breecker (2017), who, following more extensive experiments, demonstrated that HF abrasion treatment is able to restore the original δD signature of even highly surface-hydrated tephras. Therefore, all glasses and duplicates in this study were prepared following Method 3 prior to analysis.

1.3 Chlorine isotope analysis

Chlorine isotope ratios ($^{37}Cl/^{35}Cl$) were measured at the University of Texas at Austin following the protocol described in Eggenkamp (1994) and modified by Sharp et al. (2007). Glass chips free from visible alteration were hand-picked and milled in an agate mortar to produce 220-430 mg of powder. Prior to analysis, the powders were washed five

times in 18 MΩ deionized water to remove surficial contamination and dried. Then, Cl^- ions were released by pyrohydrolysis, trapped in an aqueous solution and converted to AgCl. The AgCl was reacted with CH_3I to produce CH_3Cl, which is used as the analyte. The CH_3Cl was purified on-line in a gas chromatographic column before introduction into a ThermoElectron MAT 253 IRMS. The reported error of $1\sigma = 0.2$ ‰ is based on a long-term average of internal standards.

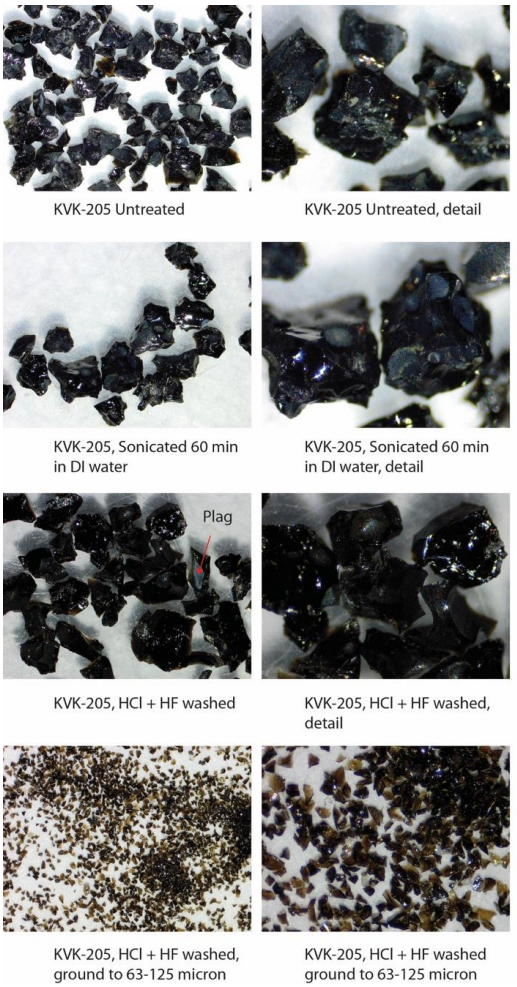

Figure S1. Sample preparation. Care was taken to pick only the freshest pillow rim glasses from each sample. However, minor "rust" or clays is sometimes observed in vesicle walls of untreated, handpicked glasses (upper row). Sonication in MilliQ-DI water removes some of the secondary materials (second row). After triple wash with dilute HCl and HF, glasses are free from remains of secondary infills (third row). The final sieved HF-washed glass fragments are free from any visible alteration, and no secondary minerals were observed (bottom row). The sieved 63-125 μm fraction, that is used for analysis, consists only of fresh looking glass and minor amount of anhydrous primary mineral (plagioclase, cpx, olivine, magnetite).

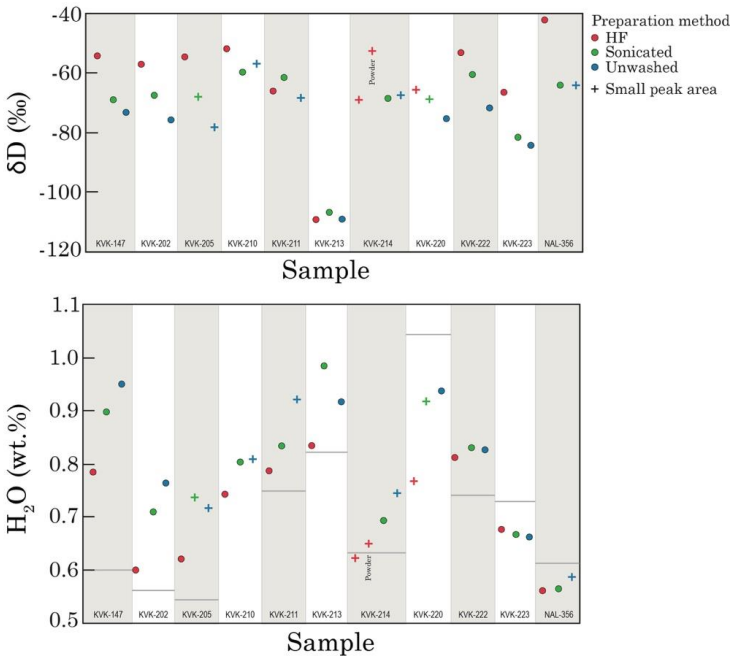

Figure S2. Comparison of the effects of three different sample preparations (unwashed, sonicated in DI water, and HCl-HF washed) on (a) δD and (b) H_2O contents measured by TC/EA. The HF-washed glass grains generally have TC/EA H_2O concentrations closest to the FTIR-measured H_2O, and on average higher δD values. This likely results from the removal of a minor amounts of low-δD clays, or potentially a mildly hydrated glass surface layer, by the HCl-HF-wash.

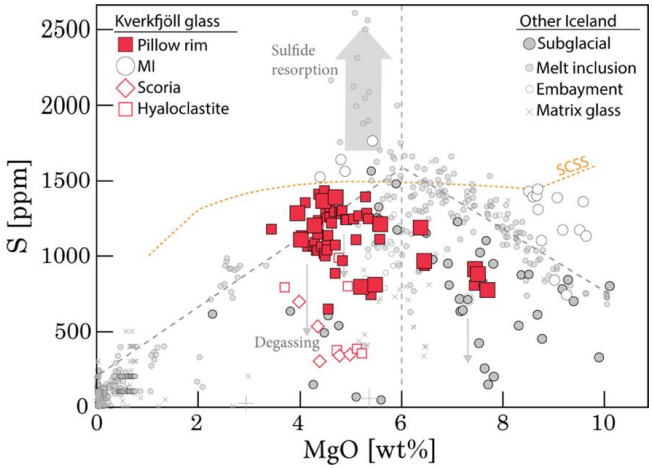

Figure S3. Sulfur systematics. Kverkfjöll pillow rim glasses retain relatively undegassed S contents, similar to many other Icelandic subglacial units (large grey symbols; Ranta et al. 2021). Kverkfjöll samples that were analyzed for δD and $\delta^{37}Cl$ are enlarged. Scoria and hyaloclastite glasses are more degassed than pillow rim glasses, whereas the S concentrations of some Kverkfjöll MIs are unusually high compared to other Icelandic MIs (data from a compilation of Icelandic MI data from Chapter 1). Sulfur concentration at sulfide saturation (SCSS curve) and the approximate onset of sulfide saturation in Icelandic melts (grey vertical dashed line) drawn after Ranta et al. (2021).

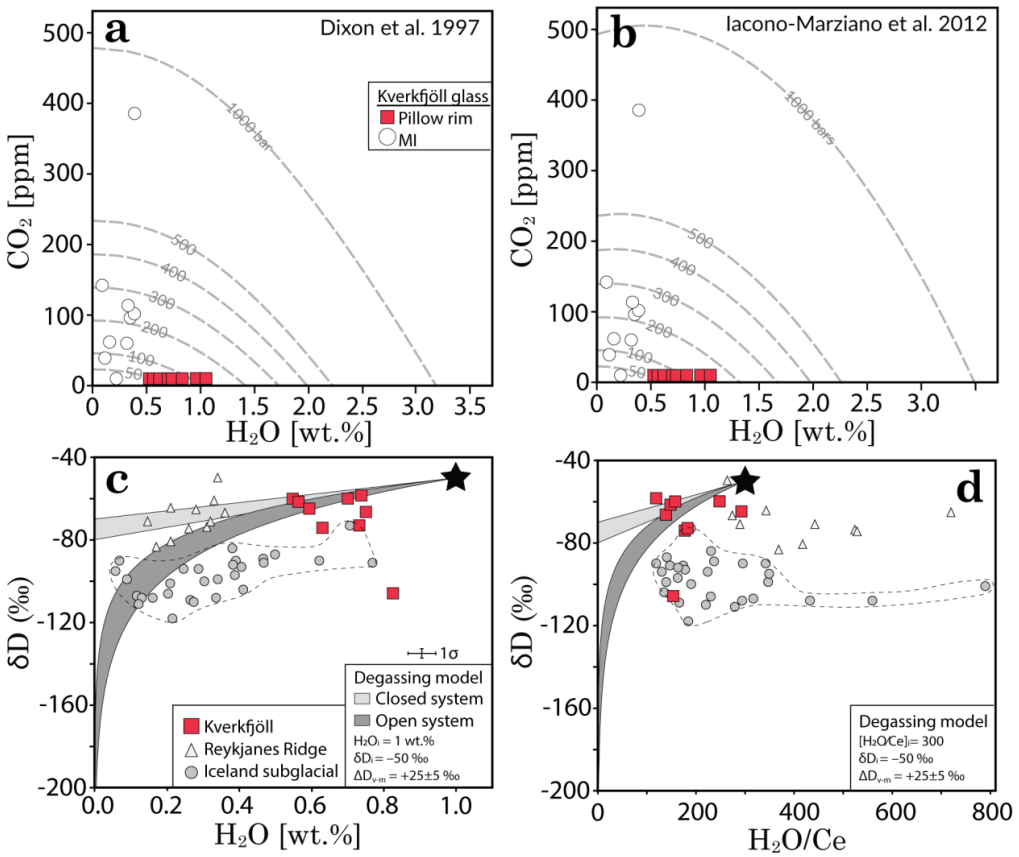

Figure S4. Effect of degassing on H_2O and δD. (a)-(b) Kverkfjöll melt inclusion and pillow rim glass CO_2-H_2O concentrations are plotted together with isobars that indicate the CO_2-H_2O solubility limits calculated in the VESIcal 1.0.2 software (Iacovino et al. 2021) using the solubility models of Dixon et al. (1997) (in (a)) and Iacono-Marziano et al. (2012) (in (b)). The two models yield similar saturation pressures, indicating MI trapping pressures of 26-780 bars. However, these pressures are minimum estimates, as post-entrapment loss of CO_2 may have occurred. The suggested pillow rim quenching pressures of 45-170 bars are equivalent to an ice thickness of 500 to 1900 meters assuming an ice density of 917 kg/m^3. (c) δD versus H_2O. (d) δD versus H_2O/Ce. Closed and open system degassing paths are calculated from a hypothetical initial melt with $\delta D_i = -50$ ‰, H_2O = 1 wt.% and H_2O/Ce = 300 resembling the Kverkfjöll glasses, using a vapor-melt fractionation factor of $\Delta D_{v\text{-}m} = +25 \pm 5$ ‰ (Pineau et al. 1998). The Icelandic subglacial and submarine (Reykjanes Ridge; Poreda et al. 1986, Kelley et al. 2013) glasses show large range in H_2O concentrations and H_2O/Ce, but these do not correlate well with δD. The glass data does not appear to follow modelled degassing trends. Thus, the variability in δD values is interpreted to be related to source heterogeneity and melt mixing.

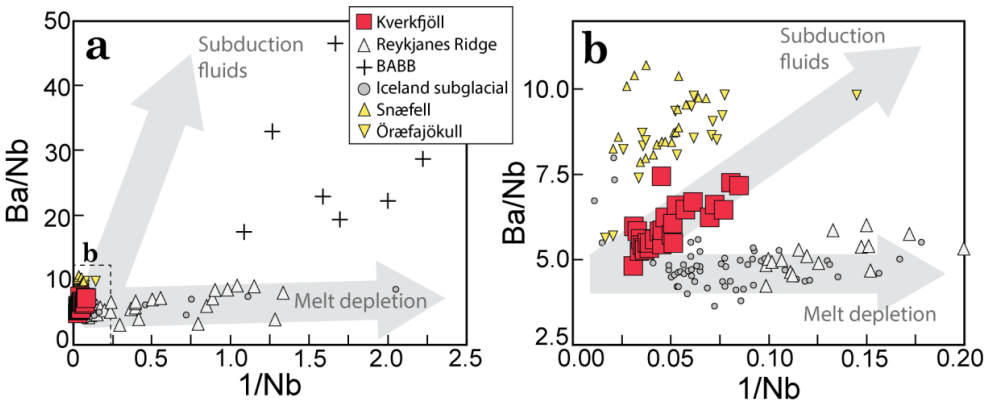

Figure S5. Ba/Nb vs 1/Nb. Snæfell (yellow triangle) and Öræfajökull (yellow top-down triangle) data from Hards et al. (2000), Prestvik et al. (2001), Peate et al. (2010). Other data sources and symbols as in Figs. 6.1-6.3.

Supplementary references

Cassel, E. J., & Breecker, D. O. (2017). Long-term stability of hydrogen isotope ratios in hydrated volcanic glass. *Geochimica et Cosmochimica Acta*, *200*, 67-86.

Dixon, J. E. (1997). Degassing of alkalic basalts. *American Mineralogist*, *82*(3-4), 368-378.

Eggenkamp, H.G.M. (1994). The geochemistry of chlorine isotopes. PhD thesis. Universiteit Utrecht, pp 151.

Hards, V. L., Kempton, P. D., Thompson, R. N., & Greenwood, P. B. (2000). The magmatic evolution of the Snaefell volcanic centre; an example of volcanism during incipient rifting in Iceland. *Journal of Volcanology and Geothermal Research*, *99*(1-4), 97-121.

Iacono-Marziano, G., Morizet, Y., Le Trong, E., & Gaillard, F. (2012). New experimental data and semi-empirical parameterization of H_2O–CO_2 solubility in mafic melts. *Geochimica et Cosmochimica Acta*, *97*, 1-23.

Matthews, S., Shorttle, O., Maclennan, J., & Rudge, J. F. (2021). The global melt inclusion C/Ba array: Mantle variability, melting process, or degassing?. *Geochimica et Cosmochimica Acta*, *293*, 525-543.

Prestvik, T., Goldberg, S., Karlsson, H., & Grönvold, K. (2001). Anomalous strontium and lead isotope signatures in the off-rift Öræfajökull central volcano in south-east Iceland: Evidence for enriched endmember (s) of the Iceland mantle plume?. *Earth and Planetary Science Letters*, *190*(3-4), 211-220.

Rasmussen, D. J., Plank, T. A., Wallace, P. J., Newcombe, M. E., & Lowenstern, J. B. (2020). Vapor-bubble growth in olivine-hosted melt inclusions. *American Mineralogist: Journal of Earth and Planetary Materials*, *105*(12), 1898-1919.

Sharp, Z. D., Atudorei, V., & Durakiewicz, T. (2001). A rapid method for determination of hydrogen and oxygen isotope ratios from water and hydrous minerals. *Chemical geology*, *178*(1-4), 197-210.

Sharp, Z. D., Barnes, J. D., Brearley, A. J., Chaussidon, M., Fischer, T. P., & Kamenetsky, V. S. (2007). Chlorine isotope homogeneity of the mantle, crust and carbonaceous chondrites. *Nature*, *446*(7139), 1062-1065.

Shishkina, T. A., Botcharnikov, R. E., Holtz, F., Almeev, R. R., Jazwa, A. M., & Jakubiak, A. A. (2014). Compositional and pressure effects on the solubility of H_2O and CO_2 in mafic melts. *Chemical Geology*, *388*, 112-129.

Silver, L. A., Ihinger, P. D., & Stolper, E. (1990). The influence of bulk composition on the speciation of water in silicate glasses. *Contributions to mineralogy and petrology*, *104*(2), 142-162.